



HAL
open science

Influence of surface texturing on the biocompatibility of breast implants

Charles Garabedian

► To cite this version:

Charles Garabedian. Influence of surface texturing on the biocompatibility of breast implants: upstream and clinical approaches. Engineering Sciences [physics]. Université Polytechnique Hauts-de-France, 2019. English. NNT : 2019UPHF0007 . tel-03359321

HAL Id: tel-03359321

<https://uphf.hal.science/tel-03359321>

Submitted on 16 Apr 2024

HAL is a multi-disciplinary open access archive for the deposit and dissemination of scientific research documents, whether they are published or not. The documents may come from teaching and research institutions in France or abroad, or from public or private research centers.

L'archive ouverte pluridisciplinaire **HAL**, est destinée au dépôt et à la diffusion de documents scientifiques de niveau recherche, publiés ou non, émanant des établissements d'enseignement et de recherche français ou étrangers, des laboratoires publics ou privés.



Distributed under a Creative Commons Attribution 4.0 International License

Thèse de doctorat
Pour obtenir le grade de Docteur de
l'UNIVERSITÉ POLYTECHNIQUE HAUTS-DE-FRANCE

Discipline, spécialité selon la liste des spécialités pour lesquelles l'Ecole Doctorale est accréditée :
MECANIQUE

Présentée et soutenue par Charles, GARABEDIAN.

Le 25/10/2019, à Valenciennes

Ecole doctorale :

Sciences Pour l'Ingénieur (ED SPI 072)

Equipe de recherche, Laboratoire :

Laboratoire d'Automatique, de Mécanique et d'Informatique Industrielles et Humaines (LAMIH – UMR 8201)

Influence de la texturation de surface sur la biocompatibilité des implants mammaires. Approches amont et clinique.

JURY

Président

- LeHouerou, Vincent. Pr, Head of International Master on Polymer Science (IMPolyS). Laboratory ICube UMR 7357, Strasbourg.

Rapporteurs

- Amédée, Joëlle. DR1 INSERM, Bioingénierie Tissulaire (BioTis). Inserm U1026, Bordeaux.
- Mazeran, Pierre-Emmanuel. MCF HDR, Enseignant-Chercheur. Laboratory Roberval, FRE CNRS 2012, Compiègne.

Examineurs

- Bosc, Romain. MCU, Praticien Hospitalier. Service de Chirurgie Plastique, Reconstructrice, Esthétique et Maxillofaciale, Hôpital Henri Mondor, Créteil.
- Brigaud, Isabelle. IR. Laboratory IS2M, Mulhouse.
- Vayron, Romain. MCF. Laboratory LAMIH, Valenciennes.

Co-directeurs de thèse

- Anselme, Karine. DR1 CNRS. Laboratory IS2M, Mulhouse.
- Bigerelle, Maxence. Pr, Head of Department of Mechanical Engineering. Laboratory LAMIH, Valenciennes.

Membre invité

- Gomes, Christophe. Scientific Director Groupe Sebbin, Boissy-l'Aillerie.

Contents

LIST OF ABBREVIATIONS	5
ACKNOWLEDGEMENTS	6
LIST OF FIGURES	7
LIST OF TABLES	9
GENERAL INTRODUCTION	11
CHAPTER I: INTRODUCTION	15
1.1. HISTORICAL BACKGROUND	15
1.2. BIA-ALCL	22
1.2.1. FDA alert	22
1.2.2. Clinical features	22
1.2.3. Association between breast implant and BIA-ALCL and estimation of a risk	24
1.2.4. Epidemiologic barriers	26
1.2.5. Epidemiologic methodologies to rationalize the risk analysis	29
1.2.6. First BIA-ALCL related epidemiologic structures	30
1.2.7. First recommendations from national regulatory agencies	38
1.3. BREAST IMPLANT SURFACE PROCESS, MEASUREMENT AND DESCRIPTION	40
1.3.1. Breast implant manufacturing and texture	40
1.3.2. The standards related to breast implant surface measurement	45
1.3.3. Breast implant surface measurements published in the literature	46
1.3.4. Breast implant surface description	49
1.4. NOMENCLATURE AND CLASSIFICATION OF BREAST IMPLANT SURFACE	54
1.5. CLINICAL EVALUATION OF BREAST IMPLANT SURFACE	58
1.5.1. Objectives and general principles of clinical evaluation via literature review	58
1.5.2. Clinical evaluation of a link between some types of textures and the incidence of capsular contracture	60
1.5.3. Clinical evaluation of a potential link between some types of textures and the incidence of BIA-ALCL	80
1.5.4. Clinical evaluation of a potential link between some types of textures and the incidence of late seroma or double capsule	97
1.6. BIOLOGICAL MODELS	98
1.6.1. In vivo models	98
1.6.2. In vitro models	102
1.6.3. Ex vivo models	106
CHAPTER II: MEASUREMENT INSTRUMENT AND MULTI-SCALE ANALYSIS	115
2.1. MULTI-SCALE ANALYSIS	116
2.2. MEASUREMENT AND FIRST ANALYSIS OF BREAST IMPLANT SURFACE WITH SEM AND 3D RECONSTRUCTION SOFTWARE	129

2.3. CONCLUSIONS _____	132
CHAPTER III: BIOLOGICAL RELEVANCE OF THE PROPOSED CLASSIFICATION _____	135
3.1 INTRODUCTION _____	135
3.2 ARTICLE _____	136
3.3 OUTLOOK _____	179
CHAPTER IV: TOPOGRAPHICAL RELEVANCE OF THE PROPOSED CLASSIFICATION _____	181
4.1. INTRODUCTION _____	181
4.2. METHODOLOGY _____	184
4.3. RESULTS _____	187
4.3.1. One variable discriminant analyses _____	187
4.3.2. Two variables discriminant analyses _____	191
4.3. DISCUSSION _____	193
4.4 CONCLUSIONS _____	199
CHAPTER V: <i>IN VIVO</i> DAMAGES OF DIFFERENT TEXTURED BREAST IMPLANTS _____	201
5.1 INTRODUCTION _____	201
5.2 MATERIALS & METHODS _____	204
5.3 RESULTS _____	208
5.3.1 Cereform texture (Cereplas) (PV) _____	209
5.3.2 Sebbin round implant texture (Sebbin) (OC) _____	211
5.3.3 Cristalline Micro-texture (Eurosilicone) (OC) _____	213
5.3.4 Nagotex texture (Nagor) (OC) _____	215
5.3.5 Sebbin shaped implant texture (Sebbin) (SOC) _____	217
5.3.6 Biocell texture (Allergan) (SOC) _____	219
5.4 DISCUSSION _____	220
5.4.1 Validation of the breast implant classification _____	220
5.4.2 The transfer function of the implant / explant roughness _____	222
5.4.3 Damage of PV structure _____	223
5.4.4 Damage of OC and SOC structures _____	225
5.5 CONCLUSION AND OUTLOOK _____	232
CHAPTER VI: GENERAL CONCLUSIONS AND OUTLOOK _____	235
6.1 GENERAL CONCLUSIONS _____	235
6.2 OUTLOOK _____	237
APPENDIX 1: Comparative bibliometric study on Hip and Breast Implants _____	239
APPENDIX 2: Multi-scale skewness analysis for SOC-patterned prostheses _____	241
REFERENCES _____	243
THESIS SUMMARY _____	255
RESUME DE THESE _____	255

LIST OF ABBREVIATIONS

2D Two-Dimensional

3D Three-Dimensional

AFM Atomic Force Microscopy

ANOVA Analysis of Variance

ANSM Agence Nationale de Sécurité du Médicament et des produits de santé

BIA-ALCL Breast Implant-Associated Anaplastic Large Cell Lymphoma

CE Conformité Européenne

DNA Deoxyribonucleic Acid

ECM Extra-Cellular Matrix

FDA Food and Drug Administration

HP High-Pass

ISO International Organization for Standardization

IL Interleukin

LP Low-Pass

MMP Matrix Metalloproteinase

OC Open Cavities

PCA Principal Component Analysis

PCR Polymerase Chain Reaction

PDMS PolyDiMethylSiloxane

PIP Poly Implant Prothese

PU Polyurethane

PV Pics and Valleys

qRT-PCR Quantitative Reverse-Transcriptase Polymerase Chain Reaction

RNA Ribonucleic Acid

SAA1 Serum Amyloid A

SEM Scanning Electron Microscope

SOC Semi-Open Cavities

TIMP Tissue Inhibitor of Metalloproteinase

TGF Tumor Growth Factor

TNFSF11 Tumor Necrosis Factor ligand Superfamily member

ACKNOWLEDGEMENTS

I would like to express my deepest gratitude to my thesis supervisors, Dr. Karine Anselme, and Pr. Maxence Bigerelle, for their support, patience, enthusiastic guidance, valuable suggestions, advices, and constructive criticisms as well as for their expertise and scientific curiosity conveyed throughout the thesis. Their great interest in the thesis was for me the major driving force to complete the thesis.

I also wish to greatly thank Dr. Isabelle Brigaud for her considerable help provided especially during the biological part of the thesis. I also wish to express my sincere gratitude to Dr. Romain Vayron for his writing skills and his relevant analyses and to Dr. Raphael Deltombe and Dr. Rémi Delille for their technical expertise.

I would like to express my warmest thanks to Christophe Gomes for having trust in me and for his confidence. My acknowledgements are also due to Dr. Marie Chiganne for her support and her constant encouragement during the thesis.

I also would like to extend my deep thank to Dr. Nathalie Bricout and Dr. Romain Bosc for their clinical expertise and for their collaboration in the study.

This thesis was conducted as part of a CIFRE (Conventions Industrielles de Formation par la Recherche) contract between the LAMIH laboratory of the UPHF, the IS2M laboratory of the UHA and the GROUPE SEBBIN. I would like to deeply thank the LAMIH laboratory and the IS2M laboratory to have welcomed me. I wish to gratefully acknowledge the financial support provided by GROUPE SEBBIN and all my colleagues and other doctorate candidates for their interest in my work, their sympathy and the friendships forged.

Last but not least, I want to express my sincere appreciation to Dr. Joëlle Amédée et Dr. Pierre-Emmanuel Mazeran to have accepted to read this manuscript and to give their feedback.

To my family and friends.

LIST OF FIGURES

<i>Figure 1 : Cross-sections of the MSI surface pattern observed by SEM (A: magnification x65, B: magnification x150)(Peters et al.)</i>	18
<i>Figure 2 : SEM images of Silimed TRUE Texture, Mentor Siltex and Allergan Biocell textured surfaces. (magnification: x65)(20)</i>	20
<i>Figure 3 : « Salt-loss technique » (77)</i>	42
<i>Figure 4 : Workflow for the selection of articles from the scientific databases</i>	67
<i>Figure 5 : Workflow for the selection of articles from the scientific databases</i>	82
<i>Figure 6 : Three-layer composition of a periprosthetic capsule (Masson Goldner stain; magnification: x4). (119)</i>	107
<i>Figure 7 : « Velcro effect ». A : implant surface (Biocell). B : capsule surface. (SEM ; magnification : x50)(88)</i> .	110
<i>Figure 8 : Biofilm imaged in capsule specimens (SEM images; magnification: x5000)(64)</i>	112
<i>Figure 9 : Illustration of the main surface structures shared by breast implant devices binding in each of the 3 categories, namely PV, OC and SOC. Top view topography and corresponding cross-section is given for one device (underlined market reference) as a representative example of the entire category. A color calibration bar in micrometer (μm) indicates the height of the relief on the topographies where black and red represents respectively the lowest and the highest amplitude of topography. Bar scale represents 1.0 mm in length.</i>	184
<i>Figure 10 : Surface analyses processing overview. 9 samples on 3 independent localizations per breast implant examined are collected to undergo surface topography measurement (X-Ray Microtomography or interferometry). The 9 surface measurements are then filtered (high-pass (HP) or low-pass (LP) filters) at 8 different scales of depth (ranging from $8\mu\text{m}$ to $952\mu\text{m}$). A pool of 672 multi-scale parameter values per surface measurement is obtained by computing 42 surface roughness parameters on each filtered surface. Finally, these 672 multi-scale parameters are 100 times bootstrapped and then paired. An index of classification was designed in order to rank in descending relevance all the couples of multi-scale parameters and to retain the most discriminative classifications</i>	186
<i>Figure 11 : One-variable discriminant analyses. Ranking of the 42 bootstrapped roughness parameters depending on their index value. Parameters are plotted with their rank (# position) and corresponding index value in descending order (A). Distribution curves of the 17 breast implant surfaces sampled in this study using the highest ranked parameter Sdq led to the discrimination of 3 implant classes (I, II and III) but failed to discriminate between implants within a same class (B).</i>	189
<i>Figure 12 : One-variable discriminant analyses. Ranking of the 100 best bootstrapped multi-scale roughness parameters depending on their index value. Parameters are plotted with their rank (# position) and corresponding index value in descending order (A). Distribution curves of the 17 breast implant surfaces sampled in this study using the highest ranked parameter ($Sa_{HP_105.8}$) failed to discriminate any implant class (B).</i>	190
<i>Figure 13 : Two-variable discriminant analysis. Classification of the 17 breast implant surfaces sampled in this study using the highest ranked parameter couple ($m(Sdq_LP_105.8) / m(Sfd_HP_105.8)$) led to the discrimination of 4 implant classes and to the segregation between implants within a same class. An additional breast implant surface (Cristalline Textured surface manufactured by Eurosilicone) was included in the analysis as a posteriori control.</i>	192
<i>Figure 14 : Measured and filtered surfaces of a characteristic implant type for the 4 categories. A color calibration bar in micrometer (μm) indicates the height of the relief on the topographies where black and red represents respectively the lowest and the highest amplitude of topography.</i>	193
<i>Figure 15 : Distributions of the 17 implant types analyzed according to the parameters Sdr (A) and Sa (B) (respective index value = [50% ; 50%]) retained after discriminant analysis performed only on parameters</i>	

<i>computed on measured surfaces, i.e. on m(param*)_LP_8. Identification of 4 categories of implant types corresponding to the 4 differently-colored areas on the Sa-distribution.</i>	<i>198</i>
<i>Figure 16 : Micrometric particles observed in the capsule. (SEM x7500) (Danino et al.)</i>	<i>201</i>
<i>Figure 17 : Principle of surface filtering (example given with a threshold of 105µm). (A) Measured surfaces containing the full range of roughness scales, once filtered by a High-Pass (HP) filter, retain the roughness scales below the threshold value and up to the instrument resolution. (B) Low-Pass filter (LP) filtered surfaces only contain roughness scales above the threshold value.</i>	<i>207</i>
<i>Figure 18 : Multi-scale curves of Sa_{implant} and Sa_{explant} and F for Cereform texture (PV)</i>	<i>209</i>
<i>Figure 19 : "Smoothing" of micro-roughness on Cereform explants (left: implant, right: explant)</i>	<i>210</i>
<i>Figure 20 : Multi-scale curves of Sa_{implant} and Sa_{explant} and F for Sebbin round implant texture (OC).....</i>	<i>211</i>
<i>Figure 21 : Damage on Sebbin round textured explants (left: implant, right: explant).....</i>	<i>212</i>
<i>Figure 22 : Multi-scale curves of Sa_{implant} and Sa_{explant} and F for Eurosilicone Cristalline Micro-texture (OC)</i>	<i>213</i>
<i>Figure 23 : Appearance of very small irregularities on the Eurosilicone Cristalline Micro-texture explant (left: implant, right: explant)</i>	<i>214</i>
<i>Figure 24 : Multi-scale curves of Sa_{implant} and Sa_{explant} and F for Nagotex texture (OC)</i>	<i>215</i>
<i>Figure 25 : Macroscopic irregularity of the cavities on the Nagor explant (left: implant, right: explant).....</i>	<i>216</i>
<i>Figure 26 : Multi-scale curves of Sa_{implant} and Sa_{explant} and F for Sebbin shaped implant texture (SOC).....</i>	<i>217</i>
<i>Figure 27 : Macroscopic opening of cavities on the explants (left: implant, right: explant)</i>	<i>218</i>
<i>Figure 28 : Multi-scale curves of Sa_{implant} and Sa_{explant} and F for Biocell texture (Allergan)</i>	<i>219</i>
<i>Figure 29 : Large heterogeneity of Allergan explant surface (left: implant, right: explant).....</i>	<i>220</i>
<i>Figure 30 : Classification of implants obtained by discriminative analysis (left) and projection of our explants database on this classification (right)</i>	<i>222</i>
<i>Figure 31 : Identification of the damage regimes of the different categories of texture and associated topographical characteristics.....</i>	<i>223</i>
<i>Figure 32 : 2-D damage modelling of the debris mill mechanism on a PV implant.....</i>	<i>225</i>
<i>Figure 33 : Appearance of microscopic irregularities within cavities of the Sebbin shaped explants</i>	<i>227</i>
<i>Figure 34 : 2-D damage modelling of the damage mechanisms on an OC implant</i>	<i>228</i>
<i>Figure 35 : 2-D damage modelling of the damage mechanisms on a SOC implant</i>	<i>228</i>
<i>Figure 36 : Schematic representation of the bias, which will appear on the Sa values during the opening of SOC structures</i>	<i>230</i>
<i>Figure 37 : The Sa evolution computed on the topographies measured (i.e. before multi-scale analysis) according to the implant duration</i>	<i>231</i>
<i>Figure 38 : OC explant's undulation characteristic of a "heterogenous stress relaxation"</i>	<i>232</i>

LIST OF TABLES

<i>Table 1 : Worldwide and nation-wide numbers of BIA-ALCL cases and related deaths as of November 2018.</i>	28
<i>Table 2 : Clinical data related to BIA-ALCL published by the newly established registries and regulatory agencies in the French- or English-speaking countries in the world</i>	37
<i>Table 3 : Textures of the major breast implant manufacturers and associated texturing processes</i>	44
<i>Table 4 : Topographical measurements and characterizations published in the literature</i>	48
<i>Table 5 : Morphological descriptions of the textures in the literature</i>	52
<i>Table 6 : Classifications of the different breast implant surfaces according to the published nomenclatures</i>	57
<i>Table 7 : Search implemented on the scientific databases</i>	66
<i>Table 8 : Selected and non-selected articles through the scientific database search</i>	77
<i>Table 9 : Cumulative risks of capsular contracture of different breast implant surfaces retrieved from the scientific database search</i>	79
<i>Table 10 : Selected and non-selected articles through scientific database search</i>	86
<i>Table 11 : BIA-ALCL cases per manufacturer reported by the French regulatory agency (ANSM) and by the Canadian regulatory agency (Health Canada)</i>	87
<i>Table 12 : BIA-ALCL cases per type of breast implant surface reported by the LYMPHOPATH network</i>	88
<i>Table 13 : BIA-ALCL cases per type of breast implant surface and hypotheses of pathogenesis retrieved from scientific and federal database search</i>	96
<i>Table 14 : Comparison of the 4 existing classifications (in color the implants analyzed in our classification: SMOOTH, PV, OC and SOC)</i>	196
<i>Table 15 : Implant characteristics and patient clinical data of the explant sampling. For clarity, the color height scale for the PV category was not represented. The approximate maximal height of this type of structure is 100μm.</i>	206
<i>Table 16 : Determination of categories of the breast implant classification</i>	221
<i>Table 17 : Difference between the Sa_{explant} and the Sa_{implant} (or Delta) for each texture at a scale of 10μm.</i>	227

GENERAL INTRODUCTION

The first surface patterning of breast implants (also called textures) only appeared in 1987. It was designed to reproduce the "immobilizing" effect of implants covered with Polyurethane (PU) foam, whose safety began to become controversial. This propensity to anchor into surrounding biological tissues has become essential for the 5th generation implants, also known as "form stable implants". Indeed, the stability of these implants, which are anatomically shaped, in the breast must be perfect to avoid disastrous aesthetic results.

Under pressure from the media, which warned patients against the paucity of the information provided by the manufacturers on the biologic profile of silicone, the American Health agency Food and Drug Administration (FDA) imposed in 1992 a moratorium on implants filled with silicone gel, allowing then in the US territory only inflatable implants filled with saline. From now on, to market breast implants in the US, manufacturers will need to provide safety for their device through large-scale clinical studies (called "Core Studies"). Once the scientific evidence of the safety of the silicone was published, the moratorium was lifted in 2006. Simultaneously, breast implants became class III medical devices.

The biological mechanisms responsible for integrating the implant into the body are beginning to be better understood. Thus, because of the foreign body reaction, any breast prosthesis once implanted is surrounded by a fibrous capsule. In some cases, this capsule may thicken and harden, causing pain in the patient. This is capsular contracture.

After a first reading of these clinical studies, a reducing effect of the capsular contracture rate of the textured implants compared to the smooth implants was thought. Motivated by all these clinical benefits (which are supposed to be), all the manufacturers started to develop implant textures. The rougher ones have been called "macrot textures", while the less rough ones have been called "micro textures". These arbitrary designations only respond to marketing logic on the part of

manufacturers. They have neither clinical sense nor topographical sense. Therefore, it was difficult because of the non-standardization of these clinical studies, to demonstrate the clinical benefit (for example in terms of reducing the risk of capsular contracture) of such type of texture compared to another type of texture.

Ten years after the commercialization of textured implants, a new pathology was identified on a woman carrying breast implants. It is a lymphoma presenting particular characteristics, such as the confinement of the pathology to the fibrous capsule. It was only after a publication in 2015 reporting an exponential increase in cases of this lymphoma and an over-representation of Allergan's Biocell texture in statistics, that Health authorities were beginning to worry about this pathology and the link between certain types of textures and the risk of lymphoma. In 2017, the World Health Organization (WHO) introduced a new category for this pathology in its lymphoma classification: Breast Implant-Associated Anaplastic Large Cell Lymphoma (BIA-ALCL). With the establishment of specific registries in some countries and clinicians' awareness, BIA-ALCL's first incidence estimates did literally explode. They increased from 1 in 500,000 in 2015 to 1 in 3,000 in 2016. An Australian study even determined that depending on the type of texture, the risk of BIA-ALCL could vary from 1 in 3,000 to 1 in 60,000. At present, such a study could not be conducted in other countries, due to registries that are not sufficiently mature to provide robust clinical data or to manufacturers reluctant to provide sales figures.

BIA-ALCL is acknowledged to be a result of chronic inflammation of the surrounding tissues. However, the origin of the inflammation remains to be identified. Various hypotheses were proposed in the literature, such as the biofilm that would develop on the surface of prostheses once implanted or the release into the tissue of silicone debris from the surface.

For the reasons previously mentioned, the paucity of data precludes a demonstration of the clinical impact of certain types of texture. Nevertheless, on the basis of the above hypotheses, the impact of the textures on the biocompatibility of the implant was analysed thereafter. As the propensity of certain surface patterns to develop a biofilm has been widely studied in the literature, this hypothesis will not be studied in

our investigations. However, the influence of the implant topography on tissue inflammation or potential post-implantation surface damage will be analyzed and will allow us to assess the relevance of these hypotheses for the pathogenesis of BIA-ALCL. Before correlating certain implant textures with biological or post mortem characteristics, the surfaces had to be measured according to an appropriate protocol, in terms of instrument, objective and resolution. Once the surface topographies were measured and the metrological parameters calculated, different measuring instruments were compared on 4 different types of implant surfaces via the multi-scale analysis. This was published in *Surface Topography: Materials and Properties*. This work allowed us to criticize the new version of the International Organization for Standardization (ISO) standard for breast implants (ISO 14607) released in 2018.

On the basis of the morphologies observed on the topographies, a classification of the textures was proposed. This classification allowed us to determine whether the topography (and more specifically the identified morphologies) has an impact on the molecular mechanisms occurring in the surrounding biological tissues. Previous transcriptomic studies have identified a number of relevant genes for an asymptomatic capsule / pathological capsule comparison. Based on this selection of genes and by restricting our study to healthy capsules, we were able to determine whether these different surface textures elicit a specific molecular response, including a particular inflammatory response. In view of the clinical complications (in particular capsular contracture), we considered relevant to integrate in the analysis some markers of the synthesis / degradation of the Extra-Cellular Matrix (ECM) (which constitutes the capsule). This study was the subject of an article that was accepted on 03/07/2019 for publication in the journal *Plastic and Reconstructive Surgery*.

Contrary to the existing nomenclatures in the literature, a statistical analysis was able to select the couple of topographical parameters and the spatial scale on which our classification is based and to demonstrate their robustness. This analysis will allow us to demonstrate putative correlations between the topographical characteristics and the obtained biological profile. This study will be the subject of an article that will be submitted for publication soon.

Before concluding on the biocompatibility of breast implants (or of any implantable device), it is fundamental to carry out tribological tests or to evaluate the potential damage to the surface of a prosthesis once implanted (or explant). Such studies on breast implants do not exist in the literature. We therefore compared at different scales the damage of 6 different explant textures. As part of this first ex vitro study, damage regimes were identified for each category of our classification. For each of these regimes, mechanisms of wear have also been suggested. This study was the subject of an article that will be submitted for publication soon.

CHAPTER I: INTRODUCTION

1.1. HISTORICAL BACKGROUND

The history of breast implant spreads over the last 50 years. Numerous attempts were led, before the development of breast implant, we know nowadays. Often the new designs introduced by the companies were conceived by individual surgeons. This history is sometimes confusing because many of the suppliers or manufacturers changed their names and ownership over the years.

A first attempt of implant-based breast augmentation based on implantation of a glass ball was performed in the 1930s by Schwarzmann and will be used until 1942. (1) Then, development of breast implant design with new polymer materials was led from 1951 to 1962. The implant was then a synthetic sponge. Thus, 3 chemically different sponges were developed: Ivalon (a polyvinyl alcohol sponge), Etheron (a polyether sponge) and Polystan (composed of fabric tapes that were cut and then wound into a ball). Dr William John Pangman formed Poly-Plastic Company to manufacture his own brand of Ivalon implants. In 1961, approximately 16 600 Ivalon implants had been inserted. The results were poor and sometimes disastrous (the breasts became firm and lost over 25% of their volume). (2)

In 1962, under the leadership of *Dow Corning Company*, two surgeons from Houston (Texas, USA), Frank Gerow and Thomas Cronin designed the first modern breast implant formed of an "anatomically" shaped (teardrop) envelope and filled with moderately viscous silicone gel. The shell of the **first-generation implants** was designed with a 0.75mm thick, smooth silicone elastomer as a 2-piece envelope with a seam along the periphery. (3) A single roughened Dacron (polyethylene terephthalate) patches was added on the posterior side of the implant to promote tissue adhesion and to avoid prosthesis displacement. (4) In 1964, 4-quadrant patches were used. In 1968, 3, 4 or 5 patches could be fixed, depending on the implant volume. (2)

This new prosthesis was marketed in the US in 1964 and was an immediate success. Dow Corning had an almost exclusive monopoly on their manufacture. From 1969 onward, all shells were seamless. However, several drawbacks were quickly reported:

- Large scar on the breast skin due to the long submammary incision required for this type of implant
- Sagging of the breast downward (or ptosis) due to the Dacron patches fixing only the posterior face of the prosthesis to the chest wall behind the gland.

Moreover, the periprosthetic capsule surrounding the implant was often too thick and contractile, resulting in a firm, hard and sometimes even distorted breast (1, 4, 5). This complication was firstly named "fibrous envelope contracture" by Freeman in 1972 (6) and will be then called "capsular contracture", which will be the most significant clinical adverse event associated with breast implant throughout the next decades.

At the same moment, in 1965 the use of inflatable saline filled implant was reported for the first time by Dr Henri Arion, in France. The implant was constituted of a 0.35mm thick elastomeric shell with a peripheral circumferential seam, a filling tube and a valve attached permanently to one side. Different companies marketed inflatable saline filled implants: Simaplast in France, Heyer-Schulte (which manufactured in the USA in 1968 the "Jenny implant") and Dow Corning (from 1970). Different silicone types were used thereafter: High Temperature Vulcanization (HTV) silicone and then Room Temperature Vulcanization (RTV) silicone. (2)

In 1968, Drs Franklin Ashley and William John Pangman developed a 1.2-2 mm polyurethane (PU) foam-coated and gel-filled implant manufactured by Polyplastic Silicone Products (PSP): the "Ashley Natural Y Implant". An inverted Y-shaped internal divider was designed to maintain the shape of the implant by preventing the gel from sagging to the deep part of the implant. (7) In 1971, Heyer-Schulte acquired the rights for the Ashley Natural Y Implants from PSP. Surprisingly, the subglandular rate of capsular contracture was drastically reduced (3.3%) compared to the existing implants. (8) Consistently, Vazquez observed a different collagenous and presumably less contractile capsule architecture around PU-coated implants. (9)

The **second-generation** implant developed in the 1970s was made of round implants with a smooth, thinner (0.13mm) and seamless shell and without Dacron patches incorporated into the shell. These implants were filled with a less viscous silicone gel than the first-generation implants. Softer implants were therefore designed with the idea that they would result in softer breasts. Although the incidence of capsular contracture was reduced, diffusion or bleed of short chains of polymeric molecules contained in the gel throughout the shell, as well as shell ruptures, were more frequent. (1, 4, 5) In 1972, Heyer-Schulte and Medical Engineering Corporation (which later became Surgitek) began to market gel-filled implants in the USA. Then, McGhan introduced its first gel-filled breast implant in 1974.

The **third generation** of smooth silicone implants, developed in the early to mid-1980s, aimed at improving the strength and permeability of the silicone shell. This generation of implants was characterized by thicker (0.30 to 0.50mm) and multi-layered shells containing a chemically different layer called "barrier". This envelope design considerably reduced gel bleed and device shell failure rate. (1, 4, 5) McGhan started to market its 3rd generation implant in the USA in 1979. The implant Silastic II was introduced by Dow Corning in the USA in 1981. Then, Surgitek Strong, Cohesive, Low-bleed (SCL) implants appeared in the USA in 1986. As a low-bleed barrier, Surgitek and McGhan incorporated within the shell a diphenyl layer, whereas Dow Corning used a 0.010mm coating of fluorosilicone on the interior surface of the shell.

As at that time the low capsular contracture profile was attributed to the PU coating, the other manufacturers then decided to imitate this type of surface structure. In 1987, all PU-coated implant brands were acquired by Cooper Laboratories and then by Surgitek in 1988. Thus, new surface processing had to be developed by the other manufacturers. The first development to make the envelope irregular and "textured" appeared in the **4th generation** of implant. The first FDA-approved texture was in 1987 the Biocell texture commercialized by McGhan (which will become later Inamed then Allergan in 2006), then Mentor Siltex[®] 2600 manufactured by Biomedic-Mentor was approved in 1988. In 1989, Dow Corning developed its Micro Structured Implants (MSI),

whose the surface exhibited regular pillars 250 μ m in diameter, 750 μ m high and 500 μ m apart. Two cross-sections of this surface pattern are exhibited in the Figure 1. (2)

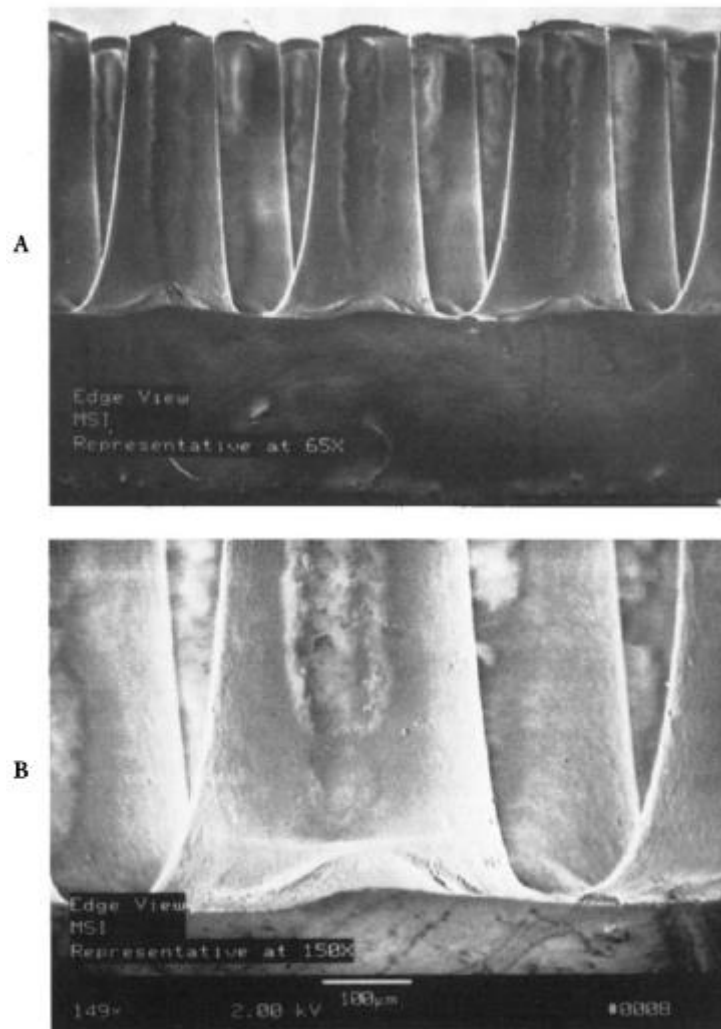


Figure 1: Cross-sections of the MSI surface pattern observed by SEM (A: magnification x65, B: magnification x150)(Peters et al.)

An enormous public pressure fuelled by unions of patients and lawyers exploded in the USA in 1990, consequently to articles in the press and talk shows, which warned patients against the paucity of the information provided by the manufacturers on the biologic profile of silicone. A few years later, the largest class action lawsuit in medical history broke out in the United States. In 1993, the *Dow Corning Company* was facing bankrupt because of 12 359 patient complaints. David Kessler (Head of FDA) established a "voluntary moratorium" on the distribution and implantation of silicone

breast implants in the USA in January 1992, only on the basis of inadequate demonstration of biocompatibility provided by the manufacturers. A month later, the "General and Plastic Surgery Devices Panel" recommended reserving silicone gel-filled implants for breast reconstruction and for teams following a rigorous scientific protocol. (4) High quality scientific researches then demonstrated no increased risk of connective tissue diseases (10-12), of neurologic disorders (13) and of any cancer (14) in women with silicone implants. The suspension was lifted in 2006, with the approval of Mentor and Allergan silicone gel-filled implants. (15)

Since the first US medical device regulations in 1976, breast implants were "grandfathered" as a Class II medical device. (16) In 1988 the FDA under pressure upgraded the breast implants as a Class III higher risk medical device. Strict premarket clinical studies were then required to be approved by the FDA. (1) A consequence of the moratorium is a shift of the Northern American implant market. From 1963 to 1992, approximately 95% of implants were silicone gel-filled. Then, since the moratorium, 95% have been saline filled. (2)

The European regulatory agencies began to restrict access to silicone gel-filled breast implants in June 1993. The European Commission released a Medical Device Directive, which obligated new devices to be certificated by an independent organism. (15) A temporary ban on silicone gel-filled breast implants was even ordered France between 1995 and 2001.

At the same time, the US sales of PU-coated implants were suspended in April 1991 because a hydrolysis of the PU foam (which was shown to release *in vitro* a toxic breakdown product: 2,4-toluenediamine or 2,4-TDA) was thought to occur during the *in vivo* macroscopic degradation of the PU foam. (17) Before 1990, PU-coated implants represented 40% of the implant market. (18) The hypothesis of toxicity was ruled out later by subsequent reports: the very small amounts of 2,4-TDA that would be released from PU-coated implants would not provide a significant health risk. (19)

In the years following the lifting of the moratorium, a **5th generation** appeared. Thanks to more cohesive gels, the concept of "form-stable" implant was achieved. Thus,

anatomically-shaped implants (tear drop) were designed. (1, 4, 5) The same surface processing designed for round implants (such as Siltex and Biocell) continued to be used for most shaped implants. (Fig. 2) On the basis of the provided clinical data, the FDA approved fifth-generation implants from all the US suppliers in the following order: Sientra (the US supplier of Silimed implants) (2012), Allergan (acquired by Actavis in 2014) (2013), and Mentor (acquired by Johnson & Johnson in 2009) (2013).

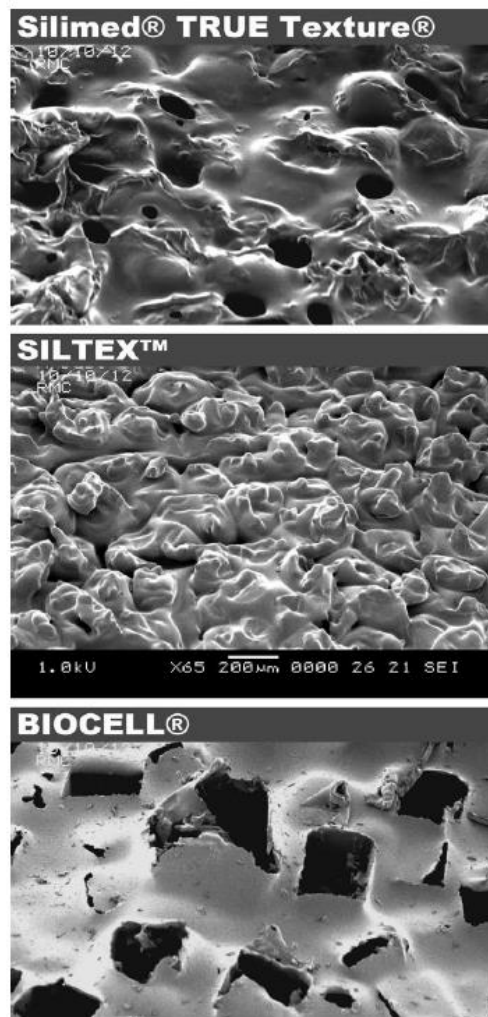


Figure 2 : SEM images of Silimed TRUE Texture, Mentor Siltex and Allergan Biocell textured surfaces. (magnification: x65)(20)

More recently, a new type of texturing process (called “microtexture” or even “nanotexture”), which uses no foreign material, is appeared. The “microtexture” of PERTHESE implant (Perouse Plastique) was the first of this type reported in the literature. (21)

The first breast reconstruction after cancer was published in 1979 and 1982 and relied on the insertion of temporary expander after the resection of tumorous tissue (mastectomy). (22, 23) Specific expanders (textured or smooth) for breast reconstruction were then designed. Once implanted, the expander is progressively filled with saline solution through a valve over a period of approximately 6 months. (24) Once the breast tissues are sufficiently distended, the expander is replaced by a definitive implant. (25) A partial resection of the capsule (capsulectomy) is also performed. Nowadays, other options exist for breast reconstruction, such as flap or lipofilling procedures. These autologous techniques consist in harvesting a section of tissue (either muscular tissue for a flap or adipose tissue for a lipofilling) from one area of the body — most often the abdomen — and relocating it to create a new breast mound).

In the last past decades, several medical controversies shadowed breast implants. The most known crisis is the suspension of exportation, distribution and sale of the Poly Implant Prothèse (PIP) silicone gel-filled breast implants in March 2010, consequently to a fraud of the manufacturer on the silicone supply. More than 300 000 women in 65 countries have received PIP silicone gel-filled implants made with nonmedical-grade silicone. (26) In September 2015, the Conformité Européenne (CE) certificate of the Silimed implants was suspended due to the discovery of particulate on device surface. In October, Sientra voluntarily suspended the sales of Silimed implants in the USA as a precaution. (15) However, the most publicized implant-related health topic, who concerned several worldwide health authority agencies, is an emerging risk of a rare type of cancer affecting immune systems (Breast Implant-Associated Anaplastic Large Cell Lymphoma or BIA-ALCL), which would be linked to breast implant. In December 2018, Allergan lost the CE mark on Microcell- and Biocell-textured implants for reasons explained below in § 1.2.7. (27)

1.2. BIA-ALCL

1.2.1. FDA ALERT

Since the safety warning issued by the FDA in 2011 on a possible association between breast implant and BIA-ALCL (<https://www.fda.gov/news-events/press-announcements/statement-binita-ashar-md-fdas-center-devices-and-radiological-health-agencys-continuing-efforts>), an increasing attention, which is now beyond the communities of breast surgeons and haematologists, was paid on this pathology.

At that time, 34 BIA-ALCL case reports were known worldwide. (28) Without any more additional epidemiologic data, they estimated the incidence of primary ALCL of the breast to be approximately three in 100 million women per year in the United States, based on data from the Surveillance, Epidemiology, and End Results (SEER) Program of the National Cancer Institute. (29)

According to this report, women with breast implants would have a very low but higher risk of developing an BIA-ALCL compared to women without breast implants, although cases of lymphoma similar to ALCL have been reported without association with breast implants. (30-33) The first case was identified in the USA in 1997 by Keech. (34) However, the number of newly diagnosed patients exploded in 2014-2015. (35) In 2017, a specific entity was created in the revised World Health Organization (WHO) classification of lymphoma under the terminology "BIA-ALCL". (36)

1.2.2. CLINICAL FEATURES

ALCLs are a proliferative disorder affecting lymphoid (or immune) cells. Different clinicopathological forms of ALCL exist: systemic ALCL, cutaneous ALCL and BIA-ALCL. While systemic ALCL is an aggressive metastatic disease, malignant lymphoid cells of BIA-ALCL are usually confined to a peri-implant seroma or capsular tissue. (37, 38) BIA-ALCL is a rare and purely T-cell lymphoma. (39, 40) A characteristic genetic subtyping of BIA-ALCL appeared: all currently reported cases were found to be anaplastic lymphoma kinase negative (ALK-) with cluster of differentiation 30 positive (CD30+). (41) Cutaneous ALCL also shows ALK- and CD30+. (42)

Clinically, approximately two thirds of BIA-ALCL cases were diagnosed consequently to breast swelling due to an effusion around the implant. This seroma fluid contained malignant cells, especially the characteristic large pleomorphic cells with horseshoe-shaped nuclei. (43) About one third of BIA-ALCL cases were characterized by a tumor mass attached to the capsule, usually perceptible by the patient. An effusion may also be observed. Metastatic disease was observed on a very small number of patients. (41, 44)

The time interval from implantation to diagnosis ranges from 2 years to 32 years with a median interval of 8-9 years. BIA-ALCL was diagnosed on both augmentation and reconstruction patients. (44) Potential ethnic and genetic predispositions may play an important role (45), with only one worldwide Asian or Asian descent case from Thailand (46). Thus, genetic aberrancies were observed in BIA-ALCL cases. Somatic mutations in JAK-STAT signalling, which are implicated in cell proliferation, differentiation and apoptosis, were the most commonly reported aberrancies. (47-50)

In term of first-line diagnosis tool, ultrasound techniques were found as specific and sensitive as more invasive techniques. (51) On suspected cases, tissue specimens should be harvested via fine-needle aspiration or biopsy for pathological examination. (41) The first National Comprehensive Cancer Network consensus guidelines for the management of BIA-ALCL developed in 2016 recommended that specimens undergo histology, flow cytometry and immunohistochemistry. The CD30 markers should be then systematically scored. (52)

BIA-ALCL as well as cutaneous ALCL are associated with a relatively slow rate of progression and a generally favourable prognosis. (42) Complete remission was reported in 93% of BIA-ALCL cases with effusion in the absence of a mass and in 72% of cases if a mass was also present. The therapy is most of the time based on a complete resection of the capsule with removal of implants. (38) Anecdotal case reports of spontaneous regression on effusion-limited BIA-ALCL patients have now been published. (53, 54)

1.2.3. ASSOCIATION BETWEEN BREAST IMPLANT AND BIA-ALCL AND ESTIMATION OF A RISK

Methodologically, to assess the efficiency of a treatment against a given pathology, a case control study must be performed. A matched control group must therefore be enrolled. This type of study is also designed to demonstrate a putative association between breast implants and BIA-ALCL. The association is quantified by the odds ratio (OR), which will indicate in one situation how many times the probability is higher that a patient diagnosed with BIA-ALCL has breast implants than no breast implant. The study design and the details of the computation are detailed in the following paragraphs.

On the basis of 5 cases identified in the Netherlands in 2008, De Jong *et al.* was the first through a case control study to demonstrate that patients with BIA-ALCL were significantly more likely to have breast implants. (55) The authors also computed an incidence estimated at 0.1 to 0.3 per 100 000 women with breast implant per year. However, they acknowledged “*uncertain data of sales figure*”. Curiously, the cases reported occurred on saline-filled implants, which were infrequently used in Europe.

In 2012, Largent *et al.* reviewed prospectively 6 clinical studies sponsored by Allergan to encompass 89 382 patients. (56) Three BIA-ALCL were diagnosed. Thus, the authors reported a crude incidence of 1.46 per 100 000 person-years from a clinical study with a median follow-up of 2.7 years

In 2015, by an extensive review of 173 cases retrieved from the literature, Brody *et al.* estimated an extremely large risk range from 1 in 500 00 to 1 in 3 000 000 women with implants from 1993 to June 1, 2014. (35)

In August 2016, Wang *et al.* reported 10 cases of BIA-ALCL on a database of 123 392 women (whose 2 990 women had breast implants). (57) Of these 10 cases, 2 patients had breast implants. The authors demonstrated a statistically significant association between breast implant and BIA-ALCL (the risk for BIA-ALCL was increased 10.9 times in patients who had a history of breast implant).

In September 2016, the French National Cancer Institute (INCa) reported 29 cases of BIA-ALCL. On the basis of a large number of assumptions, the experts computed a cumulative incidence of BIA-ALCL of approximately 1 to 2 per 100 000 person-years, which is consistent with the review led by Largent.

In November 2016, Doren *et al.* retrospectively analyzed 100 BIA-ALCL cases in the USA. (58) Based on the annualized sales data provided by the manufacturers, they estimated an incidence of 2.03 per 1 million person-years, similar to the Dutch study. Moreover, this incidence was 67.6 times higher than that of primary ALCL of the breast in the general population, according to the SEER data ($p < 0.001$). The authors assessed the lifetime prevalence (which is the ALCL risk that a woman with breast implants has throughout her entire life span) at 1 per 30 000 women with a breast implant, which is approximately 10 times higher than the rate provided by Clemens *et al.* (46) Importantly, the authors assumed that BIA-ALCL occurs only on patients with textured implants.

The European Commission-mandated Scientific Committee on Health Environmental and Emerging Risks (SCHEER) released a report in April 2017, which mitigated the possible connection between breast implants and BIA-ALCL on the basis of a review of the published scientific literature and a public call for data open to all stakeholders between 1969 and August 2016 (*"the gathered scientific information is insufficient to perform a methodologically robust risk assessment on the positive association of breast implants with the development of ALCL"*). (https://ec.europa.eu/health/sites/health/files/scientific_committees/scheer/docs/scheer_o_007.pdf) However, among the 188 articles retained by the literature review, 9 articles concluded a statistically significant positive association between breast implant exposure and risk of BIA-ALCL (51, 55, 56, 59-64), whereas only 2 articles demonstrated a statistically significant negative association according to the experts. Of these two articles, the first one drew conclusion from no identified BIA-ALCL cases on a cohort of 440 patients (65) and the conclusions of the second one were statistically inconclusive (66).

In May 2017, Clemens *et al.* published outcomes on the US FDA-mandated Continued Access Reconstruction/Revision Expansion (CARE) clinical trials, which are the largest prospective series of patients with textured implants (17 656 women). The authors estimated a lifetime prevalence of 1 in 2943. (46)

In January 2018, a case control study was led on all the breast ALCL and the other primary breast lymphoma declared in the nationwide Dutch pathology registry between 1990 and 2016. (67) The methodologically robust design of a case control

study is based on 4 groups: a group of treated and diseased patients, a group of treated and disease-free patients, a group of untreated and diseased patients and a group of untreated and disease-free patients. In the study, the treatment was the presence of breast implant. The diseased patients were all patients with breast ALCL (n=43) and the disease-free patients (or controls) gathered the women with other primary breast lymphoma (n=146). The number of patients with breast implants were then counted (n=32 among the diseased patients and n=1 among the disease-free patients). The association between breast implant and ALCL is given by the odds ratio (OR):

$$OR = \frac{\frac{32}{43-32}}{\frac{1}{146-1}} = 421.8 \quad [1]$$

On the basis of this very high OR, the authors updated the outcome given in 2008 (OR was then equal to 18.2) (55) and concluded that "*breast implants are associated with increased risk of breast-ALCL, but the absolute risk remains small*". Moreover, for the first time the authors took into account the patient age for the prevalence computation. Thus, among women with an implant, the prevalence was estimated of 1 per 35 000 at age 50 years, 1 per 12 000 at 70 years, and 1 per 7 000 at 75 years. The lifetime prevalence provided by Doren *et al.* was similar as the prevalence at age 50 years, which might be explained by the mean age of Doren study (53.2 years). In comparison, the lifetime prevalence estimated by Clemens *et al.* was much higher, which is likely due to the unique type of texture represented in the study (i.e. Biocell). As a result, the determination of an accurate risk has been elusive and a large discrepancy of BIA-ALCL incidence rate has been reported in the literature, which may reflect a combined effect of the increased awareness of this disease among the different stakeholders and geographical predisposition. (68) The following paragraph sheds light on the difficulties to have accurate epidemiologic figures.

1.2.4. EPIDEMIOLOGIC BARRIERS

To compute a risk, the number of BIA-ALCL (numerator) and the total number of patients with breast implants (denominator) must be known.

As of November 2018, 656 BIA-ALCL cases and 17 related deaths were reported throughout the world. (69) To have a nation-wide vision, the number of cases and related deaths is given per country in the Table 1. The American Society of Plastic Surgeons (ASPS) estimated 735 worldwide BIA-ALCL cases as of August 5, 2019. (<https://www.plasticsurgery.org/for-medical-professionals/health-policy/bia-alcl-physician-resources>)

Country	Cases	Deaths
Argentina	6	
Australia	81	3
Belgium	10	
Brazil	3	1
Canada	25	
Chile	2	
China	0	
Colombia	6	
Czech Republic	1	
Denmark	7	
Egypt	1	
Finland	7	
France	55	3
Germany	7	
Ireland	1	
Israel	8	
Italy	28	
Japan	0	

Mexico	4	
Netherlands	40	1
New Zealand	13	1
Norway	3	
Romania	0	
Russia	2	
Singapore	0	
South Africa	1	
South Korea	1	
Spain	29	
Sweden	6	2
Switzerland	4	
Taiwan	Not reported	Not reported
Thailand	1	
Venezuela	2	
United Kingdom	45	1
United States	257	5
Total	656	17

Table 1 : Worldwide and nation-wide numbers of BIA-ALCL cases and related deaths as of November 2018.

According to Collett *et al.*, the numerator is likely to underestimate due to an underreporting of cases in the medical device vigilance database. Basically, any serious incident occurred on a breast implant or on any medical device must be declared to the national Competent Authority, either by the clinicians or the manufacturers. Poor awareness of the disease by the surgeon as well as by the pathologist, fear of litigation or additional cost may be the root cause of these

unreported cases. An overestimation may also skew the figures: Rastogi *et al.* cautioned against duplicate case reports. (70) The FDA acknowledged that the reporting may contain incomplete, inaccurate, untimely, unverified or biased data. (<https://www.youtube.com/watch?v=wpdkXMEj60U>)

Regarding the denominator, more than 35 million of women would have textured breast implants in the world, with 1 469 606 and 70 683 breast augmentations performed in 2017 with silicone gel-filled implants and with saline implants respectively. (https://www.isaps.org/wp-content/uploads/2018/10/ISAPS_2017_International_Study_Cosmetic_Procedures.pdf)

f) Based on the sales figures provided by Allergan and Mentor, Doren estimated that approximately 3 millions of women (less than 2% of the total female population) would have textured breast implants in the US population in 2016. In 2017, 281 316 and 41 616 breast augmentations were performed in the USA with silicone gel-filled implants and with saline implants respectively. In the Netherlands, 3.3% of women had textured gel-filled breast implants in 2015. (67)

These figures reflect a globally and sharply increasing breast implant market. The exponential rise in breast implant surgery in Asia and in South Korea more particularly is the best example of this upward trend. (69) However, consistently with the numerator, the estimations of the denominator are inaccurate. Collett *et al.* detailed the list of factors, which potentially skew the denominator, such as poor records, lack of systematic follow-up and reporting of adverse events, unregulated boom in cosmetic tourism and entry of many disparate practitioners.

To overcome all these biases, it is of primer importance to constitute reliable national and international epidemiologic datasets.

1.2.5. EPIDEMIOLOGIC METHODOLOGIES TO RATIONALIZE THE RISK ANALYSIS

Two approaches exist to accurately quantify the denominator. The first one is based on sales data released by manufacturers. De Jong *et al.* (55) and Doren *et al.* (58) applied this methodology to compute the provided incidences. However, numerous manufacturer-dependent limitations exist. Sales data may not be accessible because of commercial arguments, logistic changes or bankruptcies. Moreover, it is

not reasonable to assume that the number of implants sold equates to the number of implants inserted. (69) The second approach relies on radiologic sampling of a random population. (67) Thus, radiology allows the epidemiologist to confirm the presence of breast implants. However, this technique is quite time consuming and requires an extrapolation to upscale the small sample to nation-wide statistics. (69)

Registry is the "gold standard" to accurately estimate the numerator. (69) Basically, adequate registry will be a platform, in which physicians record at least each pathologically confirmed BIA-ALCL case. By extending the input to any breast implantation, registry could be implemented to also provide the denominator. Moreover, by systematically collecting a comprehensive set of critical elements, such as demographic and clinical characteristics of patients, pathologic features, modalities of diagnosis and therapeutic regimens, registry will be a powerful tool to have more insights on the implant-specific risks, on the etiology of BIA-ALCL and on the prognosis. Until now, the implant-specific approaches are plagued by inaccurate implant exposure histories. (70)

National and international registries are now beginning to generate early high-volume datasets, which are presented in the below paragraphs.

1.2.6. FIRST BIA-ALCL RELATED EPIDEMIOLOGIC STRUCTURES

Different specific registries were developed by the regulatory agencies in the world.

The French register for breast implants was finally approved by the French Commission Nationale de l'Informatique et des Libertés (CNIL). Its effective establishment is imminent, as soon as the question of funding is resolved. (<https://www.youtube.com/watch?v=wpdkXMEj60U>) Moreover, France has established since 2010 a national network of 33 expert hematopathology reference centers, called LYMPHOPATH network. This government-supported structure is composed of multidisciplinary teams which perform a second diagnostic evaluation of all suspected cases in France (and also in Belgium) and provides a help to the clinician in order to develop an individualized treatment plan for the patient.

On an international scale, after the PIP crisis in 2010, an International Collaboration of Breast Registry Activities (ICOBRA) between Australia, Austria, Canada, France, Germany, Ireland, Italy, the Netherlands, New Zealand, South Africa, UK and the USA was developed to harmonize the breast implant registries worldwide and to allow a more efficient potential future recall of breast implant. (71)

Likewise, in the Netherlands, the Dutch Breast Implant-Associated ALCL Consortium, consisting of a multidisciplinary group of scientists, investigates BIA-ALCL occurrence in women with breast implants. (<https://static1.squarespace.com/static/56fab39ad51cd464876cceed/t/5a3c3fc39140b7cd5730b291/1513897924057/alcl-facts-figures-and-practical-guidelines.pdf>)

A breast implant registry was also implemented in Australia (Australian Breast Device Registry) in 2012. (<https://www.abdr.org.au/abdr-releases-2017-report-today/>) Deva *et al.* (2019) insisted on the high penetrance of this registry. (15)

In the USA, the PROFILE (Patient Registry and Outcomes for Breast Implants and ALCL Etiology and Epidemiology), which is a joint collaboration between the ASPS, the Plastic Surgery Foundation and the FDA, was launched in August 2012. Thus, PROFILE was designed to record and centralize all past and future pathologically confirmed BIA-ALCL cases in the USA. PROFILE is an upgrade of the existing US medical device adverse reporting program MedWatch and the corresponding publicly available Manufacturer and User Facility Device Experience (MAUDE) database. However, this surveillance system was impaired by potential incomplete, inaccurate and/or unverified data. (46) Moreover, it was not designed to capture a body of data pertaining to BIA-ALCL pathogenesis and oncologic outcomes. (28)

A European Task Force was established in 2015 by an Expert Group of the European Union Commission to examine the possible correlation between BIA-ALCL and breast implants. A European database has been therefore formed that uniformly collects all reported BIA-ALCL cases by member countries. The database is managed and updated by each national Competent Authority.

The Table 2 summarizes the most updated data provided by the newly established registries and regulatory agencies in the French- or English-speaking countries in the

world. The data were retrieved from the respective regulatory agency websites. Regarding the PROFILE registry, McCarthy *et al.* study was included because they provided more complete outcomes than the respective website. (28)

Country / countries	Name of the regulatory agency/registry	Date	Number of reports/unique cases	Number of related death	Number of pathologically confirmed cases	Number of textured implant involved	Number of smooth implants involved	Number of PU-coated implants involved	Risk
USA	FDA	Sept 30, 2018	660 reports/457 unique cases	9		310	24		The FDA reported a risk between one in 3 817 and one in 30 000 women with textured implants based on the study

									led by Loch-Wilkinson (2017) and Clemens (2017).
	PROFILE	March 2018 (McCarthy 2019)	186 distinct cases	3 (one died of disseminated BIA-ALCL, one died of metastatic breast carcinoma and one died of natural causes)		70	4 (all patients had a history of prior textured permanent implant)	2	

		Feb 8, 2019	265 suspected/confirmed cases						
Belgium	Federal Agency for Medicines and Health Products (FAMHP)			0	16				
Canada	Health Canada	Jan 1, 2019			22	20	0		
UK	Medicines and health care products regulatory authority (MHRA)	Sept, 2018	57 reports and 45 of which meet the WHO diagnostic criteria for BIA-ALCL	3 (only one of these is confirmed to meet the diagnostic criteria for BIA-ALCL)					1 per 24 000 implants sold

France	ANSM	between 2011 and November 2018	53	5 (two consequently to a breast cancer, one due to a heart attack and two related to BIA-ALCL)	50*	39 (among implants on diagnosis) and 57 (among all prior implants)	0	0 (among implants on diagnosis) and 1 (among all prior implants)	
Australia	Therapeutic Goods Administration (TGA)	11 January 2019	76 cases reported						estimated one in 1 000 to 10 000 chance of having this diagnosis

Ireland	Health Products Regulation Association (HPRA)		The HPRA has not received any reports of BIA-ALCL through its medical device vigilance reporting system.						
EU	Task Force	November 2018	214			166	0		

Table 2 : Clinical data related to BIA-ALCL published by the newly established registries and regulatory agencies in the French- or English-speaking countries in the world

*After exclusion of some patients, 46 cases were finally confirmed by the LYMPHOPATH network in February 2019. 136 implants were identified.

The main limitation is that many registries depend on voluntary reports from participating physicians. However, some tendencies may be drawn from these early data. Thus, Scandinavian countries, with excellent implant registries, had almost no reported cases until recent. (72, 73) Likewise, a greater proportion of cases within the USA was reported at a more advanced stage of disease. (38)

Due to the delay to onset (approximately 10 years) and the late recognition as a specific entity, the reported BIA-ALCL cases still belong to the “take-off” phase and the exponential increase is not planned to stop. (69) It is reasonable to wait for the “plateau phase” in order to draw representative statistics. However, some health regulatory agencies recently released recommendations.

1.2.7. FIRST RECOMMENDATIONS FROM NATIONAL REGULATORY AGENCIES

The first major recommendation was issued by the French regulatory agency (ANSM), which held in February 2019 a public consultation on textured breast implants. Different stakeholders (other regulatory agencies, breast implant manufacturers, patients, surgeons and plastic surgeon societies) were interviewed by an expert committee. At the end of the consultation, the experts had to stand up on the following points:

- Are there situations for which the use of textured implants is compulsory in cosmetic surgery? What are they?
- Are there situations for which the use of textured implants is compulsory in reconstruction surgery? What are they?

The conclusions of the committee were published by press release:

- The committee recommended smooth implants
- The macrotecture Biocell from Allergan was banned
- Other “macrot textured” implants (ie from other brands) as well as PU-coated implants had to be very carefully used
- But no need to proceed to preventive explantation of macrot textured implants at that stage

- Textured implants may be advantageous in specific cases, in aesthetics as well as in reconstruction
- The committee emphasized the need to a uniformed classification of textures at European level

The use of smooth implants had been already recommended by the French plastic surgery societies in November 2018. These recommendations were also shared by some European countries (such as Belgium, Denmark and Iceland), although the position of the European Task Force continued to state "*there is currently not enough scientific evidence of a causal relationship specifically between textured implants and BIA-ALCL*". The European opinion was shared by the Italian Ministry of Health, which argued that "*there is not statistical evidence to prove that smooth implants are not involved*".

As of April, 4th 2019 the "macrot textured" implants (i.e. Biocell-textured implants, Sebbin shaped textured implants, Arion shaped textured implants, Nagotex-textured implants and POLYtxt-textured implants) were banned in France based in part on our results presented in chapter III). (<https://www.youtube.com/watch?v=wpdkXMEj60U>) The "macrot textured" implants were then banned in Egypt and Tunisia.

Both saline and silicone-filled implants have been reported in association with BIA-ALCL without a statistical difference in frequency. (44) Therefore, it seems more likely that the silicone shell surface rather than the implant contents is involved in pathogenesis. (43) Moreover, the first case of BIA-ALCL was reported 10 years after the development of textured silicone surface implants, which approximately coincides with the median interval from implantation to diagnosis. (64) Therefore, breast implant surface, especially textured breast implant surface, is of primer importance in the pathogenesis of BIA-ALCL.

1.3. BREAST IMPLANT SURFACE PROCESS, MEASUREMENT AND DESCRIPTION

1.3.1. BREAST IMPLANT MANUFACTURING AND TEXTURE

A silicone gel-filled breast implant is composed of a thin silicone shell, inside which a silicone gel was inserted. Today, only one supplier (Nusil technology) provides all the implant manufacturers with a medical grade liquid silicone, mainly composed of straight chains of PolyDiMethylSiloxane (PDMS). (74) A silicone gel is a network of PDMS reticulated chains swollen with silicone fluid. The degree of reticulation (or cross-linking) and the average chain length (number of repeating monomers) determine the viscosity of the silicone gel and therefore the cohesiveness of the implant. (75) The implant shell is made of much more reticulated silicone elastomer. (76) The reticulation is controlled by the adding of cross-linkers and by heating, especially for the High Temperature Vulcanization (HTV) PDMS.

Basically, two parts (the "cross-linker" and the "base") are provided. The "base" contains 99% of methyl vinylpolysiloxane and the catalyst (platinum complex) in infinitesimal quantities. The "cross-linker" also contains a high percentage of methyl vinylpolysiloxane and the cross-linker (methylhydrogen polysiloxane) Silica is added to increase the viscosity and the tensile strength. The manufacturers mix them according to specific proportions. An organic solvent (xylene or ethyl benzene) is added so that the solution is enough viscous to be moulded. (74)

All the process takes place in clean room (class 1000 for the dipping room and class 10 000 for the other rooms). (77)

Many companies do not have semi-automated processes and still manually dip reusable implant-shaped mandrels into liquid silicone for several seconds to produce a layer. Implant mandrels are made of lightweight polymer (such as Ertacetal®) or stainless steel, and are designed according to the final dimension of the implant. They also have a stem to be handled. The silicone-coated mandrel is then placed under laminar flow in order to completely evaporate the solvent. The mandrel is turned up down several times to equalize the thickness of the layer. This process is then repeated to form different layers superimposed. The number of layers depends on the

manufacturer and on the type of texture. Depending on the manufacturer, breast implant shells have a thickness between 0.075 and 0.75 mm. (7)

For silicone gel-filled implants, one or several layers of another type of silicone, which have phenyl or trifluoropropyl-group in place of the methyl group, is sandwiched between PDMS layers. (76) These layers (called "low bleed barrier") will prevent bleeding of the short chains contained in the silicone gel through the shell. The shell is therefore a trilaminar structure. The position of the barrier within the shell is manufacturer-dependent.

Once all the layers were moulded, the mandrels are placed into an oven to cure the silicone. Interim curing may occur during the process. The shells are then peeled off from the mandrel. The shell surface and thickness are thoroughly controlled in order to have no defect. Destructive standardized mechanical tests are also performed. (78)

The opening created by the location of the stem is sealed by a silicone patch. Information for the implant traceability (such as manufacturer name, implant reference, serial number, volume ...) are present on the patch.

The liquid silicone gel is injected through the silicone patch with a syringe. The volume injected is computed according to the volume of the implant. A final curing allows to slightly reticulate the gel and to give the desired firmness of the implant.

The implant is finally placed into a blister and will be sterilized. (77)

The process described above is corresponding to a smooth implant. However, different surface processing (or texture) were designed to create different states of surface.

The most reported texturing processes are:

- "salt-loss technique." An additional step is introduced into the process: before curing, the silicone-coated mandrel is pushed into calibrated granular salt crystals (or other crystals). (Fig. 3) Once the surface has cured, this salt is then

dissolved in a water bath. (79) For some publications, a last silicone layer is moulded to cover the salt crystals pitted in the silicone and after the curing, the shell must be brushed in the bath to open the cavities. (80, 81)



Figure 3 : « Salt-loss technique » (77)

- A PU foam was firstly bonded on the silicone surface (the method of fixation was not specified). The PU coating has been then vulcanized on the cured silicone shell since 1989. A second PU sheeting is used to cover the base of the implant. (18)
- A pressure imprint-stamping technique: the uncured silicone coated-implant is pushed into PU foam and then removed. The silicone surface will replicate the foam structure. (7)
- Sientra uses a proprietary texturing technology. According to some authors, the process is based on "gas expansion" (82), whereas others report a "volitization of ammonium carbonate" (83).
- Other processes use rough mandrel. Thus, the moulded silicone layers replicate the state of surface present on the mandrel. Once peeled off, the shell must be turned inside out so that the textured surface is on the outer surface of the implant. (80)

On the basis of the literature, the Table 3 reports for the different major manufacturers the process of texturing used. All the types of texture do not have a commercial trademark. Thus, for the textures manufactured by Sebbin and Arion, the shape of the

implant (round or anatomical) must be specified to distinguish the different textures. Interestingly, sometimes the commercial name of the texture given by some manufacturers reflects the tactile sensing that the surgeon is susceptible to have by touching the implant, such as Silk Surface™ or Velvet Surface™.

Manufacturer	Commercial name of the implant surface*	Surface texturing process	CE marked/FDA approved
Cox Uphoff International (CUI)/Allergan, Irvine, CA, USA	Microcell	Salt loss (79)	YES/NO
Allergan	Biocell	Salt loss (84)	YES/YES
Mentor, Irvine, CA, USA	Siltex	"Negative contact imprinting with polyurethane foam" (83)	YES/YES
Silimed, Rio de Janeiro, Brazil	TRUE Texture	"Volitization of ammonium carbonate with heat" (83)	NO/YES
Silimed	Pure Polyurethane	« Polyurethane bonded foam » (85)	NO/NO
Sebbin, Boissy l'Aillierie, France	NanoSkin or Sebbin round microtextured implant	"Moulding silicone layers on a sandblasted mandrel" (80)	YES/NO
Sebbin	Round textured implant	Salt loss (80)	YES/NO
Sebbin	Shaped textured implant	Salt loss (80)	YES/NO
Cereplas	Cereform	"chuck moulded manufactured implant" (86)	Production stopped

PIP	VELVET	Salt loss (86)	Production stopped
Perouse-Plastie	Perthese	"Produced directly by the mandril" (87)	Production stopped
Eurosilicone, GC Aesthetics, Dublin, Ireland	CRISTALLINE Microtextured	Salt loss (86)	YES/NO
Eurosilicone	CRISTALLINE Textured	Salt loss (85)	YES/NO
Nagor, GC Aesthetics, Dublin, Ireland	Nagotex	Salt loss (84)	YES/NO
Polytech, Dieberg, Germany	MESMO	Unknown	YES/NO
Polytech	POLYtxt	« Vulcanisation (ammonium carbonate) » (85)	YES/NO
Arion, Mougins, France	Round and shaped micro-textured implant	Unknown	YES/NO
Arion	Round and shaped textured implant	[Sugar pitting] (88)	YES/NO
Establishment Labs SA, Coyol de Alajuela, Costa Rica	Silk Surface	"chuck moulded manufactured implant" (86)	YES/NO
Establishment Labs SA	Velvet Surface	"chuck moulded manufactured implant" (86)	YES/NO

Table 3 : Textures of the major breast implant manufacturers and associated texturing processes

*Where no commercial name exists, the shape of implant and the type of surface are given.

The silicone gel can be replaced by other types of filling (such as saline solution or hydrogel). However, the shell structure must be modified. For example, for inflatable saline-filled implants, the manufacturers use another type of silicone: the Room Temperature Vulcanized (RTV) silicone, in order not to form ripples on the shell surface. (77) Soya oil-filled implants were attempted with Trilucent breast implants from LipoMatrix in 1995. However, they were removed from the market in 2000 due to suspicion of carcinogenicity. PIP developed implants filled with hydrogel in the 1990s and were voluntary withdrawn from the market in December 2000. (15)

Manufacturing process of breast implant, especially the mechanical strength of the shell, is validated by international standards. The next paragraph reviews international and national standards relative to breast implant surface.

1.3.2. THE STANDARDS RELATED TO BREAST IMPLANT SURFACE MEASUREMENT

The only requirement relative to breast implant surface specified in the American Society for Testing and Materials (ASTM) standards is that surface texture “*may not alter the other characteristics of the device*” (ASTM F2051 – 00(20067), ASTM F703 – 07). Although informative, the Appendix H of the ISO (International Organization for Standardization) 14607:2018 standard is slightly more detailed on the methodology to measure the breast implant surface. Basically, the sampling and the instruments are specified. For the surface measurements, 3 representative shells must be used. On each shell, 15 measures of 4mm² must be performed. The instrument must be chosen among:

- the SEM with a 2D and 3D surface reconstruction software.
- White-Light Interferometry
- Laser Confocal Microscopy
- High Range Atomic Force Microscopy (AFM)

The following parameters should be reported:

- Pore size or pore diameter (μm),
- Number and height (μm) of peaks and resulting kurtosis,
- Number and depth (μm) of valleys and resulting skewness,
- Average distance between morphological features (μm), i.e. morphological density,
- Mean peak height (μm),
- Arithmetic roughness (Ra or Sa) and Root mean square roughness (Rms),
- Maximum peak height (Rz or Sz).

Only the kurtosis (Sku), the skewness (Ssk), the arithmetic roughness (Sa), the Root mean square roughness (Rms) and the maximum peak height (Sz) are metrologically standardized. (ISO 13565)

The ISO 14607:2018 standard replaces the ISO 14607:2009 standard, in which only measurements by SEM were allowed. The standard also specified that 9 measurements of 4mm^2 had to be performed and that the average characteristics of the surface (i.e. dimensions of the pores, peaks or hollows) had to be recorded.

More and more studies measuring breast implant surface were led. The next paragraph analyses their compliancy with the ISO-required measurement methodology.

1.3.3. BREAST IMPLANT SURFACE MEASUREMENTS PUBLISHED IN THE LITERATURE

The SEM were extensively used in the literature to image the surface of breast implant. In 2001, Danino published the first SEM images of the two most sold textures in the world: the Biocell texture and the Siltex texture. (89) However, topographical analysis of breast implant surface really began from 2014.

The first use of Laser Confocal Microscope was documented by Valencia-Lazcano *et al.* in 2014, who provided the first 3D images of breast implant surfaces. (90) It is only very recently that surfaces exhibiting more complex structures, such as a PU foam, were measured by Laser Confocal Microscope. (84) This instrument was then used by

Barr *et al.* (86) to measure a comprehensive range of breast implant surface and then by James *et al.* (91)

3D surface images of a textured and a smooth breast implant respectively obtained by 3D laser scanner and AFM were reported by Kyle *et al.* in 2015. (92) Barr *et al.* also specified that the smooth implant in their series was measured by AFM. (93)

The first use of Micro-tomography was published by Atlan *et al.* in 2015. (79) However, only cross-sections of the surface were provided. In 2018, Atlan *et al.* performed the same analysis on a larger range of breast implant, without more details. (94) In the same year, Jones *et al.* described a methodology to extract 3D surface images and roughness parameters from a micro-tomographic measurement, which consisted of “wrapping the sample to avoid overhangs and cavities”. (85) Jones *et al.* also concluded that the Micro-tomography provides “a more accurate morphologic assessment of the entire implant shell”.

The first study in compliance with the ISO 14607:2018 was documented by a report mandated by the French health authority (ANSM) and published online in July 2018. Basically, the authors performed measurements of a large range of breast implants with a SEM equipped with a four quadrants backscattered electron (BSE) detector, which allowed them to provide 4 images of the same surface under 4 different angles. The software of topographical analysis Mountains was then used to obtain a 3D image of the surface from the 4 images. This 3D reconstruction relies on the principle of the stereoscopy, which consists in creating an illusion of relief by superimposing two captures of the same image shot under two slightly different angles. The authors also specified that for smooth or slightly rough surfaces, a higher magnification has been used to capture the state of surface. Thus, for these surfaces, the measurements were performed on an area lower than 4mm².

The Table 4 summarizes the values reported in the literature of the most mentioned metrological parameter specified in the ISO 14607:2018 standards (i.e. Sa). To facilitate the comparison between the different studies, the surface sampling is restricted to the

two most quoted textured surfaces (Biocell and Siltex) and the two most quoted smooth surfaces (Allergan smooth implant and Mentor smooth implant).

	Kyle et al. (92)	Valencia et al. (95)	Barr et al. (86)	Jones et al. (85)	James et al. (91)
Sampling	6 repetitions	5 repetitions	5 repetitions	NP	6 repetitions
Surface area	1x1cm ² (Siltex) 90x90µm ² (smooth)	644x642µm	NP	NP	4.8mm ² ± 0.2mm ²
Compliance with the ISO 14607:2018 or ISO 14607:2009 standard?	NO	NO	NO	NO	NO
Sa values	Biocell	NP	18.83µm	80.03µm	91.7µm
	Siltex	8240nm	8.88µm	43.07µm	51.4µm
	Allergan smooth implant	NP	0.07µm	NP	8.5µm
	Mentor smooth implant	22.2nm	0.06µm	1.07µm	2.1µm

Table 4 : Topographical measurements and characterizations published in the literature

NP : Not Provided

The Sa values obtained on Biocell-textured and Siltex-textured surfaces exhibit large discrepancies between the studies of Kyle *et al.* (92) and Valencia *et al.* (95) and the ones of Barr *et al.* (86) and Jones *et al.* (85), although Valencia *et al.* (95) and Barr *et al.* (86) used the same measuring instrument. This inconsistency is also observed on smooth surfaces measured by AFM. (86, 92) The micro-tomograph with a voxel size of

15 μ m measured a 4 times higher Sa on Allergan smooth implant than Mentor smooth implant. (85)

In conclusion, the measurement methodologies published in the literature are not compliant with the ISO standards. We will now study if, although elusive (especially in the ISO 14607:2009), the surface indicators suggested by the standards are used in the literature.

1.3.4. BREAST IMPLANT SURFACE DESCRIPTION

The terms used to morphologically describe the textures in the literature were numerous and not accurate (Table 5). Authors have attempted to describe breast implant surfaces using variable terms: some referred to “*peaks and valleys*”, some to “*nodules*”, and others to “*concavities*” or “*indentations*”. Similarly, authors reported that some surfaces are more “*aggressive*” than others.

	Siltex	Biocell	Micro cell	PU-coated implant*	TRUE Texture	Sebbin anatomical implant	CRISTALLINE Microtextured	CRISTAL LINE Textured	Nago tex	POLY txt	Smooth implant*
Nodule	(79, 86, 89, 90, 95-97)										
Concavities		(98)		(98)							
Indentation		(7, 86, 97, 99)				(86)	(86)				
Depression		(86, 89, 96)				(86)					
Undulation	(98)										
Open-pore		(79, 89, 94, 96, 98, 99)	(94)	(98)				(94)	(94)		
Fully enclosed pores										(94)	
Porosity				(98)							
Wells		(79, 90, 95, 97)				(79)					
Pits		(95, 97)									(90, 95)
Spiderweb				(97)							
Mesh network				(97)							

Peaks	(79, 90, 95, 97)	(95)									
Crevasses	(90, 95, 97)										
Polyhedra		(95)									
Aggressive		(89, 96)									
Islands	(86)										
Troughs	(86)										
Surface irregularity											(86)
Nano-scale roughness											(86)
Hollow pore					(86)						
Fenestration					(86)						
Open cell				(86)							
Ridges	(97)	(95, 97)									(7, 95)
Rocky											(90, 95)
Ripples											(97)

Fibrils				(97)							
Valleys	(79, 95)										
Open dome						(79)					
Lattice structure				(99)							
Projections		(99)									
Caves										(85)	
Interconnected skeletal framework				(79)							
Irregular sponge-like surface				(94)							
Overhangs/lip		(94)									

Table 5 : Morphological descriptions of the textures in the literature

* As we suppose non-significant differences between the different smooth implants and between the different PU-coated implants sold by the different manufacturers, the latter are not mentioned for these cases. (91)

The descriptive terms are not only multiple and inaccurate: they are also inconsistent. A same term may designate very different textures. Thus, “*concavities*” or “*open pore*” characterize both salt-loss obtained texture and PU coating. Likewise, “*pits*” were used to describe Biocell textured and smooth implants.

As early as first textured implants were commercialized, categories of texture were emerged from the portfolio of manufacturers, such “*macrotecture*”, “*microecture*” or even “*nanotecture*”. By associating an intended clinical outcome and/or presumed *innovating* process (at least presumed *different* from the others), these terms rapidly became the corner stone of the marketing concept developed by the manufacturers. Thus, according to a manufacturer-sponsored study, “*the Motiva Implants are a novel breast implant technology*” and their nanotecture was “*designed to reduce the abrasion when the implant is in contact with the tissue*”. (100) Another manufacturer-sponsored study (94) claimed a “*greater tissue adherence with the Biocell texture*” through the “*Velcro effect*” (89). Consequently to the commercial success of the Biocell-textured implants sold by Allergan, the surgeons associated a sensory perception to the term “*macrotecture*”. Thus, the “*feel to the touch*” of a macrotecture implant was similar as the one of a peach or a velvet fabric (hence, the “*peach skin effect*” or “*velvet effect*”). Likewise, an implant could be qualified as “*macrotecture*”, when the surface structures are visible to the naked eye. (101) Furthermore, when an implant was not sold as “*macrotecture*” or “*nanotecture*”, the implants were either “*textured*” or “*microecture*”. Most of the time, the choice between these two terms did not rely on marketing arguments or subjective assessments any more, but often depended on the number of textures sold by the manufacturers and on the current trends. As a result, this multiplicity of trade names and jargons and the paucity of unique nomenclature preclude any relevant inter-brand comparison. (102)

As highlighted by the ANSM-mandated committee, establishment of an uniformized classification is of the utmost importance. (<https://www.youtube.com/watch?v=wpdkXMEj60U>)

1.4. NOMENCLATURE AND CLASSIFICATION OF BREAST IMPLANT SURFACE

To attempt to rationalize the different denominations, five nomenclatures based on surface parameters emerged. The first four ones proposed a quantifiable surface parameter, on which the nomenclature was based, as well as the boundaries of each category. (78, 85, 86, 94). The fifth nomenclature described in the ANSM-mandated report demonstrated for the first time by a robust statistical analysis the retained surface parameters. (<https://ansm.sante.fr/S-informer/Points-d-information-Points-d-information/Surveillance-des-implants-mammaires-par-l-ANSM-publication-d-un-avis-d-experts-de-CSST-et-d-une-etude-sur-la-texturation-Point-d-information>) Of the first four nomenclatures, one was drawn from the ISO 14607:2018 standard. (78) The other three nomenclatures provided different biological evidence to support the nomenclature, which will be discussed in the section “biological models”.

Barr *et al.* and the ANSM-mandated experts performed measurements on one of the specified instruments in the ISO 14607:2018 standard (i.e. the Laser Confocal Microscopy and the SEM with a 3D reconstruction software). (86) The two others used Micro-tomography with a voxel size of 15µm and 2.2µm for all the breast implant surfaces (including the smooth implants). (85, 94)

Barr *et al.* published in 2017 the first nomenclature established on a metrologically standardized parameter (i.e. Sa). (86) They also added a second level based on the presence or absence of porosity assessed from SEM images. Likewise, the ISO 14607:2018 standard proposed on the basis of the Sa 3 categories to describe the breast implant surfaces: “smooth”, “microtexture” and “macrotexture”. Thus, a “macrotexture” has a Sa either superior to 75µm (86) or superior to 50µm. (78) Therefore, the Sa range defining a “microtexture” is comprised between 10 and 75µm or between 10 and 50µm, according to Barr *et al.* and to the ISO 14607:2018

respectively. The major discrepancy remains on the other categories: Barr *et al.* added a mesotexture category ($Sa < 15\mu\text{m}$) and a nanotexture category ($Sa < 5\mu\text{m}$), whereas smooth implant is the third category of the ISO standard ($Sa < 10\mu\text{m}$).

Atlan *et al.* reported a nomenclature according to a custom-made parameter (called "surface area") expressed as an absolute value. (94) This article mentioned for the first time that a nomenclature must be morphologically relevant first and foremost in regard to some specific surface structures, such as pore size, pore number, texture depth or complexity.

The first nomenclature, which did not use the terms of "macrotexture" or "microtexture" was established by Jones *et al.* (85) They preferred the terms of « *high* », « *intermediate* », « *low* » and « *minimal* » surface area. The surface area was here normalized in comparison to a smooth implant. They demonstrated a correlation between surface area and Sa and insisted that the nomenclature was uncorrelated with the texturing processes. According to Rastogi *et al.*, "*this proposed grading system objectively categorizes implant texture morphology and is arguably superior to existing descriptive terms*". (70)

The ANSM-mandated nomenclature was obtained by Principal Component Analysis (PCA). This statistical analysis was designed to reduce the initial number of parameters to only two variables called Principal Components (PC), which are a linear combination of the initial parameters. The PC are mathematically built in order to maximize the variance. By only retaining the first two terms of each PC, the authors were able to constitute 4 groups: the "smooth", the "microtexture", the "macrotexture" and the "polyurethane". A linear equation of the frontiers was then found. Moreover, on the basis of SEM images, they qualitatively identified different surface structures among the "macrotextures": the "cubic structure", the "rumpled surface", the "globular surface" and the "surfaces with indeterminate imprint".

The Table 6 precise the category of each breast implant surface according to the mentioned nomenclatures. The ISO 14607:2018 did not detail the ranking of the different breast implant surfaces into the proposed groups.

	Barr et al. (86)	Atlan et al. (94)	Jones et al. (85)	ANSM report
Smooth implants*	Nanotexture	Smooth/nanotexture	Minimal	Smooth
SilkSurface	Mesotexture	Smooth/nanotexture	Minimal	Microtexture
VelvetSurface	Microtexture non-porous	Smooth/nanotexture	Minimal	Microtexture
Arion Microtextured	NM	NM	NM	Microtexture
Sebbin Microtextured	NM	NM	NM	Microtexture
Cereform	Microtexture non-porous	NM	NM	NM
MESMO	NM	Microtexture	NM	Macrotecture
Microcell	NM	Microtexture	NM	Macrotecture
VELVET	Microtexture porous	NM	NM	
Siltex	Microtexture non-porous	Microtexture	Low	Macrotecture
Sebbin round textured implant	NM	NM	NM	Macrotecture
CRISTALLINE Microtextured	Microtexture porous	NM	NM	Macrotecture
CRISTALLINE Textured	NM	Macrotecture	Intermediate	Macrotecture
POLYtxt	Microtexture non-porous	Macrotecture+	Intermediate	Macrotecture
TRUE Texture	Microtexture porous	Macrotecture	NM	Macrotecture
Nagotex	NM	Macrotecture+	Low	Macrotecture

Sebbin shaped textured implant	Macrotexture porous	NM	NM	Macrotexture
Arion textured implant	NM	NM	NM	Macrotexture
Biocell	Macrotexture porous	Macrotexture	Intermediate	Macrotexture
PU-coated*	<i>Not classed</i>	Macrotexture+	High	PU

Table 6 :Classifications of the different breast implant surfaces according to the published nomenclatures

* As we suppose non-significant differences between the different smooth implants and between the different PU-coated implants sold by the different manufacturers, the latter are not mentioned for these cases. (91)

NM: Not Measured

Numerous inconsistencies between the 4 nomenclatures of the table are observed. For example, if we exclude Jones' article (which used a totally different nomenclature system), only the Biocell texture belongs to the same category (i.e. "macrotexture") in the 3 other articles.

Moreover, a prior knowledge is often necessary to identify some types of texture analyzed in the articles, especially for the manufacturers which commercialize several types of texture without commercial names. For example, the "SL2Sebbin" texture analyzed by Barr *et al.* was identified as the texture of Sebbin shaped implant by analogy between the SEM images provided by Barr *et al.* and in the FDA-mandated report.

Once topographically consistent categories of breast implant surface will have been established, we will be able to confront the nomenclatures to the safety data in order to demonstrate or refute our hypothesis stating that a relationship exists between some

morphological structures and some clinical complications. Thus, clinical evidence categorized by implant groups must be compiled.

1.5. CLINICAL EVALUATION OF BREAST IMPLANT SURFACE

1.5.1. OBJECTIVES AND GENERAL PRINCIPLES OF CLINICAL EVALUATION VIA LITERATURE REVIEW

To study the clinical impact of some types of texture, a selective literature review was led in order to retain only the articles which:

- clearly mention the name of the implant manufacturer and the commercial type of texture
- provide safety data on severe complications which are not due to the surgery or to implant characteristics other than the texture (i.e. gel, shell integrity ...). Thus, data on complications associated to the surgery, such as infection, hematoma, early seroma, abnormal scarring or ptosis, were not retained in the analysis. Likewise, complications, for which the texture has clearly no impact, such as implant rupture or implant wrinkling/rippling, were not also taken into account. The complications, for which the assessment is not based on quantifiable markers or on a scale and relies on subjective criteria (such as implant rotation or implant malposition) were also excluded. Therefore, only the capsular contracture, BIA-ALCL, late seroma and double capsule were encompassed in the literature review. A seroma is considered as late when it occurs after 1-year post-implantation. A double capsule is constituted of a thin inner membrane adherent to the implant surrounding by an outer and totally separated membrane. (103)

The most robust clinical evidence on a medical device is provided by clinical studies. Thus, more and more regulatory agencies assess the safety of a device on the basis of clinical studies. They are even mandatory for Class III devices. Clinical studies consist to follow a cohort of patients recruited by one center (monocentric) or by several centers (multicentric) over a given period (or maximal follow-up). At regular interval, visits are scheduled between the patient and the surgeon. At each visit, any side

effects are reported. The surgeon is either free to organize the patient care (observational study) or is enforced by the study to follow a strict medical protocol (interventional study). Different designs of follow-up exist: the patients are followed from the inclusion visit to the last visit (prospective study) or the surgeon decides to include a series of patients at a given time point and all the patient history is retrieved from the patient files (retrospective study).

In our case, the most valuable studies are observational and prospective. A major drawback of these studies is that 100% of the patient are not followed until the end of the study: some patients may be "lost" because they moved to another city for example. To take into account this number of "lost" patients, the outcomes are usually given as a cumulative risk (in percentage) provided by the Kaplan-Meier statistics. The log-rank test is designed to compare two cumulative risks. (104)

In order not to be biased by some confounding variables, such as radiotherapy (usually underwent by patients after breast cancer) or anterior implant exchange (thus, the implantation of the new device is a revision surgery), the results are often presented into 4 different cohorts: the primary Augmentation cohort, the revision Augmentation cohort, the primary Reconstruction cohort and the revision Reconstruction cohort.

However, clinical studies are not designed to properly assess some rare complications, such as BIA-ALCL (see the very low incidence of the section "BIA-ALCL"). In this case, clinical evidence must be based on the report cases, which are at best compiled in published reviews or in national or international registries. Regarding double capsule, two rates were documented with Biocell-textured implants: two in 10 000 and approximately 1% in over 7 000 patients). However, an accurate estimation of incidence was plagued by clinical misreading. Late seroma incidence was assessed at one in 1 000. (103)

Capsular contracture is dependent on a myriad of different factors, including the texturing. Numerous systematic reviews and meta-analyses of randomized controlled trials demonstrated benefits to texturing in reducing rates of capsular contracture.

(105-107) However, prospective trials led on longer follow-up reported no significant differences in capsular contracture risks between smooth and textured implants. (108)

1.5.2. CLINICAL EVALUATION OF A LINK BETWEEN SOME TYPES OF TEXTURES AND THE INCIDENCE OF CAPSULAR CONTRACTURE

As mentioned previously, to establish that the risk of capsular contracture is potentially impacted by some types of texture, a selective literature review of clinical studies was led.

1.5.2.1. METHODOLOGY OF THE CLINICAL EVALUATION VIA LITERATURE REVIEW

The details of the methodology are specified below.

- Date of the research

The research was performed on February, 7th 2019.

- Literature sources used to identify articles

Both Pubmed and Google Scholar were used to identify literature data. For all searches performed in Google Scholar, patents and citations were excluded.

- Selection criteria used to choose articles

The selection criteria were the following:

- article in English or in French
- article assessing silicone gel-filled implants and more particularly one identified type of texture (commercial name of the texture and manufacturer given). If several commercial types of texture are included in the study, results must be presented by type of texture.
- multicentre clinical study
- article reporting the risk of capsular contracture per patient (computed according to the Kaplan-Meier statistics) in the primary augmentation cohort. Being graded in severity on a scale of I to IV according to the Baker classification, only the Baker III or IV will be considered as a complication. (109)

- follow-up greater or equal to 2 years for safety data
 - full text available
 - number of patients greater or equal to 500
 - no Acellular Dermal Mesh (ADM) used
- Database search details

Different searches were implemented to encompass the different textures of breast implants on the market.

Two types of search were launched on PubMed:

- One for the texture with a commercial name (Siltex, SilkSurface, VelvetSurface, Biocell, Microcell, Perthese, Cereform, Nagotex, TRUE Texture, POLYtxt, MESMO)
- Another for the texture without commercial name (Sebbin, Eurosilicone, Arion)

As the search is restricted to silicone texturing, smooth and PU-coated breast implants were excluded. Likewise, the search did not encompass VELVET (PIP) because the clinical outcomes are thought to be skewed by the use of fraudulent silicone.

As Sebbin and Eurosilicone have two different textures for their round implant and for their shaped implant (<https://www.sebbin.com/fr/page/5/>; <https://www.gcaesthetics.com/products/>), two searches were implemented with Google Scholar by precisising "round" and "anatomical". (Table 7)

The workflow of the search is schematically represented in the Figure 4.

Scientific database	Document type	Search terms	N° of documents
Medline (PubMed)	Scientific study	("breast implants"[MeSH Terms] OR ("breast"[All Fields] AND "implants"[All Fields]) OR "breast implants"[All Fields]) AND (("mentors"[MeSH Terms] OR "mentors"[All Fields] OR "mentor"[All Fields]) OR Siltex™[All Fields]) AND (multicenter[All Fields] OR multicentre[All Fields]) AND "humans"[MeSH Terms]	10
		("breast implants"[MeSH Terms] OR ("breast"[All Fields] AND "implants"[All Fields]) OR "breast implants"[All Fields]) AND (Motiva[All Fields] OR (establishment[All Fields] AND labs[All Fields]) OR SilkSurface[All Fields] OR VelvetSurface[All Fields]) AND (multicenter[All Fields] OR multicentre[All Fields]) AND "humans"[MeSH Terms]	0
		SEBBIN[All Fields] AND ("breast implants"[MeSH Terms] OR ("breast"[All Fields] AND "implants"[All Fields]) OR "breast implants"[All Fields])	4
		("breast implants"[MeSH Terms] OR ("breast"[All Fields] AND "implants"[All Fields]) OR "breast implants"[All Fields]) AND	16

		(Allergan[All Fields] OR Natrelle[All Fields] OR Inamed[All Fields] OR McGhan[All Fields] OR Biocell[All Fields]) AND (multicenter[All Fields] OR multicentre[All Fields]) AND "humans"[MeSH Terms]	
		("breast implants"[MeSH Terms] OR ("breast"[All Fields] AND "implants"[All Fields]) OR "breast implants"[All Fields]) AND (CUI[All Fields] OR Microcell [All Fields]) AND (multicenter[All Fields] OR multicentre[All Fields]) AND "humans"[MeSH Terms]	0
		("breast implants"[MeSH Terms] OR ("breast"[All Fields] AND "implants"[All Fields]) OR "breast implants"[All Fields]) AND (Perouse[All Fields] OR Perthese [All Fields]) AND (multicenter[All Fields] OR multicentre[All Fields]) AND "humans"[MeSH Terms]	0
		("breast implants"[MeSH Terms] OR ("breast"[All Fields] AND "implants"[All Fields]) OR "breast implants"[All Fields]) AND (Cereplas[All Fields] OR Cereform [All Fields]) AND (multicenter[All Fields] OR multicentre[All Fields]) AND "humans"[MeSH Terms]	0

		("breast implants"[MeSH Terms] OR ("breast"[All Fields] AND "implants"[All Fields]) OR "breast implants"[All Fields]) AND (Nagor[All Fields] OR Nagotex[All Fields]) AND (multicenter[All Fields] OR multicentre[All Fields]) AND "humans"[MeSH Terms]	0
		("breast implants"[MeSH Terms] OR ("breast"[All Fields] AND "implants"[All Fields]) OR "breast implants"[All Fields]) AND (Silimed[All Fields] OR Sientra [All Fields] OR True Texture[All Fields]) AND (multicenter[All Fields] OR multicentre[All Fields]) AND "humans"[MeSH Terms]	6
		("breast implants"[MeSH Terms] OR ("breast"[All Fields] AND "implants"[All Fields]) OR "breast implants"[All Fields]) AND (Polytech[All Fields] OR POLYtxt[All Fields]) AND (multicenter[All Fields] OR multicentre[All Fields]) AND "humans"[MeSH Terms]	0
		("breast implants"[MeSH Terms] OR ("breast"[All Fields] AND "implants"[All Fields]) OR "breast implants"[All Fields]) AND (Polytech[All Fields] OR MESMO[All Fields]) AND	0

		(multicenter[All Fields] OR multicentre[All Fields]) AND "humans"[MeSH Terms]	
		Eurosilicone[All Fields] AND ("breast implants"[MeSH Terms] OR ("breast"[All Fields] AND "implants"[All Fields]) OR "breast implants"[All Fields])	6
		Arion[All Fields] AND ("breast implants"[MeSH Terms] OR ("breast"[All Fields] AND "implants"[All Fields]) OR "breast implants"[All Fields])	10
Google Scholar	Scientific study	allintitle: breast implants Mentor	12
		allintitle: breast implants Motiva OR establishment OR labs	6
		allintitle: SEBBIN round breast implants	0
		allintitle: breast implants AND (Allergan OR Natrelle OR Inamed OR McGhan OR MacGhan)	13
		allintitle: SEBBIN shaped breast implants	0
		allintitle: SEBBIN anatomical breast implants	0
		allintitle: breast implants AND (CUI OR Microcell)	0
		allintitle: breast implants AND (Perouse OR Perthese)	0

		allintitle: breast implants AND (Cereplas OR Cereform)	0
		allintitle: breast implants AND (Nagor OR Nagotex)	0
		allintitle: breast implants AND (Silimed OR Sientra OR True Texture)	0
		allintitle: breast implants AND (Polytech OR POLYtxt)	0
		allintitle: breast implants AND (Polytech OR MESMO)	0
		allintitle: Eurosilicone round breast implants	0
		allintitle: Eurosilicone shaped breast implants	0
		allintitle: Eurosilicone anatomical breast implants	0
		allintitle: breast implants Arion	1

Table 7 : Search implemented on the scientific databases

84 articles were therefore identified.

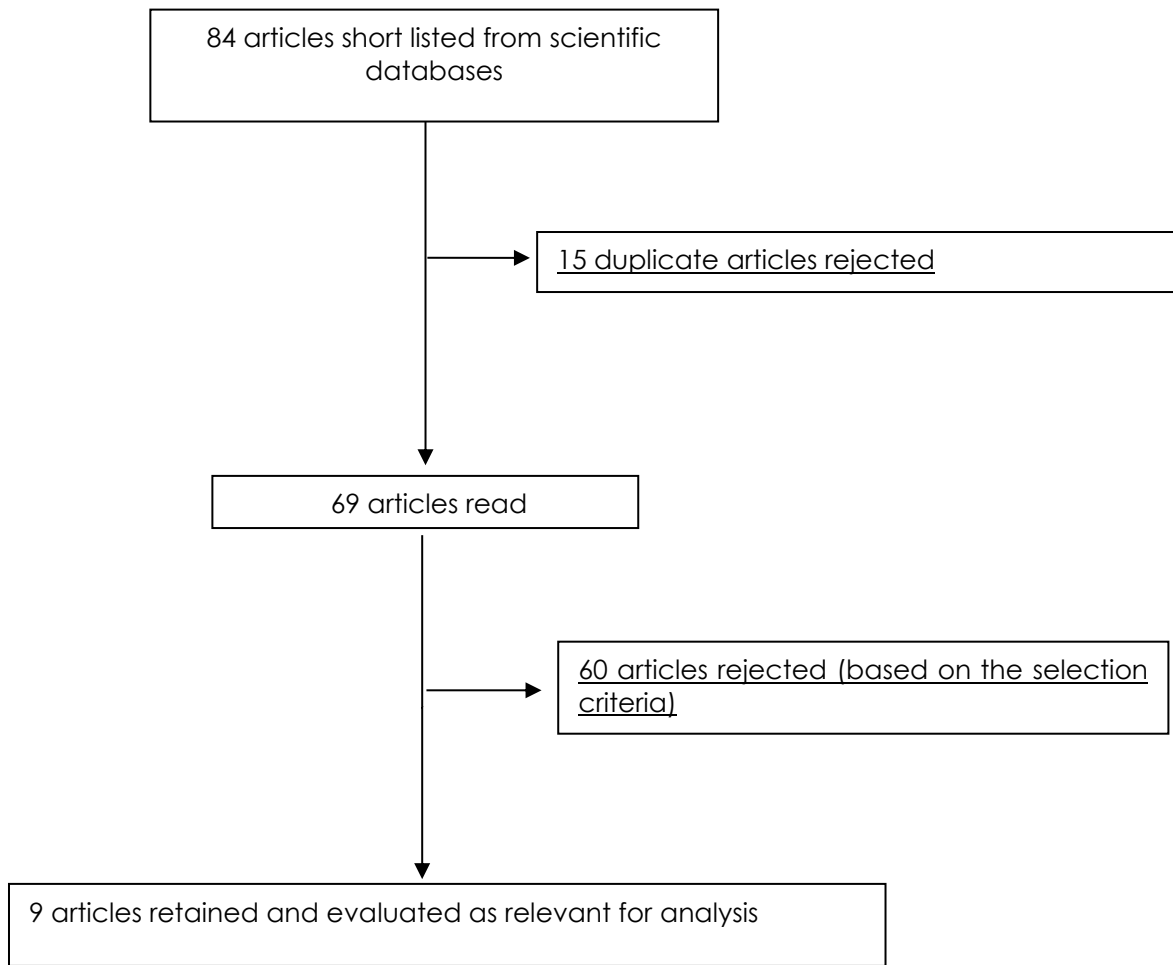


Figure 4 : Workflow for the selection of articles from the scientific databases

1.5.2.2. LIST OF THE SELECTED AND NON-SELECTED ARTICLES IN THE LITERATURE REVIEW

After deleting the 15 duplicates, 69 articles were firstly retained. The list is detailed in the Table 8, as well as the reasons for non-selection.

N°	Study title	Author	Journal	Selected / Not Selected	Reason for non-selection
1	The Mentor Study on Contour Profile Gel Silicone MemoryGel Breast Implants.	Cunningham B	Plast Reconstr Surg	Yes	
2	Breast Implant-Associated Anaplastic Large Cell Lymphoma in Australia and New Zealand: High-Surface-Area Textured Implants Are Associated with Increased Risk.	Loch-Wilkinson A <i>et al.</i>	Plast Reconstr Surg	No	No data on capsular contracture
3	Indications for the use of MemoryShape breast implants in aesthetic and reconstructive breast surgery: long-term clinical outcomes of shaped versus round silicone breast implants.	Caplin DA	Plast Reconstr Surg	Yes	
4	Breast implant rupture: causes, incidence, clinical impact, and management.	Handel N <i>et al.</i>	Plast Reconstr Surg	No	Not a clinical study
5	Mentor Contour Profile Gel implants: clinical outcomes at 6 years	Hammond DC <i>et al.</i>	Plast Reconstr Surg	No	Not a clinical study
6	Clinical experience with a fourth-generation textured silicone gel breast implant: a review of 1012 Mentor MemoryGel breast implants.	Stevens WG <i>et al.</i>	Aesthet Surg J	No	Monocentre retrospective study
7	Mentor Contour Profile Gel Implants: Clinical Outcomes at 10 Years.	Hammond DC <i>et al.</i>	Plast Reconstr Surg	Yes	

8	The Mentor Core Study on Silicone MemoryGel Breast Implants	Cunningham B	Plast Reconstr Surg	No	70% of smooth implants were used
9	Preliminary (3 years) experience with smooth wall silicone gel implants for primary breast augmentation.	Seify H <i>et al.</i>	Ann Plast Surg	No	Retrospective study on less than 500 patients
10	Saline-filled breast implant safety and efficacy: a multicenter retrospective review	Cunningham B	Plast Reconstr Surg	No	Only saline-filled breast implants were used
11	Comments on "Preliminary 3-Year Evaluation of Experience With SilkSurface and VelvetSurface Motiva Silicone Breast Implants: A Single-Center Experience With 5813 Consecutive Breast Augmentation Cases"	Duscher D <i>et al.</i>	Aesthetic Surgery Journal	No	Not a clinical study
12	Preliminary 3-Year Evaluation of Experience With SilkSurface and VelvetSurface Motiva Silicone Breast Implants: A Single-Center Experience With 5813 Consecutive Breast Augmentation Cases	Sforza M <i>et al.</i>	Aesthetic Surgery Journal	No	Monocentre retrospective study
13	Discussion: Motiva Ergonomix Round SilkSurface Silicone Breast Implants Outcome Analysis of 100 Primary Breast Augmentations over 3 Years and Technical Considerations	Disa J	Plast Reconstr Surg	No	Not a clinical study
14	Reply: Motiva Ergonomix Round SilkSurface Silicone Breast Implants: The Tale of Goldilocks: Never Be	Huemer GM <i>et al.</i>	Plast Reconstr Surg	No	Not a clinical study

	Afraid of Exploring Unknown Territory				
15	Motiva Ergonomix Round Silksurface Silicone Breast Implants: Outcome Analysis of 100 Primary Breast Augmentations over 3 Years and Technical Considerations	Huemer GM <i>et al.</i>	Plast Reconstr Surg	No	Study on less than 500 patients
16	Response to "Comments on 'Preliminary 3-Year Evaluation of Experience With SilkSurface and VelvetSurface Motiva Silicone Breast Implants: A Single-Center Experience With 5813 Consecutive Breast Augmentation Cases'"	Sforza M	Aesthetic Surgery Journal	No	Not a clinical study
17	Comparison of Allergan, Mentor, and Sientra contoured cohesive gel breast implants: A single surgeon's 10-year experience	Doren EL <i>et al.</i>	Plast Reconstr Surg	No	Less than 500 patients
18	Experience with the Mentor Contour Profile Becker-35 expandable implants in reconstructive breast surgery	Hsieh F <i>et al.</i>	J Plast Reconstr Aesthet Surg	No	No silicone gel-filled implant was used
19	Shaped Silicone Gel Implants: Mentor MemoryShape Breast Implant	Rohrich RJ	Plast Reconstr Surg	No	Not a clinical study
20	Financial Disclosure Appendix for "Shaped Silicone Gel Implants: Mentor MemoryShape Breast Implant"	Calobrace MB <i>et al.</i>	Plast Reconstr Surg	No	Not a clinical study
21	Comparison of Allergan, Mentor, and Sientra Contoured Cohesive Gel Breast Implants: A Single Surgeon's 10-Year Experience	Sisti A <i>et al.</i>	Plast Reconstr Surg	No	Not a clinical study

22	Reply: Comparison of Allergan, Mentor, and Sientra Contoured Cohesive Gel Breast Implants: A Single Surgeon's 10-Year Experience	Afrooz PN <i>et al.</i>	Plast Reconstr Surg	No	Not a clinical study
23	Clinical Experience with Mentor Contour Profile MemoryGel Breast Implants: A Single Institution's Experience with 99 Consecutive Patients	Hirsch EM <i>et al.</i>	Plast Reconstr Surg	No	Less than 500 patients
24	Important Information for Reconstruction Patients About Mentor MemoryGel® Silicone Gel-Filled Breast Implants	Mentor corporation	N/A	No	Not a clinical study (patient brochure)
25	A 10-Year Prospective Study of Implant-Based Breast Augmentation and Reconstruction.	El-Haddad R <i>et al.</i>	ePlasty	No	Smooth implants were also used.
26	Characterization of Breast Implant Surfaces, Shapes, and Biomechanics: A Comparison of High Cohesive Anatomically Shaped Textured Silicone, Breast Implants from Three Different Manufacturers.	Atlan M. <i>et al.</i>	Aesthetic Plast Surg.	No	Not a clinical study
27	Descriptive analysis of the various mammary implants available on European market in 2005	Desouches C. <i>et al.</i>	Ann Chir Plast Esthet.	No	Not a clinical study
28	A scanning electron microscopy study of the surface of porous-textured breast implants and their capsules. Description of the	Danino A.	Ann Chir Plast Esthet.	No	Not a clinical study

	"velcro" effect of porous-textured breast prostheses				
29	Eight-year follow-up data from the U.S. clinical trial for Sientra's FDA-approved round and shaped implants with high-strength cohesive silicone gel.	Stevens WG <i>et al.</i>	Aesthetic Surgery Journal	Yes	
30	Nine-Year Core Study Data for Sientra's FDA-Approved Round and Shaped Implants with High-Strength Cohesive Silicone Gel.	Stevens WG <i>et al.</i>	Aesthetic Surgery Journal	Yes	
31	Ten-year Core Study Data for Sientra's Food and Drug Administration-Approved Round and Shaped Breast Implants with Cohesive Silicone Gel.	Stevens WG <i>et al.</i>	Plast Reconstr Surg	Yes	
32	Five-year follow-up data from the U.S. clinical trial for Sientra's U.S. Food and Drug Administration-approved Silimed® brand round and shaped implants with high-strength silicone gel.	Stevens WG <i>et al.</i>	Plast Reconstr Surg	No	An overall risk rate for textured implant was given by implant.
33	Eight-Year Safety Data for Round and Anatomical Silicone Gel Breast Implants.	Duteille F <i>et al.</i>	Aesthetic Surgery Journal	No	Two different types of texture are studied (the texture of Eurosilicone round implant and the texture of Eurosilicone anatomical implant). The

					outcomes are not given separately.
34	Five-year Safety Data for Eurosilicone's Round and Anatomical Silicone Gel Breast Implants.	Duteille F <i>et al.</i>	Plast Reconstr Surg	No	Two different types of texture are studied (the texture of Eurosilicone round implant and the texture of Eurosilicone anatomical implant). The outcomes are not given separately.
35	Analytical investigations on elastomeric shells of new Poly Implant Prothèse (PIP) breast and from sixteen cases of surgical explantation.	Beretta G <i>et al.</i>	J Pharm Biomed Anal.	No	Not a clinical study
36	Investigation of the silicone structure in breast implants using ¹ H NMR.	Formes A <i>et al.</i>	J Pharm Biomed Anal.	No	Not a clinical study
37	Prospective study comparing two brands of cohesive gel breast implants with anatomic shape: 5-year follow-up evaluation.	Niechajev I <i>et al.</i>	Aesthetic Plast Surg	No	Less than 500 patients
38	[Descriptive analysis of the various mammary implants available on European market in 2005].	Desouches C <i>et al.</i>	Ann Chir Plast Esthet.	No	Not a clinical study
39	Critical review of additive mastoplastic with Arion hydrogel prosthesis.	Gatti A	Aesthetic Plast Surg	No	Not a clinical study

40	[Comment on an article:"Deflation of breast implants, pre-filled with saline or hydrogel. Results and analysis of a series of 650 treated patients" by L. Soubirac, E. Jouglu, L. Hezard, J.L. Grolleau, J.P. Chavoin. Ann Chir Plast Esthet 47 (2002) 273-279].	Arion H	Ann Chir Plast Esthet.	No	Not a clinical study
41	[Carboxymethylcellulose hydrogel-filled breast implants. Our experience in 15 years].	Arion H	Ann Chir Plast Esthet.	No	Not a clinical study
42	[On breast implants].	Arion H	Ann Chir Plast Esthet.	No	Not a clinical study
43	[Statistics and breast implants].	Arion H	Ann Chir Plast Esthet.	No	Not a clinical study
44	[On breast implants].	Arion H	Ann Chir Plast Esthet.	No	Not a clinical study
45	[Siliconomas].	Arion H	Ann Chir Plast Esthet.	No	Not a clinical study
46	[Treatment of mammary hypoplasia with Arion prosthesis].	Kari P	Maroc Med.	No	Not a clinical study
47	Comment on:" Carboxymethyl cellulose (CMC) hydrogels used to fill breast implants: a 15-year experience" by H. Arion	Sharpe DT	European Journal of Plastic Surgery	No	Not a clinical study
48	Five-Year Safety Data for More than 55,000 Subjects following Breast Implantation: Comparison of Rare Adverse Event Rates with Silicone Implants versus National Norms and Saline Implants.	Singh N <i>et al.</i>	Plast Reconstr Surg	No	No rate of capsular contracture reported
49	Novel Approach for Maximizing Follow-Up in Cosmetic Surgery	Mueller MA <i>et al.</i>	Plast Reconstr Surg	No	No safety data reported

	Clinical Trials: The Ideal Implant Core Trial Experience.				
50	Risk Factor Analysis for Capsular Contracture, Malposition, and Late Seroma in Subjects Receiving Natrelle 410 Form-Stable Silicone Breast Implants.	McGuire P <i>et al.</i>	Plast Reconstr Surg	No	No Kaplan-Meier risk given
51	Prospective Analysis of Primary Breast Augmentation on Body Image Using the BREAST-Q: Results from a Nationwide Study.	Alderman A	Plast Reconstr Surg	No	No safety data
52	Natrelle Silicone Breast Implant Follow-Up Study: Demographics, Lifestyle, and Surgical Characteristics of More Than 50,000 Augmentation Subjects	Singh N <i>et al.</i>	Plast Reconstr Surg	No	No safety data
53	Natrelle 410 Extra-Full Projection Silicone Breast Implants: 2-Year Results from Two Prospective Studies	Cordeiro PG <i>et al.</i>	Plast Reconstr Surg	No	No augmentation patient
54	Style 410 highly cohesive silicone breast implant core study results at 3 years.	Bengtson BP <i>et al.</i>	Plast Reconstr Surg	Yes	
55	Natrelle style 410 form-stable silicone breast implants: core study results at 6 years	Maxwell GP <i>et al.</i>	Aesthet Surg J	Yes	
56	Late seromas after breast implants: theory and practice.	Spear SL <i>et al.</i>	Plast Reconstr Surg	No	No rate of capsular contracture reported

57	Natrelle saline-filled breast implants: a prospective 10-year study	Walker PS <i>et al.</i>	Aesthet Surg J	No	Only saline-filled breast implants were used
58	A prospective, multi-center study of psychosocial outcomes after augmentation with natrelle silicone-filled breast implants	Murphy DK <i>et al.</i>	Ann Plast Surg	No	Less than 500 patients
59	Breast augmentation motivations and satisfaction: a prospective study of more than 3,000 silicone implantations	Gladfelter J <i>et al.</i>	Plast Surg Nurs	No	No safety data
60	Ten-year results from the Natrelle 410 anatomical form-stable silicone breast implant core study	Maxwell GP <i>et al.</i>	Aesthet Surg J	Yes	
61	Inamed silicone breast implant core study results at 6 years	Spear SL <i>et al.</i>	Plast Reconstr Surg	No	59% of smooth implants were used
62	Prevalence of rupture in inamed silicone breast implants	Hedén P <i>et al.</i>	Plast Reconstr Surg	No	Less than 500 patients
63	A modification of the parameter system and surgical techniques with McGhan anatomical implants for breast augmentation	Gao J <i>et al.</i>	Chinese Journal of Aesthetic Medicine	No	Less than 500 patients
64	Two Stage Breast Reconstruction with McGhan LV Expanders and McGhan 363 LF Implants: A Review of 82 Breast Reconstructions in 62 Consecutive Patients	Scott Gr	Congress communication	No	Less than 500 patients
65	Discussion: Risk Factor Analysis for Capsular Contracture, Malposition, and Late Seroma in Subjects Receiving Natrelle 410 Form-Stable Silicone Breast Implants	Disa JJ <i>et al.</i>	Plast Reconstr Surg	No	Not a clinical study

66	Comparison of the Explantation Rate of Poly Implant Prothèse, Allergan, and Pérouse Silicone Breast Implants within the First Four Years after Reconstructive Surgery before the Poly Implant Prothèse Alert by the French Regulatory Authority	Leduey A <i>et al.</i>	International Journal of Breast Cancer	No	Less than 500 patients
67	Allergan Style 410 Implants for Breast Reconstruction: A Prospective Study in Efficacy, Safety, and Symmetry	Unger JG <i>et al.</i>	Plast Reconstr Surg	No	Less than 500 patients
68	Risk factor analysis for capsular contracture, malposition, and late seroma in subjects receiving Natrelle 410 form-stable silicone breast implants	Quinlan CS <i>et al.</i>	Plast Reconstr Surg	No	Not a clinical study
69	Reply: Risk Factor Analysis for Capsular Contracture, Malposition, and Late Seroma in Subjects Receiving Natrelle 410 Form-Stable Silicone Breast Implants	McGuire P	Plast Reconstr Surg	No	Not a clinical study

Table 8 : Selected and non-selected articles through the scientific database search

1.5.2.3. RETRIEVED CLINICAL DATA CATEGORIZED BY BREAST IMPLANT SURFACES

On the basis of the mentioned selection criteria, 9 articles were retained [1, 3, 7, 29, 30, 31, 54, 55, 60].¹ Actually, these articles correspond to three different *Cohort studies* (currently completed). Basically, the Cohort studies are one of the Pre-Market Clinical Studies that a breast implant manufacturer must lead to obtain the FDA approval since the moratorium. These studies have a similar design:

- Observational, prospective and multicenter

¹ The references between square brackets correspond to the articles of the Table 8.

- Nonrandomized
- 10-year follow-up
- Centers located in the USA
- Outcome computed with the Kaplan-Meier methodology
- Annual visits
- 4 cohorts of patients: primary augmentation, revision augmentation, primary reconstruction and revision reconstruction

Thus, [1, 3, 7] reported the outcomes of the Cohort study led by Mentor on Contour Profile Gel implants at 2 years, 9 years and 10 years of follow-up. Actually, Caplin *et al.* [3] reported the safety data of two cohort studies led by Mentor: the Cohort study on Contour Profile Gel implants and the one on Silicone MemoryGel implants. Only the results of the first study were retained in the analysis because the second study encompassed smooth and textured implants. The clinical outcomes on Sientra round and shaped implants were published at 8 years, 9 years and 10 years [29, 30, 31]. Likewise, Allergan published the results on Natrelle 410 anatomical implants at 3 years, 6 years and 10 years [54, 55, 60].

Moreover, the implants studied in the three Cohort studies belong to the fifth-generation and more particularly are anatomically shaped for the Allergan- and Mentor-sponsored studies. In the Sientra study, approximately 10% of the implants were anatomically shaped. Thus, the outcome comparison between the three studies is all the more relevant as study design and implant characteristics are similar.

All the implants of the Cohort studies promoted by Allergan and Mentor were Biocell-textured and Siltex-textured respectively. Regarding the Sientra Cohort study, 53% of the implants were smooth. However, the cumulative risk of capsular contracture was given separately for the cohort of patients with smooth implants and for the cohort of patients with textured implants (TRUE texture). Thus, a cumulative risk of capsular contracture of patients with Biocell-textured, Siltex-textured, TRUE texture-textured and Sientra smooth implants was provided by these three Cohort studies. Maxwell *et al.* [60] reported the risk of capsular contracture in the Primary Augmentation cohort of the Allergan-sponsored Cohort study at 4 weeks, 6 months, 1 year, 2 years, 3 years, 4

years, 5 years, 6 years, 7 years, 8 years, 9 years and 10 years of follow-up. For comparison purpose between the different types of texture, only the risks at 2 years, 3 years, 6 years, 8 years, 9 years and 10 years were retained. However, some discrepancies were noted between the rates at 3 years and 6 years given by Maxwell *et al.* [60] and the ones given by Bengtson *et al.* [54] and Maxwell *et al.* [55]. The interim and the 10-year outcomes are reported in the Table 9 for the 4 different types of surface studies in the selected articles.

Follow-up	2 years	3 years	6 years	8 years	9 years	10 years
Siltex [1, 3, 7]	0.8				3.4	3.6
TRUE Texture [29, 30, 31]				7.3	8	9
Silimed smooth [29, 30, 31]				15.8	16.6	17.5
Biocell [60]	1.7	2.1	5.2	6.8	7.9	9.2

Table 9 : Cumulative risks of capsular contracture of different breast implant surfaces retrieved from the scientific database search

Moreover, on the basis of these cumulative risks, Stevens *et al.* demonstrated a statistically reduced risk of capsular contracture with Sientra textured implants compared to Sientra smooth implants at 8 years, 9 years and 10 years ($p < 0.0001$, $p = 0.0002$, $p = 0.0007$ respectively). [29, 30, 31]

More precisely, in the Mentor-sponsored Cohort study, the risk of capsular contracture at 10 years of follow-up among primary augmentation patients with a Siltex-textured implant with subglandular placement (7.7%) compared to those with submuscular placement (3.05%) was not significantly different ($p = 0.0625$ according to the log-rang test). However, by controlling prior occurrence of a hematoma or seroma and clinical site with a proportional hazards regression model, the capsular contracture rate with subglandular placement was significantly higher (hazard ratio=3.1). [7]

A single case of BIA-ALCL was reported from the three Cohort studies. [60] This case was declared on Biocell-textured implants. In 2015, Brody *et al.* theorized that some surface processing of breast implant (called texture) might play an important role: they noted that where the clinical history was known, the patient had received at least one

textured surface breast device. (35) More and more clinical evidences are in favor of an association between Biocell and BIA-ALCL. (110)

1.5.3. CLINICAL EVALUATION OF A POTENTIAL LINK BETWEEN SOME TYPES OF TEXTURES AND THE INCIDENCE OF BIA-ALCL

As mentioned previously, to establish that the risk of BIA-ALCL is potentially impacted by some types of texture, a selective literature review of compiled report cases was led. For each case, the characteristics of breast prostheses implanted at the time of BIA-ALCL diagnosis were extracted. If the patients have had beforehand other implants and if the implants were identified, these prior implants were also taken into account in the analysis and represent the implant history of the patients. The cases were retrieved from different sources (federal database, literature review, large clinical studies).

1.5.3.1. METHODOLOGY OF THE CLINICAL EVALUATION VIA LITERATURE AND FEDERAL DATABASE REVIEW

The details of the literature review are specified below.

- Date of the research

The research was performed on February, 11th 2019.

- Literature sources used to identify articles

Pubmed was used to identify literature data.

- Selection criteria used to choose articles

The selection criteria were the following:

- article in English or in French
- All the BIA-ALCL cases obtained through a chosen clinical source must be reported over a given period of time and a precise geographical location (i.e. without restriction to a texture or a manufacturer). If several articles used the same methodology and covered the same geographical location, the most recent article will be retained.

- The type of texture or the manufacturer must be known for most of the reported BIA-ALCL cases (commercial name or texturing process given). If detailed in the article or in the Supplementary Materials of the article, the characteristics of prior implants might be taken into account.
- full text available
- no Acellular Dermal Mesh (ADM) used

- Database search details

A search on Medline (Pubmed) with the term: (Breast Implant-Associated Anaplastic Large Cell Lymphoma OR BIA-ALCL OR breast-ALCL) AND (incidence OR incidences OR prevalence OR case OR cases OR risk OR risks) AND (database OR databases OR registry OR registries OR series) was implemented.

If the previously mentioned regulatory agencies reported the cases per manufacturer (or per type of texture), these statistics were also taken into account in the analysis.

The workflow of the search is schematically represented in the Figure 5.

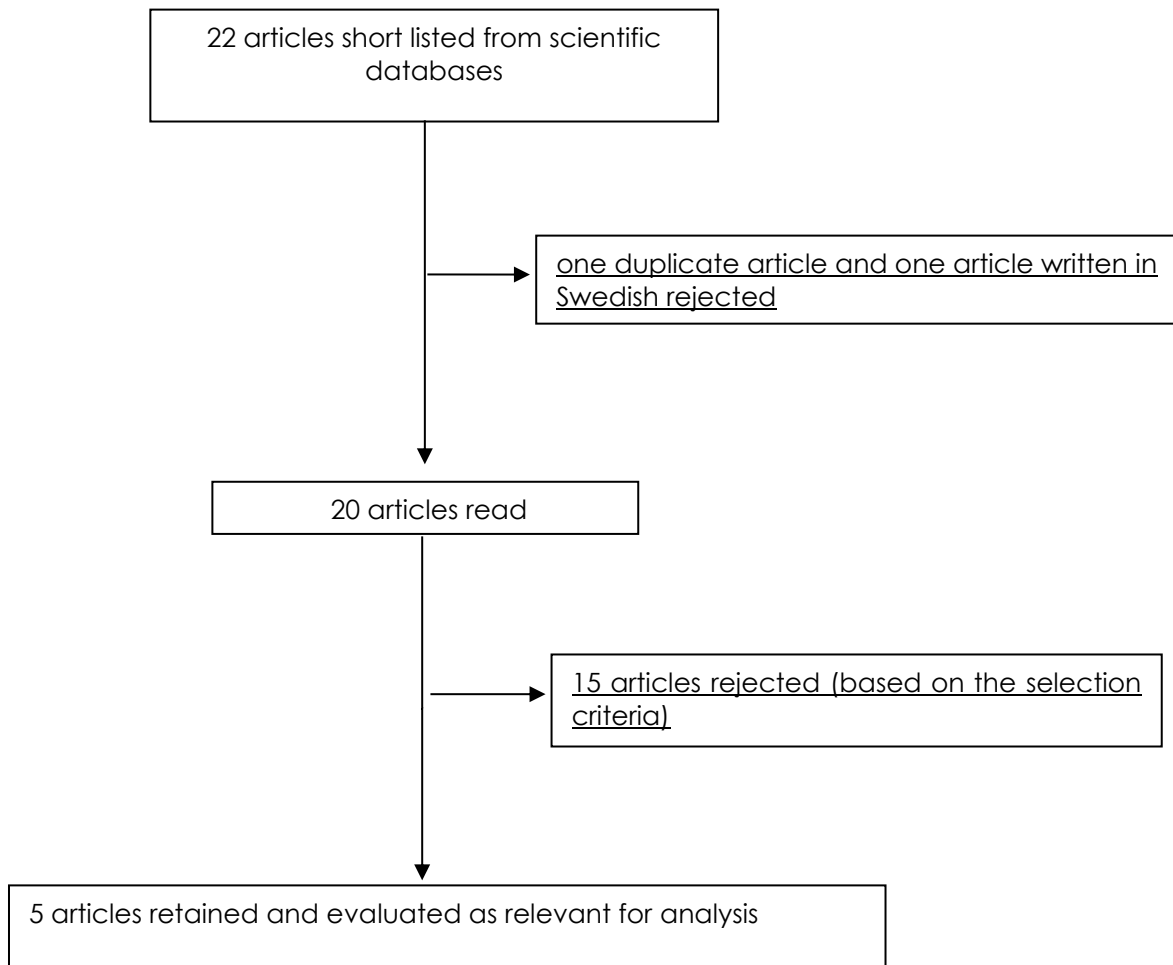


Figure 5 : Workflow for the selection of articles from the scientific databases

1.5.3.2. LIST OF THE SELECTED AND NON-SELECTED ARTICLES IN THE LITERATURE REVIEW

After exclusion of two articles (one written in Swedish and one duplicate), 20 articles were identified.

N°	Study title	Author	Journal	Selected / Not Selected	Reason for non-selection
1	Breast Implant-Associated Lymphoma.	Kricheldorf J <i>et al.</i>	Dtsch Arztebl Int.	Yes	
2	Peripheral T-Cell Lymphomas: Incorporating New Developments in Diagnostics, Prognostication, and Treatment Into Clinical Practice- PART 1: PTCL-NOS, FTCL, AITL, ALCL.	Zing NPC <i>et al.</i>	Oncology (Williston Park)	No	Not a case report
3	Breast Implants and the Risk of Anaplastic Large-Cell Lymphoma in the Breast.	de Boer M <i>et al.</i>	JAMA Oncol.	Yes	
4	22 Cases of Breast Implant-Associated ALCL: Awareness and Outcome Tracking from the Italian Ministry of Health.	Campanale A <i>et al.</i>	Plast Reconstr Surg.	No	"The Manufacturers and the Codes of the Implanted devices have not been disclosed because they are covered by confidentiality agreements and they are not relevant for the purposes of this study."
5	Breast Implant-Associated Anaplastic Large Cell Lymphoma: A Systematic Review.	Leberfinger AN <i>et al.</i>	JAMA Surg.	No	The types of texture are not reported

6	Breast Implant-Associated Anaplastic Large-Cell Lymphoma in a Transgender Woman.	De Boer M <i>et al.</i>	Aesthet Surg J.	No	Report of one case
7	Breast implant capsule-associated squamous cell carcinoma: a report of 2 cases.	Olsen DL <i>et al.</i>	Hum Pathol.	No	Report of two carcinoma cases
8	Breast implant associated anaplastic large cell lymphoma: The UK experience. Recommendations on its management and implications for informed consent.	Johnson L <i>et al.</i>	Eur J Surg Oncol.	Yes	
9	Breast Implant-Associated Anaplastic Large Cell Lymphoma in Australia and New Zealand: High-Surface-Area Textured Implants Are Associated with Increased Risk.	Loch-Wilkinson A <i>et al.</i>	Plast Reconstr Surg.	Yes	
10	Primary Breast Lymphoma in the United States: 1975-2013.	Thomas A <i>et al.</i>	J Natl Cancer Inst.	No	No details on the implants
11	NCCN Consensus Guidelines for the Diagnosis and Management of Breast Implant-Associated Anaplastic Large Cell Lymphoma.	Clemens MW <i>et al.</i>	Aesthet Surg J.	No	Not a case report
12	Global Adverse Event Reports of Breast Implant-Associated ALCL: An International Review of 40 Government Authority Databases.	Srinivasa DR <i>et al.</i>	Plast Reconstr Surg.	No	Only the manufacturers of the cases declared to the US MAUDE

					database were reported.
13	U.S. Epidemiology of Breast Implant-Associated Anaplastic Large Cell Lymphoma.	Doren EL <i>et al.</i>	Plast Reconstr Surg.	Yes	
14	Lymphomas Associated with Breast Implants: A Review of the Literature.	Rupani A <i>et al.</i>	Aesthet Surg J.	No	The types of texture are not reported
15	Anaplastic large-cell lymphoma associated with breast implants: a unique entity within the spectrum of peri-implant effusions.	Chai SM <i>et al.</i>	Diagn Cytopathol.	No	Not a case report
16	Implant-associated anaplastic large cell lymphoma of the breast: Insight into a poorly understood disease.	Weathers WM <i>et al.</i>	Can J Plast Surg.	No	Report of one case
17	Anaplastic large cell lymphoma occurring in association with breast implants: review of pathologic and immunohistochemical features in 103 cases.	Taylor CR <i>et al.</i>	Appl Immunohistochem Mol Morphol.	No	No details on the implants
18	Risk of lymphoma in women with breast implants: analysis of clinical studies.	Largent J <i>et al.</i>	Eur J Cancer Prev	No	The methodology chosen by the authors was based on clinical studies. However, only Allergan-sponsored trials were taken into account.

19	Breast implant-associated, ALK-negative, T-cell, anaplastic, large-cell lymphoma: establishment and characterization of a model cell line (TLBR-1) for this newly emerging clinical entity.	Lechner MG <i>et al.</i>	Cancer.	No	Not a case report
20	Anaplastic large-cell lymphoma in women with breast implants.	de Jong D <i>et al.</i>	JAMA.	No	A more recent case report using the same methodology and on the same country has been already retained (3).

Table 10 : Selected and non-selected articles through scientific database search

1.5.3.3. RETRIEVED CLINICAL DATA CATEGORIZED BY BREAST IMPLANT SURFACES OR MANUFACTURERS

Only two regulatory agencies (ANSM and Health Canada) provided a detail of BIA-ALCL cases per manufacturer. (Table 11) ANSM was able to retrieve the prior implants for each case, which corresponded to 80 implants.

	ANSM		Health Canada
	Through the implant history of the patients	Implant on diagnosis	Implant on diagnosis
McGhan/Inamed/ Allergan	47	32	18
Arion	2	2	
Cereplas	2	2	
Eurosilicone	1	1	
Mentor	2	1	2
Perouse-Plastie	2	1	
PIP	5	1	
Polytech	1	1	
Silimed	2	1	1
Unknown	16	8	1

Table 11 : BIA-ALCL cases per manufacturer reported by the French regulatory agency (ANSM) and by the Canadian regulatory agency (Health Canada)

However, these data are not exploitable for two reasons.

Firstly, they are absolute (i.e. not relative to the number of implanted prostheses in France or in Canada or to the sales data of the different manufacturers). This point is particularly important for a worldwide comparison because all the manufacturers are not present in all the countries or their market share may be different. Thus, in France PIP (April 2010), Perouse-Plastie (end of 2011), Cereplas (February 2014), and Silimed (2015) do not sell implant anymore. In Canada, only Allergan, Mentor and Ideal Implant implants were approved.

Secondly, the commercial names of the texture are unknown and some manufacturers (such as Allergan and Arion) commercialize several types of texture. To address this point, the LYMPHOPATH network presented during the ANSM-mandated public audition in February 2019 the most updated data summarized in the Table 12, in which the types of texture were collected as far as possible. The table takes into

account all the prior implants of each case confirmed by the network (n=46). The data are given per implant as well as per patient.

	Manufacturer	Commercial name of texture	Through the implant history of the patients	
			Per implant (n=136)	Per patient (n=46)
Textured	McGhan/Allerga	Biocell	58	32
		Microcell	1	1
		Unknown	9	5
	PIP		3	2
	Mentor	Siltex	2	1
	Other brands	Microtextured*	5	3
Unknown		6	4	
PU-coated	Polytech		2	1
Smooth	All brands		2	1
Unknown			48	21

Table 12 : BIA-ALCL cases per type of breast implant surface reported by the LYMPHOPATH network

*refer to commercial denominations

The FDA did not detail the surface characteristics on BIA-ALCL cases identified. However, for the first time, known cases in patients with only smooth-surface breast implants were reported. (<https://www.youtube.com/watch?v=wpdkXMEj60U>)

On the basis of the mentioned selection criteria of the literature review, 5 articles were retained [1, 3, 8, 9, 13].²

Doren *et al.* [13] performed a retrospective review of the unpublished cases diagnosed at their institution and the cases the authors were able to pathologically confirm from the literature from 1996 to 2015 in the USA. Thus, 100 cases were identified

² The references between square brackets correspond to the articles of the Table 10.

and confirmed. The texturing processes of the implants on diagnosis were reported. As only Allergan commercialized salt-loss-textured implants in the USA and as only Mentor sold imprint-stamping-textured implants in the USA, the identification of the type of texture was straight-forward. Based on annualized sales data of breast implants in the USA, the authors were the first to provide an incidence rate of BIA-ALCL per type of texture. Thus, the overall incidence rates for salt-loss-textured implant and for imprint-stamping-textured implant were estimated at 1.87 per 1 million person-years and at 0.33 per 1 million person-years respectively. The incidence was significantly lower with imprint-stamping-textured implant ($p < 0.001$).

A joint Australia and New Zealand task force was formed between members of the plastic surgery, breast oncology, hematology and oncology, and cosmetic surgical societies to screen all the BIA-ALCL cases between 2007 and August 2016 [9]. Thus, 55 cases were identified. All implant histories of these cases ($n=75$ implants) were obtained. 79% of implants involved in the reported cases were either Biocell-textured or PU-coated. A further statistical analysis based on the odds ratio was led by type of texture. Thus, the risk for developing BIA-ALCL was 14.11 times higher for Biocell and 10.84 times higher with PU coating as compared with Siltex texture. A Kaplan-Meier analysis determined that the risk with Biocell was particularly important from the 8th year of exposure. Moreover, the task force allowed the authors to release the sales data of the three major implant manufacturers in the region (Mentor, Allergan and Silimed) between 1999 and 2015 (Nagor did not provide sales data) and therefore to compute implant-specific risk for patients exposed to single implant texture type. Thus, the cases of BIA-ALCL per number of implantations were estimated at one in 3817 for Biocell texture, at one in 7788 for PU coating and at one in 60631 for Siltex texture, which are the highest reported incidences until now. (69) The risk with PU-coated implants was likely underestimated because the manufacturer of this type of implant (Silimed) obtained Australian regulatory approval only in 2008.

23 cases of BIA-ALCL were reported by Johnson in the UK between 2012 and 2016 [8]. The histories of implantation were known for 18 patients thanks to a close collaboration between the Association of Breast Surgery (ABS), British Association of Plastic,

Reconstructive and Aesthetic Surgeons (BAPRAS) and the British Association of Aesthetic Plastic Surgeons (BAAPS) networks.

De Boer *et al.* [3] identified 32 cases of BIA-ALCL in the Netherlands through the population-based nationwide Dutch pathology registry between 1990 and 2016. Of the 28 patients with BIA-ALCL with known implant type, 23 (82%) had “macrot textured” implants on diagnosis. Moreover, the complete implant history was detailed for the 32 cases in the Supplementary Online Content. The authors added that “*only 45% of all implants sold in the Netherlands in 2010 to 2015 were macrot textured*”. Implant-specific risk was not performed because “*our sales data lack historical information on market shares before 2010, as a result of bankruptcy or changing distributors with loss of product data files.*”

Kricheldorf *et al.* [1] reported the cases in Germany. Only 7 cases were identified by personal inquiry to the Federal Institute for Drugs and Medical Devices (BfArM), the German Society of Plastic, Reconstructive, and Aesthetic Surgeons (Deutsche Gesellschaft der Plastischen, Rekonstruktiven und Ästhetischen Chirurgen, DGPRÄC), and the German Society for Gynecology and Obstetrics (Deutsche Gesellschaft für Gynäkologie und Geburtshilfe, DGGG). The implant history was known for 6 cases.

In each of the retained articles and federal databases, the type of texture present on the implant on diagnosis and on all the prior implants of each reported case was identified, counted and summarized in the Table 13. The types of texture, which were never sold in the corresponding countries to our knowledge, were also mentioned. The hypotheses regarding the pathogenesis of the BIA-ALCL given in each article were added in the table.

From the hypotheses, the authors seemed to agree with a multifactorial etiology. Among the 5 retained articles, the “chronic inflammation” was explicitly reported in 4 articles. [1, 3, 8, 13] The fifth article [9] used a synonymous term: “chronic antigen stimulation”. Consistently, chronic inflammation related to repeated antigenic stimulation has been noted as a factor triggering lymphocyte activation, recruitment, transformation and ultimately lymphomagenesis. (111-115) Once activated, the T

lymphocytes will differentiate into different subsets with different antigen specificities. Thus, the T-helper 1 cells are specific against intracellular viral and bacterial pathogens, T-helper 17 cells are involved in mucosal immunity and autoimmune disorders and T-regulatory cells inhibit proinflammatory T cells. (116)

Different reasons were proposed to elicit this malignant host immune response: the “biofilm” (which was also reported by the authors as a “proliferation” of “adherent bacteria” on the implant surface) mentioned in 4 articles [1, 3, 9, 13], the particulate shedding of the implant surface reported in 3 articles [1, 3, 13] and an eventual chemical toxicity [3, 13]. A genetic predisposition of patients for the risk of lymphoma was also suggested [3, 9, 13].

Even though an association was demonstrated in some models (see the section 1.6 “Biological models”), these malignant triggers remain theoretical because a causative link has not been demonstrated yet. Thus, although the biofilm was the most reported hypothesis, the biological mechanism of tumorigenesis remains unelucidated. Some authors mitigated the bacterial species identified in BIA-ALCL capsule specimens because they were not properly compared with a relevant control microbiome, which is quite challenging. (117) Myckatyn *et al.* even suggested that the clusters of *Ralstonia* spp. identified by Hu *et al.* (64) would be purely “opportunistic” and that the stimulus would be actually bacterial superantigens, such as the lipopolysaccharide coat of bacteria. (118) Regarding the silicone antigenic hypothesis, Prantl *et al.* cautioned against the exact origin of the silicone particles or leachable: “*It remains unclear whether these silicone structures represent friction particles from the surface of the implant or particles of implant filler.*” (119)

	UK		Australia/ New- Zealand	Netherlands		USA	Germany		France
	Johnson [8]		Loch- Wilkinson [9]	De Boer [3]		Doren [13]	Kricheldorf [1]		LYMPHOP ATH database
	Implant on diagnosis	Through the implant history of the patients	Through the implant history of the patients	Implant on diagnosis	Through the implant history of the patients	Implant on diagnosis	Implant on diagnosis	Through the implant history of the patients	Through the implant history of the patients
Biocell	10	19	44	22	23	46	3	6	58
CRISTALLINE Microtextured			0	2	2	never sold			
Nagotex	3	4	5	1	1	never sold			
TRUE Texture			0				1	1	
POLYtxt			0			never sold	1	1	
Siltex	0	2	5	1	1	8	1	1	2

Microcell	1	1	0						1
Sebbin Microtextured			0	1	1	never sold			
Smooth implant*			4						2
VELVET									3
PU-coated implant*	3	3	15						2
Unknown	1	5	0	4	16	49		1	68

<p>Hypothesis of pathogenesis</p>	<p>"The aetiology of this disease remains unclear and, despite the growing body of evidence implicating chronic inflammation within the capsular biofilm, some authors advise caution in drawing conclusions until science catches up with this unusual entity."</p>	<p>"We propose that the higher surface area acts as a passive conduit for the growth and proliferation of bacteria, which, once they reach a threshold, cause ongoing immune activation and transformatio</p>	<p>"So far, various, not mutually exclusive causal factors have been suggested. Specifically, a local inflammatory response, elicited by silicone derived products or specific bacterial species adherent to the prosthesis surface (biofilm) may play a role, possibly via an auto-immune response. Toxic products related to the production of breast implants have been implicated as</p>	<p>"Some theories implicate the immune system response to chronic inflammation, likely induced by silicone particulate, modified silicone, or bacterial antigen in a genetically susceptible patient"</p>	<p>"A connection with implant-induced chronic inflammation has been discussed, as has genetic susceptibility in the sense of severe reactive dysplasia as a response to chronic inflammation. Other suspected causes include particle erosion of the implants, a subclinical biofilm, or chronic T-cell stimulation."</p>
--	--	---	--	---	---

		<p>n in susceptible hosts over time.</p> <p>The contamination of textured implants with a higher surface area by bacteria leading to chronic antigen stimulation in genetically susceptible hosts over a prolonged period may</p>	<p>direct mutagens.</p> <p>Whether certain groups of women have a genetically determined increased risk to develop lymphoma when exposed to breast implants, eg, via a genetically determined altered or exaggerated local immunological response, remains hypothetical."</p>	
--	--	---	---	--

		result in transformatio n of T cells into breast implant- associated ALCL."			
--	--	---	--	--	--

Table 13 : BIA-ALCL cases per type of breast implant surface and hypotheses of pathogenesis retrieved from scientific and federal database search

* As we suppose non-significant differences between the different smooth implants and between the different PU-coated implants sold by the different manufacturers, the latter were not mentioned for these cases. (91)

Two thirds of BIA-ALCL diagnoses were clinically characterized by an effusion (or seroma) in the breast implant pocket. Benign late seroma associated with breast implant were also reported. Similarly with BIA-ALCL, double capsules were predominantly observed on Biocell-textured implants. (120)

1.5.4. CLINICAL EVALUATION OF A POTENTIAL LINK BETWEEN SOME TYPES OF TEXTURES AND THE INCIDENCE OF LATE SEROMA OR DOUBLE CAPSULE

The previously described methodology was applied for late seroma and double capsules.

A similar search on Medline (Pubmed) with the term: ("double capsule") AND ("breast implant" OR "breast implants") AND (incidence OR incidences OR prevalence OR case OR cases OR risk OR risks) AND (database OR databases OR registry OR registries OR series) was implemented.

No article was identified.

Then, a second search on Medline (Pubmed) with the term: ("late seroma") AND ("breast implant" OR "breast implants") AND (incidence OR incidences OR prevalence OR case OR cases OR risk OR risks) AND (database OR databases OR registry OR registries OR series) was performed.

Among the two articles identified, the first was excluded because ADM was used (121) and the second reported between 2002 and 2011 only cases with Biocell-textured prostheses and did not mention cases on other types of texture (65).

As a result of the literature and federal database review, chronic inflammation is of primer importance in the BIA-ALCL onset and different causative hypotheses were proposed, such as biofilm-mediated or debris-mediated inflammation. However, in a clinical evidence-based medicine, biological demonstration of these hypotheses must be provided. Thus, different biological models were designed for this purpose.

Different biological models were proposed to analyse the biological reactions, in term of host tissues, host cells and microbiome, occurring around the breast implant: *in vivo* model, *in vitro* model and *ex vivo* model.

1.6.1. IN VIVO MODELS

In vivo models consisted of implanting custom-made breast implants in animals and characterizing the surrounding biological reactions. Further studies were also led to determine whether these biological reactions were modulated by some species or molecules.

The first *in vivo* model was developed in rabbits by Lilla *et al.*, who evaluated the *in situ* mobility of plain silicone, perforated silicone backed, Dacron-backed and PU-covered prostheses. (122) *In situ* mobility was assessed as the distance along which the implant could be moved under the skin. Thus, Dacron-backed implants were significantly less mobile than the plain ones and PU-covered implants were much less mobile than the average of all the others. Barone *et al.* also used rabbits to quantify some biomechanical parameters (such as the stiffness and the energy absorption) of the capsule from *in situ* measurements of pressure and volume. (99) The capsules facing the Biocell-textured and PU-coated expanders had a significantly lower stiffness and a significantly higher energy absorption than with a smooth expander implanted during 6 months. McLean *et al.* retrieved from rats host tissues in contact with breast implant samples, and performed an immunostaining with antibodies targeting the enzyme cyclooxygenase-2 (COX-2). (123) This enzyme is of particular interest because it mediates the inflammatory cascade. Cytoplasmic COX-2 expression was identified in endothelial cells, macrophages and fibroblasts from the 4th day to the 80th day after implantation. Moyer *et al.* studied whether some characteristics of breast implant other than surface (such as gel viscosity or barrier layer) elicited capsular contracture in swine. (75) Inductively Coupled Plasma-Atomic Emission Spectrometry (ICP-AES) and tensiometry were used. The stiffness measured by dynamic compression on the implant and the capsule dissected *en bloc* was correlated with the intracapsular concentration of silicon. Moreover, whatever the generation of implants, the ruptured

implants were significantly more associated with high-grade contracture than the non-ruptured implants at 1 month.

The *in vivo* biological reaction to implants coated by proteins of interest was also studied in a rabbit model by Marques *et al.* (124-126) The authors used mostly as implanted device a temporary expander with a sensor measuring the intracapsular pressure. The implants were either impregnated of fibrin, thrombin or blood, chitosan or sprayed of fibrin. All these studies were designed with a control group (i.e. implants without coating). A H&E-based histological analysis of the capsular tissue allowed the authors to score the intensity (absent, mild, moderate or severe) and to characterize the type (mononuclear/chronic, mixed/subacute or polymorph/acute) of the inflammatory infiltrate. The capsular thickness and architecture, such as the density and the organisation of collagen fibres, the degree of angiogenesis and the foreign body density, was highlighted by Trichrome staining. At 4 weeks, the fibrin- and thrombin-impregnated expanders as well as fibrin-sprayed expanders experienced significantly decreased intracapsular pressure compared to the control groups. A statistical analysis pointed out that for fibrin-impregnated and control groups, the determining factor for intracapsular pressure was the type of inflammation (mixed inflammation or mononuclear inflammation), whereas for the fibrin-sprayed group, the intracapsular pressure was correlated with capsular thickness. In the blood group, an increase of fibroblast densities and a decrease of angiogenesis were reported compared to the control group. A study quantified the levels of Interleukin 8 (IL8) by a microdialysate of the periprosthetic fluid by a solid-phase sandwich Enzyme-Linked ImmunoSorbent Assay (ELISA). (125) The chitosan group was significantly associated with Baker Grade III/IV, thick capsules, dense connective tissue and decreased IL-8 levels compared to the control.

In vivo models were also developed to analyse the impact of a deliberate inoculation of implant with a bacterial strain on the capsular architecture and inflammatory infiltrate (127), on the *in situ* bacterial colonization (60, 128, 129) and on the immune host response (60). Only strains of Coagulase-Negative Staphylococci, such as *Staphylococcus epidermidis*, were inoculated. Recently, Bergmann *et al.* quantified the capsular thickness and the thickness of the synovial-like metaplasia, the thickness

and density of parallel myofibrils, the number of layers in the capsule and the inflammatory cell number around inoculated PU-coated and textured implants in a rat model. (127) In comparison with textured implants, capsules around PU-coated implants showed significantly lower expression of parallel myofibrils, lower average thickness of synovial-like metaplasia and higher infiltration with inflammatory cells, in both contaminated and non-contaminated groups. As the only positive bacterial culture (found with PU-coated implant) had “*no signs of acute infection or tendency toward positive bacterial growth*”, the authors hypothesized that the PU-coated implants had “*no higher risk of a biofilm-dependent fibrosis*”. Jacombs *et al.* (129) and Hu *et al.* (60) used the pig model and a protocol combining ultra-sounds with enrichment culture established by Tamboto *et al.* (128) to isolate biofilm bacteria and evaluated the total number of bacteria attached to inoculated smooth or textured implants and present in capsular tissue by real-time quantitative reverse transcriptase Polymerase Chain Reaction (PCR) with the universal eubacterial primer 16S rRNA. The contracted breast capsules had 250% more bacteria than the non-contracted capsules. Moreover, a significant correlation was found between the number of bacteria attached to the implant and the Baker grade. This correlation was confirmed by standard bacterial plate culture of capsular sample. Likewise, 11-, 43- and 72-fold more bacteria were cultured on the surface of textured implants at 2, 6 and 24h respectively, compared with smooth implant. This predominance was confirmed by SEM, which highlighted a dense and mature biofilm on textured implants and a patchy biofilm on smooth implants. A quantification of the number of T-helper cell and the T-cytotoxic cell was also performed by PCR (60). All the lymphocytes were significantly more numerous on textured compared with smooth implants (63-fold increase). Immunohistochemistry with different antibodies targeting specific membrane proteins of lymphocyte phenotypes (T-cell or B-cell), confirmed T-cells represent the majority of the lymphocytic infiltrate.

In order to suggest therapeutic alternatives of bacteria-mediated complications, an immersion of implants in antimicrobial solution (composed of iodine-povidone and antibiotics), a covering of implants with antibiotic-impregnated polypropylene mesh or an injection of antibiotic were performed either simultaneously to bacterial inoculation (130, 131) or post-operatively (132). Inoculated bacteria were either

Staphylococcus epidermidis (130, 131) or Methicillin-Resistant Staphylococcus Aureus (MRSA), which was inoculated under two states: biofilm or free planktonic (132). All these studies were designed with a control group (i.e. untreated group). Mendes *et al.* histologically investigated the inflammatory reaction (i.e. numbers of polymorphonuclear cells, mononuclear cells, foreign body giant cells and macrophages) around inoculated (at different bacterial concentrations) and treated PU-coated implants in rats. (131) A discriminating analysis was performed to determine the factor which differentiated at best the treated groups and the non-treated groups. The authors found that this factor was the number of mononuclear cells. Thus, the use of antimicrobial agents would result in a low activation of mononuclear cells. Jacombs *et al.* demonstrated the protective effect of mesh against the development of capsular contracture assessed according to the Baker grading scale: the decrease of Baker III or IV capsular contracture in the mesh-treated group compared to the untreated group was highly significant. (130) Arad *et al.* quantified via viable bacterial count the bacterial colonization present in the specimens. (132) MRSA counts on the 11th day were significantly higher in the treated biofilm MRSA-infected group in comparison with treated free planktonic MRSA-infected group, whereas the counts were similar in the corresponding untreated groups. The authors concluded that vancomycin-based treatment would have a limited efficiency against mature biofilm. SEM demonstrated in situ biofilm from the 4th day on all the biofilm MRSA and free planktonic MRSA-inoculated implants. Moreover, although biofilm was detected on all implants and capsules, the biofilms on the antibiotic-treated implants and capsules were generally single-layered or isolated in contrast to the multi-layer biofilms found on all untreated implants and capsules. (130) Moreover, Arad *et al.* led a precise clinical evaluation of the rats by monitoring weight, rectal temperature and surgical wound healing. Although the wound healing scores were significantly better for untreated biofilm MRSA-infected group compared to untreated free planktonic MRSA-infected group, vancomycin significantly improved wound healing and reduced rectal temperature in free planktonic MRSA-infected group.

Recently, Atlan *et al.* led a histological analysis with H&E staining in rats on a large range of different breast implant surfaces. (94) The capsular surfaces in contact with Allergan smooth breast implants or Motiva breast implants were mostly flat, with an

alignment of the collagen fibres parallel to the surface. MESMO, Siltex and Microcell-textured implants elicited "*small tissue projections scattered*" along the surface of the capsule. The capsule surfaces facing Biocell, True Texture, Cristalline, Nagotex, Polytxt-textured and PU-coated implants exhibited "*more prominent tissue projections, resulting in irregular arrangement of collagen fibres*". The tissue adherence to the implant surface was also estimated by a peel test in this study. The adherence was significantly higher for the PU-coated implants than for all the other implant surfaces. Likewise, Biocell and Nagotex-textured implants adhered significantly more to the capsule than Allergan smooth breast implants or Motiva breast implants.

1.6.2. IN VITRO MODELS

In vitro models consisted of culturing cells of interest (i.e. either cells present in the surrounding host tissues or cell lines originated from breast implant-associated malignancies) or bacteria presumed to be involved in such malignancies. *In vitro* studies were performed on or without breast implant samples. Different types of *in vitro* models were published in the literature.

1.6.2.1. FIBROBLAST AND MACROPHAGE-BASED MODELS

The first type characterized the biological reactions of surrounding host cells cultured on breast implant surface. The cells used were mainly fibroblasts harvested from biopsies in the breast or from skin, except for two studies which cultured Peripheral Blood Mononuclear Cells (133) or THP-1 macrophages (86). Different analyses were led, such as quantification of cell attachment, proliferation and cytotoxicity through cell viability assays. (79, 90, 92, 95) After one week, fibroblasts proliferated significantly more on smooth implant surface in comparison to textured implant surface. (92) On the contrary, Valencia *et al.* (90) found that fibroblast proliferation was significantly reduced on smooth surfaces. A significant increase of cell death was observed in fibroblasts cultured on textured implant surfaces. (92) The fibroblasts adhered better on the textured implant surfaces than on the smooth implant surfaces. (79, 90, 95) This adhesion result was confirmed by confocal microscopy. (79) Moreover, an immunocytochemistry observed by confocal microscopy identified a significant number of fibroblasts trapped within the valleys of the textured breast implant surfaces and a significant number of poorly spread fibroblast morphology with a random actin

network on the smooth breast implant surfaces. (90, 92) However, Barr *et al.* did not find any preferential attachment site for macrophages over a large range of implant surface. (86) By Fluorescence Activated Cell Sorted (FACS), Cappellano *et al.* demonstrated that breast implant surfaces did not induce T-cell proliferation or activation and did not alter the proportion of T-cell subsets. (133)

The gene expression of cultured fibroblasts or macrophages was quantified by real-time quantitative PCR. (86, 92, 133) A significant down-regulation of IL-8 and Tumor Growth Factor beta1 (TGF beta1) and a significant up-regulation of Heat Shock Protein60 (HSP60) by fibroblasts were observed on textured implant surfaces in comparison to smooth implant surfaces. Cappellano *et al.* showed an up-regulation of CD14 and IL-10 by macrophages cultured on Siltex compared to on VelvetSurface-textured surfaces. Moreover, macrophages exhibited a down-regulation of CD68 on SilkSurface and a down-regulation of TNF-alpha on SilkSurface, VelvetSurface and PU-coated implants (133) and on Siltex and Mentor smooth implants (86), whereas Barr *et al.* (86) found an up-regulation of TNF-alpha on Biocell-textured implants at 12h. They also noted a significant increase in IL-6 and IL-10 expression by CUI, Eurosilicone and PIP textured surface at 24h.

The cytokines released by the cultured cells were also profiled. A peak of TGFbeta1 secretion by fibroblasts on both smooth and textured implants was determined at one week. (92) POLYtxt-textured implant elicited increased production of IL6, IL1beta and TNF-alpha by the macrophages. (133) An increased level of TNF-alpha was also found with Biocell-textured and smooth implant surfaces at 12h and with Biocell, CUI and Eurosilicone textured implant surfaces at 24h. (86)

Cappellano *et al.* mitigated the relevancy of such models by detailing the factors which were not taken into account in these studies, such as the protein coating underwent by all surfaces once implanted in the body, the *in vivo* mechanical solicitations and the particulate shedding. All these factors are of primer importance in the interaction between host cells and breast implant surfaces.

1.6.2.2. MALIGNANT CELL LINE-BASED MODELS

The second type of *in vitro* model biologically analysed established model cell lines issued from patients with T-cell breast lymphoma (134), primary cutaneous ALCL lines and BIA-ALCL lines (47) or BIA-ALCL lines, cutaneous ALCL lines, non-anaplastic

cutaneous T-cell lymphoma lines and Jurkat lymphoblastic cell line (135). Kadin *et al.* (47, 135) also used BIA-ALCL cells from clinical specimens.

Lechner *et al.* performed a large panel of biological tests on cell lines, such as karyotype analysis and histological (H&E and Wright-Giemsa staining) examinations. (134) The malignant cells were therefore characterized by an abundant cytoplasm with one to four large cytoplasmic vacuoles and an enlarged nucleus and by an abnormal, hypertriploid and complex karyotype.

Immunohistochemistry determined similar expression of the transcription factors SOCS3, JunB and SATB1 between BIA-ALCL lines and primary cutaneous ALCL lines and detected the transcription factor GATA3 and the allergy-associated immunoglobulin IgE decorating the mast cells and dendritic cells in clinical samples of BIA-ALCL. (47, 135)

A quantitative PCR of tumor suppressor genes, proto-oncogenes and apoptosis-related genes determined a significant up-regulation of the antiapoptotic genes survivin and BCL2L2 and a significant down-regulation of proapoptotic genes and tumor suppressor genes (such as BID, BAK and BBC3) by the BIA-ALCL cell lines compared to normal donor T-cells. (134) Moreover, a PCR performed on tissue section revealed a production of IL13 (which is the signature cytokine of allergic inflammation) by the BIA-ALCL cell lines and by the BIA-ALCL cells. (135) A gene array analysis highlighted the expression of Interferon gamma (IFN γ) and SOCS3 by the BIA-ALCL cell lines. (47)

FACS analyses were led to quantify the expression of normal T-cell lineage markers and transcription factors, with cytometric bead array to profile some cytokines in supernatants and with Annexin V/propidium iodide staining to count viable cells in the presence or absence of cell signalling inhibitors or chemotherapeutic drugs. (134) FACS was also performed after seeding and incubating BIA-ALCL cells in tissue culture medium by Kadin *et al.* (47) Thus, a strong activation of JAK/STAT3 signalling pathway and a strong secretion of IL-6 and IL-10 were reported on the BIA-ALCL cell lines, whereas BIA-ALCL cells exhibited a high production of IFN γ and IL-17 (which is the signature cytokine of Th1/Th17 cells) and a nuclear JunB activity. Moreover, a STAT3 inhibition or a SHP-1 activation or chemotherapy reagents effectively killed all the BIA-ALCL cell lines. The pattern of transcription factor expression was consistent with the Th1 and T-regulatory phenotypes of lineage cells.

Functionality of the lineage cells, especially the suppressive ability of T-regulatory cells, was also evaluated. Basically, the authors co-cultured cell lines with naive normal donor T-cells and measured T-cell proliferation by carboxyfluorescein succinimidyl ester dilution. Thus, all the BIA-ALCL cell lines were found to increase T-cell proliferation.

1.6.2.3. MICROBIAL MODELS

Bacterial studies of the microbiome present on breast implant surface were the third type of *in vitro* models. *In vitro* bacterial attachment assays were carried out by Jacombs *et al.* (129), Jones *et al.* (85) and James *et al.* (91) to analyze the influence of implant surface on rate of bacterial growth and adhesion to implant. Jacombs *et al.* only used *Staphylococcus epidermidis*, whereas Jones *et al.* incubated a large range of breast implant surfaces with four bacterial types: *Staphylococcus epidermidis*, *Staphylococcus aureus*, *Pseudomonas aeruginosa* and *Ralstonia pickettii*. James *et al.* used a biofilm reactor with 3 bacterial species: *Staphylococcus epidermidis*, *Pseudomonas aeruginosa* and *Ralstonia pickettii*. Quantitative bacterial analysis by standard plate culture was provided at 2, 6 and 24h of incubation. Jacombs *et al.* counted 11-, 43- and 72-fold more bacteria on textured implants at 2, 6 and 24h respectively, compared with smooth implants. Similarly, the number of *Staphylococcus epidermidis* and *Ralstonia pickettii* at 24h and the number of *Pseudomonas aeruginosa* at 2h, as well as the thickness of the biofilm observed with Confocal Scanning Laser Microscope, were significantly higher on rougher breast implant surfaces (Siltex and Biocell-textured surface) compared to SilkSurface and VelvetSurface-textured surfaces. (91) Consistently, Jones *et al.* found a significant higher number of *Staphylococcus epidermidis*, *Staphylococcus aureus* and *Ralstonia pickettii* attached to PU-coated, Biocell, Nagotex, Eurosilicone or POLYtxt textured surfaces than to smooth implant surfaces. Moreover, they determined a significant linear relationship between implant surface area and growth of the four bacteria studied. However, according to Jones *et al.* environmental factors must be considered to study the proneness of surface to form biofilm. Moreover, James *et al.* mitigated the relevancy of such studies because "*the immune response to the implant and associated bacteria/biofilm likely plays an important role*".

1.6.3. EX VIVO MODELS

A third type of model consisted in harvesting and analyzing samples from the implants or from the periprosthetic tissues or fluids surrounding the implant, once retrieved from the patient. Numerous different analyses were led.

1.6.3.1. HISTOLOGY

Different histological features were reported on the capsular samples, such as fibroblasts, inflammatory cells and immune cells (136). Thus, fibroblasts constituted the most common cell type in the capsule, with macrophages, scattered polymorphonuclear leukocytes, lymphocytes, plasma cells and mast cells. Myofibroblasts were also highlighted on the outer area of the capsule. Moreover, the myofibroblast layer with grade III contracture was significantly thicker than with grade IV contracture. (137) An examination of the H&E-stained tissue section under total polarized light highlighted birefringent materials (assumed to be silicone). (138, 139) 78% of the capsule adjacent to saline-filled Biocell-textured implants and analyzed by Lesesne *et al.* exhibited birefringent material. (138) Other studies observed extracellular silicone fragments (140), silicone-containing deposits (119), extravasated silicone or PU (141, 142) or silicone droplets (139, 143). Birefringent materials within multinucleated giant cells (138, 141), vacuolated histiocytes or macrophages (119, 140) were interpreted as an engulfment of silicone by these cells. The capsular thickness was also measured and was found to be correlated with the Baker score. (119, 136, 144) Prantl *et al.* even proposed a correlation between two scores of capsular contracture: the one clinically assessed (Baker grade) and the other histologically evaluated (Wilfingseder grade). (119) Moreover, a higher capsular thickness was associated with a higher number of silicone particles and silicone-loaded macrophages. The presence of synovial-like metaplasia (transformation of one differentiated cell type to another differentiated cell type) or hyperplasia (proliferation of cells) was also reported and found more frequently around textured implants. (144, 145) According to Wyatt *et al.*, an increase of the implant duration decreased the presence of the synovial-like metaplasia around both smooth and textured implants. (145) The density and alignment of collagen fibers were extensively analyzed. Thus, collagen fibers arranged parallel to the implant surface were more often observed around smooth implants than around textured implants after 5 years. (145) Moreover, an increasing implant duration

reduced the dense collagenous architecture and the parallel orientation of collagen fibers around textured implants (145) and around smooth implants (146). The collagen fiber alignment was found even sometimes non-uniform around an implant, especially between the plane surface and the concave surface of the implants. (146) Prantl *et al.* summarized the histological structure of periprosthetic capsule as a 3-layer structure (119) (Fig. 6):

- The first layer constituted of macrophages, fibroblasts and in some cases synovial-like metaplasia
- The second layer characterized by a loosely arranged connective tissue and by an internal vascular supply
- The third layer contained a dense connective tissue and an external vascular supply

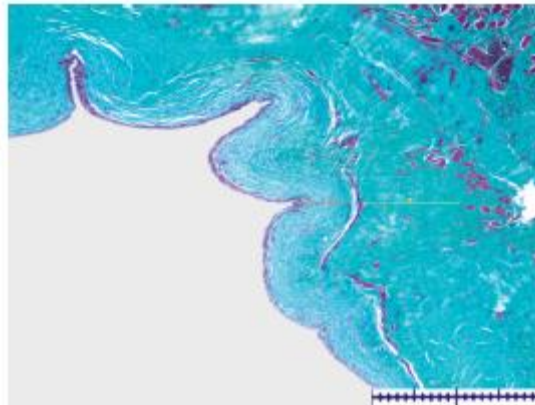


Figure 6 : Three-layer composition of a periprosthetic capsule (Masson Goldner stain; magnification: x4). (119)

Calcification was also reported in 25% of the capsules. The high degree of capsular contracture was associated with the presence of capsular calcification. (142)

1.6.3.2. IMMUNOSTAINING

Some histological analyses of the periprosthetic capsule were completed by immunohistochemical staining of the cell immune-phenotypes. (147, 148) Thus, activated T-helper cells and macrophages were detected beneath the contact zone as well as perivascularly, whereas histiocytes represented a minor cell component. Moreover, textured implants elicited a more marked T-cell response than smooth implants, with a similar proportion of T-helper and T-cytotoxic cells.

Immunohistochemistry also revealed that TGF-beta was present in all the capsules analyzed, identified two additional recurrent rearrangements (DUSP22 and TP63 rearrangements) and confirmed that the JAK-STAT3 signaling pathway was activated in all the cases tested. (42, 149) Recently, Walker *et al.* co-localized the fluorescent pattern obtained by immunostaining of host proteins (such as collagen and fibrinogen) with a bacterial fluorescent pattern in order to image the potential bacterial binding ligands on the implant surface. (117) *Staphylococcus epidermidis* predominantly co-localized with collagen, while group B streptococci and *Klebsiella pneumoniae* co-localized with fibrinogen.

1.6.3.3. CHEMICAL AND SURFACE ANALYSES

Chemical and surface analyses were performed on biological and prosthetic specimens. Rudolph *et al.* used Transmission Electron Microscope (TEM) and SEM to detect silicon around breast implant via energy dispersive X-ray analysis. (150) Silicone and other foreign materials (such as PU and Dacron) were also identified in surrounding tissues with a Raman microprobe. (151) A quantitative measurement of silicone in breast tissue was performed with an atomic absorption spectroscopy. (139) Thus, silicon was identified in half the tissue specimens (and only around gel-filled implants) by X-ray analysis and in all the capsules surrounding gel-filled implants by Raman microprobe. Likewise, PU and Dacron were detected in all the capsular tissues enveloping PU-coated and Dacron-patched gel-filled implants respectively. Moreover, on the 49 breasts with unruptured prostheses analyzed by Thomsen *et al.* (139), a positive relation between the concentration of silicone in the capsular tissue and the inflammatory reactions was determined, contrary to Siggelkow *et al.* (144). Del Rosario *et al.* observed in tissue sections the ultrastructure of cells with TEM and performed Electron Probe X-ray microanalytic studies to determine a more precise location of silicon in the capsular tissue. (152) Thus, high concentration of silicon was detected within phagocytic cells and in the collagen stroma of the breast implant capsules. Interestingly, all the cases featuring synovial-like metaplasia demonstrated abundant silicone particle deposition.

Legrand *et al.* led complementary X-ray and Nuclear Magnetic Resonance (NMR) investigations on calcifications observed in the vicinity of old breast implants (especially on those manufactured prior to the mid-eighties) removed for detected

ruptures and/or grade IV capsular contracture. (153) Micro-analyses confirmed the presence of calcium and silicon for all samples and a bone-like hydroxyapatite structure. These large crystals were detected either in contact with breast implant or in deeper collagen layers of the capsule.

Amoresano *et al.* performed chemical analyses on the gel extracted from explanted breast implants via Fourier Transform infrared spectroscopy (FTIR) and gas-chromatography mass spectrometry (GC-MS). (154) Thus, these analyses revealed the presence of organic substances (such as fatty acid) in very low concentration in all the samples and therefore the possibility of bioaccumulation and tissue contamination of the gel.

Some authors visualized the surface of the capsule in contact with the implant by SEM. (88, 89, 152, 153, 155) Danino *et al.* was one of the first suggesting on the basis of microscopic images of the capsule that the capsules enveloping Biocell or CUI textured implants “*present a mirror image with correspondence of the depressions on the prosthesis and contacts on the capsule*”. (89) This effect – called “Velcro effect” – was not present with Arion or Sebbin textured implants. (Fig. 7) From these examinations, Danino *et al.* proposed the hypothesis of a critical size of the pores, which would elicit tissue ingrowth inside the pores and therefore the “Velcro effect”. Consistently, this capsular characteristic was also found along the surface of the inner capsule in the case of double-capsules around Biocell-textured implants.

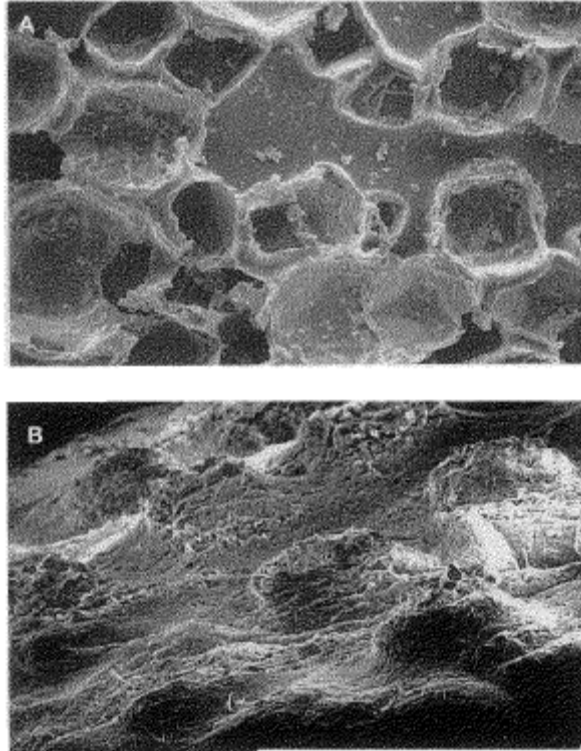


Figure 7 : « Velcro effect ». A : implant surface (Biocell). B : capsule surface. (SEM ; magnification : x50)(88)

1.6.3.4. MICROBIOLOGICAL ANALYSES

Microbiological analysis was firstly performed in order to establish a correlation between the degree of capsular contracture and bacterial presence on explanted breast implant surface (156-158) and in capsular tissue (142, 159). "Routine" culture methods were used, as well as special culture technique designed to recover bacteria adhering and encased in biofilm. Basically, this technique consisted in prolonged incubation with continuous agitation and in some cases with maceration/sonication (159) or vortexing/sonication (160). Then, both removed breast implant surface and capsular tissue were cultured. Thus, bacteria were significantly more detected on samples obtained from patients with contracted capsules than from patients with non-contracted capsules (156-161), contrary to the conclusions of Poppler *et al.* (162). The predominant isolate was Coagulase Negative species, mainly the *Staphylococcus epidermidis* group. (156, 157, 159) Pajkos *et al.* also determined that the presence of Coagulase Negative species was significantly associated with capsular contracture. (159) Other microorganisms were also isolated, such as *Propionibacterium* species

(158, 160, 161), *Corynebacterium* species (160), *Staphylococcus aureus* and *Escherichia coli* (161).

Bacterial culture may be coupled with real-time quantitative PCR technique (117), in order to quantify the total number of bacteria in the periprosthetic capsule via the 16S rRNA gene (64) and to identify bacterial species on breast implants and tissues via Next-Generation Sequencing (NGS) technique and more particularly pyrosequencing of the 16S rRNA gene (64, 117). Walker *et al.* confirmed that the predominant bacteria identified on samples from patients with capsular contracture was *Staphylococcus epidermidis*. (117) Moreover, Hu *et al.* demonstrated a different microbiome between BIA-ALCL samples and high-grade contracted capsule samples. (64) Thus, there was a significantly greater proportion of *Ralstonia pickettii* present in BIA-ALCL and contralateral breast specimens compared with high-grade contracted capsule specimens. Conversely, significantly more *Staphylococcus epidermidis* were found associated with high-grade contracted capsule specimens. However, they observed a similar total number of bacteria on BIA-ALCL samples and on high-grade contracted capsule samples (approximately $4.7\text{-}4.9 \times 10^6$ cells/mg tissue). Regarding benign cases, Walker *et al.* identified a different microbiome on clinically normal breast implants (colonized by only Gram-positive bacteria and specifically Coagulase Negative Species) and on clinically normal tissue expanders (colonized by a broader array of Gram-positive and Gram-negative bacteria).

Alternatively, SEM was used to image bacteria and biofilm on capsular and prosthetic biopsies. (Fig. 8) (64, 156, 159) The presence of bacteria was therefore confirmed by SEM on implants. (156) Biofilm was observed on the samples from patients with capsular contracture (64, 159) and without capsular contracture (159) and on the BIA-ALCL samples (64).

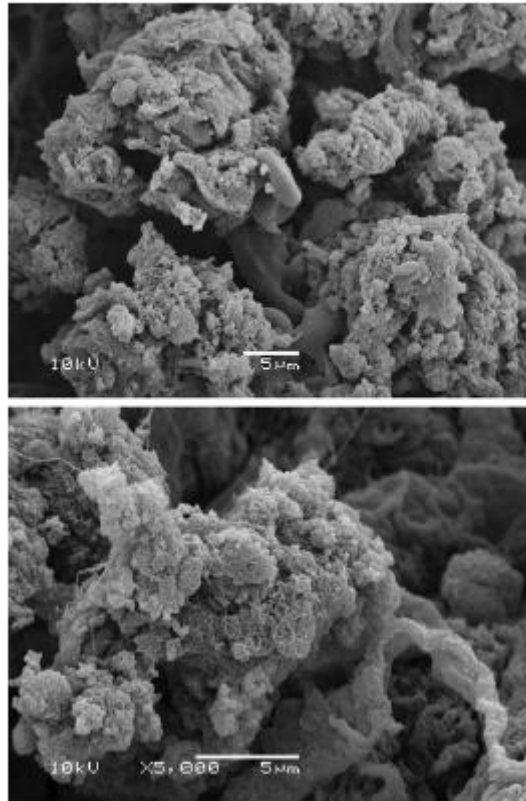


Figure 8 : Biofilm imaged in capsule specimens (SEM images; magnification: x5000)(64)

Moreover, biofilm was quantified by using the semi-quantitative scale of Van Heerden. (155) This technique consists in grading the area of biofilm coverage present on breast implant samples through SEM examination with a constant magnification.

1.6.3.5. PROTEIN EXPRESSION ANALYSES

Protein expression was quantified either directly or through retro-transcriptomic analysis. Thus, protein expression contained in biological samples, such as capsular tissue (163) and periprosthetic effusion, blood serum and blood plasma from patients with BIA-ALCL (164), was directly quantified by ELISA. More precisely, Wolfram *et al.* (2012) profiled the cytokines present in the supernatant of cultured intracapsular T-cells and determined an expression pattern consistent with a T-helper 1 or T-helper 17 immunophenotype. Hanson *et al.* demonstrated a positive detection of soluble CD30 in all BIA-ALCL effusion specimens, whereas the detection was negative or weak in BIA-ALCL serum specimens or in BIA-ALCL plasma specimens. (164)

Additionally, retro-transcriptomic studies were led by Kyle *et al.* (165) and Ulrich *et al.* (166) on both contracted and non-contracted capsular tissues. Before the qPCR assay, Kyle *et al.* performed a whole genome array analysis in order to discriminate the most dysregulated genes in contracted capsules, compared to normal capsules. Thus, the genes aggrecan, TIMP4 (Tissue Inhibitor of Metalloproteinase) and TNFSF11 (Tumor Necrosis Factor ligand Superfamily member) were significantly down-regulated in contracted capsules. Conversely, the genes MMP12 (Matrix Metalloproteinase), SAA1 (Serum Amyloid A) and IL8 were significantly up-regulated. These genes are either involved in the structure or in the degradation and the remodeling of the Extra-Cellular Matrix (ECM) (such as the genes aggrecan, TIMP4 and MMP12), or in the inflammatory reaction or in the recruitment of inflammatory or immune cells (such as the genes TNFSF11 and SAA1). Ulrich *et al.* studied more precisely the expression of a panel of genes mediating the remodeling of the ECM, according to the type of breast implant surface. The expression of MMP2 was significantly up-regulated in capsular tissues from patients with grade II/III/IV capsular contracture in comparison to grade I. This significant up-regulation was only observed with textured implants. Conversely, the up-regulation of TIMP1 and TIMP2 was significant with both smooth and textured breast implants. Then, the authors computed the MMP/TIMP ratio and concluded that the ratio was significantly lower in tissue from patients with a high degree of capsular contracture in comparison to those with grade I, whatever the type of breast implant surface. (163)

1.6.3.6. MOLECULAR BIOLOGY

NGS techniques, such as Whole Exome Sequencing (WES), were applied to screen the genetic mutations present in the effusion fluid and bone marrow (48) and in the capsules (42) of patients with BIA-ALCL. Thus, three genetic aberrancies resulting in the activation of the JAK/STAT3 pathway were reported.

Fluorescent In-Situ Hybridization (FISH) technique was also performed to confirm the presence of *Ralstonia pickettii* on BIA-ALCL samples.

1.6.3.7. BIOMECHANICAL ANALYSES

Biomechanical analyses were performed on capsular samples. The contractile ability of dissected capsule specimens was demonstrated by exposure with smooth-muscle

stimulants and relaxants. (167) Quantitatively, capsular tissues from 69% of the patients responded to smooth-muscle relaxants and 75% responded to smooth-muscle stimulants. Then, Hwang *et al.* measured the capsule tensile strength in a saline solution and determined that the tensile strength of the capsule was correlated positively with the degree of capsular contracture. (137) Moreover, the tensile strength in the myofibroblast negative group was significantly higher than in the positive group. More recently, on the basis of mechanical tests Ben Amar *et al.* implemented two mechanical models of the capsular tissue according to the Baker grading. (168) Thus, Baker grade I samples were modeled as an anisotropic material with well-oriented fibers, whereas the orientation effect was lost for Baker grade III samples.

1.6.3.8. MECHANICAL, CHEMICAL AND SURFACE ANALYSES ON RETRIEVED IMPLANTS

Several studies were led to assess the in-situ ageing of breast implants. Amoresano *et al.* (2016) performed similar mechanical tests as previously on implanted and non-implanted prostheses and reported a greater deformation on explanted outer shell samples than on the virgin materials, suggesting an *in vivo* mechanical weakening of the outer shell. (154) Bodin *et al.* led the analyses according to the ISO 14607 standard and determined that the breaking strength, the breaking stress and the elongation at break decreased with the implantation duration. (169) Tortolano *et al.* performed chemical analyses by GC-MS on saline-filled expanders, which allowed to study the release and the penetration of chemical substances of the shell without the impact of the silicone gel. (170) Thus, the authors detected cholesterol and fatty acids on all the shells and identified siloxanes in the saline solution. These chemical changes could explain the mechanical ageing of the shell. The first article, which suggested wear of the breast implant shell and therefore a release of silicone particle from the shell, was Danino *et al.* (88) They reported micrometric silicone particles released from Biocell-textured implant and embedded in the capsular tissue. A simulation was published by Ramiao *et al.*, who led an *in vitro* degradation process in a buffer solution at pH 7.4 and pH 4.0 and at a controlled temperature of 37°C according to the ISO 10993 standard (Biological Evaluation of Medical Devices). (171) Thus, they observed by SEM no morphological alteration of the textured breast implant surface over a period of 12 weeks.

CHAPTER II: MEASUREMENT INSTRUMENT AND MULTI-SCALE ANALYSIS

According to the manufacturers, the breast implant outer shells feature very different and characteristic states of surface. Some surfaces exhibit “pores” or “peaks” or “fibrils”. (see section 1.3.4) Before discussing the biological and clinical impact of these states of surface, a thorough characterization of these topographies is of primer importance. Firstly, an appropriate and validated methodology of measurement must be chosen. Thus, numerous instruments, such as SEM, laser confocal microscope or X-ray Micro-tomography, were used in the literature to measure breast implant surfaces. Moreover, the sampling and the sample size of these studies were inconsistent, which provided discrepant results. (see section 1.3.3) In order to have a robust characterization of surface and to be able to extrapolate and compare outcomes from other studies, a unique methodology (in term of instrument, sampling, sample size and cleaning) must be commonly adopted. In order to be validated, the methodology must be based on comparative studies of several instruments. Before our article published in June 2017 (which is presented below), no multi-instrument analysis was led to validate the choice of instruments. Moreover, as the biological mechanisms of interest involves several entities which have a very wide range of dimension, the analysis must be also led on a representative range of scale. This approach was considered by Barr *et al.* (97), who captured by SEM different surface areas of a same sample.

Recently, a new update of the standard relative to breast implant (ISO 14607: 2018) was released in May 2018 and proposes in an informative Annex a more complete methodology of measurement than previously. Thus, the standard requires for every type of surface (smooth or textured) a sampling of 15 measurements over 4mm² repeated on three different implants and propose four different instruments: SEM with a 2D or 3D reconstruction software, Laser confocal microscope, Interferometer or AFM. SEM with a 3D reconstruction software and more generally the methodology of the standard was grossly applied in the report mandated by the ANSM. (<https://ansm.sante.fr/S-informer/Points-d-information-Points-d-information/Surveillance-des-implants-mammaires-par-l-ANSM-publication-d-un-avis->

[d-experts-de-CSST-et-d-une-etude-sur-la-texturation-Point-d-information](#)) However, they restricted their analysis to only 9 measurements per implant and only measured 2.5mm² for implants featuring no or a slight texture.

The purpose of this chapter is to discuss the choice of measurement instrument according to the type of surface (such as “smooth”, “microtextured” or “macrotextured” surface). A multi-scale analysis was then designed to compare the instruments over a characteristic range of scales.

2.1. MULTI-SCALE ANALYSIS

A such comparison between Interferometer, Focus variation microscope and X-ray Micro-tomography was published between the different surfaces of Sebbin breast implant (Sebbin shaped textured implant, Sebbin round textured implant, Sebbin round microtextured implant and Sebbin round smooth implant), which is one of the most comprehensive portfolio of surface among manufacturers. (article below) The sampling specified in the ISO 14607: 2009 (i.e. 9 measurements over 4mm² on a single implant), which was in force at the time of the publication, was applied. The multi-scale analysis was led on the five metrological parameters stipulated in the ISO 14607:2018 (i.e. Sa, Sq, Sz, Sku, Ssk). The measurement principles and the settings of apparatus as well as the multi-scale decomposition of topographies were also explicated in the article. *In fine*, this comparison shed light on some limitations of Micro-tomography and Focus variation microscope, compared to Interferometry.

Surface Topography: Metrology and Properties



PAPER

A multi-topographical-instrument analysis: the breast implant texture measurement

RECEIVED
16 November 2016

REVISED
14 April 2017

ACCEPTED FOR PUBLICATION
11 May 2017

PUBLISHED
12 June 2017

Charles Garabédian^{1,2}, Rémi Delille¹, Raphaël Deltombe¹, Karine Anselme³ Michael Atlan⁴
and Maxence Bigerelle¹

¹ LAMIH, UMR CNRS 8201, UVHC, Valenciennes, France

² Groupe Sebbin SAS, Boissy l'Aillerie, France

³ IS2M, Mulhouse, France

⁴ UPMC Faculté de Médecine, Paris, France

E-mail: charles.garabedian@laboratoires-sebbin.fr

Keywords: breast implant, texturation, roughness

Abstract

Capsular contracture is a major complication after implant-based breast augmentation. To address this tissue reaction, most manufacturers texture the outer breast implant surfaces with calibrated salt grains. However, the analysis of these surfaces on sub-micron scales has been under-studied. This scale range is of interest to understand the future of silicone particles potentially released from the implant surface and the aetiology of newly reported complications, such as Anaplastic Large Cell Lymphoma.

The surface measurements were accomplished by tomography and by two optical devices based on interferometry and on focus variation. The robustness of the measurements was investigated from the tissue scale to the cellular scale.

The macroscopic pore-based structure of the textured implant surfaces is consistently measured by the three instruments. However, the multi-scale analyses start to be discrepant in a scale range between 50 μm and 500 μm characteristic of a finer secondary roughness regardless of the pore shape. The focus variation and the micro-tomography would fail to capture this roughness regime because of a focus-related optical artefact and of step-shaped artefact respectively.

1. Background

The fifth-generation breast implant outer surface in contact with biological tissues features an irregular texture supposed to stimulate tissue adherence on the implant and subsequently to avoid an anatomical misplacement of the prosthesis [1]. The pore size and pore depth ranges reported by Atlan *et al* [2] are in table 1.

Moreover, more and more clinical evidence is in favor of a texturation on implant surfaces to reduce the capsular contracture occurrence [3]. This complication results from the development of a thick and firm biological layer namely capsule around the implant [4]. Severe capsular contractures are responsible for implant distortion and therefore for patient discomfort, breast pain and poor aesthetic outcome [3].

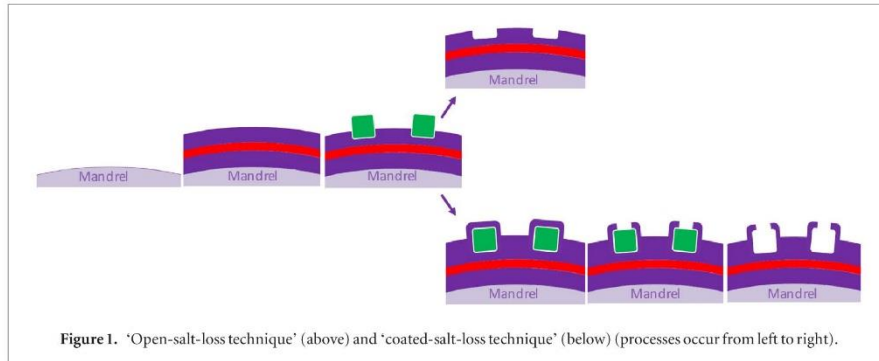
Another complication, namely Breast Implant Associated-Anaplastic Large Cell Lymphoma (BIA-ALCL), draws the attention of sanitary agencies in the

world because the case figures reported by Brody *et al* [5] have sharply increased since 1997. No case of BIA-ALCL has been reported on the Sebbin implants. The aetiology of this cancer type remains purely speculative, however 'the fluid associated with ALCL tended to be cloudy and debris filled' [5]. Danino *et al* [6] points out the micron-sized silicone particle presence in the capsule. Moreover, other newly reported complications were raised from so-called 'macro-textured breast implants', such as late seromas or double capsules [7].

According to Whitehouse [8], 'all structured surfaces are specifically designed to meet a specific functional requirement'. For implanted devices, the surface functionality is in term of biological integration. Specific biological entity targeting is the 'gold-standard' to promote implant integration. Therefore, interfaces between implanted devices and the host are ideally structured on different length-scale ranges according to the biological targets. For example, the tissue response modulation has to be performed on an approximate

Table 1. Pore sizes of two breast implant textures from [2].

	Pore size	Pore depth
Biocell® (Allergan Medical Corporation, Santa Barbara, California)	100–400 μm	100–200 μm
Sebbin anatomically-shaped implant texture (Boissy l'Aillerie, France)	150–600 μm	100–200 μm



scale of 300 μm , as reported in the literature relative to bone ingrowth promotion and consequently tissue integration of joint replacement [9]. Conversely, the characteristic scale involved in the sensing of nanometric spatial patterning by molecular mechano-sensors responsible for cell attachment on a substrate is around 3 μm [10, 11].

However, the reported measurement protocols of these interfaces were performed only at the scale of the surface target. A screening of measurement scales between the tissue scales and the cellular scales is understudied in the literature. Regarding breast implant surfaces, this analysis is all the more challenging because of the wide gap between the biological scales. Therefore, in a multi-instrument approach aiming at encompassing the scales from the pore size scale to the silicone particle scale, the accuracy of the measurement instrument will depend on the scale. Only a multi-scale analysis will be of value to compare the robustness between the measurement instruments.

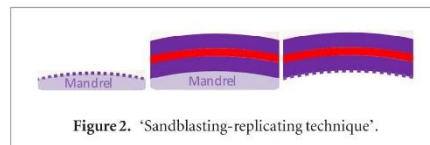
2. Materials and methods

2.1. Sample preparation

Three Sebbin brand implants featuring three different textures as well as a Sebbin smooth implant were studied.

The Sebbin company uses three processes to texture their implant. The first texturation process based on a salt-loss technique pits the last silicone layers of cuboid pores with calibrated salt crystals. Then the salt is removed in a water bath (figure 1).

Alternatively, the process is extended by covering the silicone surface imprinted of salt with a last silicone layer. After curing, this layer is washed away (figure 1).



Finally, the texturation is also obtained by moulding silicone layers on a sandblasted mandrel (figure 2).

In respect to the International Standard [12] relative to breast implants, three sample sets were peeled from the dome, the radius and the base of the implant shell, each set consisting of three 3 mm-diameter samples. The samples were sonicated in a 10% alcoholic solution during 10 min.

The surface of interest in each sample is the 2 mm-side square inside the circular sample.

2.2. Surface characterizations

To encompass a large wavelength range, measurements were performed with x-ray micro-tomography (Skyscan™ 1172, Bruker, Billerica, USA), two optical devices, namely the White-Light Interferometer (NewView™ 7300, Zygo, Middlefield, USA) and a Focus variation microscope (Infinite Focus™, Alicona Imaging GmbH, Grambach, Austria) and a Field Emission Gun-Scanning Electronic Microscope (JEOL 7100F TTLS, Tokyo, Japan).

2.2.1. X-ray micro-tomography.

The micro-tomography scan is a Skyscan™ 1172 with a resolution of 2.50 μm and a x-ray source at 80 kV and 100 μA . The scans are imaged on a 4K \times 2K pixel CCD camera

The reconstruction of scans to a stack of cross-sections along the z-axis was performed after filtering

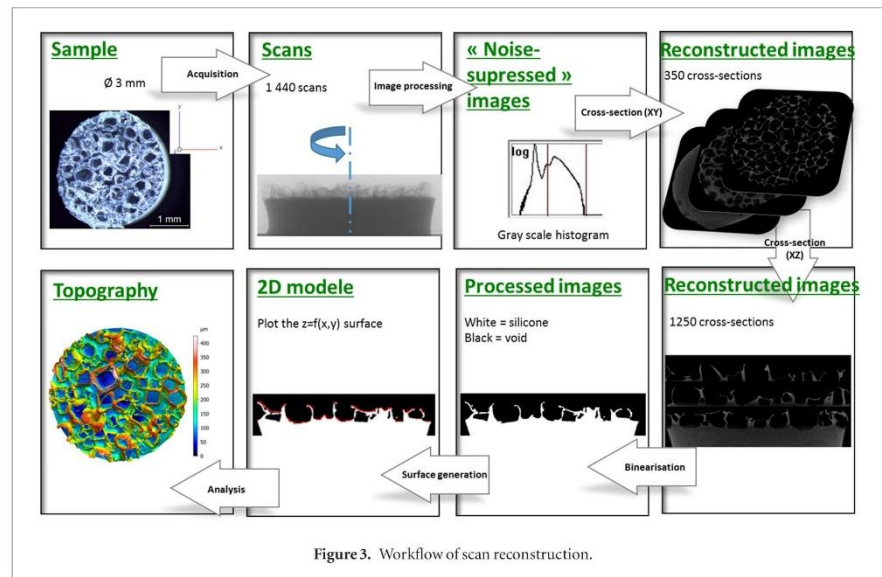


Table 2. Optical settings of White-Light Interferometer and Alicona Infinite Focus™ microscope.

Measured surfaces	Interferometry		Focus variation	
	Textured implant surface	Smooth implant surface	Salt-based textured implant surface	Sandblasted-replicated and smooth implant surface
Objective	50×	100×	10×	50×
Vertical resolution	10 nm	10 nm	1 μm	210 nm
Lateral resolution	0.52 μm	0.32 μm	6.52 μm	4 μm

the noise peak. This stack is converted to a file of cross-sections in the (xy) plane. After binarization of the cross-sections, the topography is obtained by capturing the most outer point for each (x, y) position in a matrix (figure 3).

2.2.2. White-Light Interferometer and Alicona Infinite Focus™ microscope.

The interferogram bucket is imaged on each pixel of a black and white 640×480 pixel CCD camera. Each individual surface is gathered according to the stitching method [13]. The stitching matrix of interferograms consists of 15×20 images and the overlapping is 20%. To measure all the textures, the scan length of the electric Z-device has to be extended as high as $800 \mu\text{m}$.

The focus variation was computed under a ring light source.

For the two instruments, the choice of the objective and the resulting lateral and vertical resolutions are summarized in the table 2 according to the texture type.

2.2.3. Field Emission Gun-Scanning Electronic Microscope (FEG-SEM).

The samples were pinned to the stage. The acceleration voltage is 1 kV and the working distance is approximately 15 mm.

3. Results

3.1. Surface topographies

The texture morphologies measured by the three instruments are similar (figures 4). Remarkably, sub-micrometric smooth droplets seem to spread on the smooth implant surface (figure 4(A)). The salt-based topographies exhibit randomly-arranged cuboid depressions. The open pores walls are thinner and higher in the 'coated-salt-loss texture' than in the 'open-salt-loss texture' (figures 4(B) and (C)). Many random peaks of maximal $100 \mu\text{m}$ height feature the 'sandblasting-replicating texture' (figure 4(D)).

In respect to the International Standard [12], Scanning Electronic Microscope (SEM) images were also performed to capture the three textures (figure 5).

3.2. Multi-scale analysis

In this study, all surfaces were flattened by a third degree polynomial fit to remove the form of the surface (Mountains Digital Surf™, Besançon, France). No post-measurement sampling and no refilling procedure was applied.

By applying High-Pass filters of lower and lower cut-off wavelengths to the surface, finer and finer

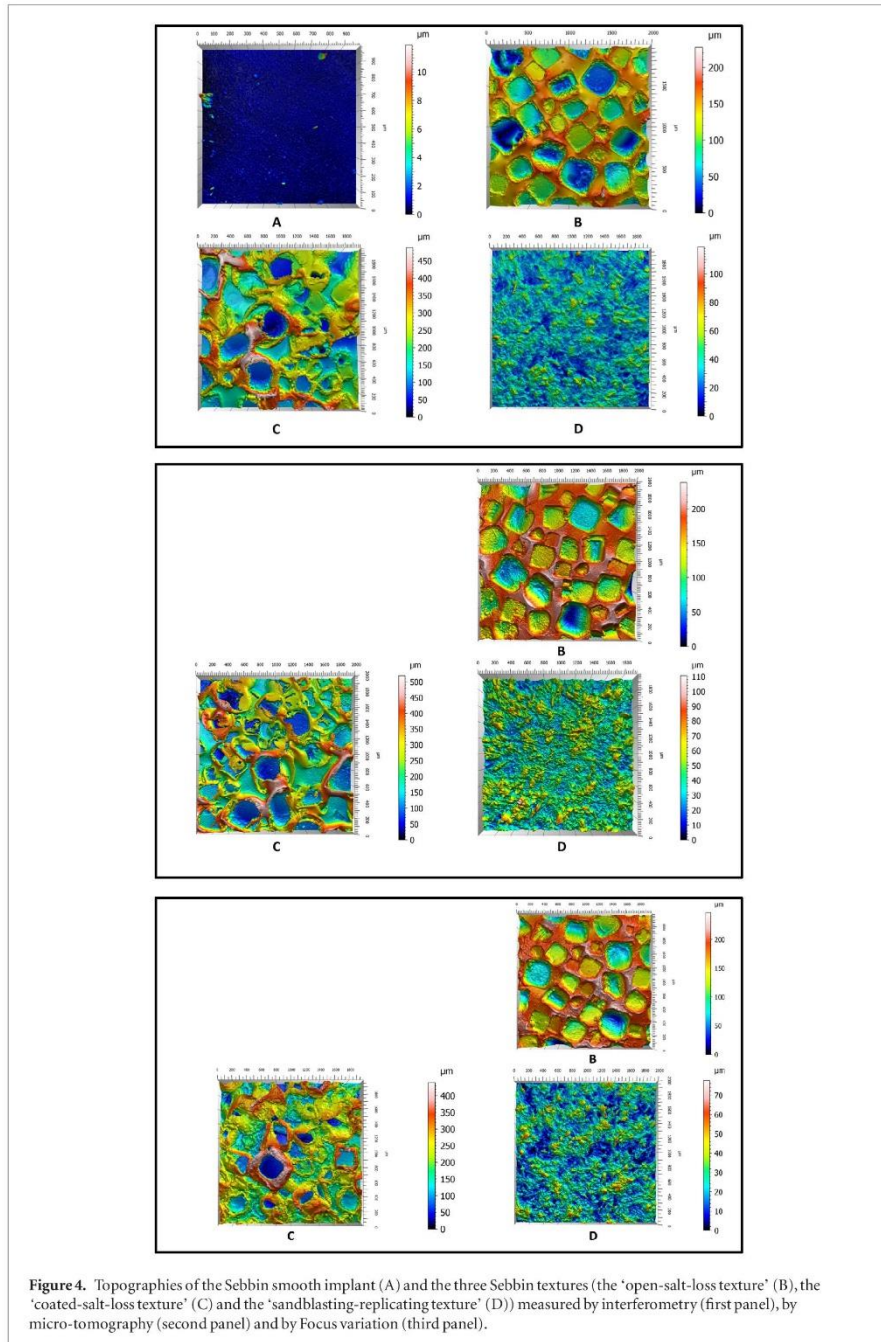


Figure 4. Topographies of the Sebbin smooth implant (A) and the three Sebbin textures (the 'open-salt-loss texture' (B), the 'coated-salt-loss texture' (C) and the 'sandblasting-replicating texture' (D)) measured by interferometry (first panel), by micro-tomography (second panel) and by Focus variation (third panel).

roughness is isolated from the surface and smaller and smaller scales are therefore captured. Firstly, the 3D arithmetic mean height (S_a) was computed on each filtered surface. This processing was implemented on the set of nine surfaces measured at different locations on

the prosthesis, resulting in the below multi-scale curves (figure 6).

The S_a was retained as a first parameter for the multi-scale analysis, from which an insight on the frequential content of the surface can be drawn.

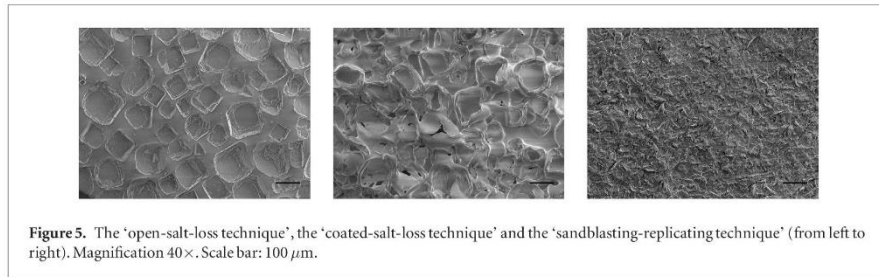


Figure 5. The ‘open-salt-loss technique’, the ‘coated-salt-loss technique’ and the ‘sandblasting-replicating technique’ (from left to right). Magnification 40×. Scale bar: 100 μm.

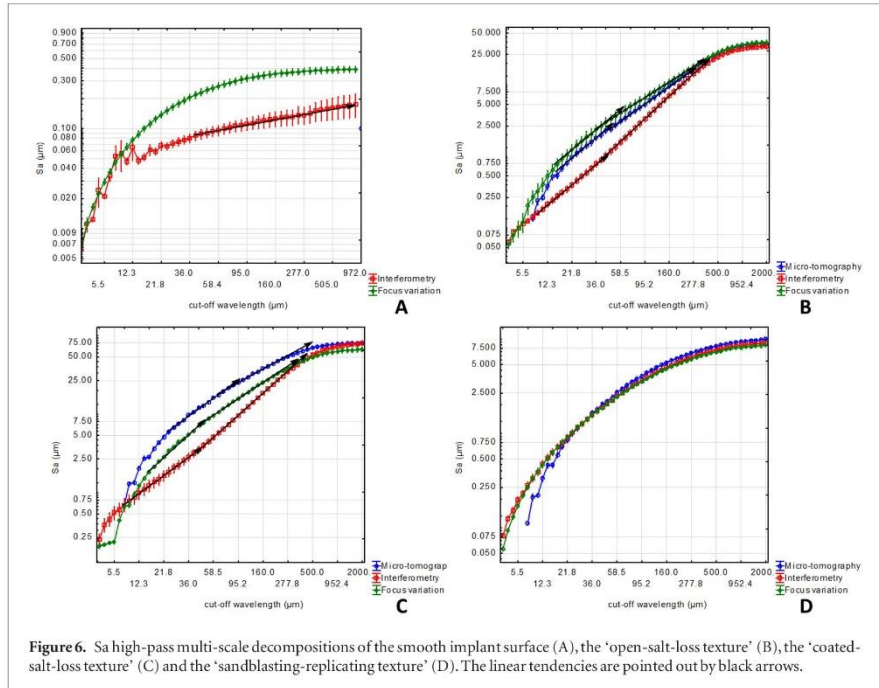


Figure 6. S_a high-pass multi-scale decompositions of the smooth implant surface (A), the ‘open-salt-loss texture’ (B), the ‘coated-salt-loss texture’ (C) and the ‘sandblasting-replicating texture’ (D). The linear tendencies are pointed out by black arrows.

3.2.1. Smooth implant surfaces.

A linear evolution—the hallmark of fractal regime—characterizes the curve measured on the smooth implant surface by Interferometry on scales superior to 40 μm (figure 6(A)). If the linear slope is mentioned H (Hurst exponent), the fractal dimension is then given by (1).

$$\Delta = 2 - H \tag{1}$$

Practically, a fractal surface exhibits the same pattern on several scales. The figure 7(A) highlights the wide range of droplet sizes on the smooth implant surface measured by interferometry microscope, contrary to the one measured by Focus variation (figure 7(B)).

Fractal structures are expected to maintain their height-diameter ratio over length scales. Wolf pruning method [14] was implemented on all filtered smooth implant surfaces with screening of minimal height motif, ranging from 0.1% to 10% of the maximal peak height (S_z). If the peak height of each motif is plotted

in function of the peak equivalent diameter in log–log scale (figure 8), the peak fractal dimension is determined as previously (1) with the slope H [15].

As highlighted in the figure 8, both curves exhibit three behaviours:

The first stage features the scales inferior to 22 μm and 14 μm, as shown respectively by the Focus variation-related curve and the Interferometry-related curve. The fractal dimension is equal to 2. Under this threshold, topographical instruments fail to measure topography. At this small scale, the output signal from the instrument is a noise. Subsequently, the watershed algorithm results in a noise discretization. Moreover, by considering these thresholds as the instrument lateral resolutions, the Focus variation lateral resolution is approximately twice less precise than the Interferometry one (22 μm and 14 μm respectively). Remarkably, this ratio is consistent with the apparatus settings since the surface is imaged with a 100× and a 50× objective, respec-

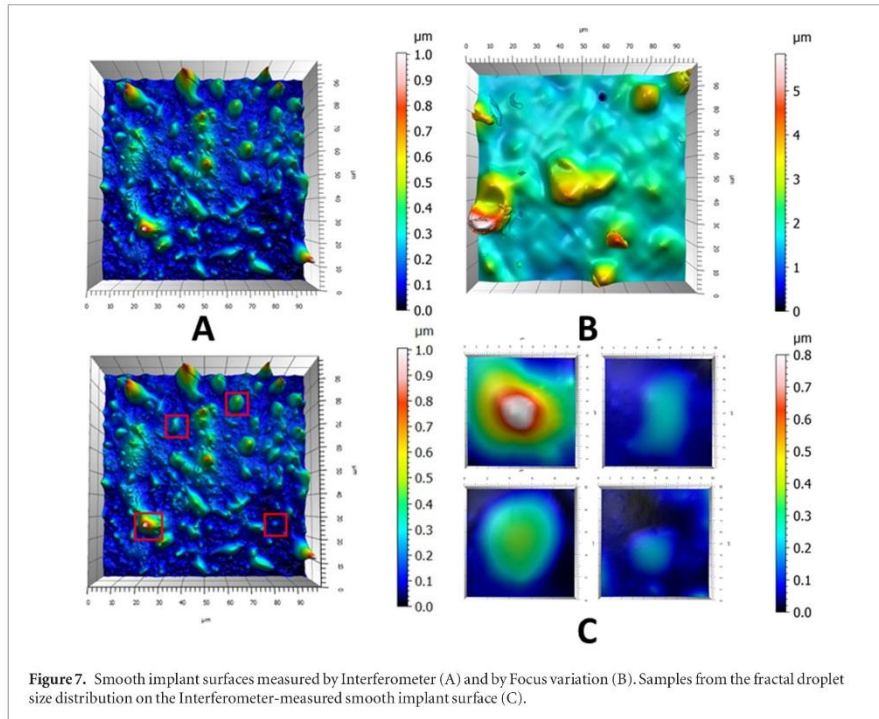


Figure 7. Smooth implant surfaces measured by Interferometer (A) and by Focus variation (B). Samples from the fractal droplet size distribution on the Interferometer-measured smooth implant surface (C).

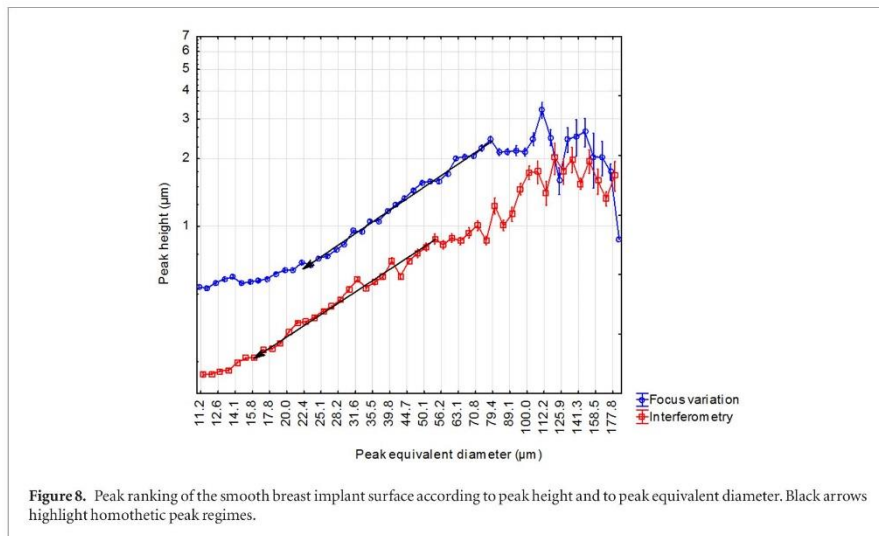


Figure 8. Peak ranking of the smooth breast implant surface according to peak height and to peak equivalent diameter. Black arrows highlight homothetic peak regimes.

tively in Interferometry and in Focus variation, resulting in the respective finest lateral resolutions $0.32 \mu\text{m}$ and $0.64 \mu\text{m}$.

The second stage ranges from $22 \mu\text{m}$ to $80 \mu\text{m}$ and from $14 \mu\text{m}$ to $50 \mu\text{m}$, respectively for the Focus variation and the Interferometry. Both curves exhibit a slope equal to 1. As a result, peak shapes are Euclidian and not fractal. Practically, a range of homothetic

peaks was measured by Interferometer and by Focus variation over these scales. Interestingly, the Focus variation measurement shifts this range to 100% upward in height and to 20% upward in diameter. The overestimation of the peak size resulting from the Focus variation measurement might be an optical artefact. By diffusing extensively light, silicone would enlarge the focus in height and in diameter compared to the real

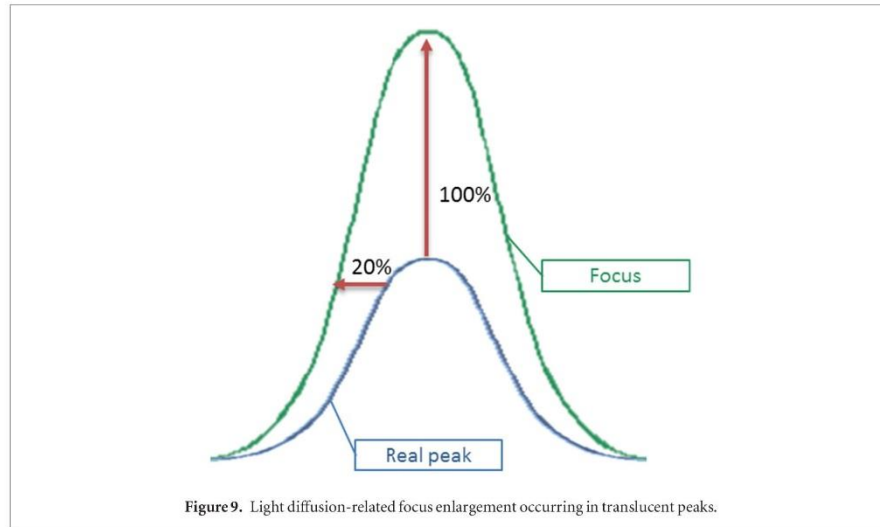


Figure 9. Light diffusion-related focus enlargement occurring in translucent peaks.

Table 3. Multi-scale parameters characteristic of the salt-based textured surfaces.

		'Open-salt-loss texture'		'Coated-salt-loss texture'	
		Hurst exponent	Lower boundary (μm)	Hurst exponent	Lower boundary (μm)
Interferometry	Second regime	0.052	35.594	0.124	45.512
	Third regime	0.023	10.593	0.075	9.762
Micro-tomography	Second regime	0.061	47.992	0.175	73.619
	Third regime	0.059	19.794	0.263	26.592
Focus variation	Second regime	0.066	40.824	0.146	46.626
	Third regime	0.074	21.669	0.173	16.004

peak (figure 9). Consequently, focalisation technique may fail to capture some translucent peaks.

The Focus variation and the Interferometry measurements start the third stage from $80\ \mu\text{m}$ and from $50\ \mu\text{m}$ respectively. The slope almost equal to zero means that peak heights remain approximately constant whatever the motif size. Therefore, the roughness correlation is completed.

3.2.2. Salt-based textured surfaces.

The multi-scale analyses of the 'open-salt-loss texturation' (figure 6(B)) and the 'coated-salt-loss texturation' (figure 6(C)) feature for each instrument 3 regimes. The Hurst exponent and the wavelength boundary values are reported for each regime in table 3.

The first stage includes scales superior to approximately $500\ \mu\text{m}$. This stationary regime is the hallmark of the macroscopic pores pitted by salt grains. As illustrated in the previously mentioned figures, the resulting measurements from the three instruments are robust to capture the salt-related macroscopic topography. This robustness between the instruments is all the more valuable as interferometric measurement captures a very reduced number of points on full sharp slopes.

The second stage is characteristic of scales between $50\ \mu\text{m}$ and $500\ \mu\text{m}$. Over these scales, roughness on

the bridging areas between the pits and on the bases of depressions is responsible for these fractal regimes. These surface features consist of silicone waviness and deformation and discrepancy in salt pitting depth. Interestingly, the Sa values are higher in the micro-tomography- and in the Focus variation-related curves than in the interferometric one. The small steps paving the micro-tomography-measured surfaces (figure 10) and the peak enlargement caused by a higher resolution in the Focus variation measurements, as mentioned previously, may be responsible for these higher Sa values.

The lower boundaries of the third stage are mentioned in the table 3 and represent the apparatus lateral resolutions. Therefore, once again the micro-tomography and the Focus variation lateral resolutions are much higher than the Interferometry one. These fractal regimes encompass the intrinsic elastomer roughness, regardless of grain shape.

3.2.3. 'Sandblasted-replicated surfaces'.

Surprisingly, no scaling law is identified on the 'sandblasting-replicating texturation'-related curves (figure 6(D)), although stochastic processes, like sandblasting, are the 'gold-standard' to manufacture a multi-scale surface. All sandblasting scales may not be imprinted on

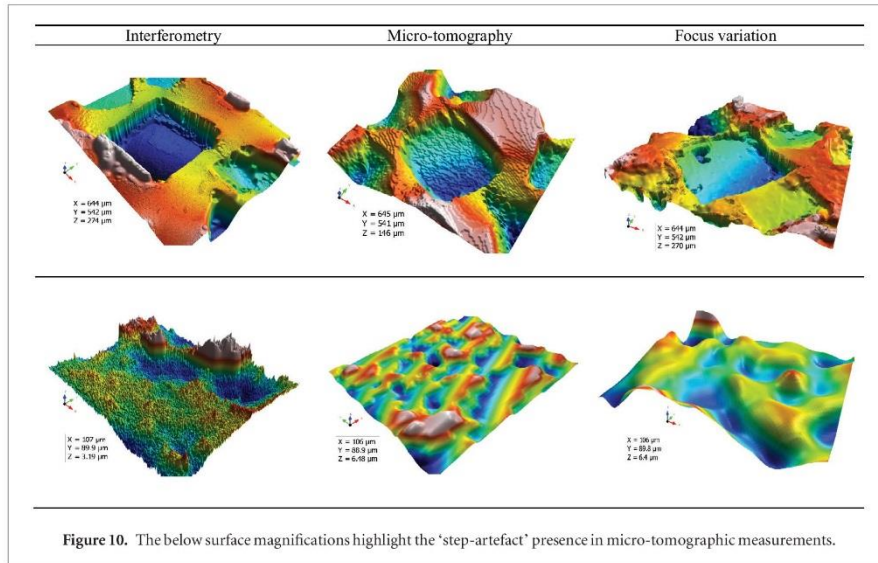


Figure 10. The below surface magnifications highlight the ‘step-artefact’ presence in micro-tomographic measurements.

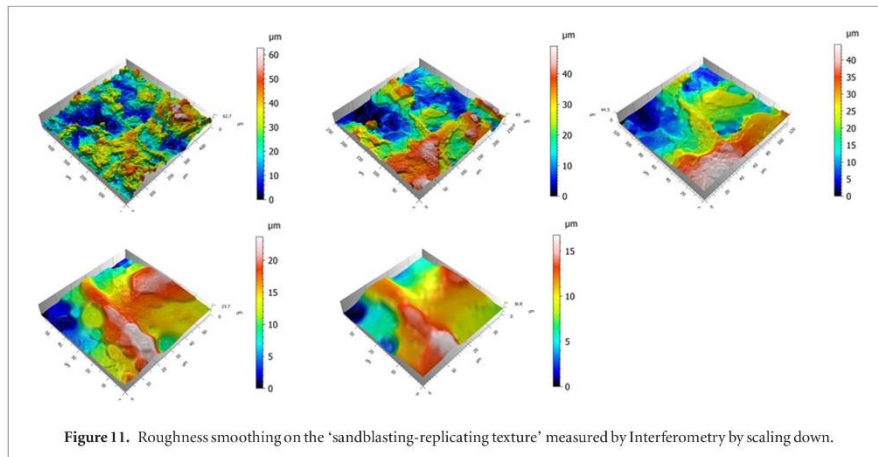


Figure 11. Roughness smoothing on the ‘sandblasting-replicating texture’ measured by Interferometry by scaling down.

the silicone replica (figure 11), resulting in roughness smoothing on the smallest scales.

3.3. Extension to other parameters

To refine the topographical characterization of such surfaces, a similar multi-scale procedure was implemented on four other height parameters: the root mean square height (Sq), the maximal height (Sz), the kurtosis (Sku) and the skewness (Ssk).

A linear correlation was established between the Sa and the Sq (figure 12) with a factor of 0.8. The factor was theoretically demonstrated on the 2D parameters [16]:

$$Ra = Rq \sqrt{\frac{2}{\pi}} \approx 0.8Rq. \tag{2}$$

The Sa and the Sz are also correlated (figure 12). Therefore, the approach led on the Sa may be easily extrapolated for the Sq and the Sz.

The multi-scale curves are in the figures 13 and 14 for the Sku and the Ssk respectively.

A scaling down of the smooth surface measured by Interferometer exhibits a decreasing Sku and Ssk to a length scale of 12 micrometers (figures 13(A) and 14(A)). Basically, the smooth surface features a range of isolated peaks. When the large scales are filtered, the highest peaks are less and less sharp (figure 15). Therefore, the Sku is expected to decrease during the filtering.

Moreover, the surface is more and more symmetrical because the peaks are less and less high, hence a reduction of the Ssk. Below the scale of 12 micrometers, the increases of the Sku and the Ssk are characteristic of the droplets described previously with a size range between 10 micrometers and 50 micrometers (figure 7). The Focus variation curves support the mentioned tendencies. However, the optical artefact of the focus is responsible for a downward shift of the values. Basically, as the peak base is wider, the Sku is lower.

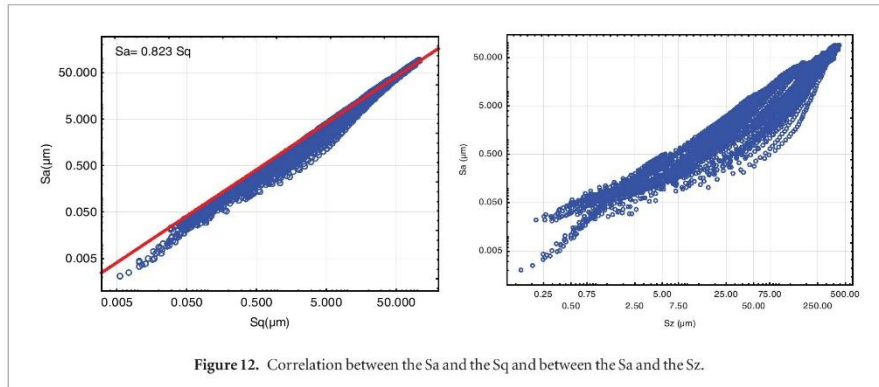


Figure 12. Correlation between the Sa and the Sq and between the Sa and the Sz.

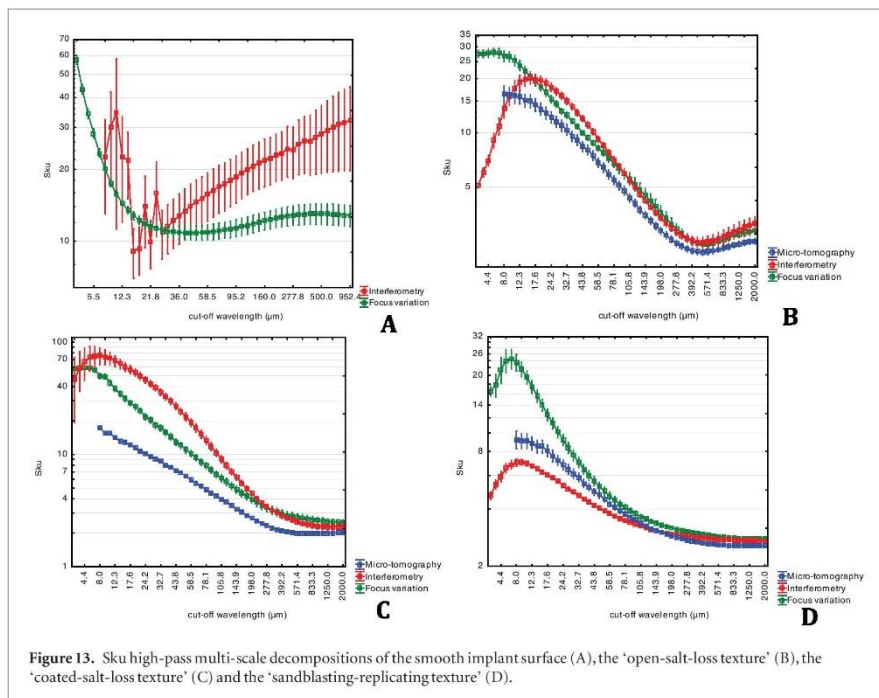


Figure 13. Sku high-pass multi-scale decompositions of the smooth implant surface (A), the 'open-salt-loss texture' (B), the 'coated-salt-loss texture' (C) and the 'sandblasting-replicating texture' (D).

For the two salt-based textured surfaces, the multi-scale curves of the Sku are similar for the three instruments (figures 13(B) and(C)). The scale range above 500 μm captures the pore regime. Then the Sku increases between 500 μm and 10 μm. Below the pore scale, a massif of peaks appears at the boundaries of the pores. These peaks are more and more spiked during the filtering (figure 16). Therefore, the Sku is expected to increase. A decrease of the Sku for the Interferometer occurs at the detection limit measured on the multi-scale curve of the Sa (figure 6).

Regarding the Ssk curves of the salt-based textured surfaces (figures 14(B) and (C)) the Micro-tomography and the Focus variation measure an approximate

symmetrical surface at every scale with a Ssk close to 0. The reference plane is therefore translated upward. The Interferometer exhibits a significant increase of the Ssk at the small scales, characteristic of some silicone pore walls abraded during the manufacturing process (figure 17). The Ssk of the 'coated-salt-loss texture' is therefore consistently higher than the Ssk of the 'open-salt-loss texture'.

As the sandblasted surface exhibits an increasing Sku (figure 13(D)), the peaks are sharper and sharper at the small sandblasting scales. Moreover, whatever the scale and the instrument, the surface is symmetrical, as proven by the small discrepancies in the Ssk values (figure 14(D)).

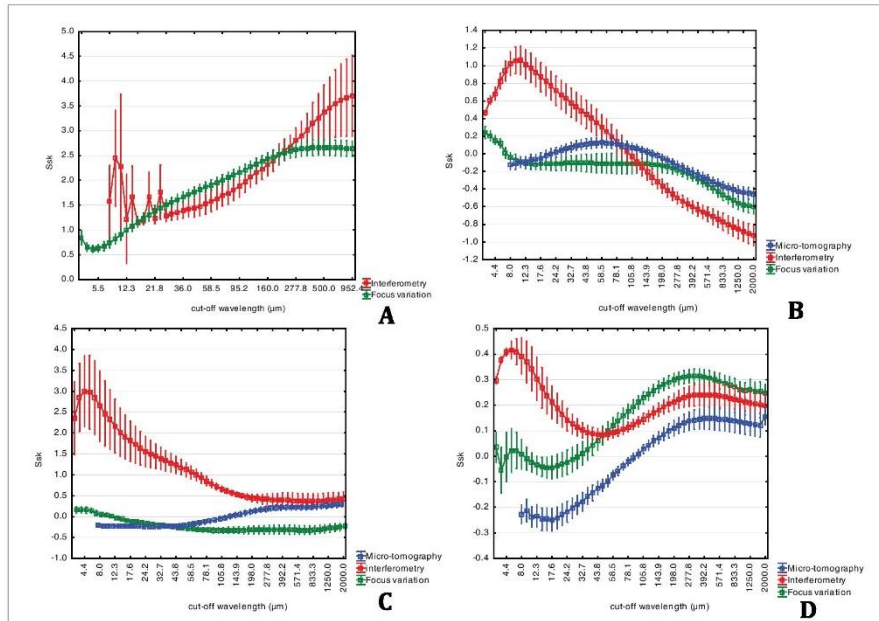


Figure 14. Ssk high-pass multi-scale decompositions of the smooth implant surface (A), the ‘open-salt-loss texture’ (B), the ‘coated-salt-loss texture’ (C) and the ‘sandblasting-replicating texture’ (D).

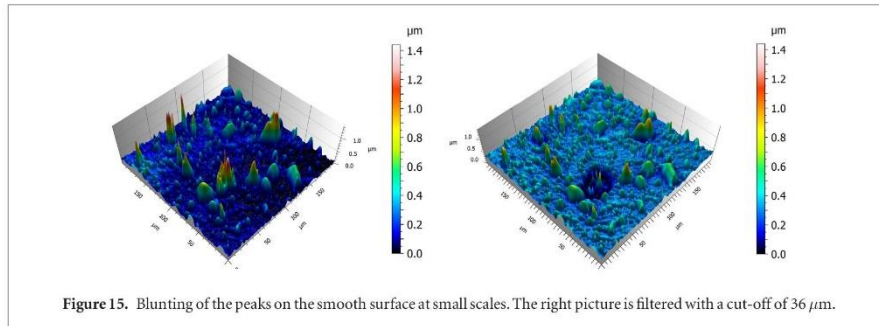


Figure 15. Blunting of the peaks on the smooth surface at small scales. The right picture is filtered with a cut-off of 36 μm .

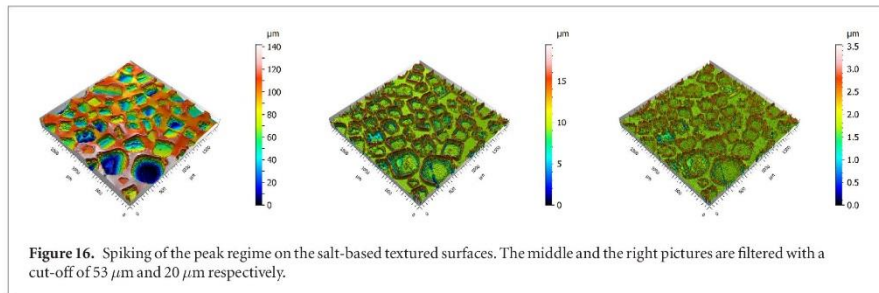


Figure 16. Spiking of the peak regime on the salt-based textured surfaces. The middle and the right pictures are filtered with a cut-off of 53 μm and 20 μm respectively.

4. Discussion

No extensive and comparative topographical analysis was performed on breast implant shells. Only preliminary surface measurements prior to biological characterizations were reported in the literature [17, 18].

Moreover, the current International Standard relative to breast implants [12] is elusive about the metrological material requirements.

This multi-instrument and multi-scale analysis highlights valuable metrological methodology and results for the editing of a breast implant texture

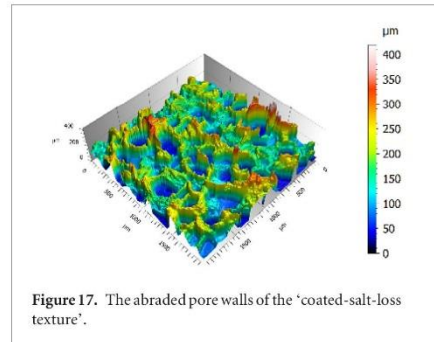


Figure 17. The abraded pore walls of the 'coated-salt-loss texture'.

measurement procedure. This study is focused on three instruments: x-ray micro-tomography, White-Light Interferometry and Focus variation microscopy. However, the methodology which aims at comparing the instrument accuracies over a wide scale range encompassing the tissue and the cellular scales is easily extrapolated to other apparatus, such as laser confocal microscopy and atomic force microscopy (AFM).

In spite of an important non-measured point number on full sharp slopes, the White-Light Interferometer is the instrument which has the most complete insight into Sebbin textured breast implant surface topography. Three roughness regimes feature its multi-scale analysis: the pore-based macroscopic structure and two fractal regimes characteristic of secondary salt-derived roughness and of intrinsic silicone roughness. Moreover, contrary to Focus variation, Interferometry captures the fractal sub-micrometric droplets present on Sebbin smooth implant surface.

Usually computer-tomography (CT) is the 'gold-standard' of volumic measurement, especially of porosity computation [19]. Remarkably, the macroscopic topography resulting from the μ -CT measurement and from the downstream reconstruction procedure is robust and metrologically of value. Sebbin textures have been already measured by x-ray micro-tomography without topographical analysis [2]. The texturation scale is also consistent with the calibration specification of the manufacturer. However, a 20 μm -wide 'step-artefact' occurring all over the surface would overestimate the secondary roughness.

The Focus variation accurately captures the primary salt-based roughness. Yet, its measuring principle must be questioned for investigating sub-micrometric translucent features. The light reflection off the surface and the computation of a non-coherent light property—the focus—would result in a non-isotropic artefact led to a 100% motif height increase and a 20% motif diameter increase in Sebbin smooth implant surface and in a higher secondary roughness than the interferometric measurements in Sebbin textured implant surface. This focus enlargement could hinder the measurement of small surface roughness on uncharged-silicone replica.

The multi-scale analysis performed on the 'sandblasting-replicating surfaces' is not conclusive because of some silicone-replicating-related artefacts. The smallest sandblasting scales are blanked out on the silicone replica because the silicone gel used does not bridge the smallest mandrel roughness. A surface analysis of the mandrel will interestingly complete the results.

According to the multi-scale curves, the three measuring protocols are robust in the capture of the Sebbin textured breast implant macro-structures. Breast implants of other manufacturers were macroscopically investigated in the literature. Valencia-Lazcano *et al* [17] measured on an Allergan Biocell[®] implant a couple of topographical parameters on a $644 \times 642 \mu\text{m}$ square, contrary to the International Standard requirements [12]. However, the reported Sa value ($Sa = 18.83 \pm 0.91 \mu\text{m}$) [17] is widely underestimated because measuring pores with a largest size of $522 \mu\text{m}$ over an area of approximate $640 \mu\text{m}^2$ is topographically irrelevant.

Valencia-Lazcano *et al* [17] and Kyle *et al* [18], both from the University of Manchester, also performed a surface analysis on a Mentor Siltex[®] implant (Mentor Corporation, Santa Barbara, California). A significant discrepancy in the maximal height of the surface ($328 \mu\text{m}$ and $40 \mu\text{m}$, respectively from [17, 18]) questions their measuring protocols and their samplings.

The secondary roughness regime is the first discriminating scale range between the three instruments. Barr *et al* [20] paved the way of a multi-scale analysis with a SEM image set capturing the Allergan Biocell[®] texturation over a surface size range from $2.5 \times 2.0 \text{ mm}$ to $27.8 \times 37.5 \mu\text{m}$. At the highest magnifications, Barr *et al* exhibits the 'lack of surface characteristics' between the pores and a 'finer wavy topography to its internal surface', which would be the hallmark of this secondary roughness regime.

Smooth Sebbin implant and smooth Mentor implant [18] surfaces feature random nano- and micro-scale peaks, contrary to ripples characteristic of smooth Allergan implant surfaces [20]. Different polymer curing processes may be responsible for these two patterns.

5. Conclusion

The White Light Interferometer captures the widest topographical content of the textured breast implant surfaces over the largest scale range (from the pore size to the scale of 10 nm). To improve the breast implant integration, which is a multi-scale challenge from the tissue scale to the cellular sensor scale, a measurement of the textures by Interferometer is the 'gold standard', compared to the Micro-tomography and the Focus variation.

References

- [1] Maxwell G P, Schefflan M, Spear S, Nava M Band Hedén P 2014 *Aesthetic Surg. J.* **34** 876–81
- [2] Atlan M, Bigerelle M, Larreta-Garde V, Hindié M and Hedén P 2016 *Aesthetic Plast. Surg.* **40** 89–97
- [3] Barnsley G P, Sigurdson L J and Barnsley S E 2006 *Plast. Reconstr. Surg.* **117** 2182–90

- [4] Barr S and Bayat A 2011 *Aesthetic Surg. J.* **31** 56–67
- [5] Brody G S, Deapen D, Taylor C R, Pinter-Brown L, House-Lightner S R, Andersen J S, Carlson G, Lechner M G and Epstein A L 2015 *Plast. Reconstr. Surg.* **135** 695–705
- [6] Danino A M, Basmacioglu P, Saito S, Rocher F, Blanchet-Bardon C, Revol M and Servant J M 2001 *Plast. Reconstr. Surg.* **108** 2047–52
- [7] Hall-Findlay E J 2011 *Plast. Reconstr. Surg.* **127** 56–66
- [8] Whitehouse D J 2010 *Handbook of Surface and Nanometrology* 2nd edn (Boca Raton, FL: CRC Press)
- [9] Kujala S, Ryhänen J, Danilov A and Tuukkanen J 2003 *Biomaterials* **24** 4691–7
- [10] Stevenson P M and Donald A M 2009 *Langmuir* **25** 367–76
- [11] Li F, Li B, Wang Q M and Wang J M 2008 *Cell. Motil. Cytoskeleton* **65** 332–41
- [12] ISO 14607 2009 Non-active surgical implants—mammary implants—particular requirements (Bruxelles European Committee for Standardization)
- [13] Roth J and de Groot P 1997 *Proc. of ASPE Spring Topical Meeting on Advances in Surface Metrology (Annapolis, MD)* pp 57–60
- [14] Scott P J 2004 *Proc. R. Soc. Lond. A* **460** 2845–64
- [15] Van Gorp A, Bigerelle M and Najjar D 2016 *Polym. Eng. Sci.* **56** 103–17
- [16] Bigerelle M 1999 *PhD Thesis* Ecole Nationale Supérieure d'Arts et Métiers, Lille, France
- [17] Valencia-Lazcano A A, Alonso-Rasgado T and Bayat A 2013 *J. Mech. Behav. Biomed. Mater* **21** 133–48
- [18] Kyle D J T, Oikonomou A, Hill E and Bayat A 2015 *Biomaterials* **52** 88–102
- [19] Evans N T et al 2015 *Acta Biomater.* **13** 159–67
- [20] Barr S, Hill E and Bayat A 2009 *Eplasty* **9** e22

However, in order to test the applicability of the ISO 14607:2018 standard, additional measurements and analyses were performed.

Contrary to the specifications of the standard, a measurement over 4m^2 with AFM is impossible: the apparatus is set up for a maximal measurement of $100\mu\text{m}^2$. Moreover, although non-stipulated in the standard, AFM is only able to measure smooth implant surface. Thus, the multi-scale analysis explicated in the article and designed for an inter-instrument comparison does not make sense with only AFM measurements.

2.2. MEASUREMENT AND FIRST ANALYSIS OF BREAST IMPLANT SURFACE WITH SEM AND 3D RECONSTRUCTION SOFTWARE

The SEM measurements must be processed with a specific reconstruction software in order to analyze the topography. Numerous techniques of SEM image reconstruction emerged over the past years. (172) They are based on the principle of stereoscopy, which consists in creating an illusion of relief by superimposing two captures of the same image shot under two slightly different angles. (173) Regarding the SEM 3D reconstruction, the tilt of the stage allows to capture the sample under different angles. The choice of the tilt value is of primer importance: it depends on the lateral resolution and roughness amplitude. (174) Moreover, the tilt must be eucentric: thus, if the tilt is performed on an axis of the stage (for example, the x-axis), only the disparity (which is the difference between the projection of a particular point of interest on the surface of the sample and the projection of the matched point on the tilted surface) on the other axis (the y-axis) is processed by the surface topography reconstruction algorithms. The mathematical details were given by Krishna *et al.* (175). The authors compared two of these algorithms: the one based on the Piazzesi model function and implemented in the Alicona's MeX software (174, 176) and the other based on the method of triangulation and configured in the Digital Surf's MountainsMap (2017 MountainsMap Reference manual Digitalsurf.com (www.digitalsurf.com/en/usermanual.html)). The Working Distance (WD) is used as a reference of distance in the algorithms. Actually, instead of point-to-point matching,

a matching extended to the small window around the point was implemented in the software. (2017 MountainsMap Reference manual Digitalsurf.com (www.digitalsurf.com/en/usermanual.html))

The standard remains elusive on the choice of the reconstruction technique. According to the comparative study led by Krishna *et al.* over a 750 x 500 μ m surface, the topographies obtained by the two algorithms were consistent with the measurements obtained by coherence scanning interferometer. However, the topographies reconstructed by the MeX software appeared to be noisier and would be more impaired by contrast and brightness settings than with MountainsMap. We chose therefore to use the later.

Different techniques of 3D rendering or reconstruction of SEM images were implanted on MountainsMap based on one, two or the four images provided by the four quadrants BSE detector (as used in the ANSM-mandated report).

The analysis was led from the 2 image-based reconstruction technique. The SEM (JEOL JSM-6480) was used with the Lower Electron Detection (LED) setting and an acceleration voltage of 1kV in order to minimize the accumulation of electron on the surface. As in the ANSM-mandated report, the Working Distance (WD) was fixed at approximately 15mm. Regarding the tilt, Krishna *et al.* specified that the value was typically comprised between 5 and 20° and that low angles were generally used for rough surfaces. As we analyzed both smooth and textured implant surfaces, we chose therefore an intermediary tilt value of 10°. Therefore, the software was implemented to process an image with a tilt = 0° (T0) and an image with a tilt = 10° (T10). The size of the window on the sample surface was fixed at 8x8pixel. The size of the matching window was based on software suggestion.

As this technique was not very documented in the literature, a statistical multi-scale analysis seemed to be premature at this stage. A preliminary study was however proposed. Two different magnifications (x70 and x140/x160) were used in order to screen two different surface areas (720x480 μ m and 1.5x1.mm). The length: width ratio

was consistent with the one used by Krishna *et al.* The analysis was led on the four types of surface measured in the enclosed article.

After inputting the SEM images in the software, a first processing, consisting in filling non-measured points, removing the form and adjusting the off-set in the (x,y) plane to co-localize the different images, was implemented on MountainsMap. Then, the topographies were reconstructed. Two reconstruction options were chosen:

- Removal of the outliers
- Use of a smoothing filter, of size 12

The Tables 14-16 exhibit the series of SEM images obtained for each magnification and for each type of surface, as well as the corresponding topographical reconstructions.

Regarding the reconstruction of Sebbin round textured implant surface, the amount of detail captured was reasonable on the smallest surface areas. For example, the topographies obtained on one cavity were comparable with the ones measured by Micro-tomography. (article enclosed to the chapter) However, the discrepancy was non-negligible for the largest surfaces. Over a surface area of 1.5x1mm, only the form of the structuration was approximately captured. The bottom of some cavities was not measured: an artefact comparable to an oil slick (due to the filling procedure) was then visible inside some cavities. Moreover, the roughness as well as the micro-roughness were not reconstructed.

Regarding the Sebbin round microtextured implant surface, whatever the reconstructed surface area, the topography of peaks was very grossly captured and much smoother than on the topographies depicted in the enclosed article to the chapter.

The reconstruction of the Sebbin shaped textured implant surface was very poor on a surface area of 720x480 μ m. Due to the very low measured area, numerous filling-related artefacts dominate the resulting morphology. The reconstructions of the larger surface areas – prone to be even more discrepant - were not then performed.

As a result, the technique could be used only to measure the topography of the Sebbin round textured implant surface on one cavity (over a maximal surface area of approximately 0.3mm²). This limitation was also highlighted in the ANSM-mandated report: by using a different reconstruction technique, they had to restrict their analysis to a surface area of 2.5mm² for surface exhibiting "*fine texturation or without texturation*".

2.3. CONCLUSIONS

This chapter allowed us to compare the relevancy of 5 instruments (namely SEM with a 3D reconstruction software based on two images, Interferometer, X-ray Micro-tomography and Focus variation microscope) to measure breast implant surface. Among the instruments suggested by the standard, only confocal microscope was not studied. The instrument, which seems from the multi-scale analysis to be the most robust on the widest scale range and for the greatest number of topographies, is Interferometry. However, the volume characterization of the samples captured by Micro-tomography (especially the cross-sections provided) allows to have further insight (such as the presence of over-hang or re-entrance) on some topographies than the Interferometry.

As the measurement methodology is validated, the obtained topographies will be then analyzed in order to select a couple of relevant surface parameters. These parameters will allow to establish robust classification of topographies and putative correlation between topographical data and biological or clinical outcomes.

Magnification	x160		x70	
Surface area	720x480 μ m		1.5x1mm	
Tilt	T0	T10	T0	T10
Series of SEM images				
Reconstructed topographies				

Table 14: A series of SEM images and the corresponding reconstructed topography of the Sebbin round textured surface for each magnification used.

Magnification	x140		x70	
Surface area	720x480 μ m		1.5x1mm	
Tilt	T0	T10	T0	T10
Series of SEM images				
Reconstructed topographies				

Table 15: A series of SEM images and the corresponding reconstructed topography of the Sebbin round microtextured surfaces for each magnification used.

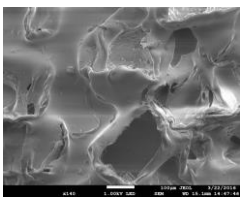
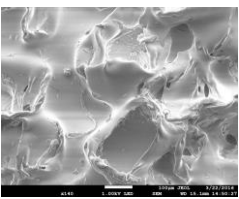
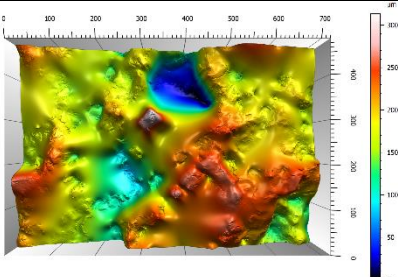
Magnification	x140	
Surface area	720x480µm	
Tilt	T0	T10
Series of SEM images		
Reconstructed topographies		

Table 16: A series of SEM images and the corresponding reconstructed topography of the Sebbin anatomical textured surfaces for each magnification used.

CHAPTER III: BIOLOGICAL RELEVANCE OF THE PROPOSED CLASSIFICATION

3.1 INTRODUCTION

The multiplicity of terms used to classify the breast implant surfaces, such as “macrotecture”, “texture”, “microtexture” or “nanotecture”, is as confusing as the measurement methodologies. Mostly, these designations rely on marketing or commercial considerations (such as the portfolio proposed by the manufacturers or presumed clinical benefits), without scientific basis. Before incriminating a type of surface as an increased risk factor of some rare pathologies (such as BIA-ALCL), a metrologically-relevant classification of breast implant surface must be established first. Basically, the categories of the classification must be consistent from a point of view of morphologies exhibited by the implant surfaces. Moreover, because of the paucity of reliable clinical data (such as the occurrence of BIA-ALCL cases or the risk of capsular contracture according to the type of surface) due to the late establishment of specific registries or standardized long-term clinical studies, no clinical validation of the classification is currently conceivable. Therefore, the nomenclature must be demonstrated from a biological point of view by *in vivo*, *in vitro* or *ex vivo* assays.

Recently, three major classifications based on topographies and surface parameters (such as Sa or surface area) and supported by biological evidence (such as *in vivo* assay on rats, *in vitro* bacterial attachment assay or *in vitro* macrophage-based assay) were published in the literature. (85, 86, 94) However, although these assays were designed to validate a hypothesis (such as respectively the tissue adherence to the implant surface, the proneness of implant surface to develop biofilm or to elicit inflammatory reactions), it is quite challenging to extrapolate outcomes on the clinical performance and biocompatibility of the device from *in vivo* studies carried out on small animals and from *in vitro* studies which consist of culturing cells or bacteria of interest on implant samples. Given the clinical problematic (i.e. the impact of the different breast implant surfaces on the clinical outcomes, such as the Baker's grade),

an *ex vivo* study consisting of harvesting and analyzing specific human tissues seems to us much more valuable and will be developed in this chapter.

Before biological testing, a classification according to the characteristic morphological structures featured by the measured topographies and cross-sections was proposed. The discriminant analysis, on which is based the selection of relevant surface parameters and the clustering of implant surface into consistent categories, will be detailed in the Chapter IV. Then a molecular approach led on human breast capsular tissues was chosen to validate our nomenclature. The classification of breast implant surfaces as well as the transcriptomic analyses of the biological samples were recently accepted for publication (article below). The acceptance mail from the editor is also enclosed.

Briefly, our analysis targets some genes involved in the inflammatory and immunological reactions and in the remodeling of the ECM, which were demonstrated as significative in two studies comparing non-contracted (Baker I or II) and contracted (Baker III or IV) capsular tissues. (165, 166) Transcriptomic studies (qPCR) were performed to quantify the relative expression levels of these genes, compared to a referent sample (chosen among the most uniform category). In order to quantify the impact of surface topography on biological mechanisms and to minimize bias, the samples were retrieved only on non-contracted capsular tissues and around non-ruptured implant. Moreover, harvesting was performed by a unique surgeon.

3.2 ARTICLE

Surface texturation of breast implant impacts extracellular matrix and inflammatory gene expression in asymptomatic capsule

Isabelle **Brigaud**^{1,2}(PhD), Charles **Garabédian**³ (MSc), Nathalie **Bricout**⁴ (MD), Laurent **Pieuchot**^{1,2} (PhD), Arnaud **Ponche**^{1,2} (PhD), Raphaël **Deltombe**³ (PhD), Rémi **Delille**³ (PhD), Michael **Atlan**^{5,6} (MD, PhD), Maxence **Bigerelle**³ (PhD), Karine **Anselme**^{1,2} (PhD)

1. Université de Haute-Alsace, CNRS, IS2M UMR 7361, F-68100 Mulhouse, France

2. Université de Strasbourg, France

3. Université de Valenciennes et du Hainaut-Cambrésis, LAMIH UMR CNRS 8201, Valenciennes, France

4. Private Hospital Saint Germain, Saint-Germain-en-Laye, France

5. Plastic Reconstructive Surgery, Microsurgery, Tissular Regeneration Department, Tenon Hospital Paris, F-75020 Paris, France.

6. Université de Médecine de la Sorbonne, Paris VI, F-75013 Paris, France.

Corresponding authors:

Brigaud Isabelle, PhD

Institut de Science des Materiaux de Mulhouse

IS2M - UMR CNRS 7361 - UHA

15 rue Jean Starcky, B.P. 2488

68057 Mulhouse Cedex, France

isabelle.brigaud@uha.fr

Karine Anselme, PhD

Institut de Science des Materiaux de Mulhouse

IS2M - UMR CNRS 7361 - UHA

15 rue Jean Starcky, B.P. 2488

68057 Mulhouse Cedex, France

karine.anselme@uha.fr

Financial disclosure statement: the authors have the following to disclose

Dr Bricout is an R&D consultant for Groupe Sebbin. Mr Garabédian is employed by Groupe Sebbin. His PhD research is funded by Sebbin, as part of the French government CIFRE program (grant CIFRE 2015–0843). The other authors declare no potential conflicts of interest with respect to the research, authorship, and publication of this article.

Presented at:

1) **IMCAS**, Paris, France, 31th January-2nd February 2019. “Surface texturation of breast implant impacts extracellular matrix and inflammatory gene expression in asymptomatic capsule” (oral). I Brigaud, C Garabédian, N Bricout, K Anselme

2) **MATERIAUX**, Strasbourg, France, November 19-21th 2018; “New, simple and biologically validated breast implant classification” (poster). C. Garabédian, I. Brigaud, L. Pieuchot, A. Ponche, M. Bigerelle, K. Anselme

3) **ESB**, Maastricht, Holland, September 9-13 2018. Molecular biology-based breast implant surface classification (poster). C. Garabédian, I. Brigaud, K. Anselme, M. Bigerelle

4) **BIOMAT, Ambleteuse, France, June 12-16 2017**. Biomarker-based evidence of the breast implant texturation benefit (oral). C. Garabedian, I. Brigaud, M. Bigerelle, K. Anselme

Short Running Head: Breast implant surface texturing effects

ABSTRACT

Background: Texturing processes have been designed to improve biocompatibility and mechanical anchoring of breast implants. However, high texturing degree has been associated with severe pathologies. Here, we aimed to determine whether implant surface topography could also affect physiology of asymptomatic capsules.

Methods: We collected topographical measurements from 17 different breast implant devices by interferometry and X-ray microtomography. Morphological structures were statistically analyzed to obtain a robust breast implant surface classification. We obtained 3 topographical categories of textured implants (“peak and valleys”, “open cavities”, and “semi-opened cavities”) based on the cross-sectional aspects. We simultaneously collected 31 Baker I capsules, sorted them according to the new classification, established their molecular profile, and examined the tissue organization.

Results: Each of the categories showed distinct expression patterns of genes associated with the extracellular matrix (*Timp* and *Mmp* members) and inflammatory response (*Saal*, *Tnfr11*, *Il8*), despite originating from healthy capsules. Besides, slight variations were observed in the organization of capsular tissues at the histological level.

Conclusions: We combined a novel surface implant classification system and gene profiling analysis to show that implant surface topography is a bioactive cue that can trigger gene expression changes in surrounding tissue, even in Baker I capsules. Our new classification system avoids confusions around the word “texture”, and could be transposed to implant ranges of every manufacturer. This new classification could prove useful in studies on potential links between specific texturations and the incidence of certain breast-implant associated complications.

INTRODUCTION

Breast implant design involves the selection and combination of several features such as implant filling (silicone gel or saline solution), shape (round or anatomically shaped), volume, and surface (smooth or textured). Implant surface is essential to the performance and safety of breast implant devices. Surface topography -the intricate relief of the outer implant shell- directly affects soft tissue reaction and fibrous tissue formation around the implant, which, if disrupted, could lead to post-surgery complications such as capsular contracture^{1,2}. The link between texturation of implant surface and medical outcomes remains controversial. “Macrottextures” were designed to promote tissue adhesion to the implant.³ However, their impact on capsular contracture⁴⁻⁷ and rare long-term complications such as double capsule⁸, late seroma, and breast implant-associated anaplastic large cell lymphoma (BIA-ALCL)⁹⁻¹³ remains unclear. The relationship between the mechanisms governing breast implant biocompatibility associated with implant surface properties is therefore of great interest.

The formation of capsular tissue around an implant is a physiological wound-healing response to foreign elements. The host organism reacts to the presence of an implant by eliciting local extracellular matrix (ECM) reorganization. These events are tightly regulated by the TGF β signaling pathway, which directly mediates downstream expression of about 60 ECM-related genes, including the expression balance of matrix-remodeling enzymes such as metalloproteinases (*MMPs*) or tissue inhibitors of proteinases (*TIMPs*).¹⁴ The inflammatory response plays a major role in implant integration¹⁵, which can also be promoted by *MMPs*.¹⁶ We hypothesized that breast implant topography could mediate cell signaling, particularly during the initial formation of capsular tissue. We assumed that different degrees of surface texturation would elicit specific gene activation/response profiles in peri-prosthetic cells, even in healthy tissues such as Baker I capsules.¹⁷

In this study, we conducted a statistically robust but simple and comprehensive classification of breast implants based on the degree of surface texturation. We then compared the impact of different categories of implants on the expression of a panel of ECM and inflammatory genes in healthy capsules. We also examined the effect of such implants on peri-prosthetic tissue organization.

MATERIALS AND METHODS

Substrate surface measurement

Surface topography of 17 implant types from 11 independent companies were measured and analyzed as a representative sample of available marketed implants (see table, supplemental digital content 1). The devices examined were new, sterile, and within their period of use. We collected 3 sets of samples from 3 separate locations (dome, edge, and base), obtaining 9 independent measures per implant. Each sample was taken from the implant shells by using a punch to obtain a final circular area of 10 mm², and sonicated in 10% alcohol solution for 10 minutes for cleaning. Samples were measured by interferometry (NewView™ 7300 Optical Surface Profiler; Zygo Corp., Middlefield, CT, USA) for “peak and valley” (PV)-patterned surfaces or X-ray Microtomography (SkyScan™ 1172; Bruker BioSpin Corporation, Billerica, MA, USA) for “open-cavities (OC)” and “semi-opened cavity” (SOC)-patterned surfaces, as described previously.¹⁸ Based on the international breast implant standard (ISO 14607:2018), we restricted our measurements to 4mm² within the circular sample.

Classification

Topography-based breast implant classification was established using robust statistical discriminant analyses, which will be described in detail in a subsequent publication. Briefly, surface topography measurements were computed using Mountains® software (Digital Surf, Besançon, France) and MesRug® (MesRug Data System, Lieu Saint Amand, France). By

applying filters, surfaces were decomposed in elementary surfaces to scale down intricate surface roughness properties. This process was applied independently to the 42 most common roughness parameters (defined in ISO 25178 and EUR 15178N). Classification was established based on the resulting values. Implants were categorized according to morphological features observed from surface cross-section and topography analyses as “peak and valley” (PV), “open-cavities (OC)”, and “semi-opened cavity” (SOC). Cross-sections based on samples analyzed by X-ray microtomography were established after image reconstruction as described previously.¹⁸ For the interferometric measurements, a 2mm-long profile was extracted from the topography, by using the Mountains[®] software, to construct the cross-section. Illustration of the methods used to establish the final classification is given in supplemental digital content 2.

Patient information and related breast implant capsule sampling

Twenty female patients with 7 different types of textured breast implants, who underwent breast revision surgeries between February 2017 and February 2018, were recruited for this study (average age: 51 ± 15 years). A single surgeon performed all surgeries and tissue collection. Ethical approval was obtained from the institutional review board. Patients gave informed consent prior to participating. Thirty-one capsular tissue samples were collected based on uni or bilateral capsulectomies; 5 were harvested from reconstructed breasts, and the rest from aesthetic surgeries. Fig.1 shows the reasons for revision surgery. The mean duration of implantation was 9 ± 6 years (range: 1–21 years). Implant location was subglandular for 11 implants and submuscular for 18 implants. Two devices were implanted under a flap while the positions. Twenty-eight implants were silicone gel-filled and 3 were saline-filled. The mean implant volume was 286 ± 96 ml (range: 120-525 ml). Samples from patients with assessed implant rupture were excluded. For more clarity, data are summarized in Fig. 2. In this study, we restricted our sampling to Baker I-classified capsular tissues¹⁷.

RNA extraction, cDNA synthesis, and quantitative PCR

Collected tissues (0.5cm in at least one dimension in size) were immediately stored in RNA later solution (Invitrogen™) and preserved at -20°C until further use. For RNA extraction, tissues were sequentially chopped into pieces with a razor, placed in an Eppendorf containing glass beads and 300 µL of chilled Trizol, and crushed manually on ice for minutes using sterile and RNase free pestles. Mixtures supplemented with additional 300µL chilled Trizol were then homogenized using a high speed shaking machine. Total RNA was extracted using the Direct-zol™ RNA MiniPrep (Ozyme), according to the manufacturer's instructions, including a DNase treatment step. RNA purity and concentration were evaluated using a NanoDrop One^C (Thermo Fischer Scientific) based on absorbance ratios A_{260}/A_{280} and A_{260}/A_{230} . RNA integrity was assessed on 1% agarose gel electrophoresis. cDNAs were synthesized from samples normalized to 350 ng RNA, by using the iScript™ cDNA synthesis Kit (Bio-Rad). qPCR was carried out as described previously.¹⁹ Calibration sample was facing an OC-patterned topography and served to calculate relative gene quantifications for all the samples, irrespectively of texture group.

qPCR statistical analyses

Molecular gene expression profiles were generated as boxplots with mean value, standard error of the mean (SEM), and outliers, by using the Plotly software. Statistical analyses were performed by using Student *t*-test and non-parametric Mann-Whitney post-test (GraphPad Prism Software, San Diego, CA, USA). From these analyses, the level of significance was considered to be $p < 0.001$. Because of intrinsic constraints linked to the qPCR technique, we considered samples as *biologically* different for expression ratios higher (overexpression) or lower (repression) than $\times 3$, even if statistical tests were positive.

RESULTS

CLASSIFICATION

Fig. 3 illustrates topographical features shared by implants grouped in the same category, giving a representative aspect of the outer implant shell which directly contacts breast tissues. PV-patterned surfaces displayed regular peak and valley structures with heights of low amplitude (<100 μm). In comparison, OC-patterned surfaces mostly presented curve-shaped open cavities features of amplitude ranging from 50 μm to 300 μm . Topographies and cross-sections of SOC-surfaces showed repetitive and regularly distributed unsealed cuboid-like patterns of high amplitude (>400 μm). Cuboid structures protruding from the main surface exposed thin and angled edges at the implant interface. This specific cuboid pattern is generated by salt-loss technique followed by surface brushing treatment.

GENE EXPRESSION

We evaluated the effects of the 3 breast implant topographical classes in healthy samples on expression of foreign body reaction and inflammatory related genes, and capsular tissue organization. We excluded any chance of expression of the BIA-ALCL markers *Cd30* and *Alk* in our sampling.²⁰ These two markers were not significantly present in our entire sample set (data not shown).

Relative expression of matrix metalloproteinases (MMPs)

Figure 4 shows the relative expression of *Mmp2*, *Mmp9*, and *Mmp12*. No significant change in *Mmp2*, *Mmp9*, or *Mmp12* expression levels were observed in peri-prosthetic cells in contact with PV-patterned surfaces compared to the OC group. On the contrary, *Mmp2* levels were unchanged (Fig. 4A), and *Mmp9* and *Mmp12* were significantly up-regulated (44 ± 11 and 46 ± 21 -fold respectively) in tissues in contact with SOC-patterned implants, compared to those in

contact with PV- and OC-patterned implants (Fig. 4B and 4C). Thus, SOC-patterned implants likely trigger *Mmp9* and *Mmp12*, but not *Mmp2*, in the surrounding tissues.

Relative expression of tissue inhibitor of metalloproteinases (TIMPs)

Because TIMP activity closely balances that of the MMPs, we focused our analyses on this gene category (Fig. 5). In tissues in contact with PV-patterned implants, we found that *Timp4* gene expression was significantly up-regulated (4.48 ± 0.94 -fold; Fig. 5C) compared to that in tissues associated with OC (1.42 ± 0.20 -fold) or SOC (0.35 ± 0.04 -fold) patterned implants. In tissues in contact with SOC-patterned implants, *Timp1* and *Timp4* gene expression varied inversely, with *Timp1* expression significantly up-regulated (4.0 ± 0.61 -fold; Fig. 5A) and *Timp4* expression down-regulated (0.35 ± 0.04 -fold) compared to the PV and OC groups (Fig. 5C). *Timp2* gene expression was not significantly different in the three groups (Fig. 5B). We concluded that contact of PV and SOC-patterned implants with peri-prosthetic tissues affects *Timp1* and/or *Timp4* expression.

Relative expression of genes related to the inflammatory response

Immunological response mechanisms are essential for implant integration. We therefore examined the expression of different genes involved in these processes (Figure 6). Variations in *Tgfb1* (Figure 6A) and *Saa1* (Figure 6B) expression were not significant among the samples tested. Capsular tissues located in the vicinity of SOC-patterned implants exhibited up-regulated expression of *Il8* (3.95 ± 0.96 -fold) compared to those in the OC and PV-patterned implant groups (Figure 6C). *Tnfs11* was drastically down-regulated in the SOC-patterned implant group (0.19 ± 0.04 -fold) compared to the OC (1.15 ± 0.20 -fold) and PV (0.88 ± 0.09 -fold) groups. Thus, peri-prosthetic cells elicit immunological responses, when in contact with an implant surface, which depend on the topography of the implant.

DISCUSSION

Elucidating the relationship between degree of breast implant surface texturation and clinical outcomes could greatly improve implant integration. In this study, we linked for the first time characteristics of implant surface topography to gene response in host healthy tissues. We used a new breast implant classification system based on robust statistical analyses, with simple and meaningful nomenclature. Detailed comparison with existing classifications (^{21,22,23}), although important, are beyond the scope of this report and will be discussed in a subsequent paper. Briefly, our new nomenclature provides a robust tool to standardize breast implant prostheses into topographical categories by giving accurate variables to define and properly discriminate between different texture degree. In light of our new classification, we examined the expression profiles of genes that are essential to foreign body reaction. The formation of capsular tissue around an implant involves inflammatory and ECM remodeling responses mediated by TGF β 1. *Tgfb1* expression was found at a basal level, indicating that wound healing was completed and the peri-prosthetic capsule had reached a steady state. Thereafter, we determined whether the establishment of appropriate bio-interfaces between peri-prosthetic cells and dissimilar breast implant topographies was associated with specific reprogramming of dynamic MMP/TIMP balance activity. ECM-related gene expression levels were significantly affected by the different surfaces. Compared to OC-patterned surfaces, our internal reference for gene variations, only PV-patterned surfaces were correlated with *Timp4* up-regulation, indicating that host organisms recognize these two types of surfaces as relatively similar.

The gene expression profile of peri-prosthetic cells in contact with SOC-patterned surfaces was drastically different. *Timp4* and *Tnfsf11* expression was down regulated. Further, *Mmp9*, *Mmp12*, *Timp1*, and *Ils* were considerably up regulated. We concluded that establishment of an adequate bio-interface for breast implant integration requires adaptation of peri-prosthetic cells to implant topography, which is molecularly modulated through differential and specific

Mmp/Timp gene expression. Two studies^{24,25} have shown that Baker III capsules also exhibit significant changes in *Timp1*, *Timp4*, and *Tnfs11* expression. It is striking that these asymptomatic capsules share molecular hallmarks with contracted (fibrotic) capsules. However, accurate comparison of the gene expression profiles observed in this study with those described previously is not possible because previous studies did not distinguish between degrees of implant texturation and used different internal calibrators for qPCR calculations. Therefore, we could not conclude which type of surface favors capsular contracture. To elucidate this point, further experiments comparing expression levels of these markers in the context of texturation degree in contracted capsules, using our internal calibrator, are required.

At the tissue level, capsules interfacing SOC-patterned implants were associated with constant higher occurrence of capillary vessels than were OC-patterned implants (Supplemental digital content 3). Interestingly, *Mmp9* gene expression, which is increased in these capsules, dominates the regulation of angiogenesis through several catalytic and non-catalytic functions. Notably, it releases proangiogenic chemokines such as IL8, whose gene expression was also up-regulated.²⁶⁻²⁸ IL8, originally identified as a neutrophil chemoattractant²⁹, is also known for its pro-inflammatory activity. However, we could not confirm this role, since this type of immune cell was not distinguished in histological sections. This issue could be addressed in further work based on immunohistochemistry analyses for example. Nevertheless, we observed an accumulation of histiocytes at the interface for any surface (Supplemental digital content 3), as described in previous studies.²⁵

Finally, we observed drastic down-regulation of *Tnfs11*, which is expressed in fibroblasts³⁰ and is involved in various physiological processes including immunity. TNFSF11 interacts with the immune system via induction of pro-inflammatory cytokines, acting on several immune cells including monocytes, T cells, and B cells. Notably, TNFSF11 is expressed on activated T-cells and activates mature dendritic cells⁽³¹⁾, two types of immune cells widely represented in

fibrotic capsules formed around silicone breast implants (³²). Besides a role in activating the adaptive immune response, it is known to regulate immune tolerance,³³ a process by which the body reduces or eliminates an immune response to chronic agents³⁴. Considering its pleiotropic activity and pivotal role in immune system, further experiments are required to elucidate TNFSF11 activity in capsular tissues.

Restricted to the subset of genes we focused on in this study, we showed that at the molecular level, peri-prosthetic cells facing PV or OC-patterned surfaces react similarly, while SOC-patterned surfaces promote drastic gene expression variations. Nevertheless, only future larger-scale studies both in term of tissue sampling and gene expression analyses (*e.g.* RNAseq) will allow to first confirm this pilot study and second to discriminate a global texturation effect at the transcriptome level.

Giot *et al*⁸ showed that “macro-texturation” (herein classified in the SOC group) clearly induces strong tissue in-growth into its cavities, which accounts for the exceptional stability of the capsule-implant complex. As illustrated in our implant cross-sections, tissue ingrowth occurs inside unsealed cuboid-like patterns with possibly fragile thin walls. Thus, the shearing forces between implant and capsule caused by natural body movements, applied on strongly attached ingrowth tissue, could induce tissue alterations. The host body is therefore forced to undergo constant tissue remodeling as highlighted by *Mmp/Timp* gene expression modulation.

Our data show that surface topography features are bioactive cues differentially integrated by surrounding healthy periprosthetic capsules and could, in combination with other factors, contribute to the development of breast implant-associated complications. Further studies on the combinatorial effects of surface topography with other factors such as presence of a biofilm, degree of capsule adhesion, and implant positioning⁶⁻³⁸ are required. In conclusion, design of surface topography is of prime importance to ensure safe and long-term physiological

integration of breast implants. Finally, we recommend the use of our classification to classify breast implant surfaces into standardized categories.

Figure 1. Recapitulative diagrams of the clinical reasons for implant removal. Percentage (%) of collected capsules A) after aesthetic surgery (n = 26) and B) after breast reconstruction (n = 5).

Figure 2. Recapitulative tab gathering implant characteristics and patient clinical data established from the periprosthetic breast capsule (Baker I) tissue sampling. Implant positions: subglandular (SG), submuscular (SM).

Figure 3. Illustration of the main surface structures shared by breast implant devices binding in each of the 3 categories, namely PV, OC and SOC. Top view topography and corresponding cross-section is given for one device (underlined market reference) as a representative example of the entire category. Note that in the course of this study, CE mark of Biocell™ breast implants has not been renewed and is now under recall within Europe³⁸. A color calibration bar in micrometer (µm) indicates the height of the relief on the topographies where black and red represents respectively the lowest and the highest amplitude of topography. Bar scale represents 1,0 mm in length.

Figure 4. Boxplots depicting relative gene expression levels Mmp2 (A), Mmp9 (B), and Mmp12 (C) in healthy tissue (Baker I grade) in contact with peak and valley (PV), open cavities (OC), or semi-opened cavity (SOC)-patterned breast implants. Empty circles correspond to outlier values, dotted and full lines correspond to the mean and median values respectively. * p < 0.001 (Student t-test and non-parametric Mann Whitney tests).

Figure 5. Boxplots depicting relative gene expression levels of tissue inhibitors of metalloproteinases Timp1 (A), Timp2 (B), and Timp4 (C) from healthy tissue (Baker I grade) in contact with peak and valley (PV), open cavities (OC), or semi-opened cavity (SOC)-patterned breast implants. Empty circles correspond to outlier values, dotted and full lines correspond to the mean and median values respectively. * p < 0.001 (Student t-test and non-parametric Mann Whitney test).

Figure 6. Boxplots depicting relative gene expression levels of the pro-fibrotic transforming growth factor beta 1 Tgf β 1 (A), TNF superfamily member11 (Tnfs11) (B), C-X-C motif chemokine ligand 8 (Il8) (C), and inflammatory markers serum amyloid 1 (Saa1) (D) from healthy tissue (Baker I grade) in contact with peak and valley (PV), open cavities (OC), or semi-opened cavity (SOC)-patterned breast implants. Empty circles correspond to outlier values, dotted and full lines correspond to the mean and median values respectively. * $p < 0.001$ (Student t-test and non-parametric Mann Whitney tests).

Supplemental digital content 1. Breast implant sampling used to establish topography-based classification. Commercial designation and company for each sample are specified.

Supplemental digital content 2. Surface analyses processing overview. 9 samples on 3 independent localizations per breast implant examined are collected to undergo surface topography measurement (X-Ray Microtomography or interferometry). The 9 surface measurements are then filtered (high-pass (HP) or low-pass (LP) filters) at 8 different scales of depth (ranging from 8 μ m to 952 μ m). A pool of 672 multi-scale parameter values per surface measurement is obtained by computing 42 surface roughness parameters on each filtered surface. Finally, these 672 multi-scale parameters are 100 times bootstrapped and then paired. An index of classification was designed in order to rank in descending relevance all the couples of multi-scale parameters and to retain the most discriminative classifications.

Supplemental digital content 3. Hematoxylin-eosin staining of histological sections (3 μ m thickness) revealing discrete tissue organization differences between Baker I breast tissues when in contact either with OC-patterned implants or SOC-patterned implants. Images from 2 independent patients for each condition. No malignancies were identified. Tissues facing OC- or SOC- patterned implants exhibit tightly woven fibroblast fibers oriented parallel to the implant surface. Irrespective of the implant texturation, tissues commonly exhibited a layer of mononucleated cells at the implant interface (dotted line) together with discrete and scattered

distribution of histiocytes within the inner part of the capsules. Compared to tissues facing OC-patterned surfaces, tissues facing SOC-patterned surfaces exhibited more fibro-hyaline structures together with small congestive capillary vessels (black arrows). ×20 objective. Scale bar: 100 μm.

Acknowledgments We thank Nayana TusamdaWakhloo for feedback on this work and Dr Maria Rosa Katunar (PhD) for help with statistics. We also thank the « NANOTRANSMED » project co-funded by the European Regional Development Fund (ERDF) in the framework of the INTERREG V Upper Rhine program (« Transcending borders with every project ») and by the Swiss Confederation and the Swiss cantons of Aargau, Basel-Landschaft and Basel-Stadt." The topographical measurements were supported by the Project TRIBOSURF and the Platform MORPHOMECA from the ELSAT2020 project, co-financed by the European Union with the European Regional Development Fund, the French state, and the Hauts de France Region Council.

REFERENCES

1. Abramo AC, De Oliveira VR, Ledo-Silva MC, De Oliveira EL. How texture-inducing contraction vectors affect the fibrous capsule shrinkage around breasts implants? *Aesthetic Plast Surg.* 2010;34(5):555-560. doi:10.1007/s00266-010-9495-9
2. Arpino V, Brock M, Gill SE, et al. Capsular contracture after breast augmentation: An update for clinical practice. *Arch Physiol Biochem.* 2015;116(2):532-543. doi:10.1038/onc.2013.568
3. Wynn T a, Wolfram D, Rabensteiner E, et al. Physico-chemical characteristics of coated silicone textured versus smooth breast implants differentially influence breast-derived fibroblast morphology and behaviour. *Aesthetic Plast Surg.* 2015;34(5):81-91. doi:10.1016/j.jaut.2004.03.005
4. Wong CH, Samuel M, Tan BK, Song C. Capsular contracture in subglandular breast augmentation with textured versus smooth breast implants: A systematic review. *Plast Reconstr Surg.* 2006;118(5):1224-1236. doi:10.1097/01.prs.0000237013.50283.d2
5. Liu X, Zhou L, Pan F, Gao Y, Yuan X, Fan D. Comparison of the postoperative incidence rate of capsular contracture among different breast implants: A cumulative meta-analysis. *PLoS One.* 2015;10(2):1-18. doi:10.1371/journal.pone.0116071
6. Poepl N, Schreml S, Lichtenegger F, Lenich A, Eisenmann-Klein M, Prantl L. Does the surface structure of implants have an impact on the formation of a capsular contracture? *Aesthetic Plast Surg.* 2007;31(2):133-139. doi:10.1007/s00266-006-0091-y
7. Headon H, Kasem AA, Mokbel K. Capsular contracture after breast augmentation: An update for clinical practice. *Arch Plast Surg.* 2015;42(5):532-543. doi:10.5999/aps.2015.42.5.532
8. Giot JP, Paek LS, Nizard N, et al. The double capsules in macro-textured breast implants. *Biomaterials.* 2015;67:65-72. doi:10.1016/j.biomaterials.2015.06.010

9. Ramos-Gallardo G, Cuenca-Pardo J, Rodríguez-Olivares E, et al. Breast Implant and Anaplastic Large Cell Lymphoma Meta-Analysis. *J Investig Surg.* 2017;30(1):56-65. doi:10.1080/08941939.2016.1215576
10. Loch-Wilkinson A, Beath KJ, Knight RJW, et al. Breast Implant-Associated Anaplastic Large Cell Lymphoma in Australia and New Zealand: High-Surface-Area Textured Implants Are Associated with Increased Risk. *Plast Reconstr Surg.* 2017;140(4):645-654. doi:10.1097/PRS.0000000000003654
11. De Boer M, Van Der Sluis WB, De Boer JP, et al. Breast implant-associated anaplastic large-cell lymphoma in a transgender woman. *Aesthetic Surg J.* 2017;37(8):NP83-NP87. doi:10.1093/asj/sjx098
12. De Boer M, Van Leeuwen FE, Hauptmann M, et al. Breast implants and the risk of anaplastic large-cell lymphoma in the breast. *JAMA Oncol.* 2018;4(3):335-341. doi:10.1001/jamaoncol.2017.4510
13. Rupani A, Frame JD, Kamel D. Lymphomas associated with breast implants: A review of the literature. *Aesthetic Surg J.* 2015;35(5):533-544. doi:10.1093/asj/sjv016
14. Bonnans C, Chou J, Werb Z. Remodelling the extracellular matrix in development and disease. *Nat Rev Mol Cell Biol.* 2014;15(12):786-801. doi:10.1038/nrm3904
15. Steiert AE, Boyce M, Sorg H. Capsular contracture by silicone breast implants: Possible causes, biocompatibility, and prophylactic strategies. *Med Devices Evid Res.* 2013;6(1):211-218. doi:10.2147/MDER.S49522
16. Issa R, Zhou X, Constandinou CM, et al. Spontaneous recovery from micronodular cirrhosis: Evidence for incomplete resolution associated with matrix cross-linking. *Gastroenterology.* 2004;126(7):1795-1808. doi:10.1053/j.gastro.2004.03.009
17. Spear SL; Baker JL Jr. Classification of capsular contracture after prosthetic breast reconstruction. *Plast Reconstr Surg.* 1995;96:1119-1124.

18. Garabédian C, Delille R, Deltombe R, Anselme K, Atlan M, Bigerelle M. A multi-topographical-instrument analysis: the breast implant texture measurement. *Surf Topogr Metrol Prop.* 2017;5(2):025004. doi:10.1088/2051-672X/aa7290
19. Brigaud I, Agniel R, Leroy-Dudal J, et al. Synergistic effects of BMP-2, BMP-6 or BMP-7 with human plasma fibronectin onto hydroxyapatite coatings: A comparative study. *Acta Biomater.* 2017;55:481-492. doi:10.1016/j.actbio.2017.04.013
20. Brody GS, Deapen D, Taylor CR, et al. Anaplastic large cell lymphoma occurring in women with breast implants: Analysis of 173 cases. *Plast Reconstr Surg.* 2015;135(3):695-705. doi:10.1097/PRS.0000000000001033
21. Barr S, Hill EW, Bayat A. Functional biocompatibility testing of silicone breast implants and a novel classification system based on surface roughness1. Barr, S., Hill, E. W. & Bayat, A. Functional biocompatibility testing of silicone breast implants and a novel classification sys. *J Mech Behav Biomed Mater.* 2017;75(May):75-81. doi:10.1016/j.jmbbm.2017.06.030
22. Atlan M, Nuti G, Wang H, Decker S, Perry TA. Breast implant surface texture impacts host tissue response. *J Mech Behav Biomed Mater.* 2018;88:377-385. doi:10.1016/j.jmbbm.2018.08.035
23. Jones P, Mempin M, Hu H, et al. The Functional Influence of Breast Implant Outer Shell Morphology on Bacterial Attachment and Growth. *Plast Reconstr Surg.* 2018;142(4):837-849. doi:10.1097/PRS.0000000000004801
24. Ulrich D, Ulrich F, Pallua N, Eisenmann-Klein M. Effect of tissue inhibitors of metalloproteinases and matrix metalloproteinases on capsular formation around smooth and textured silicone gel implants. *Aesthetic Plast Surg.* 2009;33(4):555-562. doi:10.1007/s00266-009-9335-y
25. Kyle DJT, Harvey AG, Shih B, Tan KT, Chaudhry IH, Bayat A. Identification of

- molecular phenotypic descriptors of breast capsular contracture formation using informatics analysis of the whole genome transcriptome. *Wound Repair Regen.* 2013;21(5):762-769. doi:10.1111/wrr.12077
26. Alaseem A, Alhazzani K, Dondapati P, Alobid S, Bishayee A, Rathinavelu A. Matrix Metalloproteinases: A challenging paradigm of cancer management. *Semin Cancer Biol.* 2017;(November):0-1. doi:10.1016/j.semcancer.2017.11.008
 27. Li A, Dubey S, Varney ML, Dave BJ, Singh RK. IL-8 Directly Enhanced Endothelial Cell Survival, Proliferation, and Matrix Metalloproteinases Production and Regulated Angiogenesis. *J Immunol.* 2003;170(3):3369-3376. doi:10.4049/jimmunol.170.6.3369
 28. Rundhaug JE. Matrix metalloproteinases and angiogenesis. *J Cell Mol Med.* 2005;9(2):267-285. doi:10.1111/j.1582-4934.2005.tb00355.x
 29. Baggiolini M, Loetscher P, Moser B. Interleukin-8 and the chemokine family. *Int J Immunopharmacol.* 1995;17(2):103-108. doi:10.1016/0192-0561(94)00088-6
 30. Fouque-Aubert A, Chapurlat R. Influence of RANKL inhibition on immune system in the treatment of bone diseases. *Jt Bone Spine.* 2008;75(1):5-10. doi:10.1016/j.jbspin.2007.05.004
 31. Wong BR, Josien R, Choi Y. TRANCE is a TNF family member that regulates dendritic cell and osteoclast function. *J Leukoc Biol.* 1999. doi:10.1002/jlb.65.6.715
 32. Wolfram D, Rainer C, Niederegger H, Piza H, Wick G. Cellular and molecular composition of fibrous capsules formed around silicone breast implants with special focus on local immune reactions. *J Autoimmun.* 2004;23(1):81-91. doi:10.1016/j.jaut.2004.03.005
 33. Taishin Akiyama, Yusuke Shimo JQ. RANKL signaling controls the development of regulatory T cells RANKL signaling regulates lymph node development RANKL signaling regulates the microenvironment of the thymus. 2009;23(1):258-262.

34. Rao S, Cronin SJF, Sigl V, Penninger JM. RANKL and RANK: From Mammalian Physiology to Cancer Treatment. *Trends Cell Biol.* 2017;28(3):213-223. doi:10.1016/j.tcb.2017.11.001
35. Chong SJ, Deva AK. Understanding the Etiology and Prevention of Capsular Contracture. *Clin Plast Surg.* 2015;42(4):427-436. doi:10.1016/j.cps.2015.06.007
36. Brown T, Harvie F, Stewart S. A Different Perspective on Breast Implant Surface Texturization and Anaplastic Large Cell Lymphoma (ALCL). *Aesthetic Surg J.* 2019;39(1):56-63. doi:10.1093/asj/sjy091
37. Mempin M, Hu H, Chowdhury D, Deva A, Vickery K. The A, B and C's of Silicone Breast Implants: Anaplastic Large Cell Lymphoma, Biofilm and Capsular Contracture. *Materials (Basel).* 2018;11(12):2393. doi:10.3390/ma11122393
38. Cohen D. Breast implants linked to rare cancer are removed from European market. *BMJ.* 2018;363(December):k5401. doi:10.1136/bmj.k5401

Figure 1A

[Click here to access/download;Figure;Fig 1A_pending revision.jpg](#)

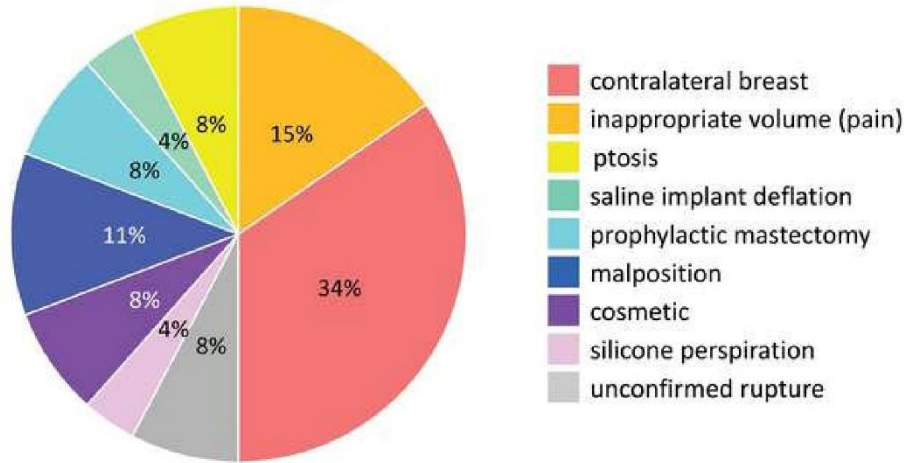
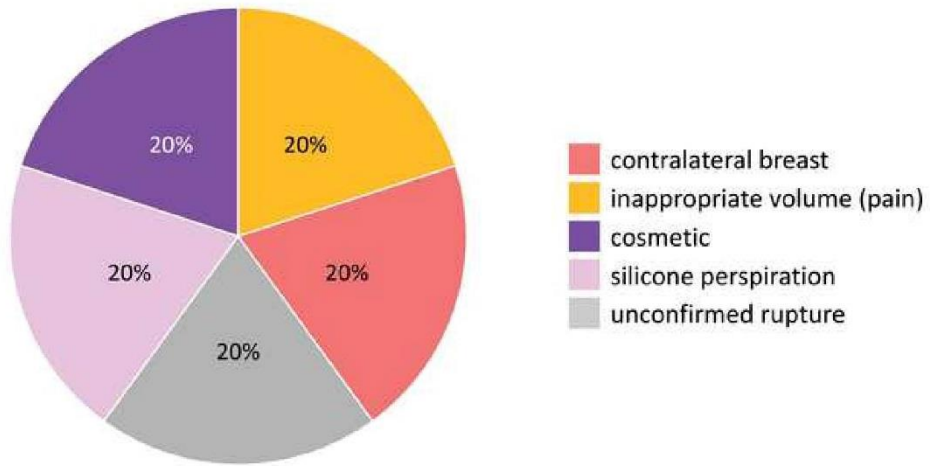


Figure 1B

[Click here to access/download;Figure;Fig 1B_pending revision.jpg](#)



reference to classification	substrate types of the harvested tissues	capsules		age or mean age of the patients (years)	implant position		
		total sampling = 31 capsules including 20 patients	duration or mean duration of implantation (years)		SG	S M	F L A P
peaks and valleys (PV)	round microtextured implant (Sebbin)	2 (including 1 patient)	1	25	-	2	-
	Cereform® (Ceraplas)	5 (including 3 patients)	7.2 (from 4 to 9)	43.6 (from 34 to 47)	5	-	-
open cavities (OC)	Siltex® (Mentor)	1 (including 1 patient)	18	43	-	1	-
	round textured implant (Sebbin)	9 (including 6 patients)	10.3 (from 1 to 15)	54.8 (from 20 to 79)	5	4	-
	TRUE Texture® (Sientra)	2 (including 1 patient)	21	58	-	2	-
semi-opened cavities (SOC)	shaped textured implant (Sebbin)	8 (including 6 patients)	7.8 (from 5 to 10)	58.1 (from 46 to 71)	1	5	2
	Biocell™ (Allergan)	4 (including 2 patients)	5 (from 2 to 8)	47 (from 46 to 48)	-	4	-

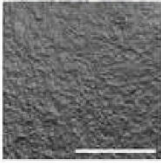

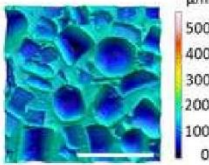

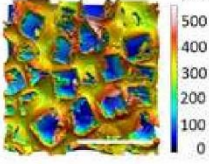
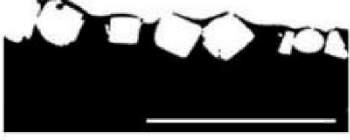
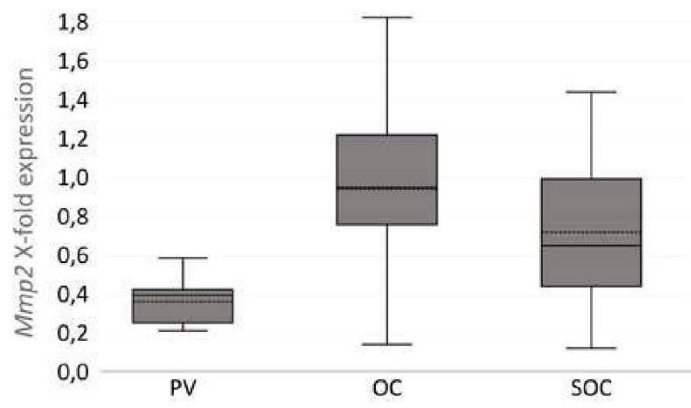
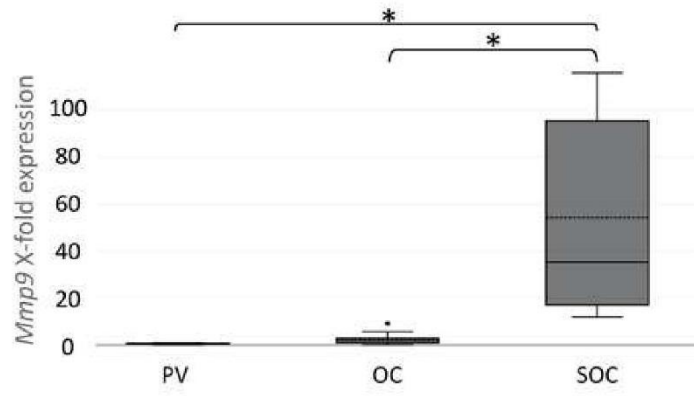
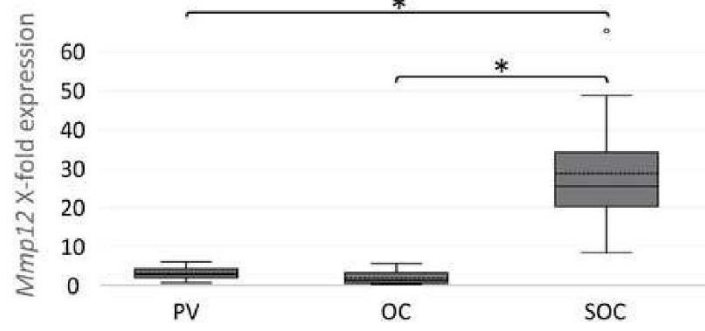
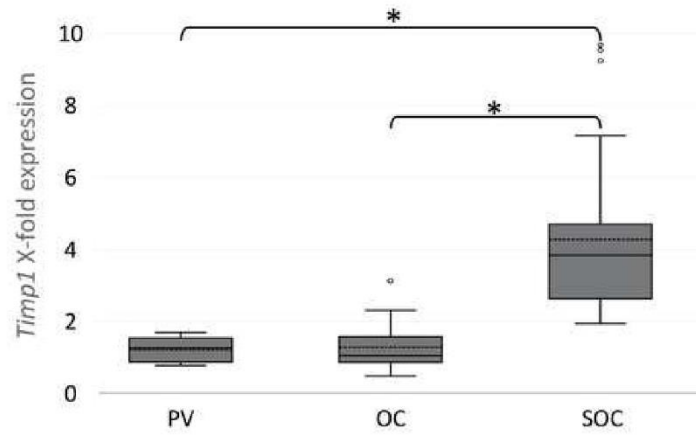
classes	prostheses sampling	topographies	cross-sections
peak and valley-patterned surfaces (PV)	<ul style="list-style-type: none"> SilkSurface™ (Motiva) Round microtextured implant (Arion) Perthese® (Perouse) Cereform® (Cereplas) <u>Round microtextured implants (Sebbin)</u> 		
open cavity-patterned surfaces (OC)	<ul style="list-style-type: none"> Round textured implant (Sebbin) TRUETexture® (Silimed) MESMO® sensitive (Polytech) Nagotex® (Nagor) Microcell™ (Allergan) <u>Cristalline Micro-textured (Eurosilicone)</u> POLYtxt® (Polytech) Siltex® (Mentor) 		
semi-opened cavity-patterned surfaces (SOC)	<ul style="list-style-type: none"> Cristalline Textured (Eurosilicone) Shaped textured implant (Sebbin) Shaped textured implant (Arion) <u>Biocell™ (Allergan)</u> 		

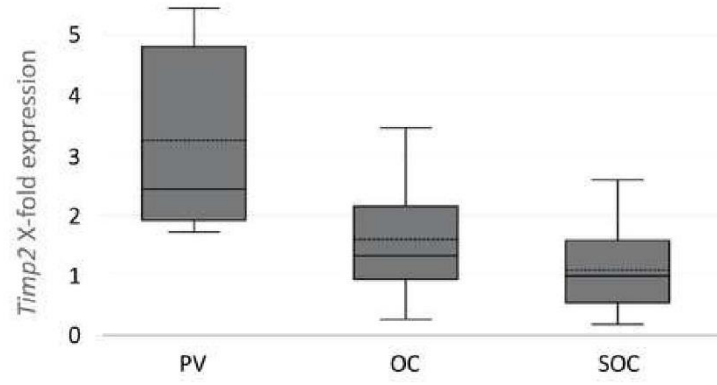
Figure 3. illustration of the main surface structures shared by breast implant devices binding in each of the 3 categories, namely PV, OC and SOC. Top view topography and corresponding cross-section is given for one device (underlined market reference) as a representative example of the entire category. A color calibration bar in micrometer (μm) indicates the height of the relief on the topographies where black and red represents respectively the lowest and the highest amplitude of topography. Bar scale represents 1,0 mm in length.

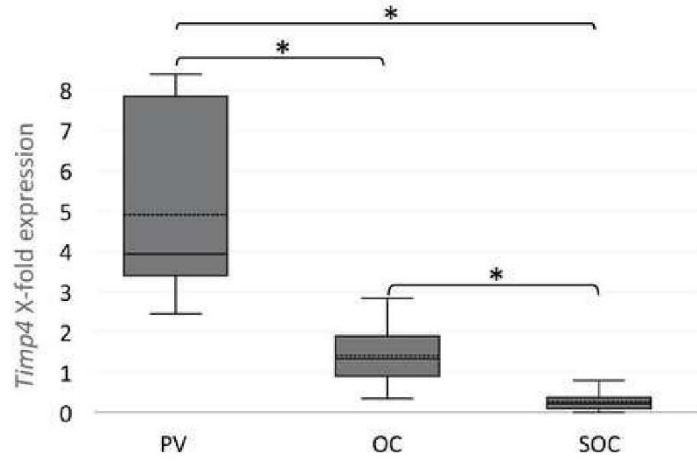


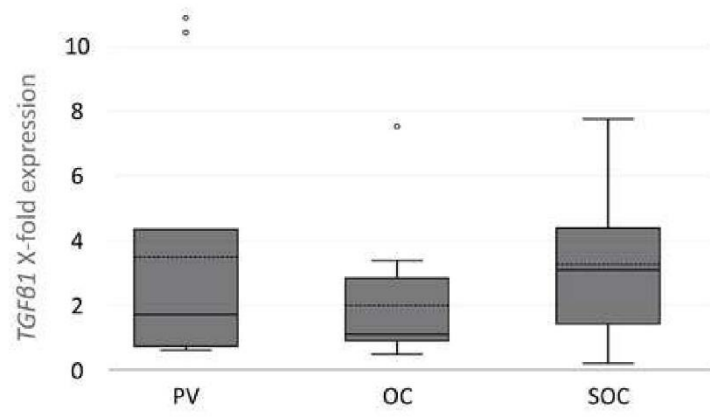


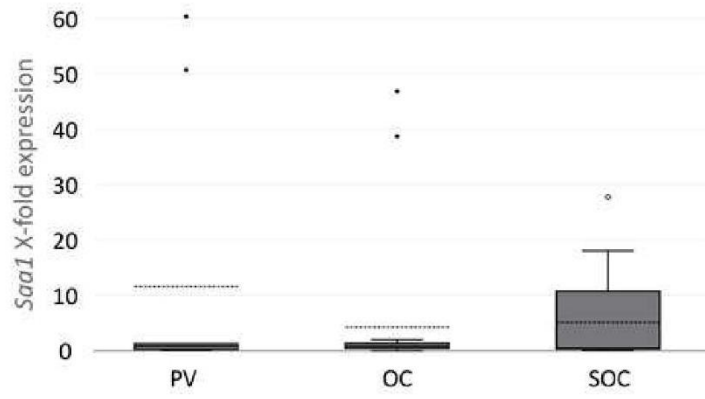


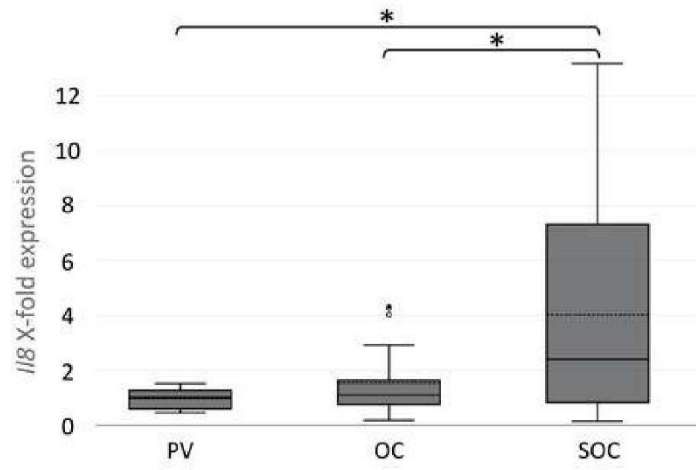


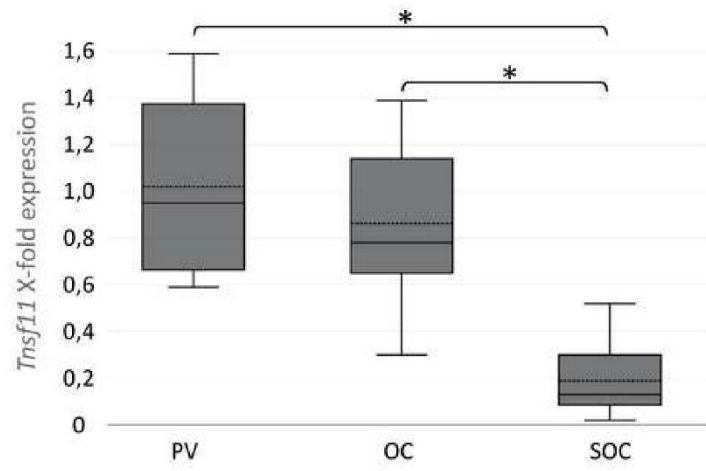




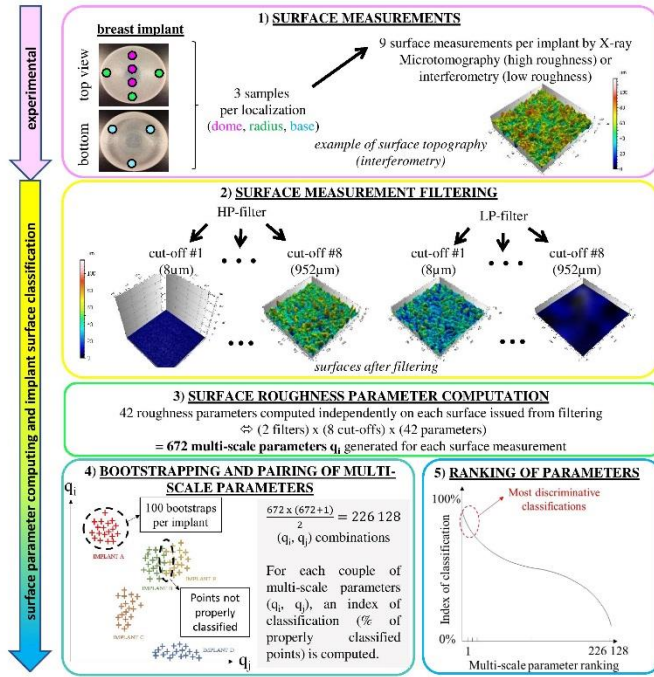


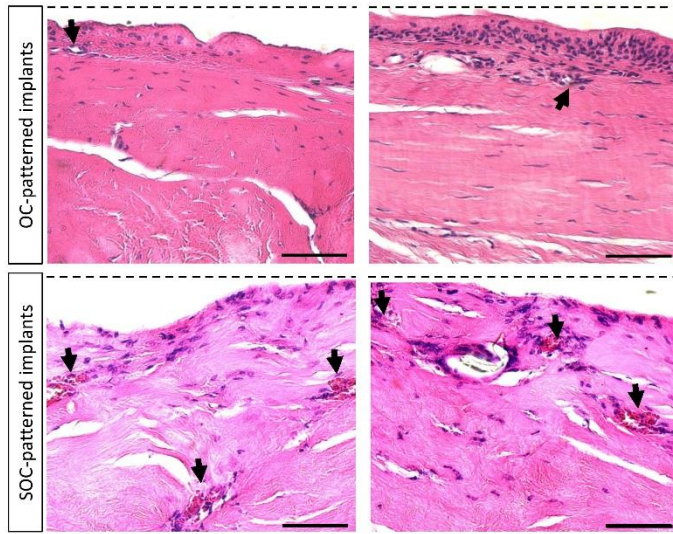






Implant type	Company
Biocell™ Microcell™	Allergan (Dublin, Ireland)
Round microtextured implant Round textured implant Shaped textured implant Round smooth implant	Sebbin (Boissy, l'Aillerie, France)
Cereform®	Cereplas (Sailly lez Cambrai, France)
Siltex®	Mentor (Irvine, CA, USA)
TRUE Texture®	Sientra (Santa Barbara, CA, USA)
Cristalline Micro-textured Cristalline Textured	Eurosilicone (Apt, France)
POLYtxt® MESMO® sensitive	Polytech Health and Aesthetics (Dieburg, Germany)
SilkSurface™	Motiva/Establishment Labs (Alajuela, Costa Rica)
Nagotex®	Nagor (Glasgow, UK)
Perthese®	Perouse Plastic (Bornel, France)
Round microtextured implant Shaped textured implant	Arion (Mougins Sophia-Antipolis, France)







Charles Garabédian <charlesgarabedian59@gmail.com>

PRS Decision

1 message

PRS Journal Editorial Team <em@editorialmanager.com>
 Répondre à : PRS Journal Editorial Team <prs@plasticsurgery.org>
 À : Charles Garabedian <charlesgarabedian59@gmail.com>

31 juillet 2019 à 22:36

You are being carbon copied ("cc:d") on an e-mail "To" "Isabelle Brigaud" isabelle.brigaud@uha.fr
 CC: "Charles Garabedian" charlesgarabedian59@gmail.com, "Nathalie Bricout" bricout.nathalie@wanadoo.fr,
 "Laurent Pieuchot" laurent.pieuchot@uha.fr, "Arnaud Ponche" arnaud.ponche@uha.fr, "Raphael Deltombe"
raphael.deltombe@uphf.fr, "Remi Delille" remi.delille@uphf.fr, "Mickael Atlan" drmichaelatlan@gmail.com, "Maxence
 Bigerelle" maxence.bigerelle@gmail.com, "Karine Anselme" karine.anselme@uha.fr

RE: PRS-D-19-00779R2, entitled "Surface texturation of breast implant impacts extracellular matrix and inflammatory gene expression in asymptomatic capsule"

Dear Dr Brigaud,

I am pleased to inform you that your work has now been accepted for publication in *Plastic and Reconstructive Surgery*. Congratulations! All manuscript materials will be forwarded immediately to the production staff for placement in an upcoming issue. The Editorial Office will request any remaining necessary materials and inform you of the publication date once your manuscript has been assigned to a specific issue.

There are many authorized ways for you to increase your work's reach, visibility, and potential citations. Review our **new accepted author toolkit** today to see how you can help us promote your article. Download the toolkit here: <http://links.lww.com/PRS/B45>.

Start now, by spreading the good news about your article's acceptance:

- Facebook - <http://goo.gl/4p6auA>
- Twitter - <http://goo.gl/3hKVVW0>

NOTES:

- You can include your article title or short title in your social media post.
- Here's a ready-made Facebook post you can copy and paste: "PRS just accepted my paper! Read "Surface texturation of breast implant impacts extracellular matrix and inflammatory gene expression in asymptomatic capsule" on PRSJournal.com soon."
- To increase visibility of your post:
 - On Twitter, add #PlasticSurgery
 - On Facebook, add @Plastic and Reconstructive Surgery (and click on our icon when it appears)
 -
- You **should not** include your article itself or abstract in your post.

Important: if you have not already done so, please do the following:

- 1) Inform us immediately if you or any co-authors have any financial relationships with any company whose products are mentioned in your article or a company making a competing product if not already stated in the manuscript.
- 2) Have each author sign and return the copyright release form if it is not already attached to your submission.

Acceptance for publication is made with the understanding that the material in your submission has not been previously published and will not be submitted for publication elsewhere before it appears in the journal.

Thank you for submitting your interesting and important work to the journal. We look forward to receiving more

<https://mail.google.com/mail/u/0?ik=768e9f72b8&view=pt&search=all&permthid=thread-f%3A1640607616606151734&simpl=msg-f%3A1640607...> 1/2

26/08/2019

Gmail - PRS Decision

manuscripts from you in the future.

<https://www.editorialmanager.com/prs/>

username: *****

password: *****

With Kind Regards,

Rod J. Rohrich, M.D.
Editor-in-Chief
Plastic and Reconstructive Surgery



In compliance with data protection regulations, you may request that we remove your personal registration details at any time. ([Remove my information/details](#)). Please contact the publication office if you have any questions.

3.3 OUTLOOK

As a result, the surface morphologies highlighted by the classification elicit a specific expression pattern on the selected genes. Even though the pathways (in which are involved the genes studied) are potentially upstream from clinical complications or pathologies, it is out of the scope of the article to conclude on the causative link between some surface topographies and the onset of pathologies because only a restricted set of genes was analyzed. For example, the genetic pool should be extended to the 60 ECM-related genes to have a comprehensive view on the role of fibrosis initiator or inhibitor of some implant surfaces. Moreover, as the biofilm was the most reported causative hypothesis for BIA-ALCL, transcriptomic studies might also be performed on bacterial RNA to identify and quantify bacteria within capsular tissues. Thus, we will be able to test this hypothesis and to determine whether the obtained expression pattern is more correlated with the presence of a specific bacteria than with topographical characteristics of implant surface or vice versa.

In addition, our transcriptomic study might be validated on the protein level by tissue-scale analysis. More particularly, immunohistochemistry could be performed on a piece of capsular tissue using specific antibodies targeting the selected gene-derived proteins. Thus, the protein expression might be localized within the tissue cross-section and correlated with some histological hallmarks (such as the presence of inflammatory or immune cells) or clinical characteristics (such area of adherence between implant and tissue and local thickness of capsular tissue).

Finally, even though the proposed nomenclature is morphologically consistent, it is of utmost importance to select surface indicators and to determine distinct range of values to define each category in order to discontinue the confusions around the current terms of implant surfaces and to rationalize the choice of these designations. Thus, a manufacturer of implant (which is not included in our analysis) could know unequivocally in each category their implant falls. That will be the focus of the next chapter.

CHAPTER IV: TOPOGRAPHICAL RELEVANCE OF THE PROPOSED CLASSIFICATION

4.1. INTRODUCTION

A classification of breast implant surface must be based at least on one topographical parameter in order to be relevant. Four different classifications of breast implant surfaces were established in this manner yet. All these classifications include 4 categories. Three classifications were based on only one topographical parameter, which was either the average roughness amplitude (Sa) (86), the surface area or the surface area ratio (85, 94). The surface area and the surface area ratio are custom-made indicators: they quantify the area of the developed surface, which is either absolute or relative to a "smooth" implant surface. These parameters were arbitrarily chosen by the authors. In addition to its first parameter (Sa), Barr *et al.* introduced a sub-level in its classification, by determining the presence or absence of porosity. (86) Two linear combinations of parameters obtained by Principal Component Analysis (PCA) were used for the fourth classification. (<https://ansm.sante.fr/S-informer/Points-d-information-Points-d-information/Surveillance-des-implants-mammaires-par-l-ANSM-publication-d-un-avis-d-experts-de-CSST-et-d-une-etude-sur-la-texturation-Point-d-information>) This statistical analysis was designed to reduce the initial number of parameters to only two variables called Principal Components (PC1 and PC2), which are a linear combination of the initial parameters. The PC are mathematically built in order to maximize the variance. This technique allows to group the samples according to a set of relevant variables. Then, to define the different categories, a linear equation of the frontiers between each scatterplot was then performed. Three classifications reuse the designations of the manufacturers (such as "smooth", "nanotexture", "microtexture" and "macrottexture") with slight differences (such as "mesottexture" and "macrottexture +") while the nomenclature of the fourth one is completely different ("minimal", "low", "intermediate" and "high") (85). The pool of implant analyzed in each study is slightly larger than our sampling. For example, the authors measured a large range of smooth implants.

The boundary values of each category are specified in the Table 17. When a category does not exist in a classification, the corresponding cases are shaded. The equations of the PC are also given.

	Barr et al. (86)	Atlan et al. (94)	ANSM-mandated report
Smooth	Sa < 5 µm	80 < surface area < 100mm ²	PC1* > 0.7
Nanotexture			
Mesotexture	Sa < 15µm		
Microtexture	10 < Sa < 75 µm	Porous	100 < surface area < 200mm ²
		Non-porous	
Macrotexture	Sa > 75 µm	Porous	200 < surface area < 300mm ²
		Non-porous	
Macrotexture +		surface area > 300mm ²	
PU			statistical analysis not performed

	Jones et al. (85)
Minimal	surface area ratio < 2
Low	2 < surface area ratio < 3
Intermediate	3 < surface area ratio < 5
High	surface area ratio > 5

Table 17: Existing classifications of breast implants based on topographical parameters. A second table is used for Jones et al. because they use another system of classification. The two couples of PC used in the ANSM-mandated classification are distinguished by one or two asterisks.

A comparison between the four classifications is not straight-forward because the parameters or the calculus of parameters are different. For example, contrary to Barr et al., Atlan et al. used absolute values of surface area, which were measured over a 10-mm diameter disk. (94) Noteworthy, the “smooth” and the “mesotexture” categories of the Barr’s classification overlap.

Even if these nomenclatures enable the ranking of implant according to relevant surface parameters, the ANSM classification is the only one which statistically justifies the choice of its parameters. (<https://ansm.sante.fr/S-informer/Points-d-information-Points-d-information/Surveillance-des-implants-mammaires-par-l-ANSM-publication-d-un-avis-d-experts-de-CSST-et-d-une-etude-sur-la-texturation-Point-d-information>)

Basically, the parameters of the PC are graded with a coefficient, which reflect their significance in the analysis. The retained parameters are therefore the most graded

ones. Moreover, by a segregation of the different groups on the 2D mapping, they also justify the boundaries between each category

Even though the choice of the parameters and the boundaries are more rationalized in the ANSM report, none of the 4 nomenclatures assessed statistically the robustness of their classification nor its comparison with the others.

It's the reason why in this section we will assess the statistical robustness of the nomenclature we proposed and validated biologically in the previous chapter. Basically, we will describe how we raised a statistically relevant and comprehensive classification from which we were able to optimally discriminate between different classes of breast implant surfaces.

As a reminder, the proposed nomenclature is mentioned again in the Figure 9, that was the Figure 3 of the article enclosed to the Chapter III.

classes	prostheses sampling	topographies	cross-sections
peak and valley-patterned surfaces (PV)	<ul style="list-style-type: none"> ▪ SilkSurface™ (Motiva) ▪ Round microtextured implant (Arion) ▪ Perthese® (Perouse) ▪ Cereform® (Cereplas) ▪ <u>Round microtextured implants (Sebbin)</u> 		
open cavity-patterned surfaces (OC)	<ul style="list-style-type: none"> ▪ Round textured implant (Sebbin) ▪ TRUETexture® (Silimed) ▪ MESMO® sensitive (Polytech) ▪ Nagotex® (Nagor) ▪ Microcell™ (Allergan) ▪ <u>Cristalline Micro-textured (Eurosilicone)</u> ▪ POLYtxt® (Polytech) ▪ Siltex® (Mentor) 		
semi-opened cavity-patterned surfaces (SOC)	<ul style="list-style-type: none"> ▪ Cristalline Textured (Eurosilicone) ▪ Shaped textured implant (Sebbin) ▪ Shaped textured implant (Arion) ▪ <u>Biocell™ (Allergan)</u> 		

Figure 9 : Illustration of the main surface structures shared by breast implant devices binding in each of the 3 categories, namely PV, OC and SOC. Top view topography and corresponding cross-section is given for one device (underlined market reference) as a representative example of the entire category. A color calibration bar in micrometer (μm) indicates the height of the relief on the topographies where black and red represents respectively the lowest and the highest amplitude of topography. Bar scale represents 1.0 mm in length.

4.2. METHODOLOGY

In order to establish statistically robust breast implant classification, we implemented sequential discriminant analyses using SAS v9.3 software (SAS Institute, Cary, NC, USA). As a first step, we performed a one-variable discriminant analysis on the 42 roughness parameters (such as previously defined in international standards ISO 25178 and EUR 15178N) computed over the whole surface area. This approach evaluated the possibility to classify breast implant topography when considering the global range of measured roughness scales. Values of parameters were then oversampled by being bootstrapped 100 times and the resulting averages were noted $m(\text{XX}^*)$. At each roughness parameter was associated an "index value". This index provides the probability for each parameter to be properly assigned into their respective category.

In order to discriminate more accurately the topographies (i.e. to have higher index values), we took into consideration the decomposition of the surfaces into elementary surfaces of roughness (providing multi-scale parameters). Basically, the topographies were first analyzed using the Mountains® software (Digital Surf, Besançon, France) from the raw measurements. Two Gaussian spatial filters, namely High-Pass (HP) and Low-pass (LP) filters, were applied to decompose all the roughness scales contained in each measured surface. By applying an HP filter, we remove the roughness scales above a defined threshold and obtain only the lowest roughness scales. Conversely, an LP filter extracts the roughness scales higher than the defined threshold. By sequentially increasing or decreasing the threshold value, we are able to reveal the spectrum of all the topographical scales included in each measured surface, namely the surface roughness with HP filter and the surface waviness with LP filter. Then, we calculated for each surface of the spectrum a large number of topographical parameters.

Then, we performed a second one-variable discriminant analysis, using bootstrapped and multi-scale parameter values (the resulting averages of each parameter will be designated by $m(XX_filter(HP/LP)_cut-off(in\ \mu m))$). The multi-scale decomposition of topographies was described in the Chapter II. At each multi-scale parameter was associated a new index value. From the analysis, we retained the multi-scale parameters with the first 100 index values only.

Since the one variable discriminant analysis was not satisfying to classify breast implant surfaces, we underwent a two-variable discriminant analysis of the bootstrapped multi-scale parameters. From this analysis, we retained only couples of parameters 1) belonging to the 100 best ones and 2) with a HP and a LP filter of the same cut-off value (i.e. to not have any rupture scale).

An overview of the surface analysis process is illustrated in the Figure 10 that was the Supplemental Digital Content 2 of the article enclosed in the Chapter III.

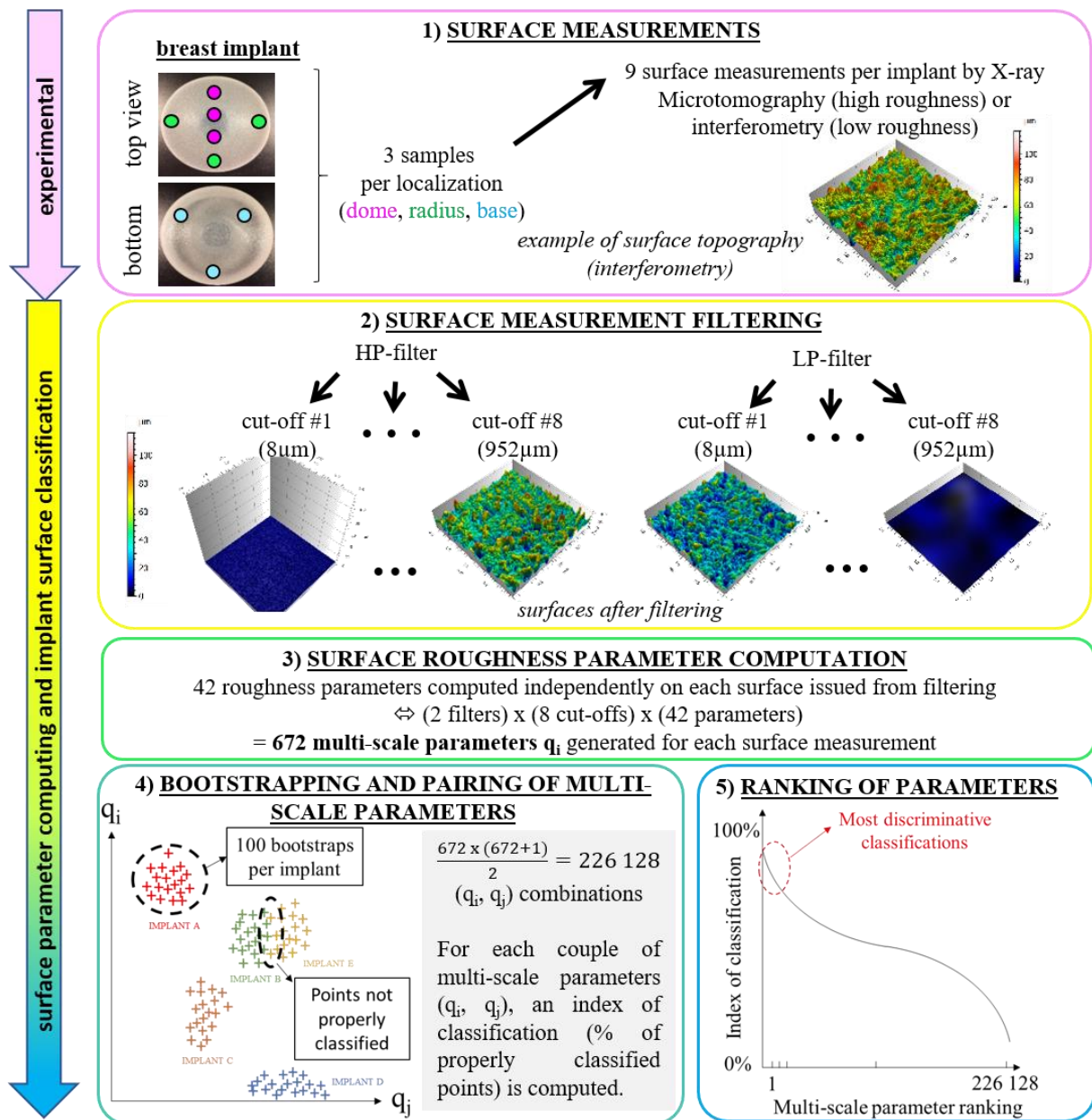


Figure 10 : Surface analyses processing overview. 9 samples on 3 independent localizations per breast implant examined are collected to undergo surface topography measurement (X-Ray Microtomography or interferometry). The 9 surface measurements are then filtered (high-pass (HP) or low-pass (LP) filters) at 8 different scales of depth (ranging from 8µm to 952µm). A pool of 672 multi-scale parameter values per surface measurement is obtained by computing 42 surface roughness parameters on each filtered surface. Finally, these 672 multi-scale parameters are 100 times bootstrapped and then paired. An index of classification was designed in order to rank in descending relevance all the couples of multi-scale parameters and to retain the most discriminative classifications.

4.3. RESULTS

4.3.1. ONE VARIABLE DISCRIMINANT ANALYSES

As a first step, we evaluated if one single topographical parameter, directly retrieved from surface measurement and without multi-scale analysis implementation, was sufficient to discriminate between the 17 different prostheses sampled herein. From this analysis, the 42 bootstrapped roughness parameters were ranked according to an index value. We found that the parameter $m(Sdq^*)$ which characterizes the mean quadratic gradient (calculated as the root mean square of slopes at all points in the examined area), has the highest index (0.54), meaning that the highest-score parameter has only 54% of probability to discriminate properly between the different implant topographies. In comparison, the parameter $m(Sa^*)$ (arithmetic mean height) or $m(Sdr^*)$ (developed surface ratio), used by Barr *et al.* and Atlan *et al.* to classify breast implant topography, have both an index value reaching 50% (Fig. 11A). Interestingly, this approach allowed to segregate our sampling into 3 independent classes, named I, II and III with Sdq values ranging from [0], [0.6 to 3.9] and [5.6 to 8.9] for each of the 3 categories that comprised respectively 1, 12 and 4 implants. (Fig. 11B) Although fruitful to discriminate between classes of breast implant surface topography, this approach was not conclusive to distinguish singularities between the implant topography. Indeed, among class II and III, we found distribution curves overlapping partially or entirely between each other (e.g Arion shaped textured implant versus Sebbin shaped texture implant in the Class III group). Therefore, the stringency of this classification was not sufficient to discriminate between the different implant characteristics within a same class.

Since this approach was not conclusive, we implemented the same process (one-variable discriminant analysis) but using multi-scale values. The parameter ranking according to their index values is given for the first 100 positions in Fig. 12A. The robustness of the classification is slightly higher than without multi-scale analysis: $m(Sal^*_{HP}_{105.8})$ has the highest index (62%). This parameter characterizes the autocorrelation length (which is a measure of the distance over the surface such that the new coordinates will have minimal correlation with the original coordinates) of the microscopic roughness (i.e. over scales lower than 105.8 μ m).

However, this analysis failed to discriminate any classes of breast implant surfaces. (Fig. 12B)

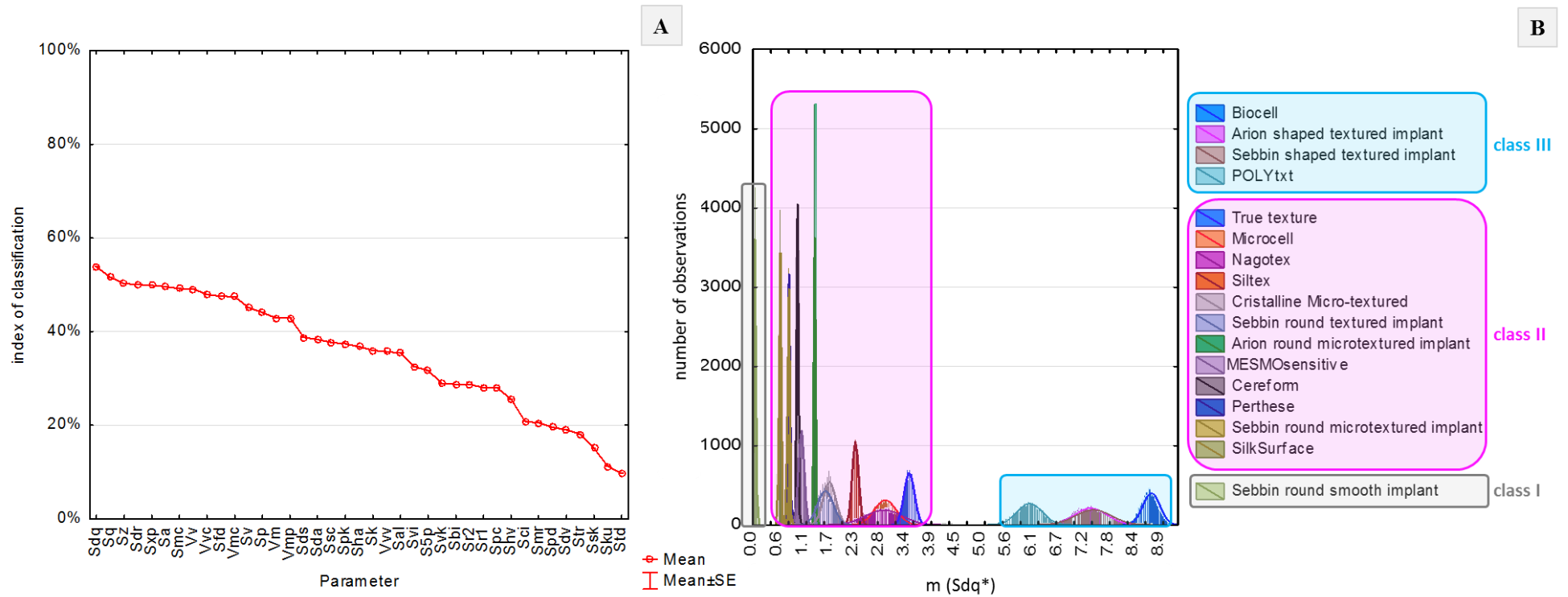


Figure 11 : One-variable discriminant analyses. Ranking of the 42 bootstrapped roughness parameters depending on their index value. Parameters are plotted with their rank (# position) and corresponding index value in descending order (A). Distribution curves of the 17 breast implant surfaces sampled in this study using the highest ranked parameter Sdq led to the discrimination of 3 implant classes (I, II and III) but failed to discriminate between implants within a same class (B).

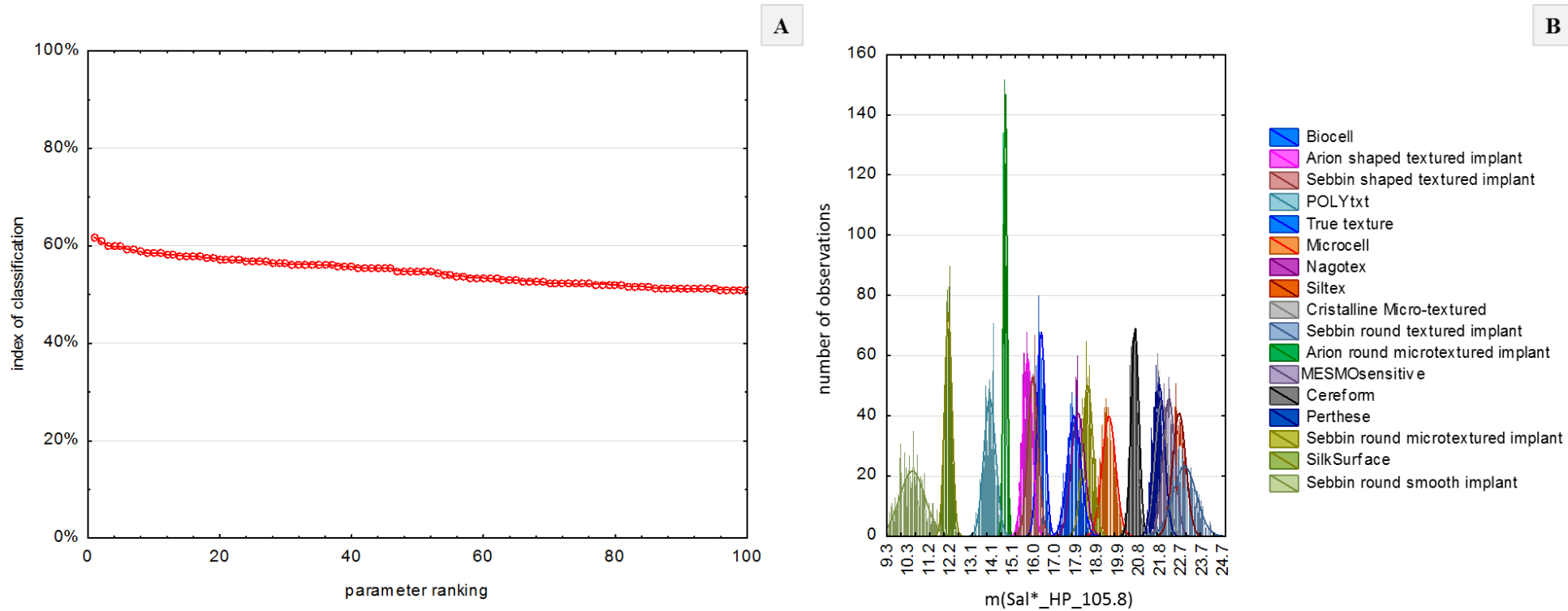


Figure 12 : One-variable discriminant analyses. Ranking of the 100 best bootstrapped multi-scale roughness parameters depending on their index value. Parameters are plotted with their rank (# position) and corresponding index value in descending order (A). Distribution curves of the 17 breast implant surfaces sampled in this study using the highest ranked parameter (Sal_HP_105.8) failed to discriminate any implant class (B).

The discriminant analysis was then extended to two variables. Basically, we searched for two independent bootstrapped multi-scale parameters (non-correlated) able to recapitulate an appropriate classification.

4.3.2. TWO VARIABLES DISCRIMINANT ANALYSES

Once again, the analysis was led on multi-scale parameters. We then chose the best couple of parameters able to discriminate between and within different prostheses classes and without scale rupture between the two elements of the couple. Finally, the parameter ranking according to their index values for the first 100 positions over 226 128 possible combinations was performed. The robustness is much higher than the previous one-variable discriminant analyses (first index value = 99%).

The couple $m(Sdq^*)_{LP_105.8} / m(Sfd^*)_{HP_105.8}$ is the first couple in the ranking (70th position), which does not present scale rupture between the two elements of the couple. The first element of the couple characterizes the mean quadratic gradient (i.e. the mean slope for all the points) of the macroscopic roughness (i.e. over scales higher than 105.8 μ m). The second element is the fractal dimension (or tortuosity) of the microscopic roughness (i.e. over scales lower than 105.8 μ m). The fractal dimension is an adimensional number comprised between 2 and 3 for a surface, which quantifies the degree of tortuosity ($Sfd = 2$ for a smooth surface and $Sfd = 3$ for a highly tortuous surface). It was estimated by the "box counting method", which consists of paving the surface with elementary motifs of given dimension (ϵ). Then, for each dimension of the motif, the number of motifs used is counted (N). Sfd is the slope of the linear regime of the curve $\log(N) = f(\log(\epsilon))$. Therefore, more Sfd is important, more the surface is tortuous on the small scales.

Interestingly, this approach allowed to segregate our sampling into 4 independent classes, named I, II, III and IV with $Sdq_{LP_105.8}$ values ranging from [0], [0 to 0.4], [0.4 to 1.4] and [1.6 to 2.7] and with $Sfd_{HP_105.8}$ values ranging from [2.17 to 2.32], [2.5 to 2.8], [2.25 to 2.6] and [2.3 to 2.6] respectively for each of the 3 categories that comprised respectively 1, 5, 8 and 4 implants (An additional breast implant surface (Cristalline Textured surface manufactured by Eurosilicone) was included in the

analysis as an *a posteriori* control). (Fig. 13) Moreover, this approach is able to discriminate between the different implant characteristics within a same class.

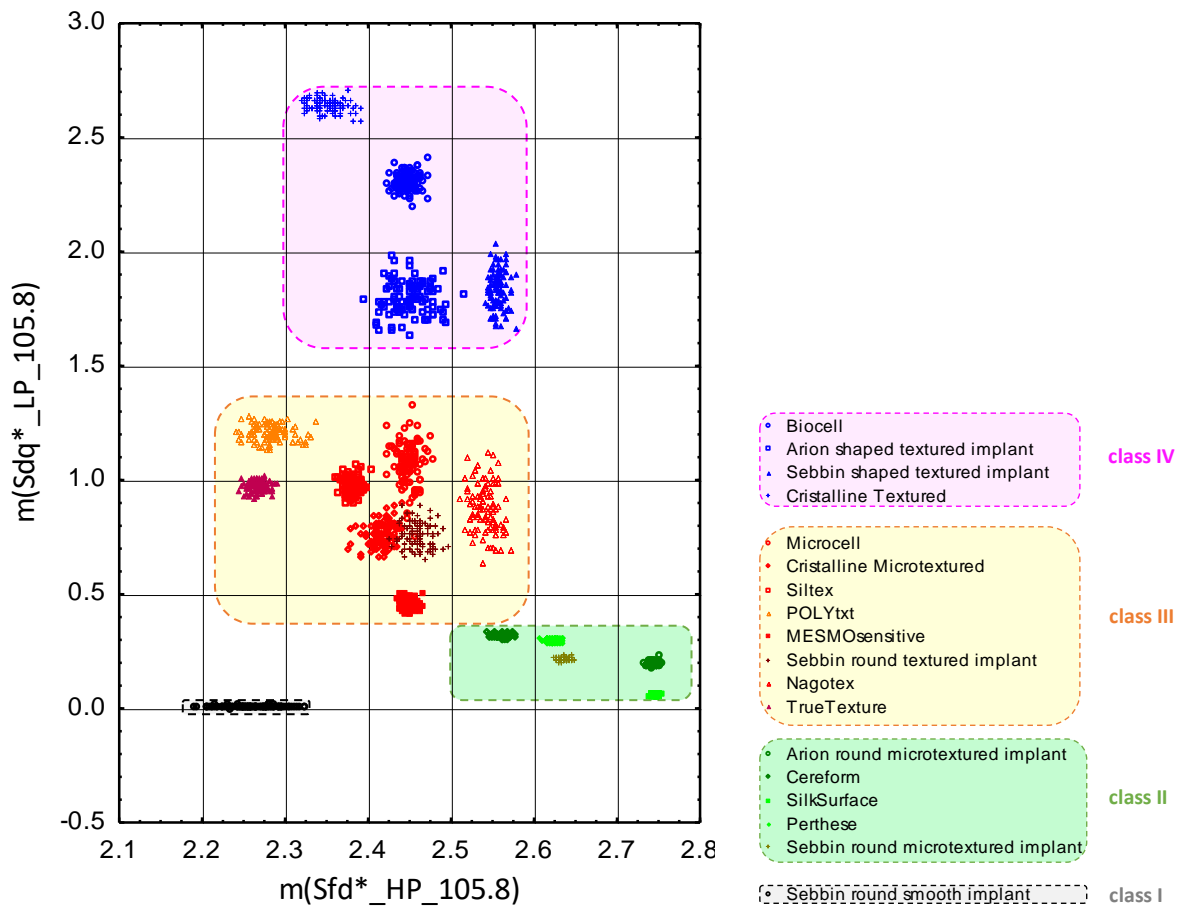


Figure 13 : Two-variable discriminant analysis. Classification of the 17 breast implant surfaces sampled in this study using the highest ranked parameter couple ($m(Sdq*_LP_{105.8}) / m(Sfd*_HP_{105.8})$) led to the discrimination of 4 implant classes and to the segregation between implants within a same class. An additional breast implant surface (Cristalline Textured surface manufactured by Eurosilicone) was included in the analysis as a *a posteriori* control.

Importantly, this analysis validates the topographical consistency of the nomenclature proposed in the Chapter III because the classes I, II, III and IV exactly encompass the smooth surface category, the PV-patterned surface category, the OC-patterned surface category and the SOC-patterned surface category. The categories are mainly discriminated by $Sdq_{LP_{105.8}}$ and therefore by the slope of the macroscopic roughness: OC- and SOC- surfaces have the highest slope because their LP-filtered surfaces exhibit pore walls, which are almost vertical, contrary to PV- and smooth surfaces. (Fig. 14) The slope of SOC-surfaces is more important than OC-surfaces because they present deeper structure. PV-surfaces have the highest fractal

dimension of the microscopic roughness because contrary to the others, their HP-filtered surfaces do not feature any smooth area.

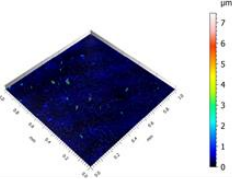
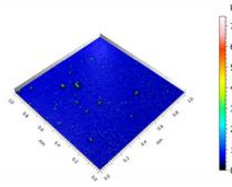
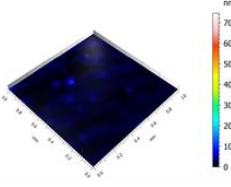
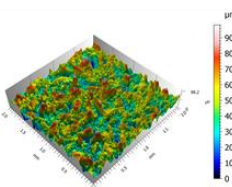
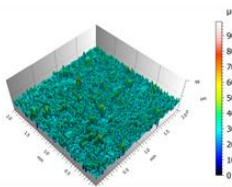
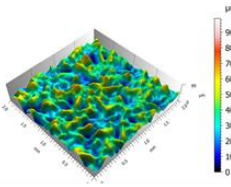
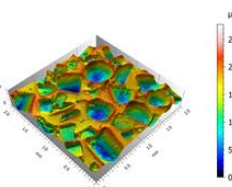
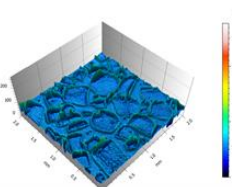
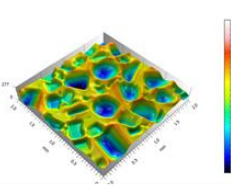
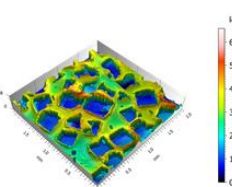
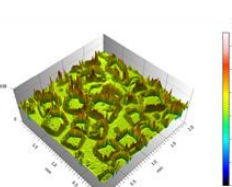
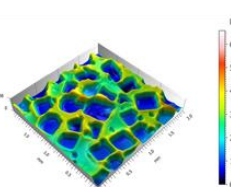
CATEGORY	Characteristic implant type	Measured surface	HP-filtered surface (cut-off= 105.8µm)	LP-filtered surface (cut-off= 105.8µm)
SMOOTH	Sebbin round smooth implant			
PICS AND VALLEYS	Perthese			
OPEN CAVITIES	Cristalline Micro-textured			
SEMI-OPEN CAVITIES	Biocell			

Figure 14 : Measured and filtered surfaces of a characteristic implant type for the 4 categories. A color calibration bar in micrometer (µm) indicates the height of the relief on the topographies where black and red represents respectively the lowest and the highest amplitude of topography.

4.3. DISCUSSION

The discriminant analysis statistically justifies the choice of the parameters and the boundaries, on which the proposed nomenclature is based. Moreover, the robustness of the classification was validated by means of an index. In comparison to the index

value obtained with our classification (99%), the classifications published by Barr *et al.*, Atlan *et al.* and Jones *et al.* have an index of 50%. Moreover, our classification is the first one able to discriminate between AND within different classes of breast implant surfaces. Basically, almost all the implant surfaces are discriminated between each other with the retained couple of parameters. Thus, the classification is so accurate that it is able to represent even the lowest differences between two types of texture and therefore to reveal the specificity of each one.

Even though they are not able to discriminate all the implant surfaces between each other and the designations of the categories are different, the grouping performed by Barr *et al.*, Jones *et al.* and Atlan *et al.* are consistent with ours. The classification of implants into the different categories of each nomenclature is detailed in Table 14. A color was assigned for each category of our classification. We can remark that the "smooth" and the "nanotexture" categories as well as the "minimal" category gather mainly the smooth implants. Most of the implants in the "microtexture" category in the ANSM-mandated report have PV-patterned surface, whereas they have OC-patterned surface for Barr *et al.* and Atlan *et al.* Similarly, the "low category" in Jones *et al.* groups only OC implants. The "macrotexture" categories in Barr *et al.* and Atlan *et al.* as well as the "intermediate" category in Jones *et al.*, exhibit primarily SOC-patterned implants whereas Atlan *et al.* finds more OC implants in the "macrotexture" category than in the "macrotexture +" category. PU-coated implants are also ranked in the "macrotexture +" category, whereas the ANSM-mandated report and Jones *et al.* added a specific category for those implants.

	Barr et al. (86)		Atlan et al. (94)	ANSM-mandated report
Smooth	Mentor smooth		Allergan smooth SilkSurface VelvetSurface	Arion smooth Allergan smooth Sebbin smooth Silimed smooth Eurosilicone smooth Nagor smooth Polytech smooth Mentor smooth
Nanotexture				
Mesotexture	SilkSurface			
Microtexture	<i>Porous</i>	TrueTexture Eurosilicone Microtexture PIP	MESMO Siltex Microcell	Arion Microtextured Sebbin Microtextured VelvetSurface SilkSurface
	<i>Non-porous</i>	Siltex Polytxt Cereplas VelvetSurface		
Macrotexture	<i>Porous</i>	Biocell Sebbin	Biocell TrueTexture Eurosilicone textured	Arion Textured Microcell Biocell Polytxt MESMO Nagotex Sebbin Macrotextured Sebbin Textured Silimed Textured Eurosilicone textured Eurosilicone Microtextured Siltex
	<i>Non-porous</i>			

Macrotecture +		Polytech PU Nagotex Polytxt	
PU			Polytech PU Silimed PU

Jones et al. (85)	
Minimal	Mentor smooth Allergan smooth VelvetSurface SilkSurface
Low	Nagotex Siltex
Intermediate	Eurosilicone textured Biocell Polytxt
High	Silimed PU

Table 14 : Comparison of the 4 existing classifications (in color the implants analyzed in our classification: SMOOTH, PV, OC and SOC)

The slight discrepancies between classifications would be due to the measurement methodologies. Thus, the “smooth” or “nanotexture” or “minimum” category mainly corresponds to our smooth category. SilkSurface (a PV-patterned surface) is the only inconsistency in these categories, which could be explained by the instrument used. Indeed, the X-ray Micro-tomography with a voxel size of 2.2µm or 15µm is not appropriate for these types of surface. Then, the “microtexture” or “low” category primarily encompasses the OC-patterned implants. Only Cereplas (a PV-patterned surface) is not a OC implant in these categories, probably because of the overlap between the boundaries. Then, the “macrotecture” or “intermediate” category principally gathers SOC-patterned implants. TrueTexture and Polytxt (OC-patterned surfaces) are the only discrepancies in these categories. Similarly, Polytxt was also

upgraded to the “*Macrotecture +*” in the classification proposed by Atlan *et al.* Their singularity (described by Atlan *et al.* and Jones *et al.* as “*sequestered surface area*” or “*enclosed pore*”) was also observed on our classification map. Effectively, a sub-category of the OC-group containing TrueTexture and Polytxt could be easily added. Finally, contrary to our study, Atlan *et al.* and Jones *et al.* were able to include PU-coated implants in their last category probably because they used custom-made indicators (such as “*surface area*” or “*surface area ratio*”) whereas we used standardized surface parameters.

This can be confirmed by our approach. The Figure 15 plots the distribution curves of the 17 implants surfaces obtained by one variable discriminant analysis with the metrological parameter used by Barr *et al.* (i.e. Sa) and with a metrological parameter similar to the indicator used by Atlan *et al.* and Jones *et al.* (i.e. Sdr). The 4 categories (SMOOTH, PV, OC and SOC) are identified on the two charts.

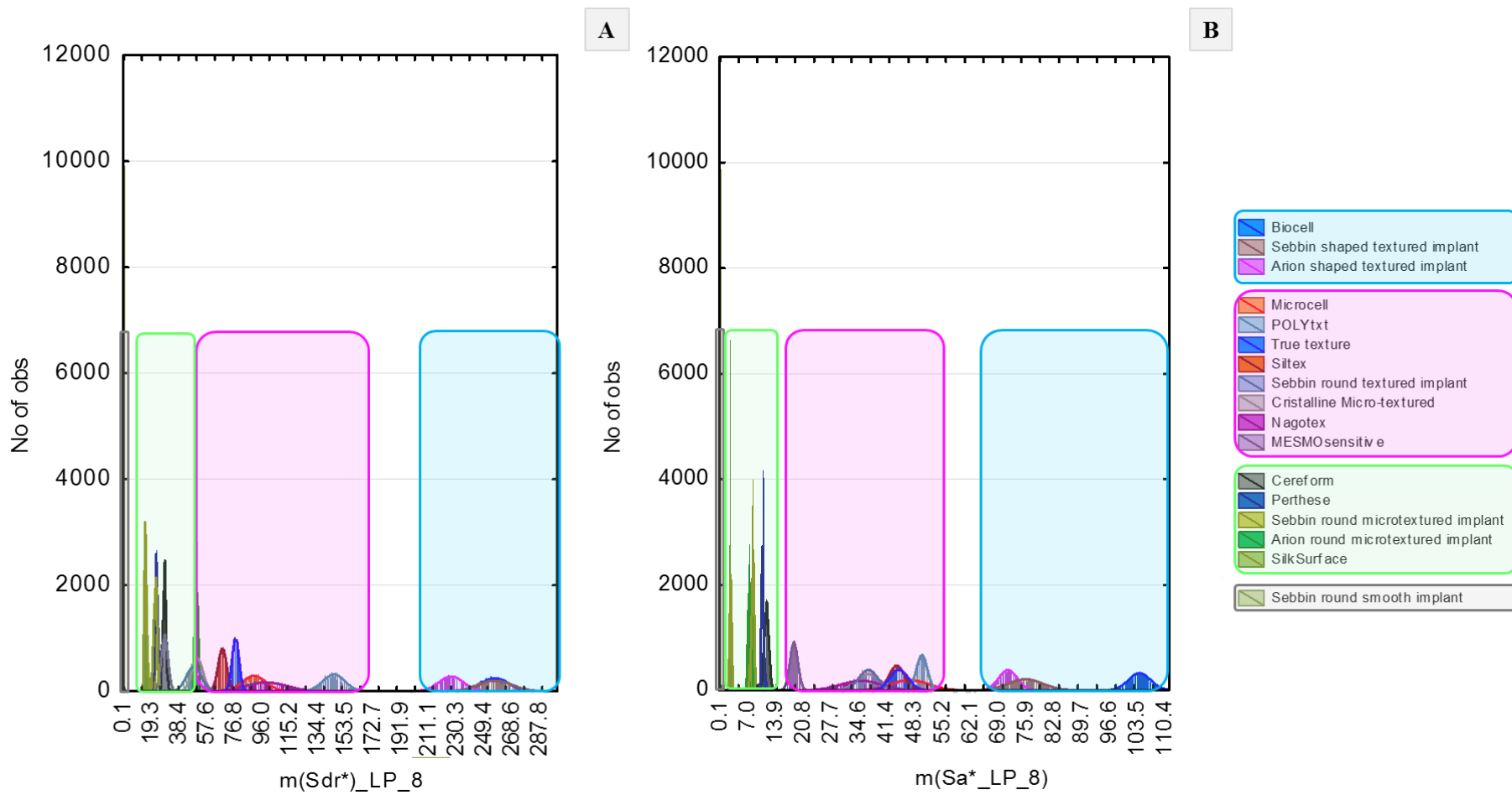


Figure 15 : Distributions of the 17 implant types analyzed according to the parameters Sdr (A) and Sa (B) (respective index value = [50% ; 50%]) retained after discriminant analysis performed only on parameters computed on measured surfaces, i.e. on $m(param^*)_{LP_8}$. Identification of 4 categories of implant types corresponding to the 4 differently-colored areas on the Sa -distribution.

Finally, the classification released in the ANSM-mandated report is not more consistent than the others because the PCA, which is an exploratory technique, is not designed to discriminate categories. The obtained categories (“smooth”, “microtexture” and “macrotexture”) are even more discrepant than the groups identified without statistical analysis. For example, the “macrotexture” category gathers both OC-patterned and SOC-patterned implants. This inaccuracy is probably due to the SEM measurements used in the ANSM-mandated report, which have to be stereoscopically reconstructed before to be analyzed. (cf. CHAPITRE II).

In addition to be an exploratory technique, the topographical meaning of the PC (even simplified to 2 terms) are difficult to determine, whereas a correlation between our classification and the topographical characteristics is much more straight-forward. The identification of morphologically-relevant group on the classification is therefore much easier.

4.4 CONCLUSIONS

Although one topographical parameter (such as the Sa or the developed surface) is able to recapitulate the proposed classification, these parameters do not allow us to discriminate each texture between each other. For this purpose, the discriminant analysis has to be based at least on a couple of two parameters. The analysis allowed us to select the couple constituted of the mean slope of the macroscopic roughness and the fractal dimension of the microscopic roughness. Contrary to the nomenclatures published, the statistical technique used validated the robustness of this couple of parameters.

Silicone debris release from the implant surface could be involved in the pathogenesis of BIA-ALCL. It is of primer importance to study the putative damage on the surface of breast prostheses once implanted, which has been performed in the literature yet. A such *ex vivo* study should firstly verify whether our classification is able to be extended to explants, in term of morphologies and obtained values on the retained parameters. In other words, we will be able to test the *in vivo* robustness of our classification,

Basically, do an implant exhibiting a PV structure remains identifiable as a PV structure, after implantation? Then, in order to assess the biological criticality of such silicone particles, damage must be measured and compared between the different categories of our biologically-validated classification. That will be the focus of the next chapter.

CHAPTER V: *IN VIVO* DAMAGES OF DIFFERENT TEXTURED BREAST IMPLANTS

5.1 INTRODUCTION

The surface patterning of breast implants (also called texture) is a highly topical subject since, even if the causal link remains to be definitively demonstrated, certain types of texture would represent an increased risk factor for the development of BIA-ALCL. (110)

All these cases raised the question of the etiology of BIA-ALCL. It is acknowledged that BIA-ALCL results from an inflammatory process. Indeed, among the five articles selected in the review of the CHAPTER I, "*chronic inflammation*" is explicitly reported in 4 articles. (58, 67, 177, 178) Some hypotheses are mentioned in the literature, such as the biofilm or possibly silicone debris released from the surface of the implant. (58, 67, 177) Indeed, Brody *et al.* noted that "*the fluid associated with ALCL tended to be cloudy and debris filled*". (35) Moreover, Danino *et al.* observed micrometric particles in the tissue, which would be released from the Biocell texture. (88) (Fig. 16)

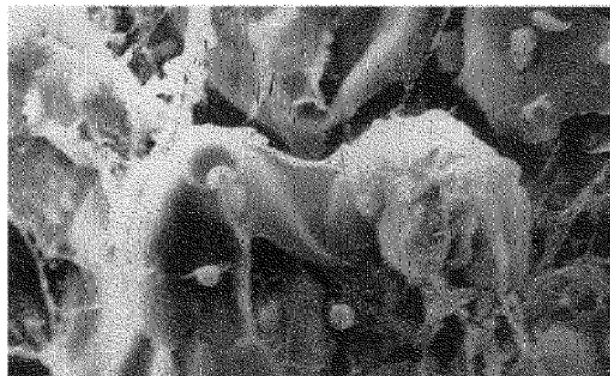


Figure 16 : Micrometric particles observed in the capsule. (SEM x7500) (Danino *et al.*)(88)

For the understanding of biological mechanisms, it is of primer importance to evaluate the mechanical stability of these surface structures. Two *in vitro* wear simulations were published on breast implants: Webb *et al.* characterized qualitatively by SEM the damage of three different textures (Biocell, Siltex and TRUE Texture) by peeling an adhesive polymer off the implant surface. (179) The other one performed by Ramajo

et al. imaged also by SEM the damage of the implants of two brands after immersion in a phosphate-buffered saline solution and in a potassium hydrogen phthalate buffer solution at controlled temperature and pH for 12 weeks. (171) Briefly, Webb *et al.* observed a particulate shedding for the three textures, which is particularly emphasized for Biocell texture. On the contrary, Ramajo *et al.* failed to see any change on the implants' shell structures after immersion during 12 weeks.

However, it is noteworthy that the mechanical stresses that the surface structures could undergo locally in the breast are not known. They are estimated only approximately and globally. (180) Moreover, in general biomechanical studies on soft tissues «oversimplify the structure of the tissues». (168)

Therefore, in the absence of valid biomechanical data on the tissue surrounding breast implants, it seems somewhat pretentious to want to reproduce the wear conditions of the textures and therefore to propose an *in vitro* wear protocol.

In addition to being weakly representative from a biomechanical and anatomical point of view, a study of the *in vivo* wear of textures on animals is difficult to carry out if we take into account the long-life of the implants (which is approximately 10 years).

Consequently, the best compromise to characterize the structural evolution of breast implant textures once implanted in the body of the patient is to topographically analyze the surface of implants removed from the human body (called "explant"). However, until now there was no article in the literature relating a *post-mortem* (or *ex vivo*) topographical study of breast implant surface although such studies are very numerous on orthopedic implants. This is all the more surprising since the numbers of breast implantations and hip procedures are similar, as evidenced by the statistics of 2017 in the USA (322,932 breast augmentations (https://www.isaps.org/wp-content/uploads/2018/10/ISAPS_2017_International_Study_Cosmetic_Procedures.pdf) versus 313 246 hip procedures (<https://www.ajrr.net/media-news/press-releases/500-ajrr-releases-2017-annual-report-on-hip-and-knee-arthroplasty-data>)).

A bibliometric analysis on the Web Of Science has quantitatively substantiated this fact over the last 20 years with "hip implant" (or "prosthesis") and "breast implant" (or "prosthesis") as keywords. (Appendix 1) Briefly, over the last 20 years, there is 10 times less articles on breast implants than on orthopedic implants.

Actually, several barriers still persist to carry out a topographical expertise of the surface of the breast explants.

- Some barriers are related to handling in the operating room: it is not usual to store explants in the breast surgery field.
- Other barriers concern the protocol of explant decontamination, which does not provide for a systematic *a posteriori* analysis of the explant. For example, it is common that after these procedures, fragments of biological tissue remain, which, once hardened, become adherent to the surface of the explant. Topographical measurement of the explant surface at these locations is therefore impossible.
- Traceability is not systematically implemented in breast surgery. Thus, the characteristics of the explant (such as the name of the manufacturer and the device reference) are hardly known because they can be poorly readable on the device or unknown to the patient. Consequently, a straight-forward implant / explant comparison, by measuring the surface of the same prosthesis before and after implantation, would require an average traceability of 10 years, which is rarely performed.
- One of the most impeding barriers is the weak clinical follow-up existing on breast implants, and therefore the few robust statistical elements available. This can be explained by the "aesthetic" connotation of breast implants, which reduces the number of research topics on these implants in favor of implants considered more "functional" such as orthopedic implants.
- Finally, the last barrier, which is all the more blocking as the previous one, is linked to the new version of the ISO 14607: 2018 standard which presents metrological aberrations, in particular on the choice of measuring instruments. For example, according to the standard, the AFM (which is used for measurements of extremely fine roughness and very small surfaces) should be

able to measure all types of textures (including those with almost vertical cavity walls) over a 2mm² area.

In order to be able to characterize for the first time the topographical evolution of breast implant textures after implantation, a study has been set up. As detailed below, our approach is based on a topographical and clinical expertise.

- We relied on a preliminary study that allowed us to validate the choice of our methodology for measuring and analyzing breast implant surfaces. (80) Textures obtained by mold replication was characterized by interferometry. The latter becoming inadequate for textures obtained by “salt-loss” processes because of their strong topographical slopes, X-ray micro-tomography was chosen to measure these last textures.
- A nomenclature of implant textures in three categories, namely Peaks and Valleys (PV), Open Cavities (OC) and Semi-Open Cavities (SOC), has been defined, allowing harmonization of the different designations using terms independent from those used in marketing denominating a texture and that are topographically meaningless.
- To collect the explants of this study, a scientific collaboration was set up with a clinician with 40 years of experience in the field of breast implantation. Statistical analysis was therefore facilitated by the fact that the surgeon explanted what she had implanted, minimizing the loss of information about the device and the patient.
- This approach allowed us to present the first results on a possible *ex vivo* degradation of different types of texture. A comparison of the degradations between the different textures was also possible.

5.2 MATERIALS & METHODS

In this study the patients were followed by the surgeon from the placement to the explantation. The reasons for reintervention could be related to aesthetic reasons (such as too small cup or unsatisfactory breast shape) or postoperative complications

(such as implant rupture, hardening of the breast or pain). All the explants were filled with silicone gel.

These data categorized according to the implant nomenclature we proposed are summarized in Table 15. The texturing processes of the implants are also detailed.

As described by Garabedian *et al.*, surface measurements were made with an interferometer for the PV-assimilated explants and with a micro-tomograph for the OC- and SOC-assimilated explants. (80) Interferometer measurements were performed under white light and with a x50 objective. Regarding the micro-tomograph, the X-ray source was powered by a voltage of 80kV and an intensity of 100 μ A. The size of the voxels was set at 2.5 μ m. As often only a fragment of the explant's apex was harvested, three measurements of 4mm² were performed by explant.

For the implant / explant comparison, one implant for each type of texture detailed in the Table 15 (Cereform, Sebbin round implant texture, Micro-textured Crystalline, Nagotex, Sebbin shaped implant texture and Biocell) was analyzed.

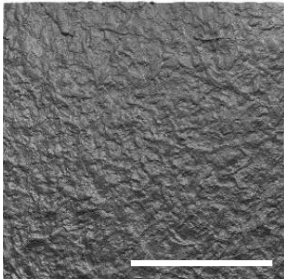
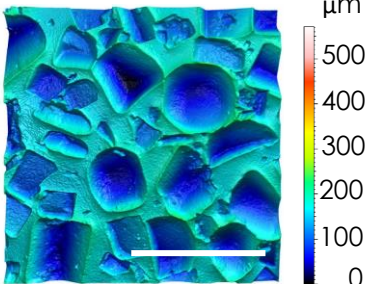
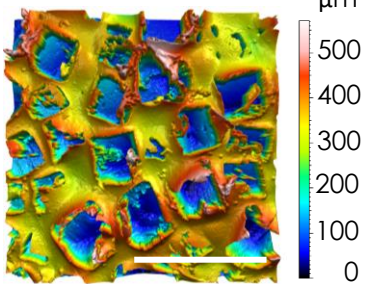
Reference to implant category	Implant topographies	Types of textures (manufacturer)	Texturing process	Total sampling = 41 explants including 29 patients
PV		Cereform (Cereplas)	Mould replication	3 explants (including 3 patients)
OC		Sebbin round implant texture (Sebbin)	« Salt-loss »	21 explants (including 15 patients)
		Micro-textured Cristalline (Eurosilicone)	« Salt-loss »	2 explants (including 1 patient)
		Nagotex (Nagor)	« Salt-loss »	1 explant (including 1 patient)
SOC		Sebbin shaped implant texture (Sebbin)	« Salt-loss »	13 explants (including 8 patients)
		Biocell (Allergan)	« Salt-loss »	1 explant (including 1 patient)

Table 15 : Implant characteristics and patient clinical data of the explant sampling. For clarity, the color height scale for the PV category was not represented. The approximate maximal height of this type of structure is 100µm.

To determine the scale at which the implant / explant comparison is the most relevant in regards to biological phenomena, a multi-scale decomposition of the surfaces was conducted. Basically, the topographies were first analyzed using the Mountains®

software (Digital Surf, Besançon, France) from the raw measurements. Two Gaussian spatial filters, namely High-Pass (HP) and Low-pass (LP) filters, were applied to decompose all the roughness scales contained in each measured surface. By applying a HP filter, we remove the roughness scales above a defined threshold and obtain only the lowest roughness scales. Conversely, an LP filter extracts the roughness scales higher than the defined threshold. (Fig. 17)

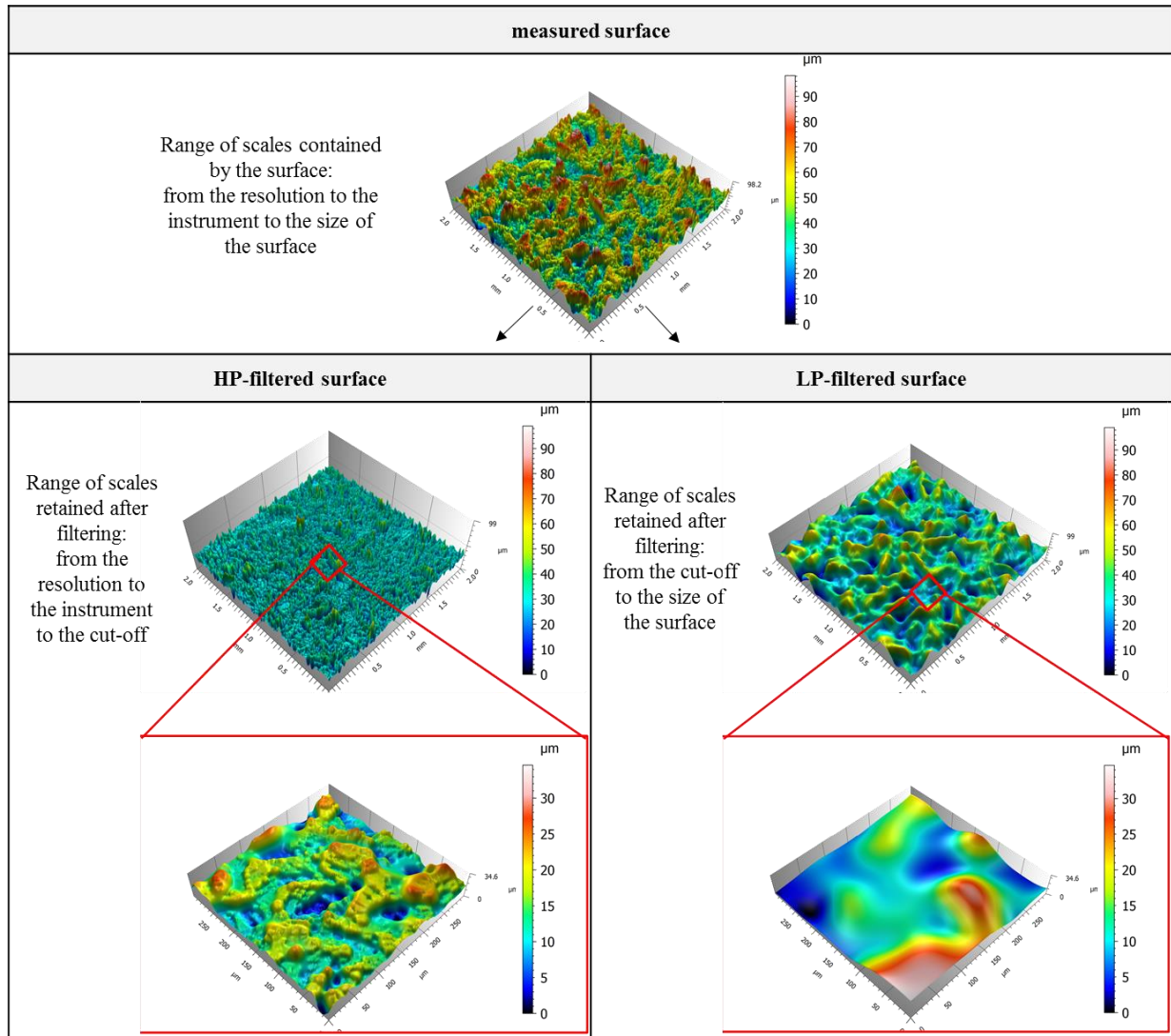


Figure 17 : Principle of surface filtering (example given with a threshold of $105\mu\text{m}$). (A) Measured surfaces containing the full range of roughness scales, once filtered by a High-Pass (HP) filter, retain the roughness scales below the threshold value and up to the instrument resolution. (B) Low-Pass filter (LP) filtered surfaces only contain roughness scales above the threshold value.

By sequentially increasing or decreasing the threshold value, we are able to reveal the spectrum of all the topographical scales included in each measured surface, namely

the surface roughness with HP filter and the surface waviness with LP filter. Then, we calculated for each surface of the spectrum a large number of topographical parameters. We are able to easily obtain for each of these parameters its evolution according to the filter threshold and therefore according to the scale. Basically, these plots describe their multi-scale behavior.

In this publication, we restricted our study to the multi-scale analysis of Sa by HP filter because the latter is sufficient to describe the multi-scale behavior of breast implant surfaces. (80)

The damage was finally quantified as the relative difference between the Sa of the implant and that of the explant over the entire wavelength range, as explained in formula [1].

$$\text{Damage amplitude} = \frac{Sa_{\text{implant}} - Sa_{\text{explant}}}{Sa_{\text{implant}}} \quad [1]$$

An analysis of variance (ANOVA) between the Sa values of the implants and those of the explants, as well as the calculation of the Fisher value (F) was conducted on all the scales studied. The multi-scale curve of the F superimposed on those of the Sa allowed us to graphically represent an area of relevance and an area of non-relevance defined from a threshold of relevance (which is hereafter fixed at 1).

5.3 RESULTS

From the multi-scale analysis, we were able to compute the average value of the Sa at a given scale and to plot its evolution according to the scales. At small scales, the Sa characterized only the micro-roughness, which is low. The latter was completed by waviness on the large scales, especially the roughness of the cavities which has a much larger Sa. Thus, this evolution, which will be represented in a logarithmic coordinate system, was increasing. The confidence intervals obtained on the averages were represented by dashed lines.

We thus obtained the multi-scale curve of the average Sa and its confidence interval for the implants, as well as for the explants. We then were able to draw the F value according to the scales, to quantify the degree of significance. Thus, the higher the F value, the larger the difference between the Sa_{implant} and Sa_{explant} . Conversely, the closer the F value is to 1, the more non-significant the difference.

The combined multi-scale analysis of Sa_{implant} and Sa_{explant} as well as the one of the F were initially explained separately for each type of texture. (Fig. 18, 20, 22, 24, 26, 28) The differences between the topographies of the implants and those of the corresponding explants were illustrated in parallel. (Fig. 19, 21, 23, 25, 27, 29)

5.3.1 CEREFORM TEXTURE (CEREPLAS) (PV)

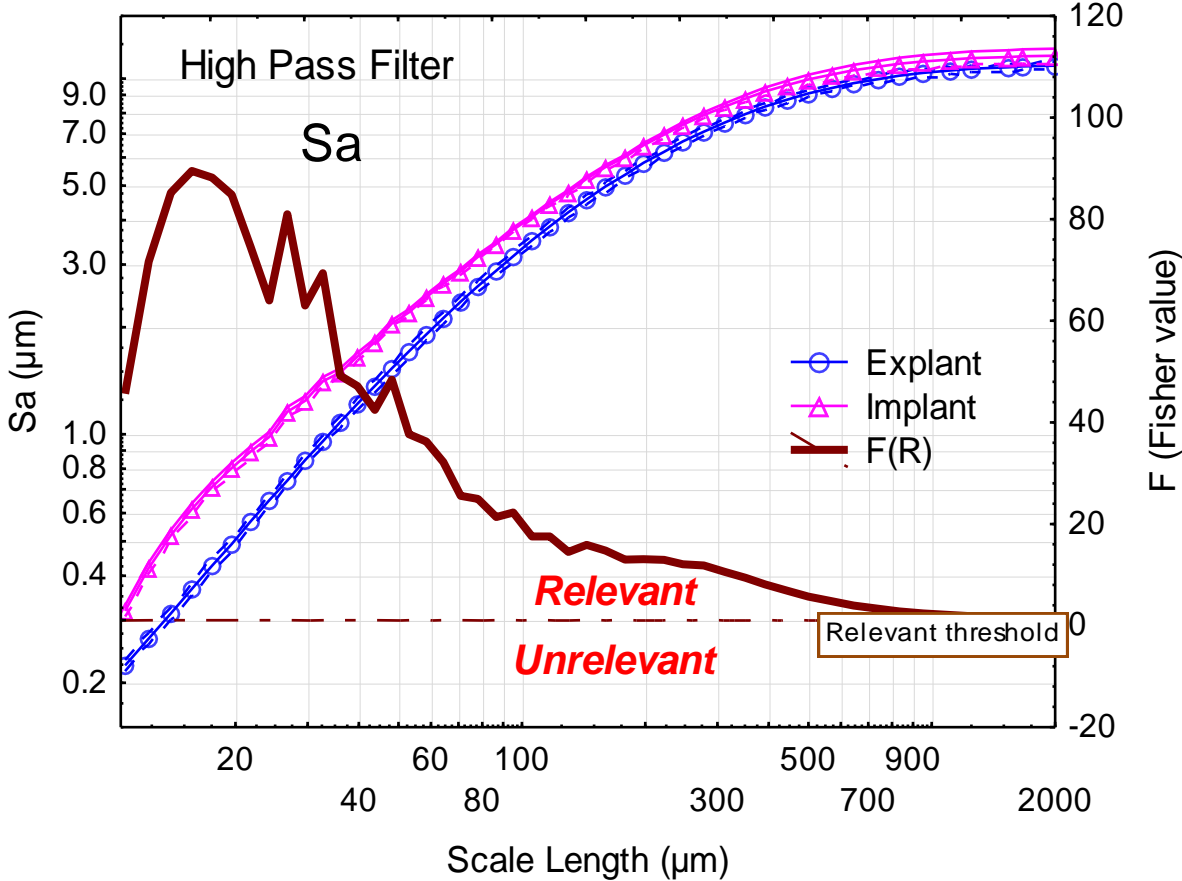


Figure 18 : Multi-scale curves of Sa_{implant} and Sa_{explant} and F for Cereform texture (PV)

At all scales, the Sa of Cereform explants is smaller than the Sa of the Cereform implant, which is characteristic of a wear phenomenon. The measurements are extremely homogeneous. Given the small dispersions, this difference is significant over all the scales studied, as evidenced by the F curve which is constantly above the threshold of relevance. The wear of the Cereform explants is therefore multi-scale. The damage is gradually less and less pronounced by increasing the scales.

By examining the topographies, we observe a "smoothing" of the micro-roughness, as shown in the Figure 19.

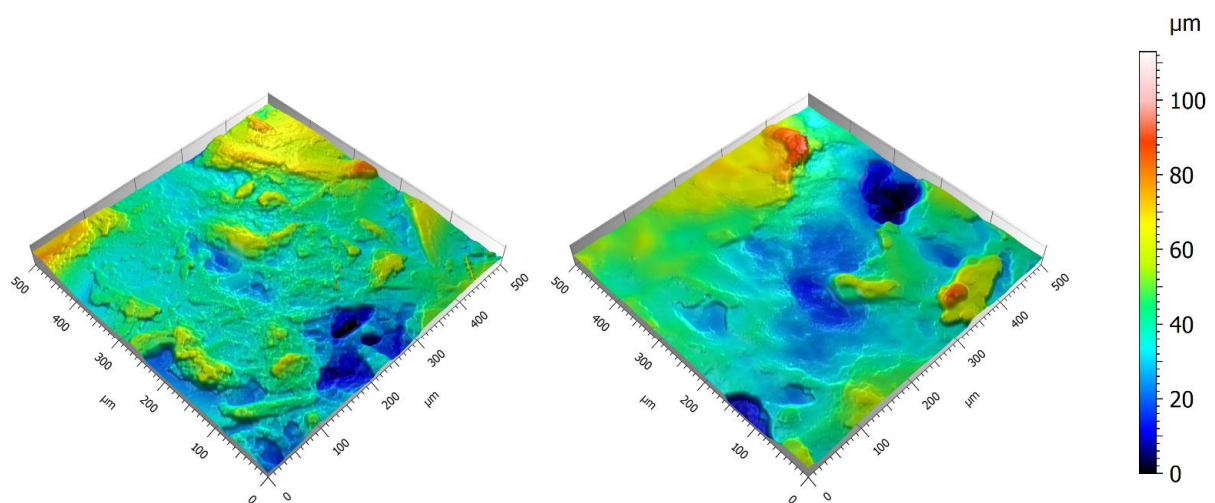


Figure 19 : "Smoothing" of micro-roughness on Cereform explants (left: implant, right: explant)

5.3.2 SEBBIN ROUND IMPLANT TEXTURE (SEBBIN) (OC)

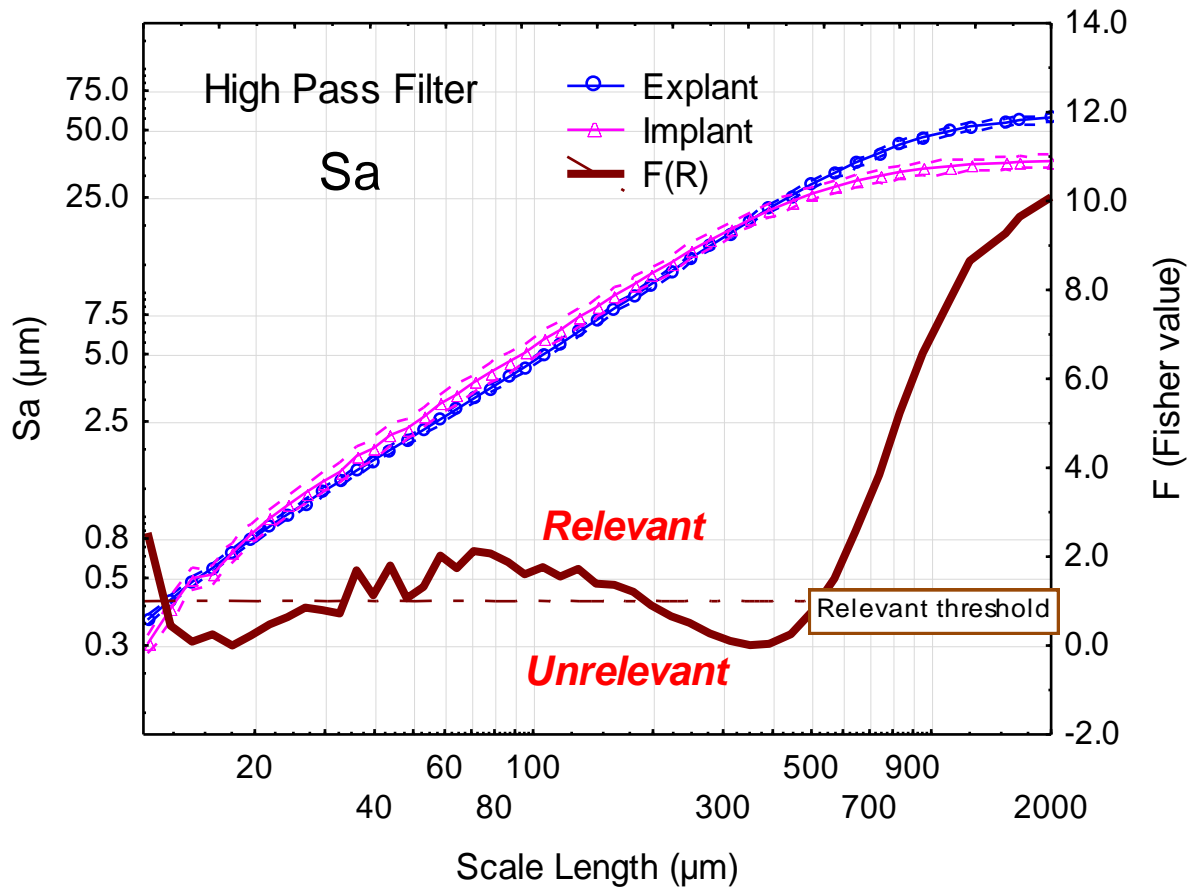


Figure 20 : Multi-scale curves of Sa_{implant} and Sa_{explant} and F for Sebbin round implant texture (OC)

Once again, the explant curve is below the implant curve except for the very low and the very high scales, which are characterized respectively by a small peak and by an exponential rise on the F-curve. Therefore, the multi-scale analysis of this texture reveals a small increase in roughness amplitude at the low scales and a sharp increase in roughness amplitude at the high scales.

On the other scales, as the dispersion of the measurements on the implant surface is larger than for PV implant, this difference remains within the significance limit. The multi-scale curve of Sa calculated on these explants does not attest much damage. In addition, we note on this scale range a fractal regime (characterized in a logarithmic coordinate system by a linear evolution of the Sa according to the spatial length) on the implant curve as well as on the explant curve.

This type of texture, obtained by indentation of calibrated salt crystals on the surface of the non-crosslinked silicone envelope is characterized by cuboidal cavities. It is therefore distinguished by a good stability (and therefore by low damage) at all scales. The damage to the characteristic structures of these cavities (such as the edges, the bottom of the cavities and the plateaus) is topographically confirmed. Indeed, the edges are almost at right angles and the bottom of the cavities and plateaus exhibit a step pattern even on the explant. (Fig. 21)

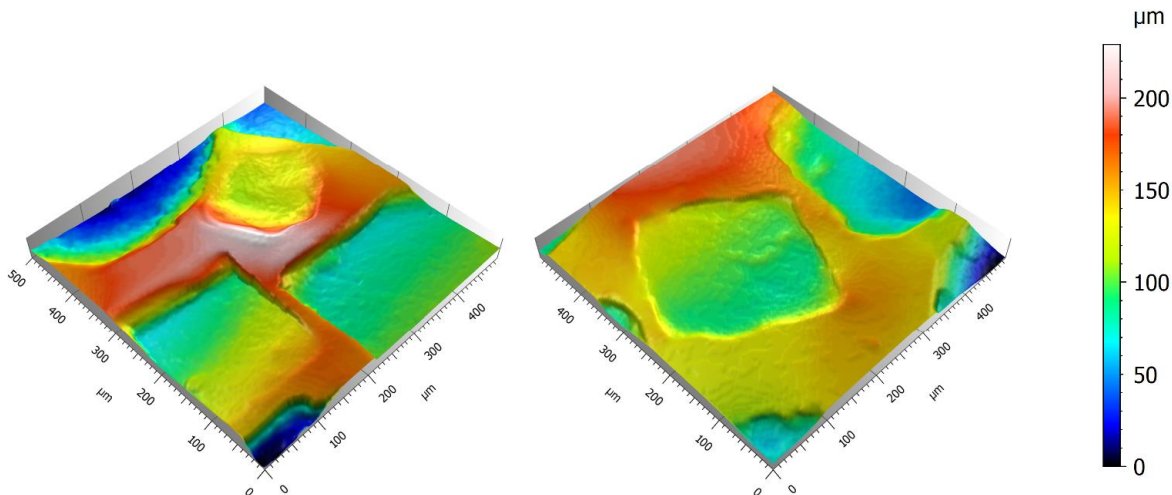


Figure 21 : Damage on Sebbin round textured explants (left: implant, right: explant)

5.3.3 CRISTALLINE MICRO-TEXTURE (EUROSILICONE) (OC)

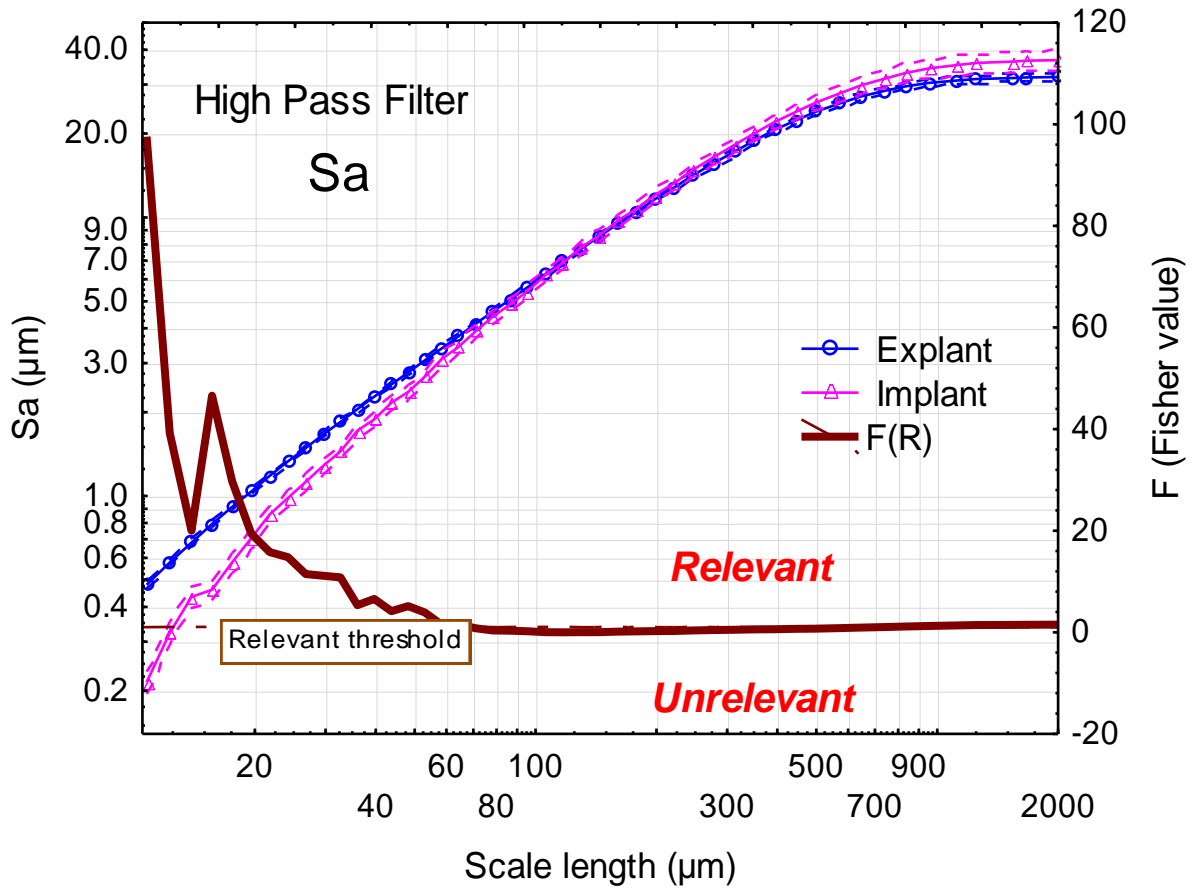


Figure 22 : Multi-scale curves of Sa_{implant} and Sa_{explant} and F for Eurosilicone Crystalline Micro-texture (OC)

A similar implant / explant behavior is observed on the scales higher than 100 µm with a fractal behavior and perfectly superimposable curves on Crystalline Micro-texture. Below 100µm, the decline of the implant curve is more important than for the explant curve. This deviation gradually increases on the very low scales. Then, this increase in the Sa value of the explant (which is almost double at the very low scales) reflects a phenomenon of micro-roughness "creation", which is confirmed by the F-curve. Indeed, the threshold of relevance is exceeded on the scales lower than 60µm and a peak at the very low scales is again observed.

Topographically, the explants are characterized by the homogeneous appearance of very small peaks on the bottom of the cavities and on the plateaus between the

cavities, which is not observed on the implant surface. The edges of these cavities remain almost at right angles (Figure 23).

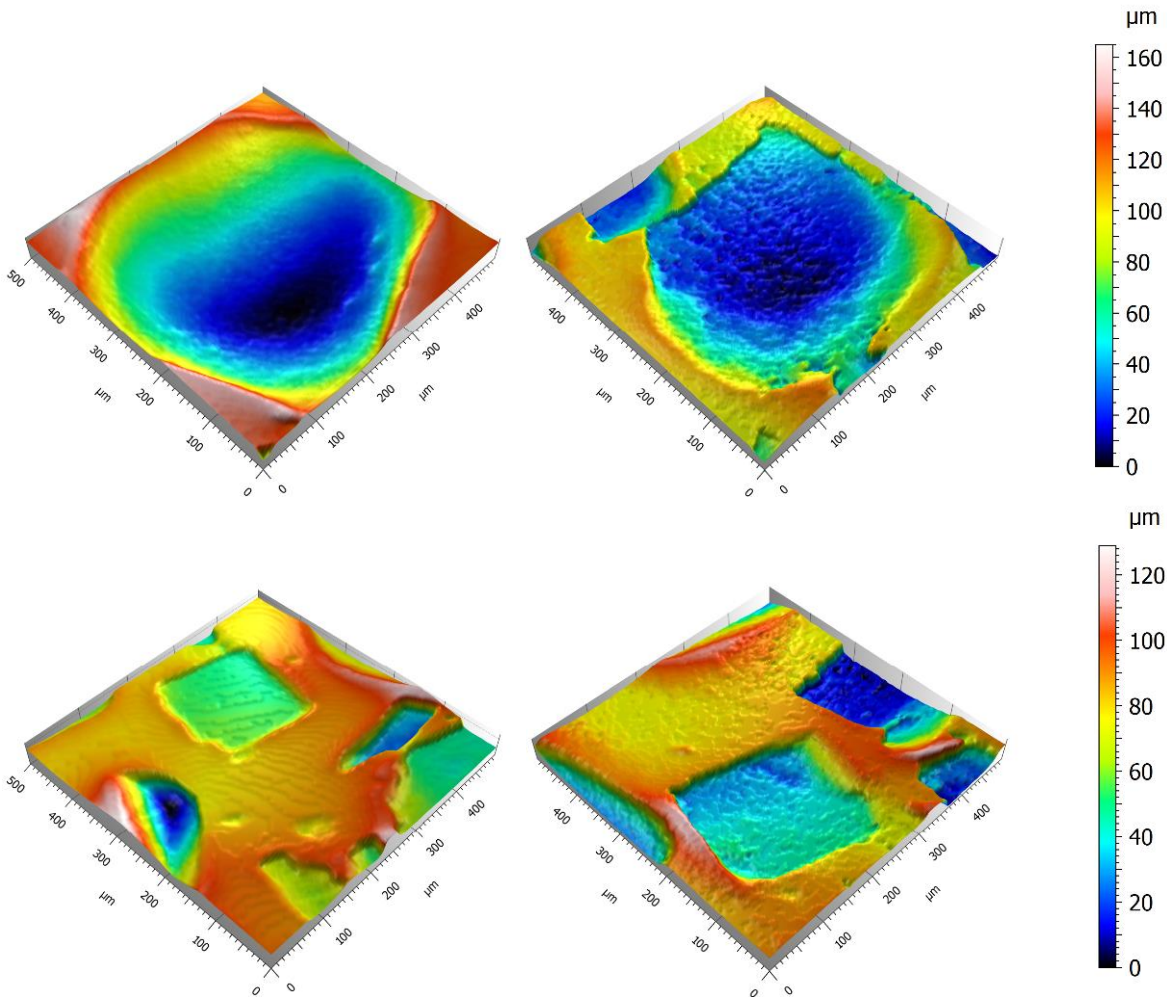


Figure 23 : Appearance of very small irregularities on the Eurosilicone Crystalline Micro-texture explant (left: implant, right: explant)

5.3.4 NAGOTEX TEXTURE (NAGOR) (OC)

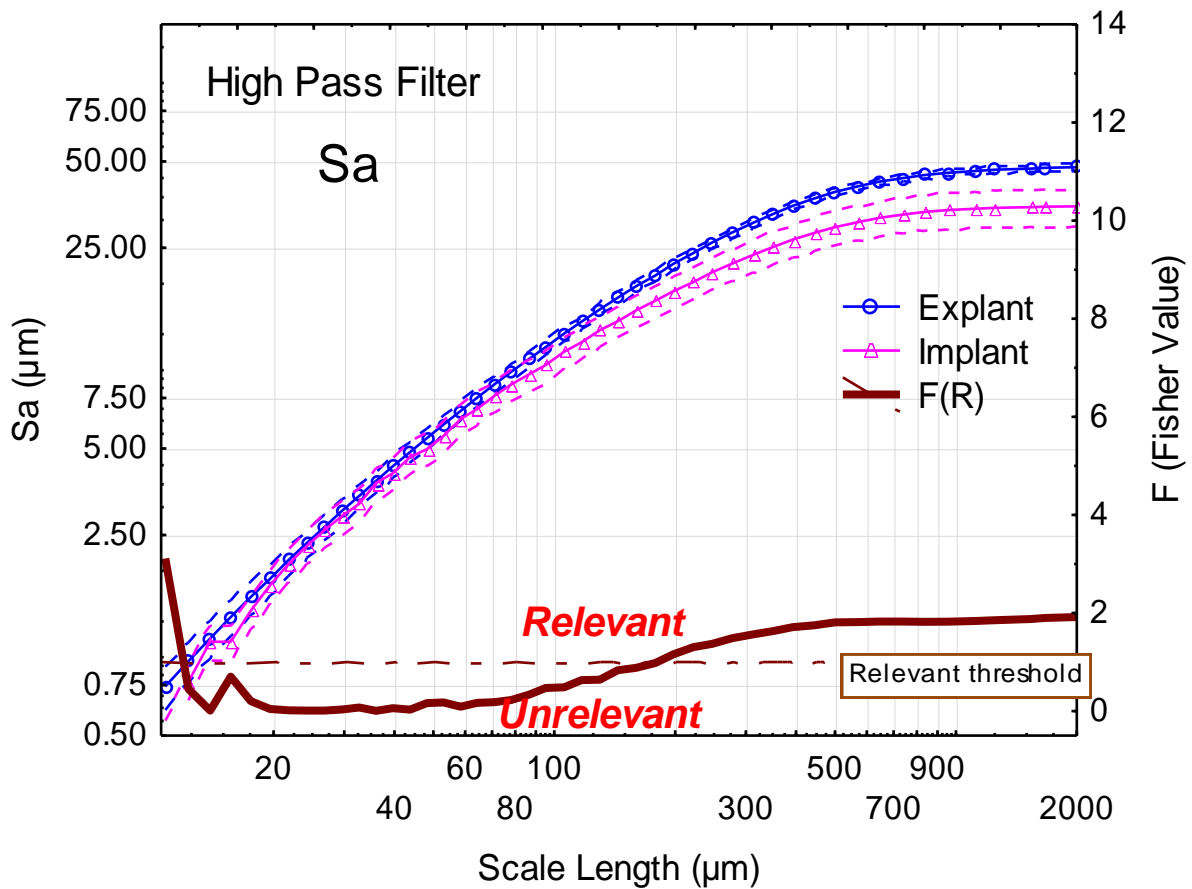


Figure 24 : Multi-scale curves of Sa_{implant} and Sa_{explant} and F for Nagotex texture (OC)

Contrary to Eurosilicone explant, the Nagor explant exhibits a good stability of its texture on the low scales (less than 100µm), although it displays a larger dispersion than the implant. However, on the higher scales, the roughness of the explant is increased, while having the same dispersion. The roughness difference becomes significant from 200µm, as indicated by the threshold crossing of the F-curve. Once again, a peak is present on the F-curve at the very low scales. It represents the creation of micro-roughness.

Based on the Figure 25, the topography of the explant is characterized by an increase in the width of the cavities with some cavities 4-5 times wider than those on the implant. Those cavities are also deeper with a depth value of about 270µm on the explant and

200 μm on the implant. In addition, cavities on the explant are much more heterogeneous in size and less cubic and more irregular in shape than on the implant.

Noteworthy, the roughness present on the edges of the cavities of the implant is preserved on the explant.

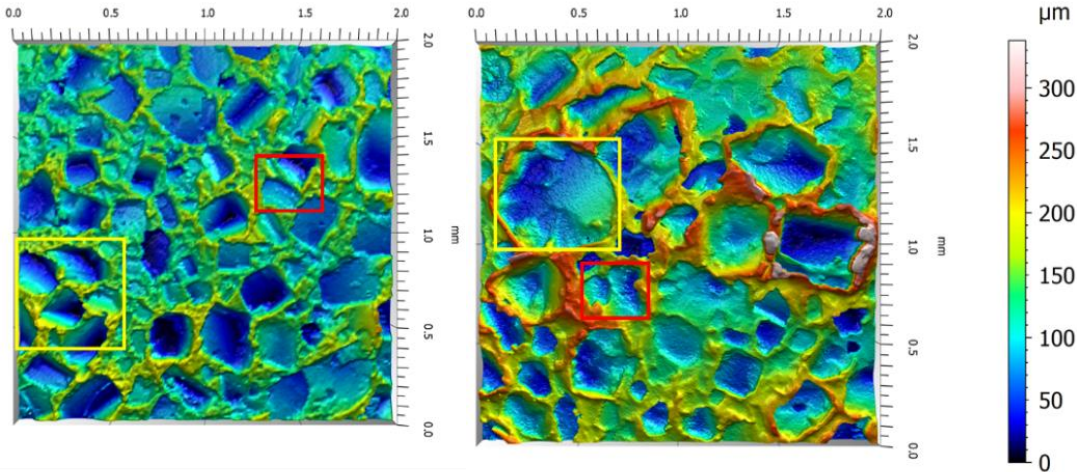


Figure 25 : Macroscopic irregularity of the cavities on the Nagor explant (left: implant, right: explant)

5.3.5 SEBBIN SHAPED IMPLANT TEXTURE (SEBBIN) (SOC)

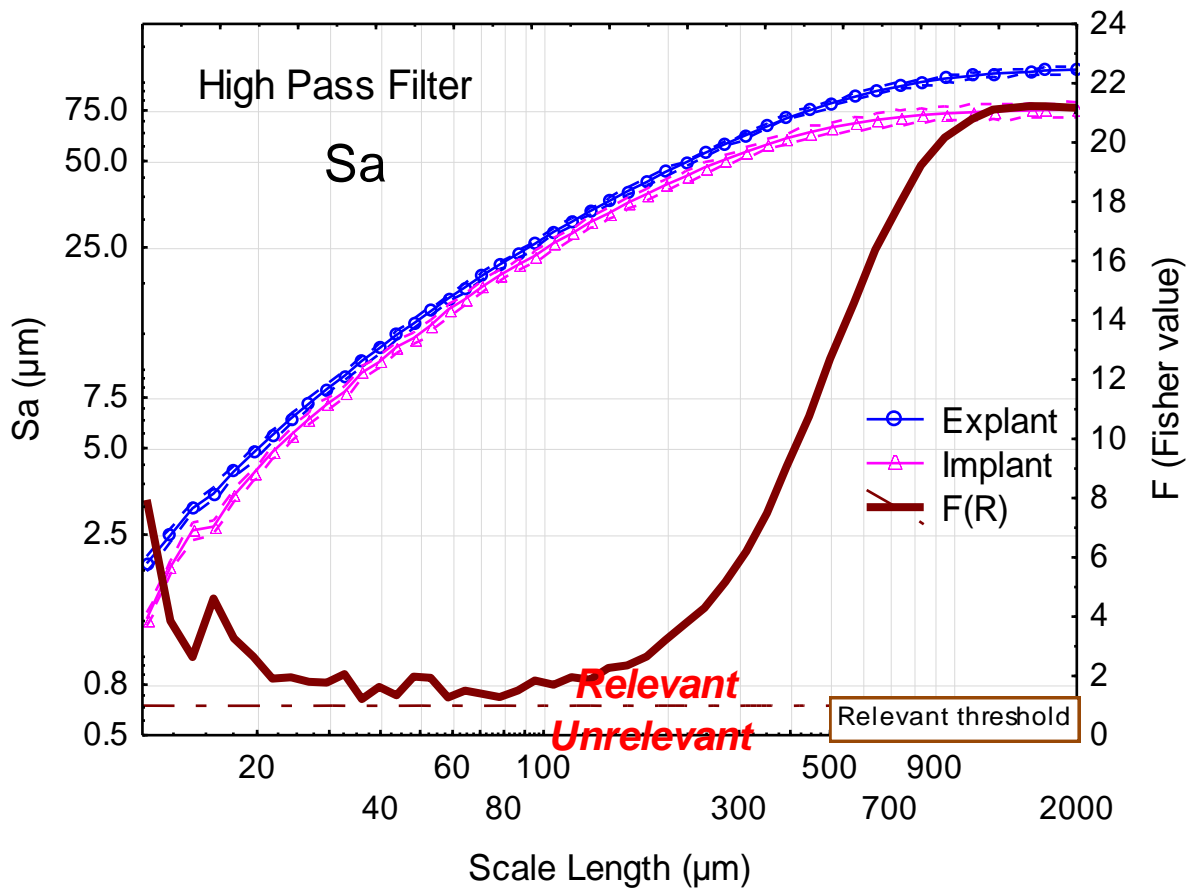


Figure 26 : Multi-scale curves of Sa_{implant} and Sa_{explant} and F for Sebbin shaped implant texture (SOC)

The multi-scale plot for Sebbin shaped implant texture reveals three regimes. The first regime extends on the scales less than $30\mu\text{m}$. It is characterized by a more important decrease on the implant curve than on the explant curve. The second regime is between $30\mu\text{m}$ and $200\mu\text{m}$. The behavior of the two curves is fractal and the gap between the curves is in the range of the dispersion. Since $200\mu\text{m}$, a third regime starts, featured by an inflection of the implant curve. The multi-scale curve of the explants thus demonstrates a larger roughness on the very low scales (less than $30\mu\text{m}$) and a larger roughness on the very high scales (higher than $200\mu\text{m}$). The F-curve confirms these 3 regimes. There is a sharp increase in F below $30\mu\text{m}$ and above $200\mu\text{m}$ and an intermediate regime characterized by a plateau slightly above the threshold of relevance.

The surface of Sebbin shaped implants is more complex and heterogeneous than OC implants: it exhibits more or less semi-open cavities. Topographically, the explants feature the appearance of very small peaks (their amplitude is in the range of ten microns) within the majority of the cavities, whereas they were completely smooth on the implant. On the higher scales, there is a destruction of their "cap". As only the vertical walls of the cavities remain, the latter appear topographically more open. (Fig. 27)

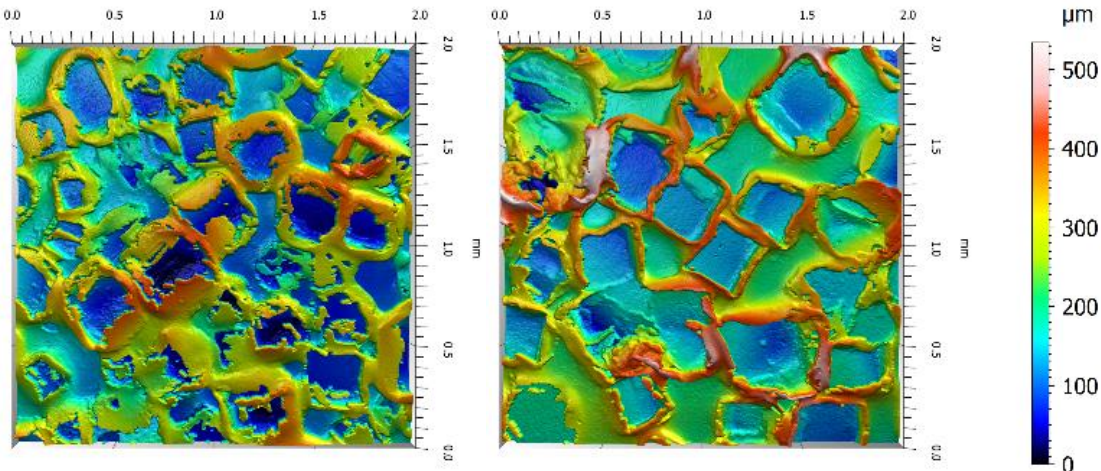


Figure 27 : Macroscopic opening of cavities on the explants (left: implant, right: explant)

5.3.6 BIOCELL TEXTURE (ALLERGAN) (SOC)

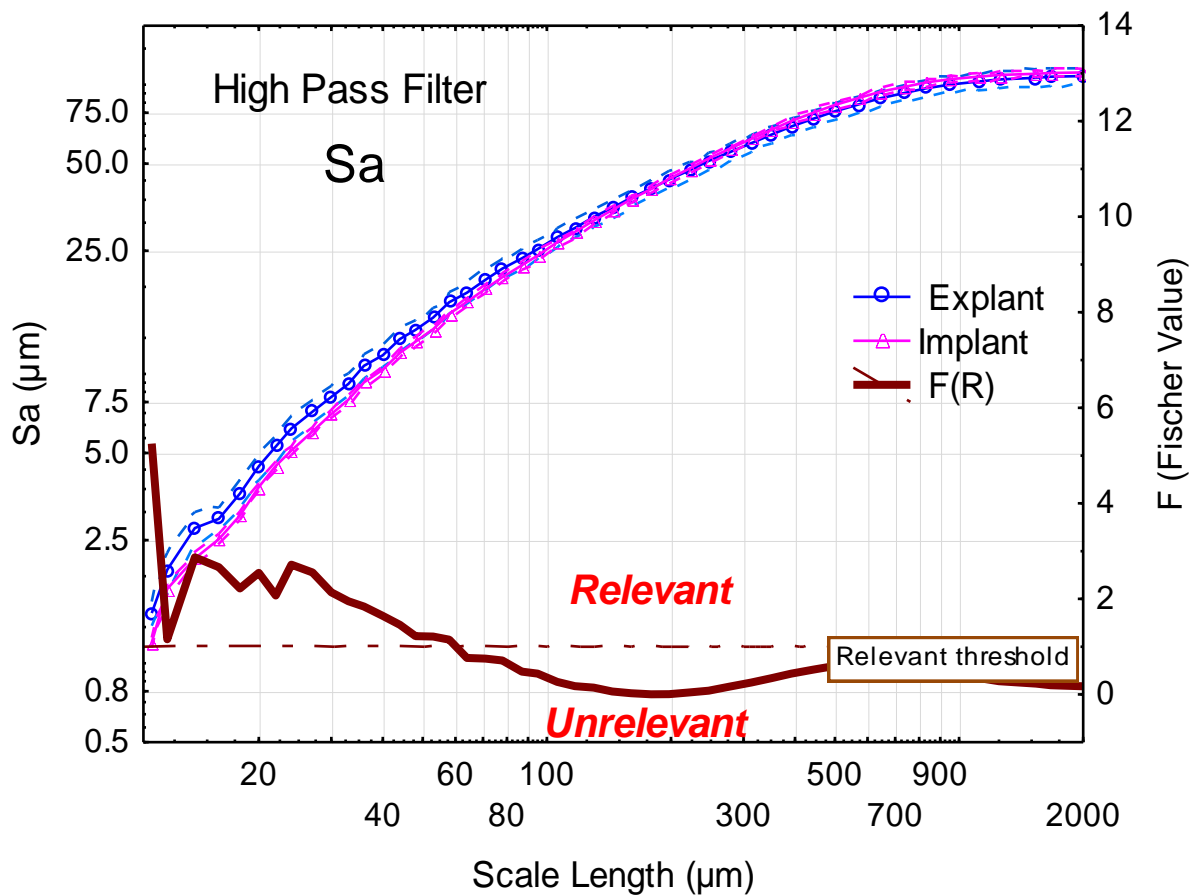


Figure 28 : Multi-scale curves of Sa_{implant} and Sa_{explant} and F for Biocell texture (Allergan)

Compared with the previous curves, the multi-scale dispersion of the Allergan explant (dashed curves) is much larger, which indicates a very important variability in topographical measurements.

As a result, the multi-scale behavior of the explant is not significantly different from that of the implant over the entire wavelength range, with the exception of small scales, where a peak is once again observed.

The topographies of the Figure 29 illustrate the heterogeneity in size of the cavities present on the surface of the explants, compared to the implant. If you draw a diagonal on the topography of the explant, two areas can be easily identified. In addition, apparently the damage of the "cap" is much more heterogeneous than on the Sebbin shaped explant.

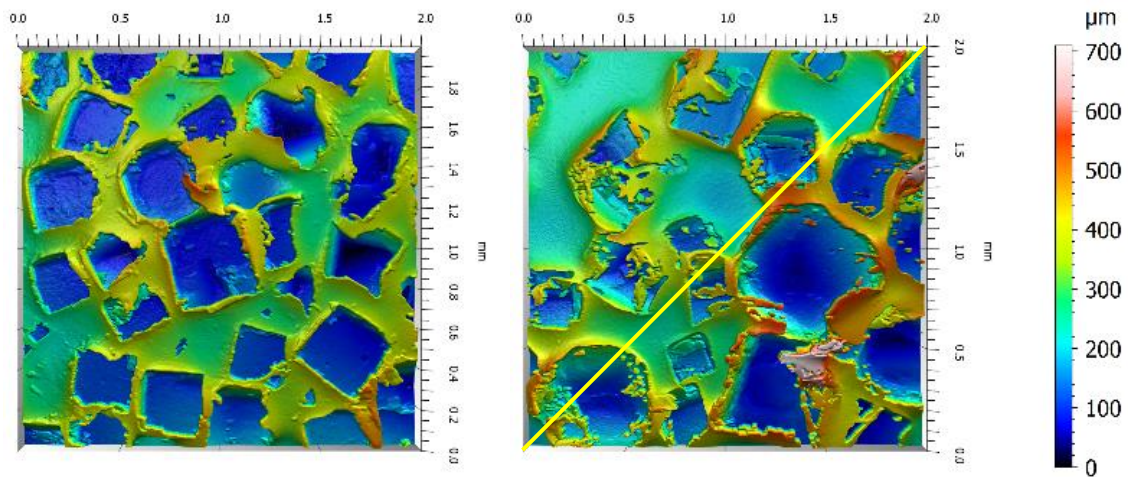


Figure 29 : Large heterogeneity of Allergan explant surface (left: implant, right: explant)

5.4 DISCUSSION

5.4.1 VALIDATION OF THE BREAST IMPLANT CLASSIFICATION

On the basis of a much more extended sampling of implants (17 different types of textures from 7 manufacturers) and a more important database of topographical parameters, we have previously defined a new classification of implants. (cf. CHAPTER III) This classification relies on a complete and robust 2-variable discriminant analysis.

After data bootstrapping, screening of all possible couples of topographical parameters and calculation of a classification index, the classification was obtained with the selected parameter set:

- the average slope (Sdq) of the waviness that has a characteristic scale higher than $105\mu\text{m}$
- the tortuosity (Sfd) of the roughness that has a characteristic scale lower than $105\mu\text{m}$

The classification allowed us not only to discriminate 4 categories of implants (SMOOTH, PV, OC, SOC), but also to determine the singularities of each type of texture

(which had never been performed until now). These four categories were determined according to the values of these two parameters, as detailed in the Table 16.

	Average slope of waviness (cut-off=105µm, LP filter) (no unit)	Tortuosity of roughness (cut-off=105µm, HP filter) (no unit)
SMOOTH	0	[2.17 to 2.32]
PV]0 to 0.4]	[2.5 to 2.8]
OC]0.4 to 1.4]	[2.25 to 2.6]
SOC]1.6 to 2.7]	[2.3 to 2.6]

Table 16 : Determination of categories of the breast implant classification

Once the different categories of implant textures have been quantitatively identified, it is necessary to wonder whether a prosthesis with a given initial texture is maintained post implantation in its category. For example, does an implant with a PV structure remain identifiable as a PV structure, even after a long implantation time? This interrogation is crucial because it implies that the putative *in vivo* damage to the prosthesis does not alter the discriminating classification structure, for example a SOC prosthesis manufactured by the manufacturer Allergan remains a SOC prosthesis. An affirmative answer to this question would imply that the positive or negative impact of surface texture remains effective during the entire placement of the prosthesis (varying from 1 to 15.3 years in our experimental layout).

On our explant sampling, the selected parameters were calculated and then bootstrapped, in order to apply our classification matrix to the explants. (Fig. 30) The dispersion of the explant scatterplots is comparable to that of implants, with the exception of Allergan. This suggests heterogeneous damage to the Allergan implants. When comparing the scatterplots of the Sebbin shaped implant texture, the Nagotex texture and the Cereform texture with the corresponding explants, there is a slight decrease in the tortuosity of roughness and a slight increase in the average slope of waviness. Regarding the Cristalline Micro-texture, there is only a small increase in the macroscopic slope. However, despite these slight deviations, the categories (as defined on the implants in the Table 16) remain valid on the explants. Unlike orthopedic implants for which friction parts create a new topography after abrasion (181, 182), the initial topographies of breast implants remain the same. Breast

prostheses therefore retain their classification once implanted. Lastly, this structural stability allows us to validate the robustness of the parameters retained for the classification since they even are able to discriminate the textures post-implantation.

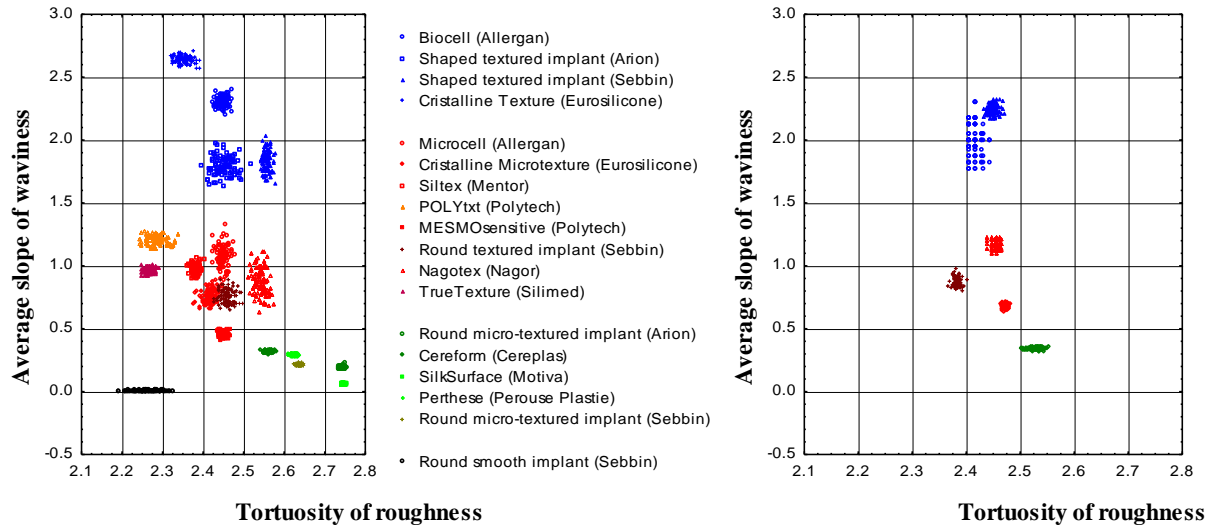


Figure 30 : Classification of implants obtained by discriminative analysis (left) and projection of our explants database on this classification (right)

5.4.2 THE TRANSFER FUNCTION OF THE IMPLANT / EXPLANT ROUGHNESS

The comparative multi-scale analysis of the Sa allowed us to specify the ranges of scale on which the roughness is preserved, destroyed or created. The implant / explant study gathers together three categories depicted in our classification (PV, OV and SOC). As the explants remain identifiable in their category, we grouped the explants according to these categories namely PV, OC and SOC. Thus, we were able to quantify and therefore to compare the multi-scale damage of the different categories of texture defined in the classification (Fig. 31).

Thus, the PV_{explant} category consists of the Cereform explant, the OC_{explant} category of the Sebbin round textured explants, the Nagor explant and the Eurosilicone explant and the SOC_{explant} category of the Sebbin shaped textured explants and the Allergan explant.

The multi-scale curves of the damage of these 3 categories allowed us to identify different regimes, as indicated in the Figure 31.

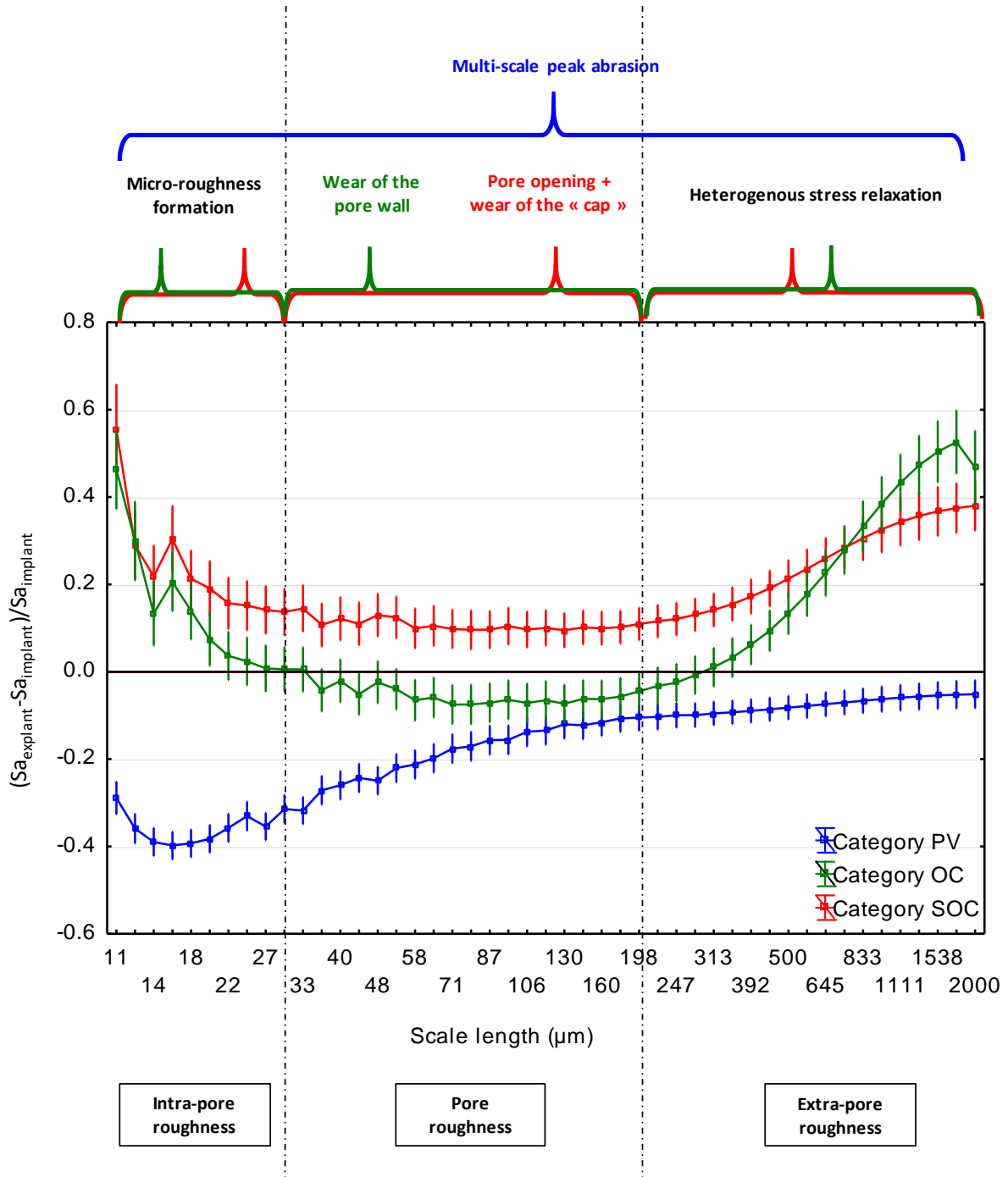


Figure 31 : Identification of the damage regimes of the different categories of texture and associated topographical characteristics

5.4.3 DAMAGE OF PV STRUCTURE

As the PV category is only represented by the Cereform texture, the damage curve entirely reflects the multi-scale behavior of this texture, i.e. a decline of the Sa on all the scales studied but which gradually becomes more important on the low scales.

Due to the texturing process (sandblasting), the Cereform texture is a multi-scale surface. (80) Indeed, the impact of the grains of sand creates craters first. Then, since sandblasting is a stochastic process, craters of much smaller amplitude appear on the initial craters.

According to the multi-scale curves, these are firstly the smallest peaks for which the amplitude decreases. This decrease in amplitude of the peaks becomes smaller and smaller on the high scales, ending up almost stable. This amplitude drop on the low scales is symptomatic of a material removal, which is much more favored for small than for large peaks. This suggests a mechanical action on the surface, which is attributable to wear. Thus, a damage of these prostheses in the body by multi-scale abrasion is worth considering. If this hypothesis is confirmed, a generation of small debris is expected. Given that a 40% decrease in S_a occurs for a spatial scale of $9\mu\text{m}$, it is reasonable to assume a release of debris smaller than this size.

Noteworthy, for scales between $10\mu\text{m}$ and $25\mu\text{m}$, the transfer function has a U-shape curve. Although the transfer coefficient remains negative, we distinguish a rise in the transfer coefficient for a critical length of $15\mu\text{m}$. A U-shape curve is often the hallmark of two antagonistic mechanisms. In our case, another mechanism (which will also be noted for OC- and SOC-patterned prostheses) simultaneously occurs. Thus, while we have an erosion more and more important at the low scales due to a preferential erosion of small peaks, a micro-roughness is created due to an abrasion between the silicone and the biological tissue.

In order to validate this hypothesis, a 2-D phenomenological model was applied to reproduce the effect of different damage mechanisms. This model is similar to that implemented to simulate the abrasion of metal components. (183) It remains, however, to analyze more finely whether the wear is distributed all over the contact which, given the softness of the connective tissues, seems highly likely. In our model, we assumed that the wear was concentrated on the positive curvature part of the roughness profile.

To model the damage of PV implants, only a mechanism called “debris mill” was taken into account. Basically, our model allowed us to simulate the 2-D roughness attributable to the debris mill mechanism and to visualize the impact of this roughness on the initial 2-D roughness of the implant. In our case, the model was applied on a profile characteristic of the PV implant. (Fig. 32)

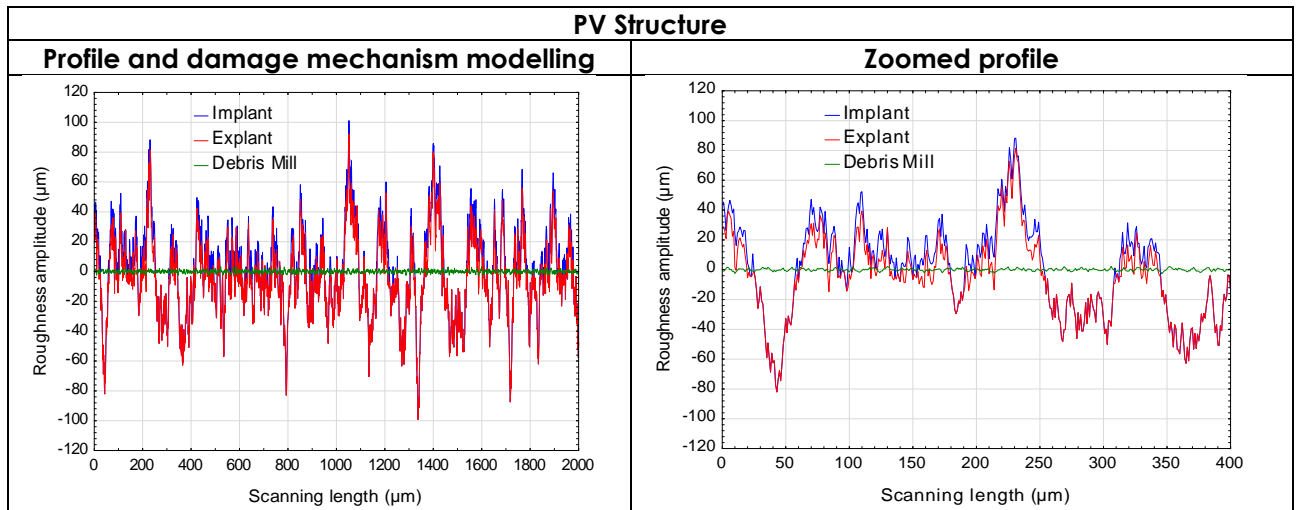


Figure 32 : 2-D damage modelling of the debris mill mechanism on a PV implant.

5.4.4 DAMAGE OF OC AND SOC STRUCTURES

For the other textured surfaces (i.e. OC and SOC), the following features are common and define three regimes:

- An increase in roughness below 25µm: intra-pore roughness regime
- A multi-scale stabilization of roughness between 30 and 200µm: pore roughness regime
- An increase of the roughness from 200µm: extra-pore roughness regime

These behaviors are completely different from that of PV structure. Indeed, for the latter, no increase in roughness and no stabilized regime was observed.

There are, however, two fundamental differences between SOC and OC structures:

- The SOC structure exhibits an increase in roughness (of around 10%) in the stabilized regime (between 30 and 200µm), whereas the OC structure presents a 5% decrease in roughness in the same regime.

- The amplitude rise on the high scales (superior to 1 mm) is larger for OC structure (50%) than for SOC structure (35%).

5.4.4.1 INTRA-PORE ROUGHNESS REGIME

Concerning the damage curve of OC and SOC structures, there is a very sharp increase in roughness for the low scales which decreases further to stabilize at a common spatial scale of approximately 30 μ m. We note that this type of damage on these spatial ranges also occurred on the PV prostheses. Importantly, we therefore have a common mechanism of damage between all the textures, which we will call the debris mill. The abrasion (probably coupled with adhesive wear) creates a micro-roughness with release of elastomeric particles of size inferior to 30 μ m. As this roughness is always increasing (and tends to an exponential growth) as the scale decreases, it appears that the damage only occurs on the scales much lower than 10 μ m, suggesting the generation of submicron debris. The amplitude or severity of this mechanism (characterized for example by the volume of debris released per unit time) cannot be deduced from a purely geometric study. However, it is possible, from the surface morphology, to propose a first quantification of the prosthesis' resistance regarding the mechanisms of abrasive damage. If we assume that the wear is abrasive, then a larger roughness created by this abrasive mechanism will potentially create a larger particle flow. OC and SOC-patterned prostheses have a sharp increase of roughness at the low scale (a rise of 40% at a scale of 10 μ m). This would suggest that the damage is important on these textured prostheses. The presence of a crenel-shaped structure could lead to a concentration of shear on the plateaus of the surface morphology thus facilitating abrasion. However, not all prostheses (manufacturers) have the same degree of roughness creation. (Table 17)

	Delta at a scale of 10 μm (μm)
Sebbin shaped implant texture	0.711
Cristalline Micro-texture	0.266
Nagotex	0.247
Sebbin round implant texture	0.072
Biocell	-0.024
Cereform texture	-0.095

Table 17 : Difference between the $S_{a_{explant}}$ and the $S_{a_{implant}}$ (or Delta) for each texture at a scale of 10 μm .

The Sebbin shaped implant texture has the most important degree of roughness creation, as confirmed topographically (Fig. 33)

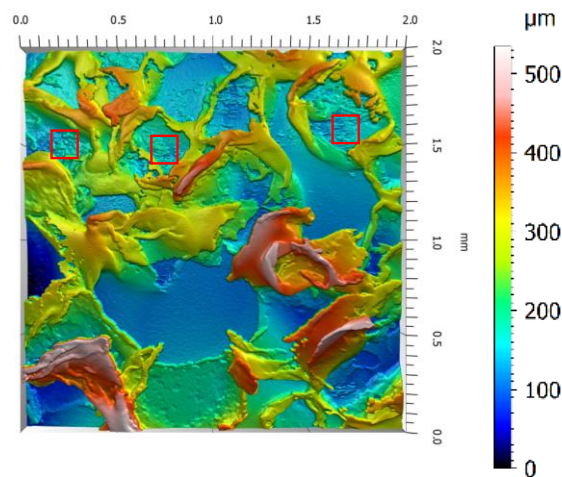


Figure 33 : Appearance of microscopic irregularities within cavities of the Sebbin shaped explants

This difference in term of damage can be caused by either the silicone mechanical properties or the macroscopic (shearing and normal) shear forces generated by the macroscopic shape (superior to 200 μm) of the surface topography. In summary, the topographical analysis on the low scales of explants can help to determine the basic mechanism of abrasion damage on breast implants and the potential origin of debris release.

As previously, we modeled damage to OC and SOC-patterned prostheses including the debris mill (Fig. 34 and 35). However, other mechanisms characteristic to the damage of these types of implant (such silicone heterogenous stress relaxation,

silicone homogeneous stress relaxation, wear of the pore wall and wear of the “cap”) were included in the model.

The results of the model will be commented later on with the study of the two other regimes (pore roughness regime and extra-pore roughness regime).

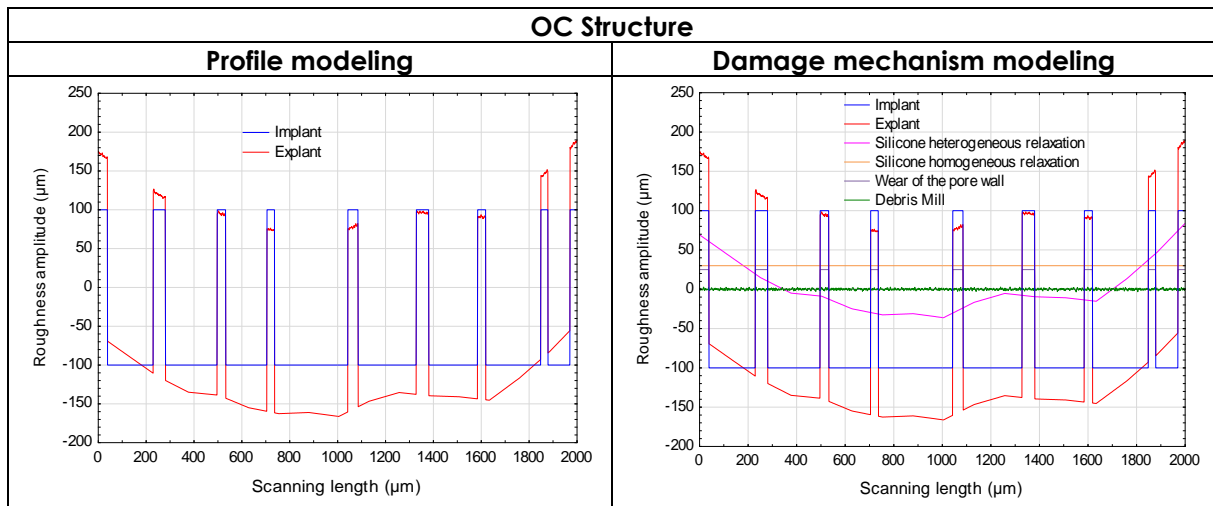


Figure 34 : 2-D damage modelling of the damage mechanisms on an OC implant

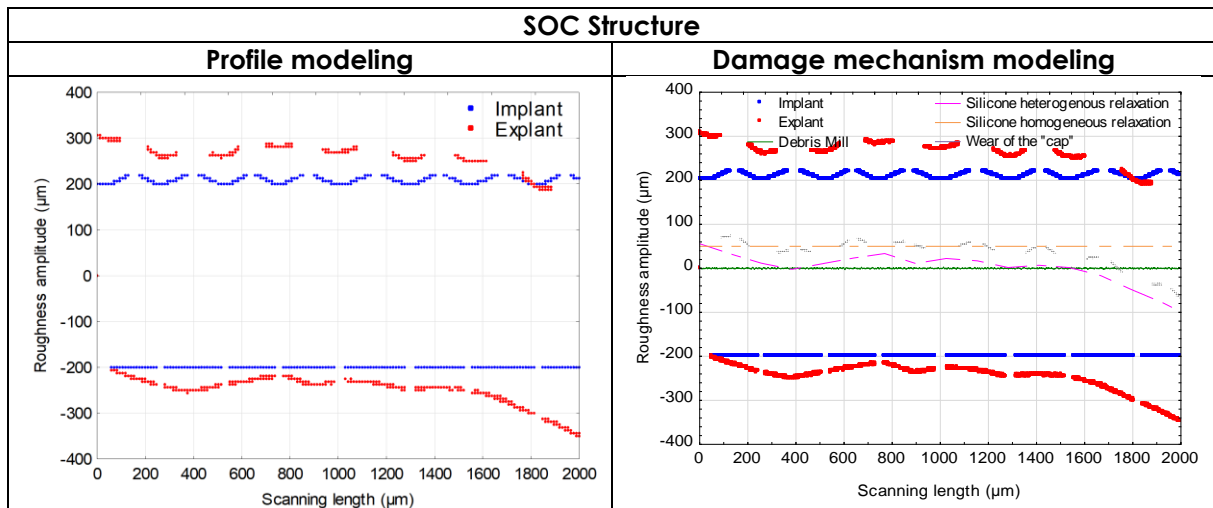


Figure 35 : 2-D damage modelling of the damage mechanisms on a SOC implant

5.4.4.2 PORE ROUGHNESS REGIME

This regime is described by a multi-scale stabilization of the roughness between 30 and 200µm. The SOC structure exhibits a slight increase in roughness (of approximately 10%)

in this stabilized regime, whereas the OC structure presents over the same regime a slight decrease of 5% in roughness.

This spatial range characterizes the roughness of a pore. Remarkably, the transfer function remains constant, therefore the transfer is uniform in this roughness range.

For OC-patterned prostheses, the transfer function is negative (a 5% decrease in amplitude) which is therefore characteristic of wear. However, contrary to PV-patterned prostheses, this wear is constant. This constant regime could be explained only if the damage is uniform on this range. The only mechanical explanation to that observation would consist in an erosion of the walls, which has an almost constant surface with depth, thus presenting a constant wear over a wide range of spatial scales (Fig. 31). Once again, wear is generated by the debris mill previously described on the very low spatial scales.

For SOC-patterned prostheses, the transfer function is positive (a 10% rise of amplitude), which seem counterintuitive compared to the wear mechanism previously presented for SOC structure. However, the morphology of SOC prevents an integral measurement of the pore roughness. Indeed, the presence of a "cap" precludes an integral estimation of the roughness on the bottom of the pore. No roughness parameter is designed to characterize this morphology. Likewise, with the exception of a particular analysis methodology specific for the 4-D morphology, very few instruments are able to measure a complete topography with micrometric resolution. Therefore, a bias will appear in the measurement of S_a . (Fig. 36) The opening of the explant pores shown on the measurements of the Figure 27, will therefore increase the S_a by revealing a larger mass of valley (bottom of the pore). A more detailed analysis is proposed in the Appendix 2 by the multi-scale study of Skewness (S_{sk}). Once again, wear is generated by the debris mill previously described on the very low spatial scales. It should be noted, according to the Figure 29, that the Allergan implants (particularly incriminated in the BIA-ALCL appearance (110) exhibit a more heterogeneous damage to the "cap" causing a very strong dispersion on the roughness, which is not observed on the Sebbin prostheses. Noteworthy, the skewness of the micro-roughness of the Allergan explant is positive ($S_{sk} = 0.1$) while it is negative ($S_{sk} = -0.2$) for the Sebbin

shaped textured explants (result not shown). This reflects the presence of sharper roughness peaks for Allergan explants than for Sebbin shaped textured explants (Fig. 27 and 29). The Ssk study also showed that the Allergan implant has more open pores than Sebbin shaped textured implants. It could be hypothesized that the stronger constraints applied during manufacturing to the Allergan prosthesis to open the pores may be responsible for the heterogeneity of the explants. This heterogeneity is liable to generate locally more sharp micro-roughness and therefore more intense debris mill.

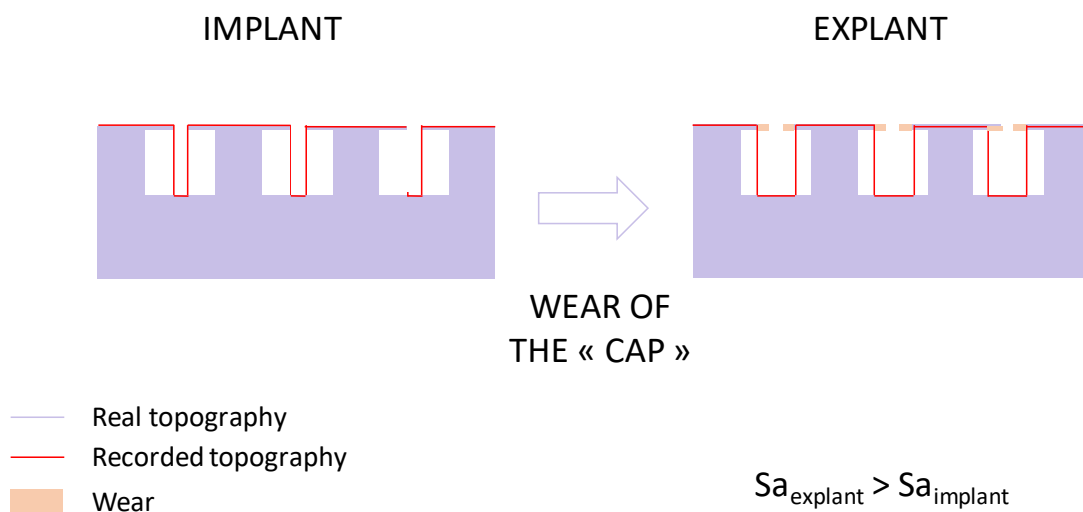


Figure 36 : Schematic representation of the bias, which will appear on the Sa values during the opening of SOC structures

5.4.4.3 EXTRA-PORE ROUGHNESS REGIME

For OC and SOC-textured surfaces, they have in common an increase in roughness above 200µm: an extra-pore roughness. However, the increase in amplitude on the high scales (superior to 1 mm) is larger for OC structure (50%) than for SOC structure (35%). This behavior is completely different from that of the PV structure for which no increase in roughness was observed.

Several hypotheses can be made to explain this increase in extra-pore roughness for OC and SOC-textured surfaces. Wear at high scale must be rejected since it is clearly impossible to increase topography by wear (scratch) at this scale and if present, it would clearly appear on topographical map. Also, it could be shown that this extra-

pore roughness does not depend on the implantation time (Fig. 37) meaning that a pure homogeneous process of materials creep or relaxation must be rejected.

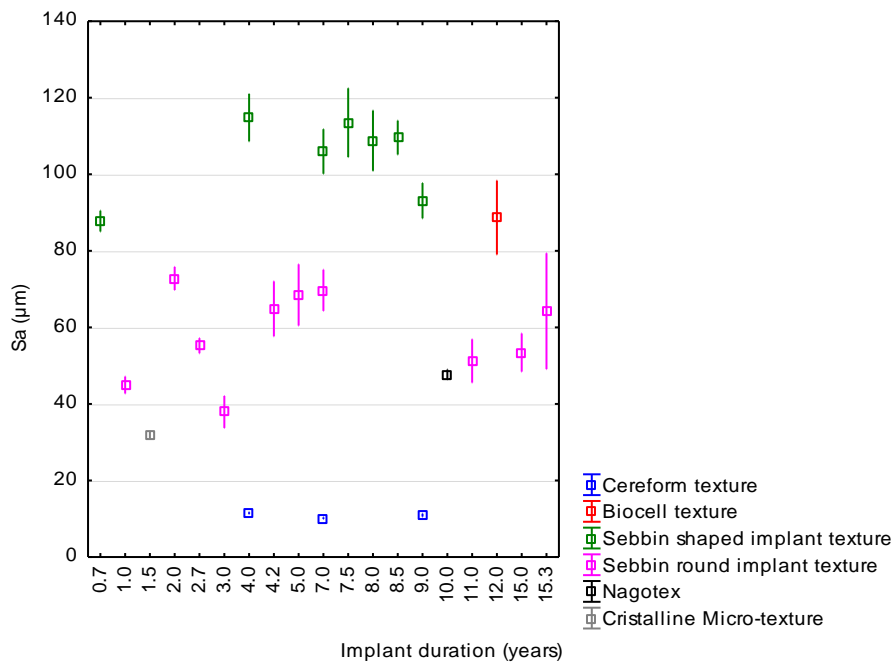


Figure 37 : The Sa evolution computed on the topographies measured (i.e. before multi-scale analysis) according to the implant duration

Another hypothesis can be proposed to explain the increase in extra-pore roughness for OC and SOC-textured surfaces.

Due to irregularities and stochastic nature of the salt-imprint process of texturation, stress heterogeneities may be created during curing. After implantation, and under normal stress, shear stress and activation energy, local stress heterogeneities may disappear and during this stress relaxation, a waviness greater than the mean size between 2 consecutives salt imprints ($> 500\mu\text{m}$) may appear. Then, this waviness may increase the Sa on a critical length higher than the individual salt-imprint size. This phenomenon was named "heterogeneous stress relaxation". The visualization of the OC explant's undulation shows this relaxation well (Fig. 38). We have phenomenologically modelled this heterogeneous stress relaxation (Fig. 34) showing a persistent wave on the global profile. Contrary to OC and SOC-textured surfaces, the amplitude does not increase for long wavelength on PV structures. That can be

explained by their quite homogeneous structure due to the multi-scale aspect of the grinded surfaces that minimizes the effect of stress relaxation.

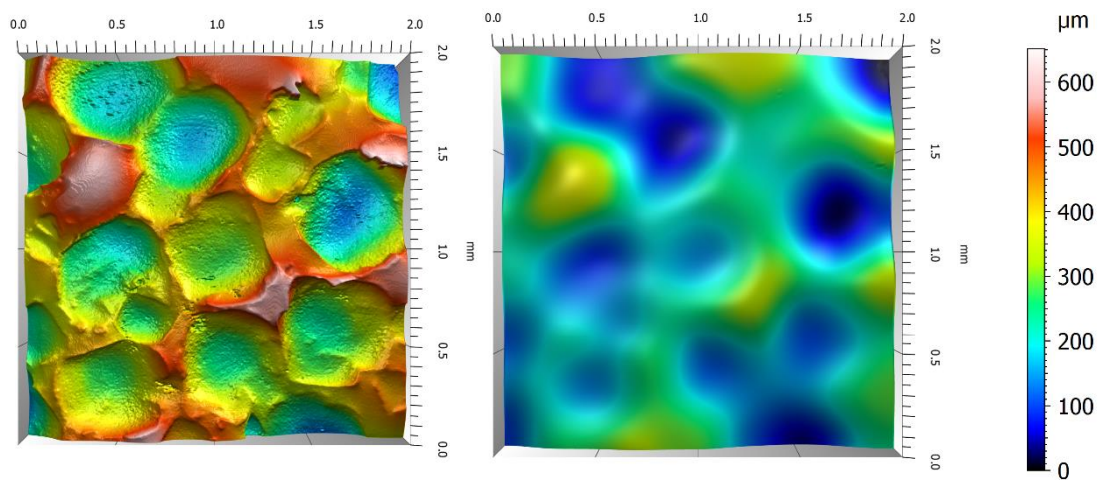


Figure 38 : OC explant's undulation characteristic of a "heterogenous stress relaxation"

5.5 CONCLUSION AND OUTLOOK

This study is the first study of *in vivo* damage. With the use of the most optimal techniques (i.e. interferometry and micro-tomography), the damage of different types of breast implant texture was quantified, compared and justified topographically on all the scales. These two experimental techniques are not mentioned in the ISO 14607 standard.

Various conclusions could be drawn from this study:

- Damage is described by a morphology at all the scales.
- Despite their damage, prostheses retain their original morphological appearance. There is no complete destruction of their initial morphological structure.
- The proposed universal damage mechanism for all these prostheses is an abrasion mechanism (according to the debris mill mechanism), which releases debris on micrometric or even submicrometer scales.
- The debris mill erodes peaks and valleys for PV structures, pore walls for OC structures, and pore "cap" for SOC structures. A 2-D model has been proposed

to qualify and quantify it, which will have to be extended in 3-D and with a refinement of the physical constants.

Once the *in vivo* mechanical, biological and chemical context of the implant is further defined, tribological tests, which will reproduce this context as accurately as possible, will enable the characterization of granulometry and the tribological elementary mechanisms responsible for erosion.

CHAPTER VI: GENERAL CONCLUSIONS AND OUTLOOK

6.1 GENERAL CONCLUSIONS

The biocompatibility of breast implant textures is a highly topical subject, which is becoming more and more critical, both in the media and medically. We have shown that surface measurements and nomenclatures of breast implant surfaces are numerous in the literature. However, a lack of scientific rigor plagued most of these studies.

This thesis is located at the forefront of these studies. Indeed, a first justification of the methodology of breast implant surface measurement and a first biologically and topographically relevant classification of the topographies of these implants were published within the framework of this thesis. Moreover, a first analysis of the states of implant surfaces post implantation will be submitted for publication soon. These different results have all been obtained through a statistical approach, which is based on the multiscale analysis of surface topographies.

A summary of the main findings of these 3 different studies is presented below.

One of our first conclusions is that it is necessary to use two measuring instruments to encompass the range of the topographies of implant surfaces. This simple fact nullifies the ISO 14607 standard that proposes to use only one instrument among 4 (SEM with a 2D and 3D surface reconstruction software, White-Light Interferometry, Laser Confocal Microscopy, High Range AFM). In addition to the instruments, the standard is metrologically incorrect at the sampling level: an AFM measurement over 2mm^2 is simply out of the scope of the apparatus.

Once the criticism of the standard was topographically argued, we were able to propose a new methodology for measuring breast implant surfaces from a comparative multi-instrumental study. Taking into account the area imposed by the standard (2mm^2), the interferometry is perfectly adapted to the surface structures obtained by sandblasting. It can also be used for the measurement of smooth

implants, provided to reduce the area to 1mm². Moreover, X-ray micro-tomography and Focus variation microscope completely measure the structures obtained by the "salt-loss" process, contrary to interferometry. Indeed, the latter would provide only very local measures for this type of texture. In addition, although artefacts have been identified, micro-tomography and Focus variation microscope are able to measure on these surfaces the 3 roughness regimes, which were highlighted by the multi-scale analysis of interferometric measurements. Micro-tomography was finally chosen on the following studies for the structures obtained by the "salt-loss" process because we thought that an X-ray measurement would allow us not to depend on the light-related problems inherent to optical measurements on a translucent material (such as the silicone).

Once a metrologically-validated measurement protocol was justified for each of the different structures, the used measurement, visualization and analysis techniques allowed us to identify complex 3D structures. Thanks to the instruments we used which are able to provide a view of the topography and a view of the section, these structures were entirely characterized for the first time. It was then possible to propose a classification based on these morphological characteristics (i.e. PV, OC and SOC).

It is then important to consider whether the fibroblasts and the surrounding biological tissues are sensitive to these characteristics. From a relevant selection of genes involved in both remodeling of extracellular matrix and inflammatory reactions and by an original retro-transcriptomic analysis of peri-prosthetic capsular tissues harvested from asymptomatic patients, the biological relevance of the classification proposed has been validated. This is the first classification based on an *ex vivo* study of healthy human tissues. It was then shown that the different categories of the proposed classification induce a specific pattern of expression of these genes. Basically, these molecular mechanisms are modulated by the topography of the implant. At the tissue level, differences in structure and organization were also observed on histological sections of peri-prosthetic capsule.

It then seemed important to us to define the classification topographically and quantitatively (otherwise than by morphological terms). An in-depth statistical analysis

was implemented for the first time to demonstrate the robustness of the selected couple of parameters. Moreover, since the classification is based on a simple pair of two parameters, the topographical meaning of the classification is easily extricable. Finally, since we correlated the tissue response to the surface topography of the prosthesis before implantation, it seemed interesting to us to confirm whether the tissues remain in contact with the same state of surface of the prosthesis, once implanted. It was therefore necessary to characterize the *in vivo* integrity of the different structures. This first topographical study on explanted prostheses allowed us to note the absence of major structural changes over the explant surface. More precisely, by multi-scale analysis, a different wear regime was identified for each category of the classification. Thus, PV-patterned explants exhibited multi-scale peak erosion, while OC and SOC-patterned explants were characterized at small scales (inferior to 30 μ m) by the formation of micro-roughness and at large scales (superior to 200 μ m) by a "heterogenous stress relaxation". Between these two phenomena, an intermediate regime corresponding to wear of the wall of the OC structures and to an opening and wear of the "cap" of the SOC structures.

6.2 OUTLOOK

While some regulatory authorities have banned certain types of textures and others have recommended surgeons not to implant some of them, the assessment of the clinical impact of textures and a putative link between BIA-ALCL and certain textures has not still been resolved. It is then necessary to analyze the possible further work, which will allow us to conclude on this link.

Firstly, the link must be considered statistically. However, the awareness of the authorities and clinicians of the pathology has been recent and the specific registers are not sufficiently mature to allow the published or reported data to be used for statistical analysis. Indeed, they are often fragmented.

In order to enhance these studies, it would be necessary to be able to analyze all the collected data. The only way to recover this data is to collaborate with public bodies

promoting these major national registers. Appropriate statistical models (used in biostatistics, for example) will allow us, even in the presence of incomplete data, to demonstrate a potential correlation between certain types of texture (or even certain topographical parameters) and the incidence of BIA-ALCL.

For example, studies on capsular contractures are more completed than those on BIA-ALCL. Based on the risks calculated by the Kaplan-Meier methodology, a comparison between different textures is then possible. These data were collected and graphically summarized in a publication. (184)

Secondly, regarding the causal link, different hypotheses have been mentioned in the literature. We have shown that the biological reaction in contact with SOC-patterned implants is very different from those in contact with OC- or PV-patterned implants. However, it is too early to conclude on a higher clinical risk of these structures because the mechanism upstream of inflammation has not been elucidated. Many authors reported the biofilm hypothesis. In order to validate or refute a such hypothesis, an ex vivo study of the microbiome at the surface of the explant and within the capsular tissues will have to be conducted over a wide range of surface textures and completed by a correlation study between the microbiology data and the topographical data. In a much more sporadic way, some authors mentioned among others the hypothesis of debris. As mentioned previously, in the state of the biomechanical knowledge of the soft tissues, it is pretentious to want to reproduce in a tribological test the wear conditions of the surfaces. The potential release of debris by the surface can be verified only by physico-chemical analyzes of capsular tissue sections. This study should be conducted on a large number of new generation implants, for which gel bleed through the shell is very limited.

These two studies will be all the more valuable, as a partnership with an expert center in pathology (such as the French National Cancer Institute or the LYMPHOPATH network) is set up, because once the protocols have been amended and approved, the analyzes could be performed on capsule samples harvested from patients with BIA-ALCL.

APPENDIX 1: Comparative bibliometric study on Hip and Breast Implants

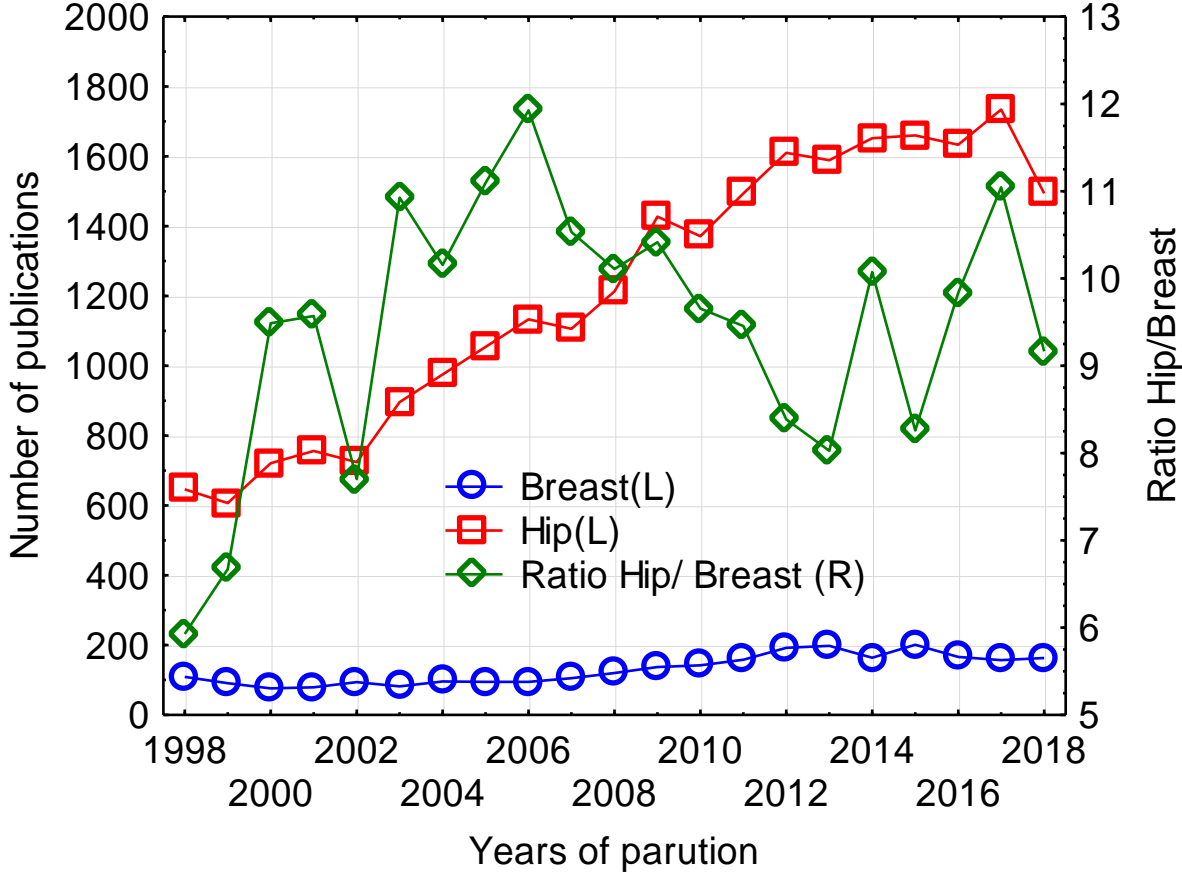


Figure S1: Number of publications related to "breast implant" (or "prosthesis") and to "hip implant" (or "prosthesis") from 1998 to 2018 according to a bibliometric analysis on the Web Of Science.

APPENDIX 2: Multi-scale skewness analysis for SOC-patterned prostheses

The skewness (Ssk) quantifies the degree of asymmetry of the amplitude distribution curve. A surface exhibiting peaks and valleys will have a Ssk close to 0. A surface presenting mostly valleys will have a Ssk positive. Conversely, a surface with mainly plateaus will have a Ssk negative.

The mathematical formula of the skewness (Ssk) is given below. The general coordinates of points on the topography are (x,y,z). The surface area of the topography is designed by A. Sq corresponds to the root mean square height.

$$Ssk = \frac{\frac{1}{A} \iint_A Z^3(x,y) dx dy}{Sq^3} \quad [2]$$

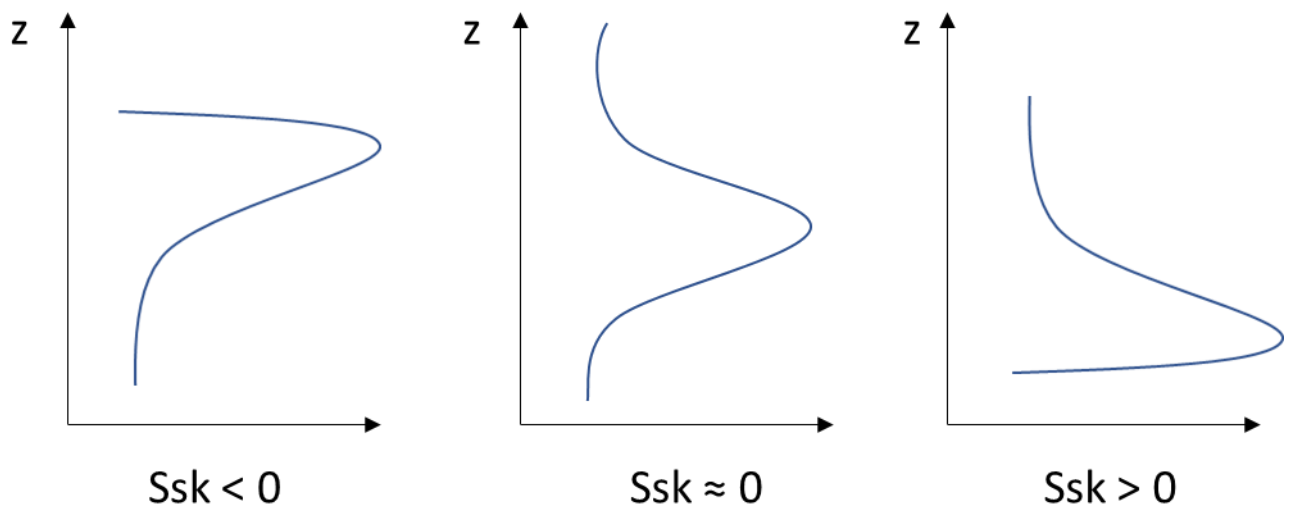


Figure S2: Topographical meaning of the Ssk.

As the skewness (Ssk) is a very sensitive parameter, the analysis has to be led on a comprehensive sampling. The Sebbin shaped implant texture was therefore chosen below to explain the mechanism of pore opening,

On the intra-pore roughness regime, the S_{sk} is negative. The micro-roughness exhibits a PV structure with valleys slightly deeper than the peaks. The explant, by a creation of a micro-roughness, has a slightly higher S_{sk} value due to the formation of small peaks during the wear.

On the pore roughness regime, the S_{sk} becomes positive as the scale increases. The walls are then taken into account in the filtering process, which introduces valleys and therefore makes S_{sk} positive. However, on this regime, at a same scale, $S_{sk_{explant}}$ is superior to $S_{sk_{implant}}$. At a same scale, the pore opening decreases then the “mass” of roughness amplitude on the extreme amplitude (“cap”), and consequently increases the S_{sk} .

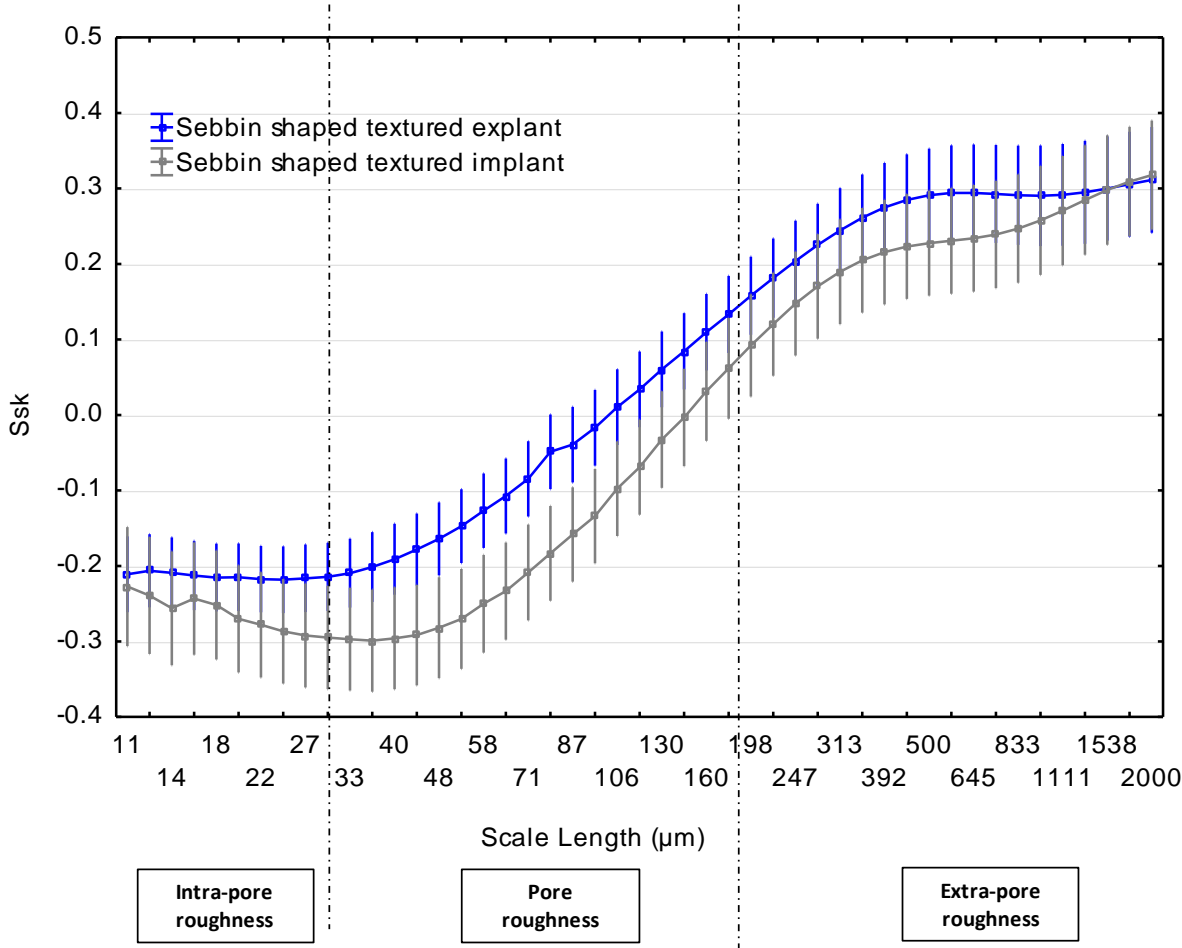


Figure S3: Multi-scale curves of $S_{sk_{implant}}$ and $S_{sk_{explant}}$ for Sebbin shaped implant texture (SOC)

REFERENCES

1. Molitor M, Mestak O, Kalinova L, Krajcova A, Mestak J. The history and safety of breast implants. *Acta chirurgiae plasticae*. 2014;56(1-2):15-9. PubMed PMID: 25484272. Epub 2014/12/09. eng.
2. Peters W. The evolution of breast implants. *Canadian Journal of Plastic Surgery*. 2002;10(5):223-36.
3. Maxwell GP, Gabriel A. The evolution of breast implants. *Plastic and reconstructive surgery*. 2014 Jul;134(1 Suppl):12S-7S. PubMed PMID: 25057743. Epub 2014/07/25. eng.
4. Glicenstein J. [History of augmentation mammoplasty]. *Annales de chirurgie plastique et esthetique*. 2005 Oct;50(5):337-49. PubMed PMID: 16185804. Epub 2005/09/28. Histoire de l'augmentation mammaire. fre.
5. Berry MG, Davies DM. Breast augmentation: Part I--A review of the silicone prosthesis. *Journal of plastic, reconstructive & aesthetic surgery : JPRAS*. 2010 Nov;63(11):1761-8. PubMed PMID: 19713165. Epub 2009/08/29. eng.
6. Freeman BS. Successful treatment of some fibrous envelope contractures around breast implants. *Plastic and reconstructive surgery*. 1972 Aug;50(2):107-13. PubMed PMID: 5045376. Epub 1972/08/01. eng.
7. Barr S, Bayat A. Breast implant surface development: perspectives on development and manufacture. *Aesthetic surgery journal*. 2011 Jan;31(1):56-67. PubMed PMID: 21239673. Epub 2011/01/18. eng.
8. Gasperoni C, Salgarello M, Gargani G. Polyurethane-covered mammary implants: a 12-year experience. *Annals of plastic surgery*. 1992 Oct;29(4):303-8. PubMed PMID: 1466525. Epub 1992/10/01. eng.
9. Vazquez G. A ten-year experience using polyurethane-covered breast implants. *Aesthetic plastic surgery*. 1999 May-Jun;23(3):189-96. PubMed PMID: 10384018. Epub 1999/06/29. eng.
10. Brody GS, Conway DP, Deapen DM, Fisher JC, Hochberg MC, LeRoy EC, et al. Consensus statement on the relationship of breast implants to connective-tissue disorders. *Plastic and reconstructive surgery*. 1992;90(6):1102-5.
11. Gabriel SE, O'Fallon WM, Kurland LT, Beard CM, Woods JE, Melton LJ. Risk of connective-tissue diseases and other disorders after breast implantation. *New England Journal of Medicine*. 1994;330(24):1697-702.
12. Blackburn WD, Everson MP. Silicone-associated rheumatic disease: an unsupported myth. *Plastic and reconstructive surgery*. 1997;99(5):1362-7.
13. Ferguson JH. Silicone breast implants and neurologic disorders: report of the Practice Committee of the American Academy of Neurology. *Neurology*. 1997;48(6):1504-7.
14. Grigg M, Bondurant S, Ernster VL, Herdman R. Information for women about the safety of silicone breast implants: National Academies Press; 2000.
15. Deva AK, Cuss A, Magnusson M, Cooter R. The "Game of Implants": A Perspective on the Crisis-Prone History of Breast Implants. *Aesthetic surgery journal*. 2019;39(Supplement_1):S55-S65.
16. Spear SL, Parikh PM, Goldstein JA. History of breast implants and the food and drug administration. *Clinics in plastic surgery*. 2009 Jan;36(1):15-21, v. PubMed PMID: 19055957. Epub 2008/12/06. eng.
17. Batich C, Williams J, King R. Toxic hydrolysis product from a biodegradable foam implant. *J Biomed Mater Res*. 1989 Dec;23(A3 Suppl):311-9. PubMed PMID: 2613741. Epub 1989/12/01. eng.
18. Batiukov D, Podgaiski V, Ladutko D. Removal of Polyurethane Implants. *Aesthetic plastic surgery*. 2019 Feb;43(1):70-5. PubMed PMID: 30311035. Epub 2018/10/13. eng.
19. Hester TR, Jr., Ford NF, Gale PJ, Hammett JL, Raymond R, Turnbull D, et al. Measurement of 2,4-toluenediamine in urine and serum samples from women with Meme or Replicon breast

- implants. *Plastic and reconstructive surgery*. 1997 Oct;100(5):1291-8. PubMed PMID: 9326795. Epub 1997/11/05. eng.
20. Stevens WG, Nahabedian MY, Calobrace MB, Harrington JL, Capizzi PJ, Cohen R, et al. Risk factor analysis for capsular contracture: a 5-year Sientra study analysis using round, smooth, and textured implants for breast augmentation. *Plastic and reconstructive surgery*. 2013 Nov;132(5):1115-23. PubMed PMID: 24056498. Epub 2013/09/24. eng.
 21. Gore SM, Lamberty BG. PERTHESE implant-identical cohesive-gel sizers in breast augmentation: a prospective report on 200 consecutive cases and implications for treatment of breast asymmetry. *Aesthetic surgery journal*. 2012 Mar;32(3):310-8. PubMed PMID: 22301618. Epub 2012/02/04. eng.
 22. Radovan C. Breast reconstruction after mastectomy using the temporary expander. *Plastic and reconstructive surgery*. 1982 Feb;69(2):195-208. PubMed PMID: 7054790. Epub 1982/02/01. eng.
 23. Radovan C, editor *Reconstruction of the breast after radical mastectomy using a temporary expander*. *Plast Surg Forum*; 1979.
 24. Fabre G, Gangloff D, Fabie-Boulard A, Grolleau JL, Chavoin JP. [Breast reconstruction after prolonged tissue expansion. About 247 cases]. *Annales de chirurgie plastique et esthetique*. 2006 Feb;51(1):29-37. PubMed PMID: 16338234. Epub 2005/12/13. Reconstruction mammaire prothetique apres expansion prealable prolongee. A propos de 247 cas. fre.
 25. Huttin-Marquelet C, Huttin C. Reconstruction mammaire par prothèse d'expansion temporaire. *Annales de Chirurgie Plastique Esthétique*. 2018 2018/11/01/;63(5):545-58.
 26. Spiegelhalter D, Knight S, Sant T. Breast implants: The scandal, the outcry, and assessing the risks. *Significance*. 2012;9(6):17-21.
 27. Cohen D. Breast implants linked to rare cancer are removed from European market. *BMJ (Clinical research ed)*. 2018 Dec 20;363:k5401. PubMed PMID: 30573474. Epub 2018/12/24. eng.
 28. McCarthy CM, Loyo-Berrios N, Qureshi AA, Mullen E, Gordillo G, Pusic AL, et al. Patient Registry and Outcomes for Breast Implants and Anaplastic Large Cell Lymphoma Etiology and Epidemiology (PROFILE): Initial Report of Findings, 2012–2018. *Plastic and reconstructive surgery*. 2019;143(3S):65S-73S.
 29. Altekruse S. SEER cancer statistics review, 1975-2007. http://seer.cancer.gov/csr/1975_2007/results_merged/sect_13_leukemia.pdf. 2009.
 30. Mulligan C, Salisbury E, Tschuchnigg M, Moradi P, Matthews A, Warriar S. ALK1-Negative Anaplastic Large Cell Lymphoma of the Breast from a Nonprosthesis Cyst. *Plastic and reconstructive surgery Global open*. 2014 Oct;2(10):e238. PubMed PMID: 25426355. Pubmed Central PMCID: PMC4236383. Epub 2014/11/27. eng.
 31. Yoon HJ, Choe JY, Jeon YK. Mucosal CD30-Positive T-Cell Lymphoproliferative Disorder Arising in the Oral Cavity Following Dental Implants: Report of the First Case. *International journal of surgical pathology*. 2015 Dec;23(8):656-61. PubMed PMID: 26261101. Epub 2015/08/12. eng.
 32. Palraj B, Paturi A, Stone RG, Alvarez H, Sebenik M, Perez MT, et al. Soft tissue anaplastic large T-cell lymphoma associated with a metallic orthopedic implant: case report and review of the current literature. *The Journal of foot and ankle surgery : official publication of the American College of Foot and Ankle Surgeons*. 2010 Nov-Dec;49(6):561-4. PubMed PMID: 20870426. Epub 2010/09/28. eng.
 33. Ozkaya N, Grogg KL, Dogan A. Seroma-associated anaplastic large-cell lymphoma arising on the background of subcutaneous calcinosis: beyond breast implants. *Histopathology*. 2016 Nov;69(5):890-2. PubMed PMID: 27271483. Epub 2016/06/09. eng.
 34. Keech JA, Jr., Creech BJ. Anaplastic T-cell lymphoma in proximity to a saline-filled breast implant. *Plastic and reconstructive surgery*. 1997 Aug;100(2):554-5. PubMed PMID: 9252643. Epub 1997/08/01. eng.
 35. Brody GS, Deapen D, Taylor CR, Pinter-Brown L, House-Lightner SR, Andersen JS, et al. Anaplastic large cell lymphoma occurring in women with breast implants: analysis of 173 cases. *Plastic and reconstructive surgery*. 2015 Mar;135(3):695-705. PubMed PMID: 25490535. Epub 2014/12/10. eng.

36. Swerdlow SH, Campo E, Pileri SA, Harris NL, Stein H, Siebert R, et al. The 2016 revision of the World Health Organization classification of lymphoid neoplasms. *Blood*. 2016 May 19;127(20):2375-90. PubMed PMID: 26980727. Pubmed Central PMCID: PMC4874220. Epub 2016/03/17. eng.
37. Jacobsen E. Anaplastic large-cell lymphoma, T-/null-cell type. *The oncologist*. 2006 Jul-Aug;11(7):831-40. PubMed PMID: 16880242. Epub 2006/08/02. eng.
38. Clemens MW, Medeiros LJ, Butler CE, Hunt KK, Fanale MA, Horwitz S, et al. Complete Surgical Excision Is Essential for the Management of Patients With Breast Implant-Associated Anaplastic Large-Cell Lymphoma. *Journal of clinical oncology : official journal of the American Society of Clinical Oncology*. 2016 Jan 10;34(2):160-8. PubMed PMID: 26628470. Pubmed Central PMCID: PMC4872006 online at www.jco.org. Author contributions are found at the end of this article. Epub 2015/12/03. eng.
39. Gholam D, Bibeau F, El Weshi A, Bosq J, Ribrag V. Primary breast lymphoma. *Leukemia & lymphoma*. 2003 Jul;44(7):1173-8. PubMed PMID: 12916870. Epub 2003/08/15. eng.
40. Kim B, Roth C, Chung KC, Young VL, van Busum K, Schnyer C, et al. Anaplastic large cell lymphoma and breast implants: a systematic review. *Plastic and reconstructive surgery*. 2011 Jun;127(6):2141-50. PubMed PMID: 21358562. Epub 2011/03/02. eng.
41. Clemens MW, Miranda RN. Coming of Age: Breast Implant-Associated Anaplastic Large Cell Lymphoma After 18 Years of Investigation. *Clinics in plastic surgery*. 2015 Oct;42(4):605-13. PubMed PMID: 26408447. Epub 2015/09/27. eng.
42. Oishi N, Brody GS, Ketterling RP, Viswanatha DS, He R, Dasari S, et al. Genetic subtyping of breast implant-associated anaplastic large cell lymphoma. *Blood*. 2018 Aug 2;132(5):544-7. PubMed PMID: 29921615. Pubmed Central PMCID: PMC6073323. Epub 2018/06/21. eng.
43. Quesada AE, Medeiros LJ, Clemens MW, Ferrufino-Schmidt MC, Pina-Oviedo S, Miranda RN. Breast implant-associated anaplastic large cell lymphoma: a review. *Modern pathology : an official journal of the United States and Canadian Academy of Pathology, Inc.* 2019 Feb;32(2):166-88. PubMed PMID: 30206414. Epub 2018/09/13. eng.
44. Miranda RN, Aladily TN, Prince HM, Kanagal-Shamanna R, de Jong D, Fayad LE, et al. Breast implant-associated anaplastic large-cell lymphoma: long-term follow-up of 60 patients. *Journal of clinical oncology : official journal of the American Society of Clinical Oncology*. 2014 Jan 10;32(2):114-20. PubMed PMID: 24323027. Pubmed Central PMCID: PMC4062709. Epub 2013/12/11. eng.
45. Ye X, Shokrollahi K, Rozen WM, Conyers R, Wright P, Kenner L, et al. Anaplastic large cell lymphoma (ALCL) and breast implants: Breaking down the evidence. *Mutation Research/Reviews in Mutation Research*. 2014 10//;762:123-32.
46. Clemens MW. Discussion: Breast Implant-Associated Anaplastic Large Cell Lymphoma in Australia and New Zealand: High-Surface-Area Textured Implants Are Associated with Increased Risk. *Plastic and reconstructive surgery*. 2017 Oct;140(4):660-2. PubMed PMID: 28953714. Epub 2017/09/28. eng.
47. Kadin ME, Deva A, Xu H, Morgan J, Khare P, MacLeod RA, et al. Biomarkers Provide Clues to Early Events in the Pathogenesis of Breast Implant-Associated Anaplastic Large Cell Lymphoma. *Aesthetic surgery journal*. 2016 Jul;36(7):773-81. PubMed PMID: 26979456. Epub 2016/03/17. eng.
48. Blombery P, Thompson ER, Jones K, Arnau GM, Lade S, Markham JF, et al. Whole exome sequencing reveals activating JAK1 and STAT3 mutations in breast implant-associated anaplastic large cell lymphoma. *Haematologica*. 2016 Sep;101(9):e387-90. PubMed PMID: 27198716. Pubmed Central PMCID: PMC5060038. Epub 2016/05/21. eng.
49. Di Napoli A, Jain P, Duranti E, Margolskee E, Arancio W, Facchetti F, et al. Targeted next generation sequencing of breast implant-associated anaplastic large cell lymphoma reveals mutations in JAK/STAT signalling pathway genes, TP53 and DNMT3A. *British journal of haematology*. 2018 Mar;180(5):741-4. PubMed PMID: 27859003. Epub 2016/11/20. eng.
50. Letourneau A, Maerevoet M, Milowich D, Dewind R, Bisig B, Missiaglia E, et al. Dual JAK1 and STAT3 mutations in a breast implant-associated anaplastic large cell lymphoma. *Virchows*

Archiv : an international journal of pathology. 2018 Oct;473(4):505-11. PubMed PMID: 29637270. Epub 2018/04/11. eng.

51. Adrada BE, Miranda RN, Rauch GM, Arribas E, Kanagal-Shamanna R, Clemens MW, et al. Breast implant-associated anaplastic large cell lymphoma: sensitivity, specificity, and findings of imaging studies in 44 patients. *Breast cancer research and treatment*. 2014 Aug;147(1):1-14. PubMed PMID: 25073777. Epub 2014/07/31. eng.

52. Clemens MW, Horwitz SM. NCCN Consensus Guidelines for the Diagnosis and Management of Breast Implant-Associated Anaplastic Large Cell Lymphoma. *Aesthetic surgery journal*. 2017 Mar 1;37(3):285-9. PubMed PMID: 28184418. Epub 2017/02/12. eng.

53. Fleming D, Stone J, Tansley P. Spontaneous Regression and Resolution of Breast Implant-Associated Anaplastic Large Cell Lymphoma: Implications for Research, Diagnosis and Clinical Management. *Aesthetic plastic surgery*. 2018 Jun;42(3):672-8. PubMed PMID: 29445921. Pubmed Central PMCID: PMC5945759. Epub 2018/02/16. eng.

54. Adams Jr WP. Discussion: Breast Implant-Associated Anaplastic Large Cell Lymphoma in Australia and New Zealand High-Surface-Area Textured Implants Are Associated with Increased Risk. *Plastic and reconstructive surgery*. 2017;140(4):663-5.

55. de Jong D, Vasmel WL, de Boer JP, Verhave G, Barbe E, Casparie MK, et al. Anaplastic large-cell lymphoma in women with breast implants. *Jama*. 2008 Nov 5;300(17):2030-5. PubMed PMID: 18984890. Epub 2008/11/06. eng.

56. Largent J, Oefelein M, Kaplan HM, Okerson T, Boyle P. Risk of lymphoma in women with breast implants: analysis of clinical studies. *European journal of cancer prevention : the official journal of the European Cancer Prevention Organisation (ECP)*. 2012 May;21(3):274-80. PubMed PMID: 22456426. Epub 2012/03/30. eng.

57. Wang SS, Deapen D, Voutsinas J, Lacey JV, Jr., Lu Y, Ma H, et al. Breast implants and anaplastic large cell lymphomas among females in the California Teachers Study cohort. *British journal of haematology*. 2016 Aug;174(3):480-3. PubMed PMID: 26456010. Pubmed Central PMCID: PMC4829485. Epub 2015/10/13. eng.

58. Doren EL, Miranda RN, Selber JC, Garvey PB, Liu J, Medeiros LJ, et al. U.S. Epidemiology of Breast Implant-Associated Anaplastic Large Cell Lymphoma. *Plastic and reconstructive surgery*. 2017;139(5):1042-50. PubMed PMID: 00006534-201705000-00003.

59. Duvic M, Moore D, Menter A, Vonderheid EC. Cutaneous T-cell lymphoma in association with silicone breast implants. *Journal of the American Academy of Dermatology*. 1995 Jun;32(6):939-42. PubMed PMID: 7751462. Epub 1995/06/01. eng.

60. Hu H, Jacombs A, Vickery K, Merten SL, Pennington DG, Deva AK. Chronic Biofilm Infection in Breast Implants Is Associated with an Increased T-Cell Lymphocytic Infiltrate: Implications for Breast Implant-Associated Lymphoma. *Plastic and reconstructive surgery*. 2015;135(2):319-29. PubMed PMID: 00006534-201502000-00001.

61. Laurent C, Delas A, Gaulard P, Haioun C, Moreau A, Xerri L, et al. Breast implant-associated anaplastic large cell lymphoma: two distinct clinicopathological variants with different outcomes. *Annals of oncology : official journal of the European Society for Medical Oncology*. 2016 Feb;27(2):306-14. PubMed PMID: 26598546. Pubmed Central PMCID: PMC4722894. Epub 2015/11/26. eng.

62. Chai SM, Kavangh S, Ooi SS, Sterrett GF, Cull G, Plunkett M, et al. Anaplastic large-cell lymphoma associated with breast implants: a unique entity within the spectrum of peri-implant effusions. *Diagnostic cytopathology*. 2014 Nov;42(11):929-38. PubMed PMID: 24687769. Epub 2014/04/02. eng.

63. Clemens MW, Clarke C, Fanale M, Miranda R, Madeiros J. Breast implant-associated anaplastic large t-cell lymphoma: Institutional experience and review of the literature. *Journal of Plastic, Reconstructive & Aesthetic Surgery*. 2014;67(10):1463.

64. Hu H, Johani K, Almatroudi A, Vickery K, Van Natta B, Kadin ME, et al. Bacterial Biofilm Infection Detected in Breast Implant-Associated Anaplastic Large-Cell Lymphoma. *Plastic and reconstructive surgery*. 2016 Jun;137(6):1659-69. PubMed PMID: 26890506. Epub 2016/02/19. eng.

65. Lista F, Tutino R, Khan A, Ahmad J. Subglandular breast augmentation with textured, anatomic, cohesive silicone implants: a review of 440 consecutive patients. *Plastic and*

- reconstructive surgery. 2013 Aug;132(2):295-303. PubMed PMID: 23584627. Epub 2013/04/16. eng.
66. Kuehlmann B, Prantl L. Breast implants and possible association with ALCL: A retrospective study including a histological analysis of 296 explanted breast tissues and current literature. *Clinical hemorheology and microcirculation*. 2016 Oct 5;63(4):439-49. PubMed PMID: 27314443. Epub 2016/06/18. eng.
67. de Boer M, van Leeuwen FE, Hauptmann M, et al. Breast implants and the risk of anaplastic large-cell lymphoma in the breast. *JAMA Oncology*. 2018.
68. Stark B, Mureau M, Hopper I, Cooter R, Deva A, Perks G, et al. Letter on breast implant safety and the role of breast implant registries sent to the FDA in preparation of their public hearing in 20192019.
69. Collett DJ, Rakhorst H, Lennox P, Magnusson M, Cooter R, Deva AK. Current Risk Estimate of Breast Implant–Associated Anaplastic Large Cell Lymphoma in Textured Breast Implants. *Plastic and reconstructive surgery*. 2019;143(3S):30S-40S.
70. Rastogi P, Riordan E, Moon D, Deva AK. Theories of Etiopathogenesis of Breast Implant–Associated Anaplastic Large Cell Lymphoma. *Plastic and reconstructive surgery*. 2019;143(3S):23S-9S.
71. Cooter R, Barnett R, Deva A, Magnusson MR, McNeil J, Perks G, et al. In Defense of the International Collaboration of Breast Registry Activities (ICOBRA). *Aesthetic surgery journal*. 2016 Jul;36(7):NP225-7. PubMed PMID: 27053073. Pubmed Central PMCID: PMC4911904. Epub 2016/04/08. eng.
72. McLaughlin JK, Lipworth L, Fryzek JP, Ye W, Tarone RE, Nyren O. Long-term cancer risk among Swedish women with cosmetic breast implants: an update of a nationwide study. *Journal of the National Cancer Institute*. 2006 Apr 19;98(8):557-60. PubMed PMID: 16622125. Epub 2006/04/20. eng.
73. Pukkala E, Boice JD, Hovi S-L, Hemminki E, Asko-Seljavaara S, Keskimaki I, et al. Incidence of breast and other cancers among Finnish women with cosmetic breast implants, 1970–1999. *Journal of long-term effects of medical implants*. 2002;12(4).
74. Formes A, Diehl B. Investigation of the silicone structure in breast implants using (1)H NMR. *Journal of pharmaceutical and biomedical analysis*. 2014 May;93:95-101. PubMed PMID: 24342752. Epub 2013/12/18. eng.
75. Moyer HR, Ghazi BH, Losken A. The effect of silicone gel bleed on capsular contracture: a generational study. *Plastic and reconstructive surgery*. 2012 Oct;130(4):793-800. PubMed PMID: 22691845. Epub 2012/06/14. eng.
76. O'Shaughnessy K. Evolution and update on current devices for prosthetic breast reconstruction. *Gland Surg*. 2015 Apr;4(2):97-110. PubMed PMID: 26005642. Pubmed Central PMCID: PMC4409673. Epub 2015/05/26. eng.
77. Sitbon E. Fabrication des prothèses mammaires : une industrie de haute technologie. *Annales de Chirurgie Plastique Esthétique*. 2005 2005/10/01;50(5):394-407.
78. Standardization BEcf. ISO 14607 Non-active surgical implants—mammary implants—particular requirements (Bruxelles European Committee for Standardization). 2009.
79. Atlan M, Bigerelle M, Larreta-garde V, Hindie M, Heden P. Characterization of Breast Implant Surfaces, Shapes, and Biomechanics: A Comparison of High Cohesive Anatomically Shaped Textured Silicone, Breast Implants from Three Different Manufacturers. *Aesthetic plastic surgery*. 2016 Feb;40(1):89-97. PubMed PMID: 26746882. Epub 2016/01/10. eng.
80. Garabédian C, Delille R, Deltombe R, Anselme K, Atlan M, Bigerelle M. A multi-topographical-instrument analysis: the breast implant texture measurement. *Surface Topography: Metrology and Properties*. 2017;5(2):025004.
81. Chang EI, Hammond DC. Clinical Results on Innovation in Breast Implant Design. *Plastic and reconstructive surgery*. 2018 Oct;142(4S The Science of Breast Implants):31S-8S. PubMed PMID: 30252757. Epub 2018/09/27. eng.
82. O'Neill AC, Zhong T, Hofer SOP. Implications of Breast Implant-Associated Anaplastic Large Cell Lymphoma (BIA-ALCL) for Breast Cancer Reconstruction: An Update for Surgical

- Oncologists. *Annals of surgical oncology*. 2017 Oct;24(11):3174-9. PubMed PMID: 28762113. Epub 2017/08/02. eng.
83. Calobrace MB, Schwartz MR, Zeidler KR, Pittman TA, Cohen R, Stevens WG. Long-Term Safety of Textured and Smooth Breast Implants. *Aesthetic surgery journal*. 2017 Sep 28. PubMed PMID: 29040370. Epub 2017/10/19. eng.
84. Loch-Wilkinson A, Beath K, Knight RJW, Wessels WLF, Magnusson M, Papadopoulos T, et al. Breast implant associated Anaplastic Large Cell Lymphoma in Australia and New Zealand - high surface area textured implants are associated with increased risk. *Plastic and reconstructive surgery*. 2017 May 05. PubMed PMID: 28481803. Epub 2017/05/10. eng.
85. Jones P, Mempin M, Hu H, Chowdhury D, Foley M, Cooter R, et al. The Functional Influence of Breast Implant Outer Shell Morphology on Bacterial Attachment and Growth. *Plastic and reconstructive surgery*. 2018 Oct;142(4):837-49. PubMed PMID: 30252806. Epub 2018/09/27. eng.
86. Barr S, Hill EW, Bayat A. Functional biocompatibility testing of silicone breast implants and a novel classification system based on surface roughness. *Journal of the mechanical behavior of biomedical materials*. 2017 Jun 27;75:75-81. PubMed PMID: 28697402. Epub 2017/07/12. eng.
87. Psillakis JM, Facchina PH, Kharmandayan P, Trillo L, Canzi WC, Aguiar HR. Review of 1,447 breast augmentation patients using PERTHESE silicone implants. *Aesthetic plastic surgery*. 2010 Feb;34(1):11-5. PubMed PMID: 19760452. Pubmed Central PMCID: PMC2812707. Epub 2009/09/18. eng.
88. Danino A, Rocher F, Blanchet-Bardon C, Revol M, Servant JM. Étude au microscope électronique à balayage des surfaces des implants mammaires à texturation poreuse et de leurs capsules. Description de l'effet « velcro » des prothèses à texturation poreuse. *Annales de Chirurgie Plastique Esthétique*. 2001 2001/02/01;46(1):23-30.
89. Danino AM, Basmacioglu P, Saito S, Rocher F, Blanchet-Bardon C, Revol M, et al. Comparison of the capsular response to the Biocell RTV and Mentor 1600 Siltex breast implant surface texturing: a scanning electron microscopic study. *Plastic and reconstructive surgery*. 2001 Dec;108(7):2047-52. PubMed PMID: 11743398. Epub 2001/12/18. eng.
90. Valencia-Lazcano AA, Alonso-Rasgado T, Bayat A. Physico-chemical characteristics of coated silicone textured versus smooth breast implants differentially influence breast-derived fibroblast morphology and behaviour. *Journal of the mechanical behavior of biomedical materials*. 2014 Dec;40:140-55. PubMed PMID: 25238227. Epub 2014/09/23. eng.
91. James GA, Boegli L, Hancock J, Bowersock L, Parker A, Kinney BM. Bacterial Adhesion and Biofilm Formation on Textured Breast Implant Shell Materials. *Aesthetic plastic surgery*. 2019 Apr;43(2):490-7. PubMed PMID: 30276456. Epub 2018/10/03. eng.
92. Kyle DJ, Oikonomou A, Hill E, Bayat A. Development and functional evaluation of biomimetic silicone surfaces with hierarchical micro/nano-topographical features demonstrates favourable in vitro foreign body response of breast-derived fibroblasts. *Biomaterials*. 2015 Jun;52:88-102. PubMed PMID: 25818416. Epub 2015/03/31. eng.
93. Barr S, Hill EW, Bayat A. Development, fabrication and evaluation of a novel biomimetic human breast tissue derived breast implant surface. *Acta Biomaterialia*. 2017 2//;49:260-71.
94. Atlan M, Nuti G, Wang H, Decker S, Perry T. Breast implant surface texture impacts host tissue response. *Journal of the mechanical behavior of biomedical materials*. 2018 2018/12/01//;88:377-85.
95. Valencia-Lazcano AA, Alonso-Rasgado T, Bayat A. Characterisation of breast implant surfaces and correlation with fibroblast adhesion. *Journal of the mechanical behavior of biomedical materials*. 2013 May;21:133-48. PubMed PMID: 23545265. Epub 2013/04/03. eng.
96. Paek LS, Giot J-P, Tétreault-Paquin J-O, St-Jacques S, Nelea M, Danino MA. The Impact of Postoperative Expansion Initiation Timing on Breast Expander Capsular Characteristics: A Prospective Combined Clinical and Scanning Electron Microscopy Study. *Plastic and reconstructive surgery*. 2015;135(4):967-74. PubMed PMID: 00006534-201504000-00005.
97. Barr S, Hill E, Bayat A. Current implant surface technology: an examination of their nanostructure and their influence on fibroblast alignment and biocompatibility. *Eplasty*. 2009

- Jun 16;9:e22. PubMed PMID: 19606207. Pubmed Central PMCID: PMC2698670. Epub 2009/07/17. eng.
98. Abramo AC, De Oliveira VR, Ledo-Silva MC, De Oliveira EL. How texture-inducing contraction vectors affect the fibrous capsule shrinkage around breasts implants? *Aesthetic plastic surgery*. 2010 Oct;34(5):555-60. PubMed PMID: 20354696. Epub 2010/04/01. eng.
99. Barone FE, Perry L, Keller T, Maxwell GP. The Biomechanical and Histopathologic Effects of Surface Texturing with Silicone and Polyurethane in Tissue Implantation and Expansion. *Plastic and reconstructive surgery*. 1992;90(1):77-86. PubMed PMID: 00006534-199207000-00012.
100. Sforza M, Zaccheddu R, Alleruzzo A, Seno A, Mileto D, Paganelli A, et al. Preliminary 3-Year Evaluation of Experience With SilkSurface and VelvetSurface Motiva Silicone Breast Implants: A Single-Center Experience With 5813 Consecutive Breast Augmentation Cases. *Aesthetic surgery journal*. 2017.
101. Cranin AN. *Handbook of biomaterials evaluation. Scientific, technical and clinical testing of Implant Materials*. Andreas F. von Recum, Editor, New York, 1986, MacMillan. With a forward by Solomon Pollack and contributions by 61 authors and 10 section editors. Index of 14 pp. \$120.00. *Journal of Biomedical Materials Research*. 1987;21(9):1167-8.
102. Henderson PW, Nash D, Laskowski M, Grant RT. Objective Comparison of Commercially Available Breast Implant Devices. *Aesthetic plastic surgery*. 2015 Oct;39(5):724-32. PubMed PMID: 26206500. Epub 2015/07/25. eng.
103. Maxwell GP, Brown MH, Oefelein MG, Kaplan HM, Heden P. Clinical considerations regarding the risks and benefits of textured surface implants and double capsule. *Plastic and reconstructive surgery*. 2011 Aug;128(2):593-5. PubMed PMID: 21788865. Epub 2011/07/27. eng.
104. Goel MK, Khanna P, Kishore J. Understanding survival analysis: Kaplan-Meier estimate. *International journal of Ayurveda research*. 2010 Oct-Dec;1(4):274-8. PubMed PMID: 21455458.
105. Barnsley GP, Sigurdson LJ, Barnsley SE. Textured surface breast implants in the prevention of capsular contracture among breast augmentation patients: a meta-analysis of randomized controlled trials. *Plastic and reconstructive surgery*. 2006 Jun;117(7):2182-90. PubMed PMID: 16772915. Epub 2006/06/15. eng.
106. Wong CH, Samuel M, Tan BK, Song C. Capsular contracture in subglandular breast augmentation with textured versus smooth breast implants: a systematic review. *Plastic and reconstructive surgery*. 2006 Oct;118(5):1224-36. PubMed PMID: 17016195. Epub 2006/10/04. eng.
107. Liu X, Zhou L, Pan F, Gao Y, Yuan X, Fan D. Comparison of the postoperative incidence rate of capsular contracture among different breast implants: a cumulative meta-analysis. *PloS one*. 2015;10(2):e0116071. PubMed PMID: 25680100. Pubmed Central PMCID: PMC4332657. Epub 2015/02/14. eng.
108. Spear SL, Murphy DK. Natrelle round silicone breast implants: Core Study results at 10 years. *Plastic and reconstructive surgery*. 2014 Jun;133(6):1354-61. PubMed PMID: 24867717. Pubmed Central PMCID: PMC4819531. Epub 2014/05/29. eng.
109. Spear SL, Murphy DK, Slicton A, Walker PS. Inamed silicone breast implant core study results at 6 years. *Plastic and reconstructive surgery*. 2007 Dec;120(7 Suppl 1):8S-16S; discussion 7S-8S. PubMed PMID: 18090808. Epub 2007/12/27. eng.
110. Taylor CR, Siddiqi IN, Brody GS. Anaplastic large cell lymphoma occurring in association with breast implants: review of pathologic and immunohistochemical features in 103 cases. *Applied Immunohistochemistry & Molecular Morphology*. 2013;21(1):13-20.
111. Roden AC, Macon WR, Keeney GL, Myers JL, Feldman AL, Dogan A. Seroma-associated primary anaplastic large-cell lymphoma adjacent to breast implants: an indolent T-cell lymphoproliferative disorder. *Modern pathology : an official journal of the United States and Canadian Academy of Pathology, Inc*. 2008 Apr;21(4):455-63. PubMed PMID: 18223553. Epub 2008/01/29. eng.
112. Story SK, Schowalter MK, Geskin LJ. Breast implant-associated ALCL: a unique entity in the spectrum of CD30+ lymphoproliferative disorders. *The oncologist*. 2013;18(3):301-7. PubMed PMID: 23429741. Pubmed Central PMCID: PMC3607527. Epub 2013/02/23. eng.

113. Talmadge JE, Donkor M, Scholar E. Inflammatory cell infiltration of tumors: Jekyll or Hyde. *Cancer metastasis reviews*. 2007 Dec;26(3-4):373-400. PubMed PMID: 17717638. Epub 2007/08/25. eng.
114. Burg G, Kempf W, Haeffner A, Dobbeling U, Nestle FO, Boni R, et al. From inflammation to neoplasia: new concepts in the pathogenesis of cutaneous lymphomas. *Recent results in cancer research Fortschritte der Krebsforschung Progres dans les recherches sur le cancer*. 2002;160:271-80. PubMed PMID: 12079224. Epub 2002/06/25. eng.
115. Meresse B, Ripoche J, Heyman M, Cerf-Bensussan N. Celiac disease: from oral tolerance to intestinal inflammation, autoimmunity and lymphomagenesis. *Mucosal immunology*. 2009 Jan;2(1):8-23. PubMed PMID: 19079330. Epub 2008/12/17. eng.
116. Pennock ND, White JT, Cross EW, Cheney EE, Tamburini BA, Kedl RM. T cell responses: naive to memory and everything in between. *Advances in physiology education*. 2013 Dec;37(4):273-83. PubMed PMID: 24292902. Pubmed Central PMCID: PMC4089090. Epub 2013/12/03. eng.
117. Walker JN, Pinkner CL, Pinkner JS, Hultgren SJ, Myckatyn TM. The Detection of Bacteria and Matrix Proteins on Clinically Benign and Pathologic Implants. *Plastic and Reconstructive Surgery-Global Open*. 2019.
118. Myckatyn TM, Parikh RP. Discussion: Breast Implant-Associated Anaplastic Large Cell Lymphoma in Australia and New Zealand: High-Surface-Area Textured Implants Are Associated with Increased Risk. *Plastic and reconstructive surgery*. 2017 Oct;140(4):655-8. PubMed PMID: 28953712. Epub 2017/09/28. eng.
119. Prantl L, Schreml S, Fichtner-Feigl S, Poppl N, Eisenmann-Klein M, Schwarze H, et al. Clinical and morphological conditions in capsular contracture formed around silicone breast implants. *Plastic and reconstructive surgery*. 2007 Jul;120(1):275-84. PubMed PMID: 17572576. Epub 2007/06/19. eng.
120. Hall-Findlay EJ. Breast implant complication review: double capsules and late seromas. *Plastic and reconstructive surgery*. 2011 Jan;127(1):56-66. PubMed PMID: 21200201. Epub 2011/01/05. eng.
121. Wu C, Cipriano J, Osgood G, Jr., Tepper D, Siddiqui A. Human acellular dermal matrix (AlloDerm(R)) dimensional changes and stretching in tissue expander/implant breast reconstruction. *Journal of plastic, reconstructive & aesthetic surgery : JPRAS*. 2013 Oct;66(10):1376-81. PubMed PMID: 23790562. Epub 2013/06/25. eng.
122. Lilla JA, Vistnes LM. Long-term study of reactions to various silicone breast implants in rabbits. *Plastic and reconstructive surgery*. 1976 May;57(5):637-49. PubMed PMID: 775511. Epub 1976/05/01. eng.
123. McLean AL, Talmor M, Harper A, Fahey TJ, 3rd, Gayle LB, Hoffman LA. Expression of cyclooxygenase-2 in the periprosthetic capsule surrounding a silicone shell implant in the rat. *Annals of plastic surgery*. 2002 Mar;48(3):292-7. PubMed PMID: 11862035. Epub 2002/02/28. eng.
124. Marques M, Brown SA, Cordeiro ND, Rodrigues-Pereira P, Cobrado ML, Morales-Helguera A, et al. Effects of fibrin, thrombin, and blood on breast capsule formation in a preclinical model. *Aesthetic surgery journal*. 2011 Mar;31(3):302-9. PubMed PMID: 21385741. Epub 2011/03/10. eng.
125. Marques M, Brown SA, Rodrigues-Pereira P, Natalia M, Cordeiro DS, Morales-Helguera A, et al. Animal model of implant capsular contracture: effects of chitosan. *Aesthetic surgery journal*. 2011 Jul;31(5):540-50. PubMed PMID: 21719867. Epub 2011/07/02. eng.
126. Marques M, Brown SA, Cordeiro ND, Rodrigues-Pereira P, Cobrado ML, Morales-Helguera A, et al. Effects of coagulase-negative staphylococci and fibrin on breast capsule formation in a rabbit model. *Aesthetic surgery journal*. 2011 May;31(4):420-8. PubMed PMID: 21551433. Epub 2011/05/10. eng.
127. Bergmann PA, Tamouridis G, Lohmeyer JA, Mauss KL, Becker B, Knobloch J, et al. The effect of a bacterial contamination on the formation of capsular contracture with polyurethane breast implants in comparison with textured silicone implants: an animal study. *Journal of plastic, reconstructive & aesthetic surgery : JPRAS*. 2014 Oct;67(10):1364-70. PubMed PMID: 24953446. Epub 2014/06/24. eng.

128. Tamboto H, Vickery K, Deva AK. Subclinical (biofilm) infection causes capsular contracture in a porcine model following augmentation mammoplasty. *Plastic and reconstructive surgery*. 2010 Sep;126(3):835-42. PubMed PMID: 20811216. Epub 2010/09/03. eng.
129. Jacombs A, Tahir S, Hu H, Deva AK, Almatroudi A, Wessels WLF, et al. In Vitro and In Vivo Investigation of the Influence of Implant Surface on the Formation of Bacterial Biofilm in Mammary Implants. *Plastic and reconstructive surgery*. 2014;133(4):471e-80e. PubMed PMID: 00006534-201404000-00009.
130. Jacombs A, Allan J, Hu H, Valente PM, Wessels WL, Deva AK, et al. Prevention of biofilm-induced capsular contracture with antibiotic-impregnated mesh in a porcine model. *Aesthetic surgery journal*. 2012 Sep;32(7):886-91. PubMed PMID: 22942116. Epub 2012/09/04. eng.
131. Mendes PR, Bins-Ely J, Lima EA, Vasconcellos ZA, d'Acampora AJ, Neves RD. Histological study on acute inflammatory reaction to polyurethane-coated silicone implants in rats. *Acta cirurgica brasileira*. 2008 Jan-Feb;23(1):93-101. PubMed PMID: 18278399. Epub 2008/02/19. eng.
132. Arad E, Navon-Venezia S, Gur E, Kuzmenko B, Glick R, Frenkiel-Krispin D, et al. Novel rat model of methicillin-resistant *Staphylococcus aureus*-infected silicone breast implants: a study of biofilm pathogenesis. *Plastic and reconstructive surgery*. 2013 Feb;131(2):205-14. PubMed PMID: 23076419. Epub 2012/10/19. eng.
133. Cappellano G, Ploner C, Lobenwein S, Sopper S, Hoerthagl P, Mayerl C, et al. Immunophenotypic characterization of human T cells after in vitro exposure to different silicone breast implant surfaces. *PloS one*. 2018;13(2):e0192108.
134. Lechner MG, Megiel C, Church CH, Angell TE, Russell SM, Sevell RB, et al. Survival signals and targets for therapy in breast implant-associated ALK--anaplastic large cell lymphoma. *Clinical cancer research : an official journal of the American Association for Cancer Research*. 2012 Sep 01;18(17):4549-59. PubMed PMID: 22791880. Epub 2012/07/14. eng.
135. Kadin ME, Morgan J, Xu H, Epstein AL, Sieber D, Hubbard BA, et al. IL-13 is produced by tumor cells in breast implant-associated anaplastic large cell lymphoma: implications for pathogenesis. *Human pathology*. 2018 Aug;78:54-62. PubMed PMID: 29689246. Epub 2018/04/25. eng.
136. Prantl L, Poppl N, Horvat N, Heine N, Eisenmann-Klein M. Serologic and histologic findings in patients with capsular contracture after breast augmentation with smooth silicone gel implants: is serum hyaluronan a potential predictor? *Aesthetic plastic surgery*. 2005 Nov-Dec;29(6):510-8. PubMed PMID: 16328636. Epub 2005/12/06. eng.
137. Hwang K, Sim HB, Huan F, Kim DJ. Myofibroblasts and capsular tissue tension in breast capsular contracture. *Aesthetic plastic surgery*. 2010 Dec;34(6):716-21. PubMed PMID: 20512331. Epub 2010/06/01. eng.
138. Lesesne CB. Textured surface silicone breast implants: histology in the human. *Aesthetic plastic surgery*. 1997 Mar-Apr;21(2):93-6. PubMed PMID: 9143423. Epub 1997/03/01. eng.
139. Thomsen JL, Christensen L, Nielsen M, Brandt B, Breiting VB, Felby S, et al. Histologic changes and silicone concentrations in human breast tissue surrounding silicone breast prostheses. *Plastic and reconstructive surgery*. 1990 Jan;85(1):38-41. PubMed PMID: 2293734. Epub 1990/01/01. eng.
140. Copeland M, Choi M, Bleiweiss JJ. Silicone breakdown and capsular synovial metaplasia in textured-wall saline breast prostheses. *Plastic and reconstructive surgery*. 1994 Oct;94(5):628-33; discussion 34-6. PubMed PMID: 7938285. Epub 1994/10/01. eng.
141. Yeoh G, Russell P, Jenkins E. Spectrum of histological changes reactive to prosthetic breast implants: a clinopathological study of 84 patients. *Pathology*. 1996 Aug;28(3):232-5. PubMed PMID: 8912351. Epub 1996/08/01. eng.
142. Peters W, Smith D, Fornasier V, Lugowski S, Ibanez D. An outcome analysis of 100 women after explantation of silicone gel breast implants. *Annals of plastic surgery*. 1997 Jul;39(1):9-19. PubMed PMID: 9229086. Epub 1997/07/01. eng.
143. Gayou RM. A histological comparison of contracted and non-contracted capsules around silicone breast implants. *Plastic and reconstructive surgery*. 1979 May;63(5):700-7. PubMed PMID: 571127. Epub 1979/05/01. eng.

144. Siggelkow W, Faridi A, Spiritus K, Klinge U, Rath W, Klosterhalfen B. Histological analysis of silicone breast implant capsules and correlation with capsular contracture. *Biomaterials*. 2003 Mar;24(6):1101-9. PubMed PMID: 12504533. Epub 2002/12/31. eng.
145. Wyatt LE, Sinow JD, Wollman JS, Sami DA, Miller TA. The influence of time on human breast capsule histology: smooth and textured silicone-surfaced implants. *Plastic and reconstructive surgery*. 1998 Nov;102(6):1922-31. PubMed PMID: 9810987. Epub 1998/11/12. eng.
146. Carpaneda CA. Inflammatory reaction and capsular contracture around smooth silicone implants. *Aesthetic plastic surgery*. 1997 Mar-Apr;21(2):110-4. PubMed PMID: 9143426. Epub 1997/03/01. eng.
147. Wolfram D, Rainer C, Niederegger H, Piza H, Wick G. Cellular and molecular composition of fibrous capsules formed around silicone breast implants with special focus on local immune reactions. *Journal of autoimmunity*. 2004 Aug;23(1):81-91. PubMed PMID: 15236756. Epub 2004/07/09. eng.
148. Meza Britez ME, Caballero Llano C, Chaux A. Periprosthetic breast capsules and immunophenotypes of inflammatory cells. *European journal of plastic surgery*. 2012 Sep;35(9):647-51. PubMed PMID: 22904602. Pubmed Central PMCID: PMC3419835. Epub 2012/08/21. eng.
149. Kuhn A, Singh S, Smith PD, Ko F, Falcone R, Lyle WG, et al. Periprosthetic breast capsules contain the fibrogenic cytokines TGF-beta1 and TGF-beta2, suggesting possible new treatment approaches. *Annals of plastic surgery*. 2000 Apr;44(4):387-91. PubMed PMID: 10783094. Epub 2000/04/27. eng.
150. Rudolph R, Abraham J, Vecchione T, Guber S, Woodward M. Myofibroblasts and free silicon around breast implants. *Plastic and reconstructive surgery*. 1978 Aug;62(2):185-96. PubMed PMID: 678332. Epub 1978/08/01. eng.
151. Centeno JA, Mullick FG, Panos RG, Miller FW, Valenzuela-Espinoza A. Laser-Raman microprobe identification of inclusions in capsules associated with silicone gel breast implants. *Modern pathology : an official journal of the United States and Canadian Academy of Pathology, Inc*. 1999 Jul;12(7):714-21. PubMed PMID: 10430276. Epub 1999/08/03. eng.
152. del Rosario AD, Bui HX, Petrocine S, Sheehan C, Pastore J, Singh J, et al. True synovial metaplasia of breast implant capsules: a light and electron microscopic study. *Ultrastructural pathology*. 1995 Mar-Apr;19(2):83-93. PubMed PMID: 7792953. Epub 1995/03/01. eng.
153. Legrand AP, Marinov G, Pavlov S, Guidoin MF, Famery R, Bresson B, et al. Degenerative mineralization in the fibrous capsule of silicone breast implants. *Journal of materials science Materials in medicine*. 2005 May;16(5):477-85. PubMed PMID: 15875259. Epub 2005/05/06. eng.
154. Amoresano A, De Stefano L, Rea I, Pane F, Birolo L, Schonauer F. Chemical and Structural Characterization of Several Mid-Term Explanted Breast Prostheses. *Materials*. 2016;9(8):678. PubMed PMID: doi:10.3390/ma9080678.
155. Giot JP, Paek LS, Nizard N, El-Diwany M, Gaboury LA, Nelea M, et al. The double capsules in macro-textured breast implants. *Biomaterials*. 2015 Oct;67:65-72. PubMed PMID: 26210173. Epub 2015/07/27. eng.
156. Virden CP, Dobke MK, Stein P, Parsons CL, Frank DH. Subclinical infection of the silicone breast implant surface as a possible cause of capsular contracture. *Aesthetic plastic surgery*. 1992 Spring;16(2):173-9. PubMed PMID: 1570781. Epub 1992/01/01. eng.
157. Dobke MK, Svahn JK, Vastine VL, Landon BN, Stein PC, Parsons CL. Characterization of microbial presence at the surface of silicone mammary implants. *Annals of plastic surgery*. 1995 Jun;34(6):563-9; discussion 70-1. PubMed PMID: 7661531. Epub 1995/06/01. eng.
158. Rieger UM, Mesina J, Kalbermatten DF, Haug M, Frey HP, Pico R, et al. Bacterial biofilms and capsular contracture in patients with breast implants. *The British journal of surgery*. 2013 May;100(6):768-74. PubMed PMID: 23468161. Epub 2013/03/08. eng.
159. Pajkos A, Deva AK, Vickery K, Cope C, Chang L, Cossart YE. Detection of subclinical infection in significant breast implant capsules. *Plastic and reconstructive surgery*. 2003 Apr 15;111(5):1605-11. PubMed PMID: 12655204. Epub 2003/03/26. eng.
160. Del Pozo JL, Tran NV, Petty PM, Johnson CH, Walsh MF, Bite U, et al. Pilot study of association of bacteria on breast implants with capsular contracture. *Journal of clinical*

- microbiology. 2009 May;47(5):1333-7. PubMed PMID: 19261794. Pubmed Central PMCID: PMC2681843. Epub 2009/03/06. eng.
161. Schreml S, Heine N, Eisenmann-Klein M, Prantl L. Bacterial colonization is of major relevance for high-grade capsular contracture after augmentation mammoplasty. *Annals of plastic surgery*. 2007 Aug;59(2):126-30. PubMed PMID: 17667403. Epub 2007/08/02. eng.
162. Poppler L, Cohen J, Dolen UC, Schriefer AE, Tenenbaum MM, Deeken C, et al. Histologic, Molecular, and Clinical Evaluation of Explanted Breast Prostheses, Capsules, and Acellular Dermal Matrices for Bacteria. *Aesthetic surgery journal*. 2015 Aug;35(6):653-68. PubMed PMID: 26229126. Pubmed Central PMCID: PMC4649701. Epub 2015/08/01. eng.
163. Wolfram D, Rabensteiner E, Grundtman C, Bock G, Mayerl C, Parson W, et al. T regulatory cells and TH17 cells in peri-silicone implant capsular fibrosis. *Plastic and reconstructive surgery*. 2012 Feb;129(2):327e-37e. PubMed PMID: 22286447. Epub 2012/01/31. eng.
164. Hanson SE, Hassid VJ, Branch-Brooks C, Liu J, Kadin ME, Miranda R, et al. Validation of a CD30 Enzyme-Linked Immunosorbant Assay for the Rapid Detection of Breast Implant-Associated Anaplastic Large Cell Lymphoma. *Aesthetic surgery journal*. 2019 Feb 21. PubMed PMID: 30789639. Epub 2019/02/23. eng.
165. Kyle DJ, Harvey AG, Shih B, Tan KT, Chaudhry IH, Bayat A. Identification of molecular phenotypic descriptors of breast capsular contracture formation using informatics analysis of the whole genome transcriptome. *Wound repair and regeneration : official publication of the Wound Healing Society [and] the European Tissue Repair Society*. 2013 Sep-Oct;21(5):762-9. PubMed PMID: 23941504. Epub 2013/08/15. eng.
166. Ulrich D, Ulrich F, Pallua N, Eisenmann-Klein M. Effect of Tissue Inhibitors of Metalloproteinases and Matrix Metalloproteinases on Capsular Formation Around Smooth and Textured Silicone Gel Implants. *Aesthetic plastic surgery*. 2009;33(4):555-62.
167. Baker JL, Jr., Chandler ML, LeVier RR. Occurrence and activity of myofibroblasts in human capsular tissue surrounding mammary implants. *Plastic and reconstructive surgery*. 1981 Dec;68(6):905-12. PubMed PMID: 7301985. Epub 1981/12/01. eng.
168. Ben Amar M, Wu M, Trejo M, Atlan M. Morpho-elasticity of inflammatory fibrosis: the case of capsular contracture. *Journal of the Royal Society, Interface*. 2015 Oct 06;12(111):20150343. PubMed PMID: 26446558. Pubmed Central PMCID: PMC4614484. Epub 2015/10/09. eng.
169. Bodin F, Jung C, Dieval F, Chakfe N, Wisniewski S, Bruant Rodier C, et al. Aging of retrieved gel breast implants: a comparison between two product generations. *Journal of the mechanical behavior of biomedical materials*. 2015 Jun;46:11-22. PubMed PMID: 25746931. Epub 2015/03/10. eng.
170. Tortolano L, Yen-Nicolaÿ S, Rogliano P-F, Alkhashnam H, Honart J-F, Manerlax K, et al. Permeability of expander breast implants: in vitro and in vivo analyses. *Journal of the mechanical behavior of biomedical materials*.
171. Ramiao NG, Martins PS, Barroso ML, Santos DC, Fernandes AA. In vitro degradation of polydimethylsiloxanes in breast implant applications. *Journal of applied biomaterials & functional materials*. 2017 Nov 10;15(4):e369-e75. PubMed PMID: 28574093. Epub 2017/06/03. eng.
172. Taffi AP, Kirkpatrick AB, Alavi Z, Owen HA, Yu Z. Recent advances in 3D SEM surface reconstruction. *Micron*. 2015;78:54-66.
173. Podsiadlo P, Stachowiak G. Characterization of surface topography of wear particles by SEM stereoscopy. *Wear*. 1997;206(1-2):39-52.
174. Bariani P, De Chiffre L, Hansen HN, Horsewell A. Investigation on the traceability of three dimensional scanning electron microscope measurements based on the stereo-pair technique. *Precision engineering*. 2005;29(2):219-28.
175. Krishna AV, Flys O, Reddy VV, Rosén BG. Surface topography characterization using 3D stereoscopic reconstruction of SEM images. *Surface Topography: Metrology and Properties*. 2018 2018/05/16;6(2):024006.
176. Piazzesi G. Photogrammetry with the scanning electron microscope. *Journal of Physics E: Scientific Instruments*. 1973;6(4):392.

177. Kricheldorf J, Fallenberg EM, Solbach C, Gerber-Schafer C, Rancso C, Fritschen UV. Breast Implant-Associated Lymphoma. *Deutsches Arzteblatt international*. 2018 Sep 21;115(38):628-35. PubMed PMID: 30373708. Pubmed Central PMCID: PMC6218708. Epub 2018/10/31. eng.
178. Johnson L, O'Donoghue JM, McLean N, Turton P, Khan AA, Turner SD, et al. Breast implant associated anaplastic large cell lymphoma: The UK experience. Recommendations on its management and implications for informed consent. *European journal of surgical oncology : the journal of the European Society of Surgical Oncology and the British Association of Surgical Oncology*. 2017 May 18. PubMed PMID: 28596034. Epub 2017/06/10. eng.
179. Webb LH, Aime VL, Do A, Mossman K, Mahabir RC. Textured Breast Implants: A Closer Look at the Surface Debris Under the Microscope. *Plastic Surgery*. 2017;25(3):179-83.
180. Gefen A, Dilmoney B. Mechanics of the normal woman's breast. *Technology and health care : official journal of the European Society for Engineering and Medicine*. 2007;15(4):259-71. PubMed PMID: 17673835. Epub 2007/08/04. eng.
181. Garabédian C, Bigerelle M, Najjar D, Migaud H. Wear pattern on a retrieved Total Knee Replacement: The "fourth body abrasion". *Biotribology*. 2017 2017/09/01;11(Supplement C):29-43.
182. Najjar D, Bigerelle M, Migaud H, lost A. About the relevance of roughness parameters used for characterizing worn femoral heads. *Tribology international*. 2006;39(12):1527-37.
183. Bigerelle M, Hagege B, El Mansori M. Mechanical modelling of micro-scale abrasion in superfinish belt grinding. *Tribology International*. 2008;41(11):992-1001.
184. El-Haddad R, Lafarge-Claoue B, Garabedian C, Staub S. A 10-Year Prospective Study of Implant-Based Breast Augmentation and Reconstruction. *Eplasty*. 2018;18.

THESIS SUMMARY

The first breast implant surface pattern approved by the American Food and Drug Administration (FDA) is Biocell texture commercialized by the American company Allergan in 1987. Most breast implant manufacturers then adopted similar surface patterning process. A report from the Agence Nationale de Sécurité du Médicament et des produits de santé (ANSM) estimated that 85% of implants sold in France between 2007 and 2016 were textured. In 2011, the FDA warned of a possible association between breast implants and a rare and specific form of lymphoma: Breast Implant-Associated Anaplastic Large Cell Lymphoma (BIA-ALCL). The number of cases of BIA-ALCL has exploded since 2014-2015, with an over-representation of the Biocell texture in the statistics, which justified the withdrawal of the French market of these prostheses by the ANSM in April 2019.

This thesis aims to evaluate the impact of breast implant surface topography on the clinical performance of the device.

Firstly, a comparative study carried out on 3 surface measurement techniques, as well as a statistical analysis based on the multi-scale decomposition of the topographies, allowed us to propose a metrologically-validated measurement methodology taking into account the surface morphology and the scale and to highlight the inconsistencies of the ISO standard related to breast implants (ISO 14607). Then, a classification and a morphologically-relevant designation of the textures were proposed and validated by an original protocol of genetic analysis on human tissues and by a discriminant analysis carried out on a large base of topographical parameters.

Similar topographical and statistical analyzes were also conducted on prostheses removed from the human body (or explant) in order to quantify the damage according to the type of texture and to the scale.

These studies will enable the GROUPE SEBBIN to design a new anatomically-shaped prosthesis, which will combine tissue anchoring and minimization of inflammation and damage processes.

Keywords: breast implant ; ALCL; texture ; surface measurement ; roughness ; surface nomenclature ; gene expression ; discriminant analysis ; *in vivo* damage

RESUME DE THESE

La première structuration de surface d'implants mammaires approuvée par l'agence sanitaire américaine Food and Drug Administration (FDA) est la texturation Biocell de l'Américain Allergan en 1987. La plupart des fabricants d'implants mammaires ont ensuite adopté des procédés permettant d'obtenir des texturations similaires pour la plupart. Un rapport de l'Agence Nationale de Sécurité du Médicament et des produits de santé (ANSM) a estimé que 85% des implants vendus en France entre 2007 et 2016 étaient texturés. En 2011, la FDA alerte sur une possible association entre les implants mammaires et une forme rare et spécifique de lymphome : le Lymphome Anaplasique à Grandes Cellules Associés aux Implants Mammaires (LAGC-AIM). Le nombre de cas de LAGC-AIM a explosé depuis 2014-2015, avec une sur-représentation de la texture Biocell dans les statistiques justifiant le retrait du marché français de ces prothèses par l'ANSM en avril 2019.

Ces travaux de thèse ont pour but d'évaluer l'impact de la topographie de surface des implants mammaires sur les performances cliniques du dispositif.

Premièrement, une étude comparative menée sur 3 techniques de mesure de surface, ainsi qu'une analyse statistique basée sur la décomposition multi-échelle des topographies, nous ont permis de proposer une méthodologie de mesure métrologiquement correcte prenant en compte la morphologie de surface et l'échelle et de jeter la lumière sur les faiblesses de la norme ISO relative aux implants mammaires (ISO 14607).

Ensuite, une classification et une dénomination morphologiquement pertinente des texturations ont été proposées et validées par un protocole original d'analyse génétique sur tissus humains et par une analyse discriminante menée sur une large base de paramètres topographiques.

Des analyses topographique et statistique similaires ont été également conduites sur prothèses retirées du corps humain (ou explant), afin de quantifier l'endommagement en fonction du type de texturation et de l'échelle.

Ces études permettront au GROUPE SEBBIN de concevoir une nouvelle prothèse de forme anatomique, qui alliera à la fois accroche tissulaire et minimisation des processus d'inflammation et d'endommagement.

Mots clés : implant mammaire ; LAGC ; texturation ; mesure de surface ; rugosité ; nomenclature des surfaces ; analyse discriminante ; endommagement *in vivo*